

**Pathogenesis of Heart and Liver Diseases in Acquired and  
Genetic Iron-overload Disorders**

*Resveratrol as potential therapy*

by

Subhash Kumar Das

A thesis submitted in partial fulfillment of the requirements for the degree of

Doctor of Philosophy

*Experimental Medicine*

Department of Medicine  
University of Alberta

© Subhash Kumar Das, 2016

## **Abstract**

Abnormal iron metabolism leads to cardiac and hepatic iron-overload disorders in an epidemic proportion. Irregular iron absorption results in iron deposition in different organs of the body including heart and liver. Iron-overload heart and liver diseases are commonly observed in patients with genetic hemochromatosis and secondary iron-overload, which are a common cause of end organ failure and mortality worldwide basis. An excess amount of iron associated with iron induced oxidative stress that leads to iron-overload cardiomyopathy and liver dysfunction respectively. We developed murine models of iron-overload with cardiomyopathy and liver disease to understand new insights into the pathogenesis and novel therapeutic effects of resveratrol.

Cardiac and hepatic iron-overload pathogenesis showed dose-dependent iron-overload, oxidative stress, lipid peroxidation and fibrosis; however reduction in SERCA2a protein with defective calcium cycling without any inflammatory response is noticed in iron-overload hearts, which are key factors for the development of diastolic and systolic dysfunction. In contrast, hepatomegaly, hepatic inflammation, hepatic cell death and hepatic steatosis are well noticed in hepatic iron-overload. Resveratrol therapy improved cardiac function by decreasing iron-induced oxidative stress, myocardial lipid peroxidation, cardiac fibrosis, and hypertrophy; normalize calcium cycling defects by improving SERCA2a. In contrast resveratrol, therapy also improved liver function by reducing hepatic oxidative stress, lipid peroxidation, hepatic inflammation, hepatic cell death and hepatic steatosis. Consistent with the role of iron-induced myocardial oxidative stress in the development of heart disease, iron-overload female mice showed normal cardiac function with better survival rate without iron

induced oxidative stress, highlighting the antioxidant properties of the female sex hormone estrogen. These results indicate that iron-induced oxidative stress is the key driver in the development of heart and liver diseases. There is no effective therapy available to prevent the global clinical burden of iron-overload, however, the mainstay therapies for iron-overload are phlebotomy and chelation therapy and these therapies have several limitations. Therefore, given the high degree of iron induced oxidative damage, we proposed that the pleiotropic effects of resveratrol represent a potential therapy to treat heart and liver diseases in iron-overloaded conditions.

**Preface:**

Non-failing human hearts were collected as part of the Human Organ Procurement and Exchange (HOPE) program for research at the Mazankowski Alberta Heart Institute. Human cardiomyocytes were used to improve the translational impact of our research. All experiments were performed in accordance with the institutional guidelines and were approved by Institutional Ethics Committee. Informed consent was obtained from all study subjects. The research projects in the current thesis are mainly performed in Dr. Gavin Oudit lab.

## **This thesis is dedicated**

*To my beloved parents for their endless love, support and encouragement, who always reminded me as follow.....*

***“Karmanye vadhikaraste Ma Phaleshu Kadachana,”***

***“Ma Karmaphalaheturbhurma Te Sangostvakarmani”***

*“Keep on performing your duties without expecting any reward in return. You get something or you don't get anything, you should not worry about it. You should lead a selfless life”*

(Verses from Bhagwat Gita)

## ACKNOWLEDGEMENTS

I would like to thank my supervisor *Dr. Gavin Y. Oudit* for the support that he has provided throughout my Ph.D. graduate studies. Without his intellectual guidance, the content of this thesis would not have been possible to accomplish.

I would also like to thank the committee members, *Dr. Jason R.B. Dyck* and *Dr. Michael Sean McMurtry*, for their guidance, advice, invaluable suggestions and constant support throughout the course of my Ph.D. program.

I sincerely would like to thank all of my collaborators, especially *Dr. Jason R.B. Dyck* and *Dr. Zamaneh Kassiri* for allowing me to work with various ongoing projects, independent from this thesis. I would also like to sincerely thank my other collaborators *Dr. Nancy C. Andrews* and *Dr. Roger J. Hajjar*, for kindly providing us the hemojuvelin knock-out mice and adenoviral SERCA2a, respectively.

My sincere gratitude is given to all my present and past lab members, for their continued peer support and friendship, a wonderful experience in life during my time in the lab.

This research would not have been possible without the financial assistance of Alberta Innovative Health solutions (AIHS) studentship and Alberta HEART STEADI-HF studentship as well as Heart and Stroke grant from Dr. Oudit.

Last but not least, I would like to thank my wife *Sushreeta Sai* for her continued and unrelenting support. I would also like to thank my mother *Susheela Das* and my father *Bhaskar Das* for letting me pursue my ambition.

# CONTENTS

<b>Chapter 1: Literature Review.....</b>	<b>1-46</b>
1.1 General Introduction	
1.2 Iron metabolism	
1.2.1 Cellular iron metabolism	
1.2.2 Systemic iron metabolism	
1.3 Pathological conditions associated with iron-overload	
1.3.1 Primary hemochromatosis	
1.3.2 Secondary Iron-overload	
1.4 Iron-overload cardiomyopathy	
1.4.1 Clinical description of iron-overload cardiomyopathy	
1.4.2 Pathophysiology of iron-overload cardiomyopathy	
1.4.3 Role of gender in the pathogenesis of iron-overload cardiomyopathy	
1.5 Hepatic Iron-overload disease	
1.6 Iron induced oxidative stress	
1.7 Current therapies	

1.8 Proposed therapies

1.8.1 Antioxidant therapy

1.8.2 Resveratrol in clinical trials

1.8.3 Amlodipine: L-Type calcium channel blocker

1.9 Hypothesis

**Chapter 2: Overview of Research Protocol.....47-56**

2.1 Iron-overload animal models

2.2 Experimental Animal Protocols

2.3 Sample size, Power of study and choice of statistical method

**Chapter 3: Iron-overload injury and cardiomyopathy in acquired and genetic models  
is attenuated by resveratrol therapy.....57-106**

3.1 Abstract

3.2 Introduction

3.3 Materials and Methods

3.4 Results

3.5 Discussion

3.6 Conclusion

**Chapter 4: Iron-overload cardiomyopathy in aged Juvenile hemochromatosis genetic murine model and prevented by resveratrol.....107-131**

- 4.1 Abstract
- 4.2 Introduction
- 4.3 Materials and Methods
- 4.4 Results
- 4.5 Discussion
- 4.6 Conclusion

**Chapter 5: Resveratrol mediates therapeutic hepatic effects in acquired and genetic murine models of iron-overload.....132-157**

- 5.1 Abstract
- 5.2 Introduction
- 5.3 Materials and Methods
- 5.4 Results
- 5.5 Discussion
- 5.6 Conclusion

**Chapter 6: Females are protected from iron-overload cardiomyopathy independent of iron metabolism: key role of oxidative stress.....158-189**

- 6.1 Abstract
- 6.2 Introduction
- 6.3 Materials and Methods
- 6.4 Results
- 6.5 Discussion
- 6.6 Conclusion

**Chapter 7: Discussion and future directions.....190-203**

- 7.1 Discussion
- 7.2 Future directions

**References.....204-241**

<b>Figure 1.1</b> Schematic view of mammalian cellular iron metabolism.....	05
<b>Figure 1.2</b> Schematic presentations of transferrin and transferrin receptor cycle.....	08
<b>Figure 1.3</b> IRE/IRP regulation of cellular iron metabolism during iron deficient state.....	12
<b>Figure 1.4</b> IRE/IRP regulation of cellular iron metabolism during iron rich state.....	14
<b>Figure 1.5</b> Schematic view of mammalian systemic iron metabolism.....	16
<b>Figure 1.6</b> Schematic presentation of worldwide distribution of iron-overload diseases.....	17
<b>Figure 1.7</b> Schematic presentation of Pathophysiology of iron-overload cardiomyopathy.....	24
<b>Figure 1.8</b> Schematic presentation of gender basis of iron-overload cardiomyopathy.....	26
<b>Figure 1.9</b> Schematic presentation of Pathophysiology of iron-overload liver diseases.....	28
<b>Figure 1.10</b> Schematic presentation of oxidative stress and consequences.....	29
<b>Figure 1.11</b> Schematic presentation of thioredoxin system.....	35
<b>Figure 1.12</b> Schematic presentation of cardiovascular and hepatic benefits of resveratrol therapy.....	39

<b>Figure 1.13</b> Schematic presentation of cardiovascular benefits of how resveratrol regulates AMPK and SIRT1 .....	41
<b>Figure 1.14</b> Schematic presentation of cardiovascular benefits of amlodipine calcium channel blocker therapy.....	44
<b>Figure 2.1</b> Overview of animal models and research protocol. ....	50
<b>Figure 3.1</b> Iron-overload alters myocardial SIRT1/FOXO1 signaling which is restored by resveratrol.....	79
<b>Figure 3.2</b> Pathological myocardial remodeling and diastolic dysfunction in early iron-overload is completely rescued by resveratrol therapy independent of myocardial iron-deposition.....	82
<b>Figure 3.2.1</b> Early iron-overload cardiomyopathy is not associated with any fibrosis or inflammation.....	83
<b>Figure 3.2.2</b> Early iron-overload cardiomyopathy is driven by downregulation of SERCA2a: rescue with adenoviral transfer of SERCA2a and resveratrol.....	86
<b>Figure 3.3</b> Iron-induced pro-oxidant effects in human and murine cardiomyocytes and in murine models of iron-overload are prevented by resveratrol.....	89
<b>Figure 3.3.1</b> Iron metabolism in wild type and hemojuvelin knockout mice.....	90
<b>Figure 3.3.2</b> Iron-induced oxidative stress in early and chronic murine models of iron-overload is prevented by resveratrol.....	91
<b>Figure 3.3.3</b> Iron-induced oxidative stress in early and chronic murine models of iron-overload is prevented by resveratrol.....	92

<b>Figure 3.4</b> Iron-induced profibrotic effects in human and murine cardiofibroblasts are suppressed by resveratrol.....	94
<b>Figure 3.4.1</b> Increased myocardial fibrosis associated with chronic iron-overload cardiomyopathy is completely rescued by resveratrol therapy.....	96
<b>Figure 3.4.2</b> Lack of inflammation associated with chronic iron-overload cardiomyopathy.....	97
<b>Figure 3.4.3</b> Resveratrol therapy completely rescued the cardiac dysfunction in chronic iron-overloaded wildtype and hemojuvelin knockout mice.....	98
<b>Figure 4.1</b> Abnormal iron metabolism in murine models of aged genetic hemochromatosis.....	116
<b>Figure 4.2</b> Resveratrol therapy prevents the advanced cardiomyopathy in aged iron-overloaded hemojuvelin knockout mice.....	118
<b>Figure 4.3</b> Kaplan-Meier curves showing severe mortality in aged iron-overloaded HJVKO mice, salutary effects with resveratrol treatment.....	121
<b>Figure 4.4</b> Resveratrol therapy prevents myocardial fibrosis and defective calcium cycling proteins associated with advanced iron-overload cardiomyopathy.....	123
<b>Figure 4.5</b> Neutrophil inflammatory staining in advanced iron-overload cardiomyopathy.....	124
<b>Figure 4.6</b> Macrophage (F4/80) inflammatory staining in advanced iron-overload cardiomyopathy.....	125
<b>Figure 4.7</b> Iron-induced oxidative stress in advanced murine models of iron-overload is prevented by resveratrol.....	127

**Figure 5.1** Hepatic iron-overload increases nuclear FOXO1 acetylation which is restored by resveratrol.....143

**Figure 5.2** Increased hepatic fibrosis, abnormal iron metabolism in chronic hepatic iron-overload is rescued by resveratrol therapy.....145

**Figure 5.2.1** Hepatic iron-overload is associated with hepatosplenomegaly.....146

**Figure 5.3** Iron-induced oxidative stress in chronic hepatic iron-overload is suppressed by resveratrol therapy.....148

**Figure 5.4** Iron-induced hepatic inflammation and apoptosis in chronic hepatic iron-overload is suppressed by resveratrol.....150

**Figure 5.5** Resveratrol therapy prevents iron-induced oxidative stress, fibrosis and steatosis at an advanced stage of hepatic iron-overload in aged hemojuvelin knockout mice.....152

**Figure 5.6** H&E and Oil-O-Red staining showing hepatocyte vacuolation and lack of hepatosteatosis.....153

**Figure 5.7** Oral glucose tolerance testing and hepatic inflammation in advanced iron-overloaded HJVKO livers.....154

**Figure 6.1** Marked gender differences in iron-overload cardiomyopathy.....170

**Figure 6.2** Female mice are protected against iron-overload induced oxidative stress.....174

**Figure 6.3** Female mice are protected against iron-overload induced myocardial fibrosis and heart disease.....176

**Figure 6.4** Lack of myocardial apoptosis in chronic iron-overloaded mice based on TUNNEL.....177

**Figure 6.5** H&E staining of ovaries from ovariectomized mice.....179

**Figure 6.6** Ovariectomy precipitates diastolic and systolic dysfunction in response to myocardial iron-overload.....180

**Figure 6.7** Ovariectomy does not modulate myocardial iron deposition but suppressed the upregulation of ferritin expression.....182

**Figure 6.8** Iron-overload induced myocardial oxidative stress is potentiated in ovariectomized female mice.....184

**Figure 6.9** Exacerbation of pathological myocardial remodeling in iron-overloaded ovariectomized female mice.....186

**Figure 7.1** Schematic presentation iron induced oxidative stress and cellular effects that lead to cardiomyopathy.....195

**Figure 7.2** Schematic presentation resveratrol therapeutic action in reducing iron induced oxidative stress and different stages of iron-overload cardiomyopathy.....197

**Figure 7.3** Schematic presentation showing hepatoprotective benefits of resveratrol hepatic iron-overload.....199

**Figure7.4** Schematic presentation showing summary of iron-overload pathophysiology in heart and liver and gender .....202

**LIST OF TABLES****PAGE #**

---

<b>Table 1.1</b> Diseases associated with iron-overload.....	21
<b>Table 3.1</b> List of TaqMan Primers and Probes.....	70
<b>Table 3.2</b> Echocardiographic assessment of cardiac function in early iron-overloaded male WT mice.....	84
<b>Table 3.3</b> Pressure-Volume loop assessment of cardiac function in early iron-overloaded WT mice.....	85
<b>Table 3.4</b> Echocardiographic assessment of cardiac function in chronically iron-overloaded male WT mice.....	99
<b>Table 3.5</b> Echocardiographic assessment of cardiac function in chronically iron-overloaded male HJV knockout mice.....	100
<b>Table 3.6</b> Pressure-Volume loop assessment of cardiac function in chronically iron-overloaded male WT mice.....	101
<b>Table 3.7</b> Pressure-Volume loop assessment of cardiac function in chronically iron-overloaded male HJV knockout mice.....	102
<b>Table 4.1</b> List of TaqMan probe and primer.....	114
<b>Table 4.2</b> Echocardiographic and Pressure-Volume assessment of cardiac function in advanced iron-overloaded male HJV KO mice at 1 yr of age.....	119
<b>Table 4.3</b> Echo-MRI assessment in iron-overloaded male HJV KO mice at 1 year of age group.....	120
<b>Table 5.1</b> List of TaqMan probe and primer.....	140

**Table 6.1** Invasive Pressure-Volume (PV) loop assessment of cardiac function in iron-overloaded WT male and female mice.....171

**Table 6.2** Invasive Pressure-Volume (PV) loop assessment of cardiac function in iron-overloaded HJV knockout male and female mice.....172

## LIST OF ABBREVIATIONS

---

A.....	late diastolic filling velocity during atrial contraction
A'.....	late diastolic myocardial velocity using tissue Doppler
AAV9.....	adeno associated virus 9
AC.....	adenylyl cyclase
ATP.....	adenosine triphosphate
ANF.....	atrial natriuretic factor
AMPK.....	AMP-Activated Protein Kinase
ALAS2.....	5-aminolevulinic acid synthase2
AU.....	Arbitrary unit
$\alpha$ -SKA.....	Alpha-skeletal actin
$\alpha$ -SMA.....	Alpha-smooth muscle actin
BNP.....	Brain natriuretic peptide
BSA.....	Bovine serum albumin
$\beta$ -MHC.....	Beta-Myosin Heavy Chain
CAT.....	Catalase
cAMP.....	Cyclic Adenosine monophosphate
cGMP.....	Cyclic Guanosine monophosphate
CO.....	Cardiac output
DAPI.....	4',6-diamidino-2-phenylindole
DHE.....	Dihydroethidium
DT.....	Deceleration Time

DTT.....Dithiothreitol  
 DMT1.....Divalent metal transporter 1  
 DNA.....Deoxyribonucleic acid  
 Dyc7b.....Duodenal cytochrome b  
 E.....early diastolic filling velocity during atrial contraction  
 E'.....early diastolic myocardial velocity using tissue Doppler  
 ECG.....Electrocardiography  
 ECM.....Extracellular matrix  
 EDPVR.....End diastolic pressure-volume relationship  
 EDV.....End diastolic volume  
 EDP.....End diastolic Pressure  
 EDTA.....Ethylenediaminetetraacetic acid  
 ETS.....Electron transport system  
 EF.....Ejection fraction  
 ERE.....Estrogen receptor Element  
 ER- $\alpha$ .....Estrogen receptor Alpha  
 ER- $\beta$ .....Estrogen receptor Beta  
 ESPVR.....End-systolic pressure-volume relationship  
 ESV.....End systolic volume  
 ESP.....End systolic Pressure  
 FOXO1.....Forkhead box-O 1  
 FAC.....Ferric ammonium citrate  
 Ft1.....Ferritin light chain1

Fth1.....Ferritin heavy chain1  
FLVCR.....Feline leukemia virus type C receptor  
FPN.....Ferroportin  
GFP.....Green fluorescent protein  
Gpx-1.....Glutathione peroxidase-1  
GRX.....Glutaredoxin  
GSH.....Reduced Glutathione  
GSSG.....Glutathione disulfide  
HBSS.....Hanks balanced salt solution  
HCV.....Hepatitis C Virus  
HFE.....High Iron  
Hmox-1.....Heme oxygenase-1  
HJV.....Hemojuvelin  
HJVKO.....Hemojuvelin knockout  
HAMP1,2.....Hepcidin1,2  
HMOX1.....Hemeoxygenase1  
HR.....Heart rate  
HRP.....Horseradish peroxidase  
ILs.....Interleukins  
IRE.....Iron-responsive elements  
IRP.....Iron regulatory proteins  
IREG1.....Iron-regulated protein1  
IVRT.....Isovolumetric relaxation time

JH.....Juvenile hemochromatosis  
KPE.....potassium phosphate extraction  
LA.....Left atrium  
LIP.....Labile iron pool  
LV.....left ventricle  
LVEDD.....LV end-diastolic diameter  
LVESD.....LV end-systolic diameter  
LTCC.....L-Type Calcium channel  
LPS.....Lipopolysaccharide  
MDA.....Malondialdehyde  
MT-1,2.....Metallothionein  
MTP1.....Metal transporter protein1  
MnSOD.....Manganese superoxide dismutase  
NAC.....N-acetylcysteine  
NADPH.....Nicotinamide adenine dinucleotide phosphate  
NCX-1.....Sodium-Calcium exchanger-1  
NTBI.....Non-transferrin bound iron  
NT.....Nitrotyrosine  
NMPI.....N-methyl-2-phenylindole  
NO.....Nitric oxide  
OVX.....Ovariectomy  
ORO.....Oil red O  
OGTT.....Oral glucose tolerance test

PBS.....Phosphate Buffered Solution  
PDGF.....Platelet-derived growth factor  
PDE.....Phosphodiesterase  
PGC-1 $\alpha$ .....Peroxisome proliferator-activated receptor c coactivator 1- $\alpha$   
PLN.....Phospholamban  
PSR.....Picro Sirius Red  
PVDF.....Polyvinyl difluoride  
PRSW.....preload recruitable stroke work  
RT-PCR.....real-time polymerase chain reaction  
RGMc.....Repulsive and Guidance Molecules  
RSV.....Resveratrol  
ROS.....Reactive oxygen species  
RNS.....Reactive nitrogen species  
RNA.....Ribonucleic acid  
RV.....Right ventricle  
RR.....Relative ratio  
SR.....Sarcoplasmic reticulum  
SH.....Sulfhydryl  
SV.....Stroke volume  
SW.....Stroke work  
SERCA2a.....Sarcoendoplasmic reticulum Calcium ATPase2a  
SREBP1.....Sterol regulatory element binding protein1  
SDS-PAGE.....Sodium dodecyl sulphate-poly acrylamide gel electrophoresis

SCI.....Starlings contractile index  
SCD.....Sickle cell disease  
TDI.....Tissue Doppler imaging  
Trfc1.....Transferrin receptor1  
Tf.....Transferrin  
TRX1,2.....Thioredoxin 1, 2  
TIMP.....Tissue inhibitor of metalloproteinase  
TNF.....Tumor necrosis factor  
TGF- $\beta$ .....Transforming growth factor- $\beta$   
TTCC.....T-Type Calcium channel  
TUNEL.....Terminal deoxynucleotidyl transferase-mediated dUTP nick-end  
labeling  
UTR.....Untranslated regions  
VSMC.....Vascular smooth muscle cell  
WT.....Wild type

## LIST OF PREFIXES

---

M.....mega ( $10^6$ )

K.....kilo ( $10^3$ )

C.....centi ( $10^{-2}$ )

m.....milli ( $10^{-3}$ )

$\mu$ .....micro ( $10^{-6}$ )

n.....nano ( $10^{-9}$ )

## LIST OF UNITS

---

Hz.....hertz

L.....litre

m.....meter

g.....gram

Da.....dalton

$^{\circ}\text{C}$ .....degree Celsius

Wk.....week

d.....day

## LIST OF SYMBOLS

---

$\alpha$  .....alpha

$\beta$  .....beta

$\gamma$  .....gamma

$\mu$  .....mu

# CHAPTER ONE

# Literature Review

**Part of this chapter has been adapted from**

Das SK, Oudit GY. *European Journal Haematology*. 2012;88(6): 476-7.

**Voltage-gated Ca<sup>2+</sup> channels as key mediators of iron-transport and iron-overload cardiomyopathy: L-type vs T-type Ca<sup>2+</sup> channels.**

And

Das SK, Zhabyeyev P, Oudit GY. *Transl Res*. 2014 Feb;163(2):141-4.

**Role of sex steroids and sexual dimorphism on cardiac iron metabolism in iron-overload cardiomyopathy.**

## 1.1 General Introduction:

Iron is an important transition element which is predominately present in our environment and absolutely necessary for all forms of life.<sup>1-6</sup> It is available to living system in two different forms, heme iron (organic form) and ionic form iron (inorganic form) and the ionic form exist in two different states: ferrous state ( $\text{Fe}^{2+}$ ) and ferric state ( $\text{Fe}^{3+}$ ), because of this unique transition property iron perform one electron transfer oxidation-reduction reactions in biological systems.<sup>1, 4</sup> Many proteins and enzymes require iron for their function, in which they act as cofactor. Iron-containing proteins perform different kinds of function such as gas transport, electron transfer in the respiratory chain, the catalyst for biodegradation and biosynthesis, transcription factors, DNA replication, and repair etc. Besides these many beneficial effects iron also causes hazardous effects, because of its redox properties.

Healthy adult men contain 35 to 45mg of iron per kilogram of body weight.<sup>4</sup> Majority of body iron confined to red blood cells and erythroid precursors, besides this liver hepatocytes and reticuloendothelial macrophages stores most body iron.<sup>4, 7</sup> In mammals as there are no efficient iron excretion pathways, and the amount of iron present efficiently recycled to meet the demands of the body and any loss of iron due to bleeding, sloughing off of tissues and sweating will be replaced by iron absorption from dietary sources.<sup>3, 4</sup>

## **1.2 Iron metabolism:**

Many vital functions of life require iron. Iron associated with several proteins and carry out essential housekeeping functions of body.<sup>3, 6</sup> Iron-mediated cellular damage plays a key pathophysiological role in many disorders such as acute iron toxicosis, iron-overload cardiomyopathy, Friedreich ataxia associated cardiomyopathy, neurodegenerative disorders, and myocardial ischemia-reperfusion injury. Improper iron metabolism associated with detrimental pathophysiological consequences, which may lead to iron-overload (excess iron) or iron-deficiency (low iron) and to avoid these pathophysiological conditions, iron metabolism tightly regulated at the cellular level and systemic level.<sup>4, 8</sup>

### **1.2.1 Cellular iron metabolism:**

Iron metabolism at the cellular level is a tightly regulated process. Iron cannot passively enter cells because it cannot cross plasma membrane, without the aid of specific carrier/channel proteins thus cells evolved with specialized molecules for acquisition, transport and storage of iron (**Figure 1.1**). Following traditional cellular proteins involved in iron metabolism in the cell.

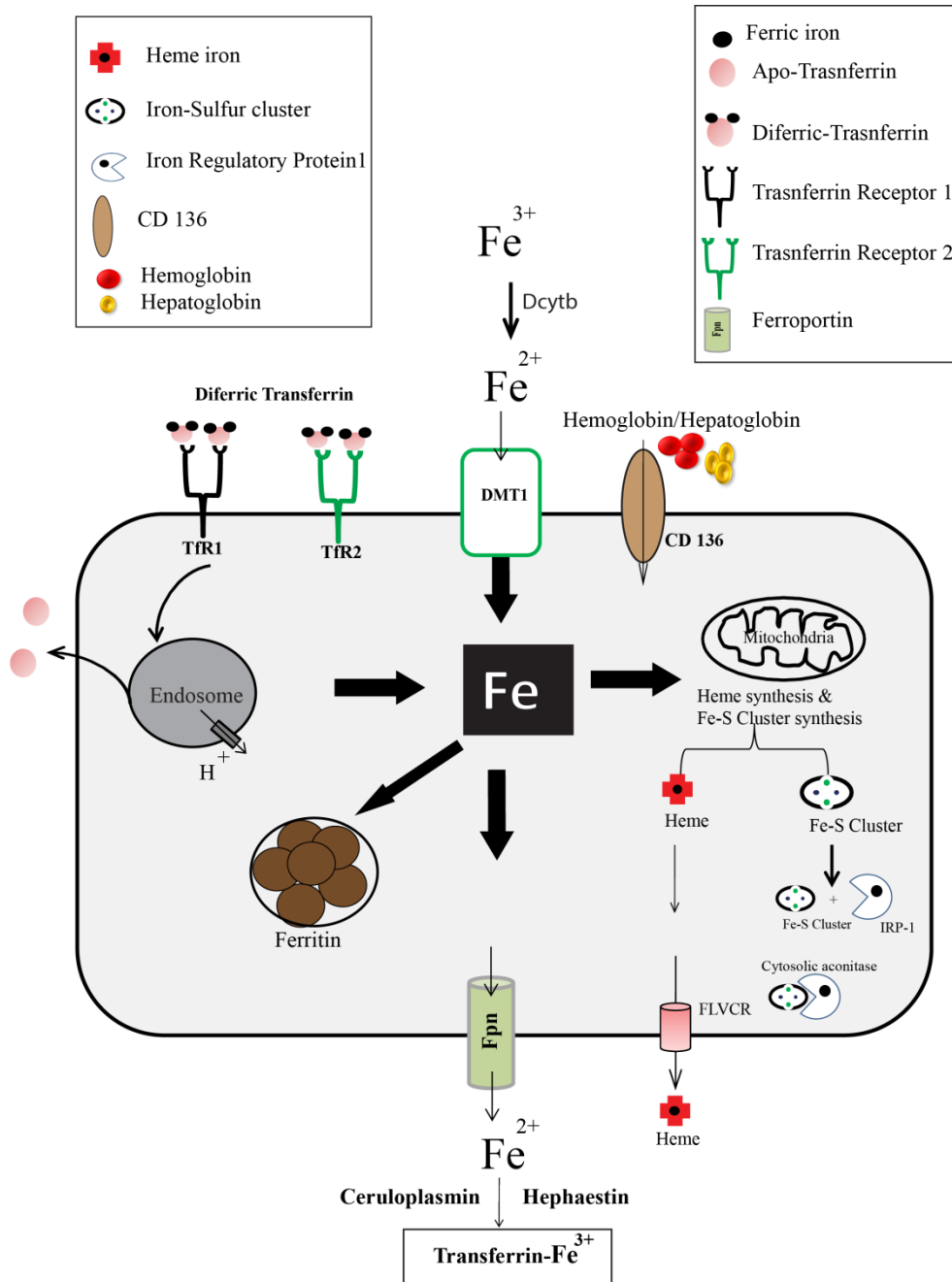


**Figure 1.1 Schematic presentation of mammalian cellular iron metabolism.** A general mammalian cell depicted with iron importers (top) and iron exports (bottom). Transferrin receptors majorly play a role in transferrin-mediated iron uptake. DMT1 also plays a role in iron import in intestinal cells with Dcytb which converts  $Fe^{2+}$  into  $Fe^{3+}$  before entering cells. CD136 act as heme transporter. Heme degradation occurs by heme oxygenase. Inside the cell iron translocated into different compartments for storage (ferritin), utilization (mitochondria). Iron is exported by only putative exporter named ferroportin found in duodenal cells and reticuloendothelial macrophages. Iron enters mitochondria for Fe-S cluster synthesis and Heme synthesis both are very important for cellular function. Sometime heme also exported by special exporter called heme exporter FLVCR. Dcytb= Duodenal cytochrome b; DMT1= Divalent metal transporter; FLVCR= Feline leukemia virus type C receptor; FPN1= Ferroportin1; IRP1= Iron regulatory protein1

**Transferrin (Tf):** Under physiological conditions, iron is stored and transported by a specific iron transporter called Transferrin (Tf) into blood compartments. Tf is a well characterized nearly 80kDa plasma glycoprotein, majorly transports and mobilization of iron for absorption and storage.<sup>1</sup> Transferrin protein consists of two homologous domains which are high-affinity iron binding sites and mostly bind to a ferric ( $\text{Fe}^{3+}$ ) form of iron.<sup>3</sup> Each Tf molecule can associate with two ferric iron molecules and this iron loaded transferrin molecules also called as diferric transferrin (Diferric-Tf).<sup>1,3</sup>

**Transferrin Receptor (Tfr1/2):** Tfr1 is ubiquitously expressed membrane receptor protein which plays an important role in physiological iron acquisition in most cell types.<sup>9</sup> It was also documented that Tfr1 play important role in cardiac iron uptake and inactivation of Transferrin Receptor1 (Tfr1) leads lethal cardiomyopathy due to cardiac iron deficiency.<sup>10</sup> Transferrin Receptor 2 (Tfr2) is predominantly found in liver hepatocytes, erythroid cells and some cells of duodenum.)<sup>7, 11, 12</sup> however both receptors expressed in hepatocytes of liver and enterocytes of small intestine, especially in the duodenum.<sup>3, 11, 12</sup> In hepatocytes Tfr1 allows entry of iron into liver cells and Tfr2 senses the iron levels and modulate the hepatic hepcidin expression.<sup>13, 14</sup> Both Transferrin receptors (Tfr1/2) regulate differently in response to iron levels, the expression of Tfr1 is downregulated during iron-overloaded condition and the expression of Tfr2 is up-regulated in iron-overload condition.

**Transferrin-Transferrin Receptor1 cycle:** The existence of transferrin receptor for transferrin was proposed by Jandl *et.al.*<sup>15, 16</sup> It is one of the most important pathway

through which iron enters and circulate in the body.<sup>1, 4, 8, 17</sup> It was well documented that the affinity of iron binding sites are  $P^H$  dependent.<sup>1, 3, 17-20</sup> Transferrin cycle allows binding of iron with high affinity at  $P^H$  approximately 7.4 ( $P^H$  of blood), diferric transferrin bind to transferrin receptor1 (TfR1) and this Tf-TfR1 complex internalized, (**Figure 1.2**) invaginate to form clathrin-coated endosomes.<sup>16, 19-21</sup> The endosome has a proton pump which reduces the  $P^H$  and decreases the affinity of Ferric to Tf, meanwhile the released ferric ( $Fe^{3+}$ ) iron converted to Ferrous ( $Fe^{2+}$ ) iron by unidentified ferrireductase and transported through a specific transporter called divalent metal transporter-1 (DMT-1) into the cytoplasm.<sup>4, 8, 17, 20</sup> Finally the Apo-Tf and TfR1 are recycled to the cell surface to (**Figure 1.2**) carry out another round of Transferrin cycle.<sup>22, 23</sup> Transferrin-bound iron is soluble in nature and serves as a major form of transported iron that utilized in many metabolic processes with low toxic side effects.<sup>3</sup> Some of this released iron enters into mitochondria for heme and iron-sulfur cluster synthesis, few associates with proteins, some of them stored in Ferritin for eventual iron supply (**Figure 1.2**). This transferrin bound iron is non-toxic and soluble in nature and distributed to different tissues and organs with the specific functional requirement.

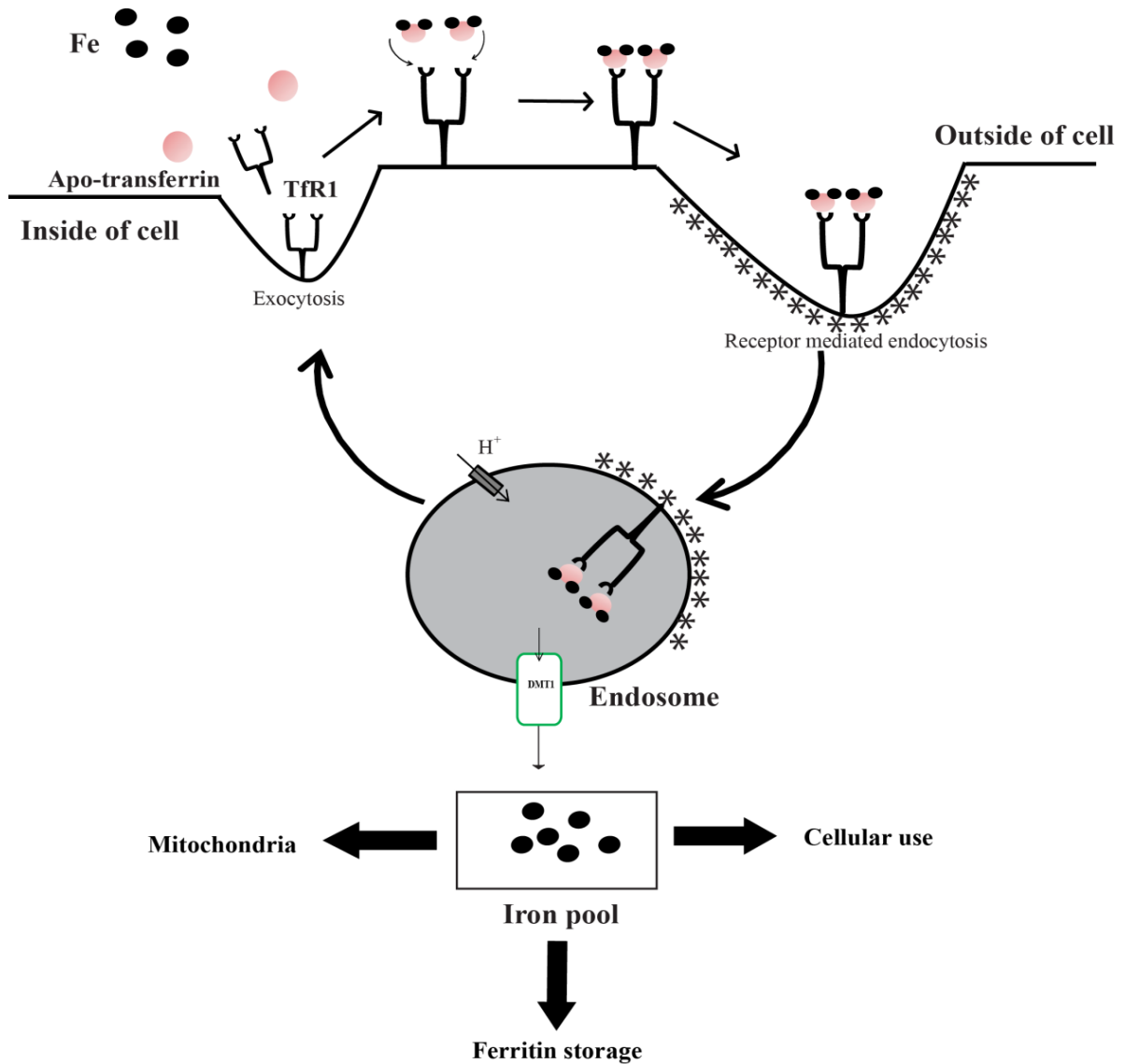


**Figure1.2 Schematic presentation of Transferrin-Transferrin receptor cycle.** Outside of cell apo-transferrin binds with iron to form diferric transferrin. Diferric transferrin bind to transferrin receptor present on the cell surface, followed by internalization via receptor-mediated endocytosis having special clathrin coat to form endosome. The endosome contains a proton pump which reduces the  $P^H$  (making acidic) and favors the iron release from transferrin receptor and diferric transferrin. The released iron transported via DMT 1. The transported iron allocated in the body for different functions.

Plasma transferrin saturation in human is normally about 30% saturated with iron; however, in certain pathologies, it varies. A transferrin saturation < 16% indicates iron deficiency and >45% saturation indicates iron-overload.<sup>3</sup> When the plasma transferrin iron saturation exceeds 60% non-transferrin bound iron (NTBI) starts to accumulate which is highly toxic.<sup>3</sup>

**Divalent metal transporter1 (DMT1):** Besides transferrin-bound iron, iron also transported into the cell via additional transports called divalent metal transporter1 (DMT1).<sup>24</sup> Divalent metal transporter1 also called as DCT1 or Nramp2 or SLC11A2 and predominantly expressed in duodenal enterocytes, kidney and less expressed in brain and in heart, beside divalent iron ( $\text{Fe}^{2+}$ ) it also transports various divalent metals such as  $\text{Mn}^{2+}$ ,  $\text{Cu}^{2+}$  and  $\text{Cd}^{2+}$ .<sup>25-27</sup> The intestine containing brush border cells transport iron from dietary sources via DMT1 with the help of Dcytb (duodenal cytochrome b, an intestinal ferrireductase which reduces ferric iron to ferrous iron) into enterocytes.

**Ferritin:** Free iron has redox chemical properties and produces free radical, if not properly regulated inside the cell, to prevent such deleterious effects cells evolved with iron sequestering and storage proteins called ferritin.<sup>1, 3, 4</sup> Ferritin is a ubiquitous multimeric protein made up of 24 subunits of heavy (H) and light (L) chains and forms a shell-like structure, and Ferritin molecule accommodates up to 4500  $\text{Fe}^{3+}$  ions in their cavity.<sup>28</sup> The ratio of H and L chains of ferritin varies based on tissue type pathological states (inflammation) and iron availability.<sup>1</sup> Ferritin contains enzymatic activity (inherent ferroxidase activity), which is largely confined to H sub-unit.<sup>1, 29</sup> Mitochondria also contain unique ferritin called mitochondrial ferritin, which consists

of a homodimer of H sub-units and plays an important role in mitochondrial iron homeostasis.<sup>29</sup>

***Feline leukemia virus type C receptor (FLVCR):*** It is a multi-transmembrane protein that exports heme iron.<sup>3, 30-32</sup> However, the physiological role of heme export is unclear, but FLVCR is highly essential for murine proerythroblast differentiation and macrophage iron recycling.<sup>31</sup> Mice with FLVCR deficiency develop severe hypochromic and microcytic anemia.<sup>1</sup> Excess heme is also detrimental to the cell and is catabolized by heme oxygenase.

***Ferroportin:*** The only putative iron exporter known is ferroportin (FPN), predominantly found in duodenal enterocytes, macrophages, hepatocytes, placental syncytiotrophoblast and cells of the central nervous system.<sup>1, 33</sup> It is also called an iron-regulated protein (IREG1) or metal transporter protein (MTP1), besides it is also called a solute carrier family 40 iron-regulated transporter.<sup>33-35</sup> Ferroportin is located at the basolateral surface of duodenal enterocytes and exports dietary absorbed iron into the blood stream and also associates with the ferroxidase enzyme called hephaestin.<sup>36</sup> Similarly, iron export from non-intestinal cells requires a unique exporter named ferroportin coupled with multicopper oxidase ceruloplasmin produced from the liver. Ceruloplasmin is homologous to hephaestin and ceruloplasmin deficiency leads to hepatocyte and macrophage iron accumulation which converts  $Fe^{2+}$  into  $Fe^{3+}$  before export.<sup>37</sup> Non-classical type-4 primary hemochromatosis occurs due to a mutation in the ferroportin exporter, which prevents hepcidin-induced ferroportin degradation process.<sup>38</sup>

### 1.2.2 Regulation of cellular iron metabolism:

Cellular iron metabolism is regulated post-transcriptionally by RNA binding proteins called iron regulatory proteins (IRPs). There are two different iron regulatory proteins such as iron regulatory protein1 (IRP1) and iron regulatory protein2 (IRP2).<sup>1, 39, 40</sup> These orthologous iron regulatory proteins bind to iron-responsive elements (IREs), having conserved hairpin loop structure located 3' and 5' untranslated regions (UTRs) of mRNA transcript.<sup>1</sup> A single hairpin loop structure IRE located at 5' UTR of several iron metabolic transcripts such as Ferritin L, Ferritin H, 5-aminolevulinic acid synthase2 (ALAS2) and hypoxia inducible factor 2 $\alpha$  etc.<sup>1, 3, 39, 40</sup> (**Figure 1.3 and 1.4**), however multiple IRE located at 3' UTR of transferrin receptor and DMT1 mRNA (**Figure 1.3 and 1.4**).<sup>1, 3, 39, 40</sup> During iron deficient state, IRPs are active and bind to IREs located 3' and 5' untranslated regions (UTRs) of mRNA transcript.

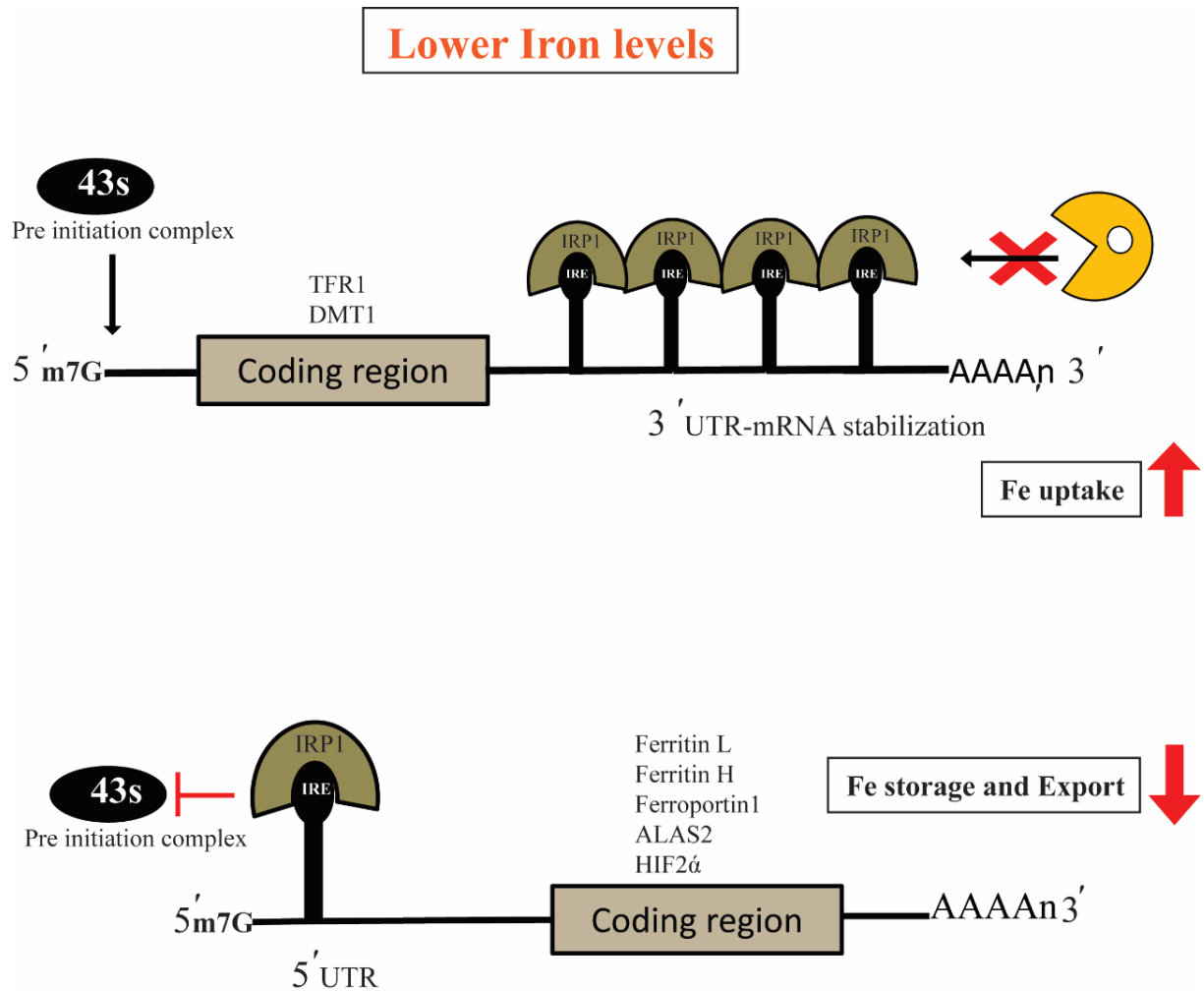


**Figure 1.3 IRE/IRP regulation of cellular iron metabolism during iron deficient state.** The binding of IRPs to IREs at 3' end during iron deficient state stabilizes the transcript and upregulates iron uptake protein levels (Tfr1, DMT1). Meanwhile, the binding of IRPs to IREs at 5' end during iron deficient state prevents the translation pre-initiation complex to bind 5' cap to initiate protein synthesis, so the iron storage and export protein levels will decrease. IRP= Iron regulatory protein; IRE=Iron regulatory element; UTR=Untranslated region.

IRE/IRP interactions at 3' UTR leads to stabilization of mRNA (TfR1, DMT1) and prevents its endonucleolytic cleave (**Figure 1.3**), results in increased iron uptake via TfR1 and DMT1.<sup>1, 3</sup> However, IRE/IRP interactions at 5' UTR results in inhibition of protein synthesis and decrease the production of ferritin L/H, ferroportin 5-aminolevulinic acid synthase2 (ALAS2) and hypoxia inducible factor 2 $\alpha$  etc. (**Figure 1.3**), Due to this the iron storage and export will decrease.<sup>1, 3</sup>

In the setting of high iron state, the IRPs become inactive and do not interact with IREs at 3' and 5'UTR of mRNA transcripts (**Figure 1.4**).<sup>1, 3</sup> During high iron rich environment IRP1 associate with Fe-S cluster to form cytosolic aconitase, beside this at high oxygen state the IRP1/2 undergoes ubiquitin-mediated proteolytic cleavage and degradation (**Figure 1.4**).<sup>1, 3</sup> Due to lack of IRPs, the 3' UTR containing IREs undergo endonucleolytic cleavage and degradation of transcripts (TfR1, DMT1).<sup>1, 3</sup> However, the 5' UTR containing IRE allows 43S preinitiation complex binding at 5' end and translation of ferritin L/H, ferroportin 5-aminolevulinic acid synthase2 (ALAS2) and hypoxia inducible factor 2 $\alpha$  etc. as a result the levels of the iron storage and export will increase as shown (**Figure 1.4**).<sup>1, 3</sup>

## High Iron levels

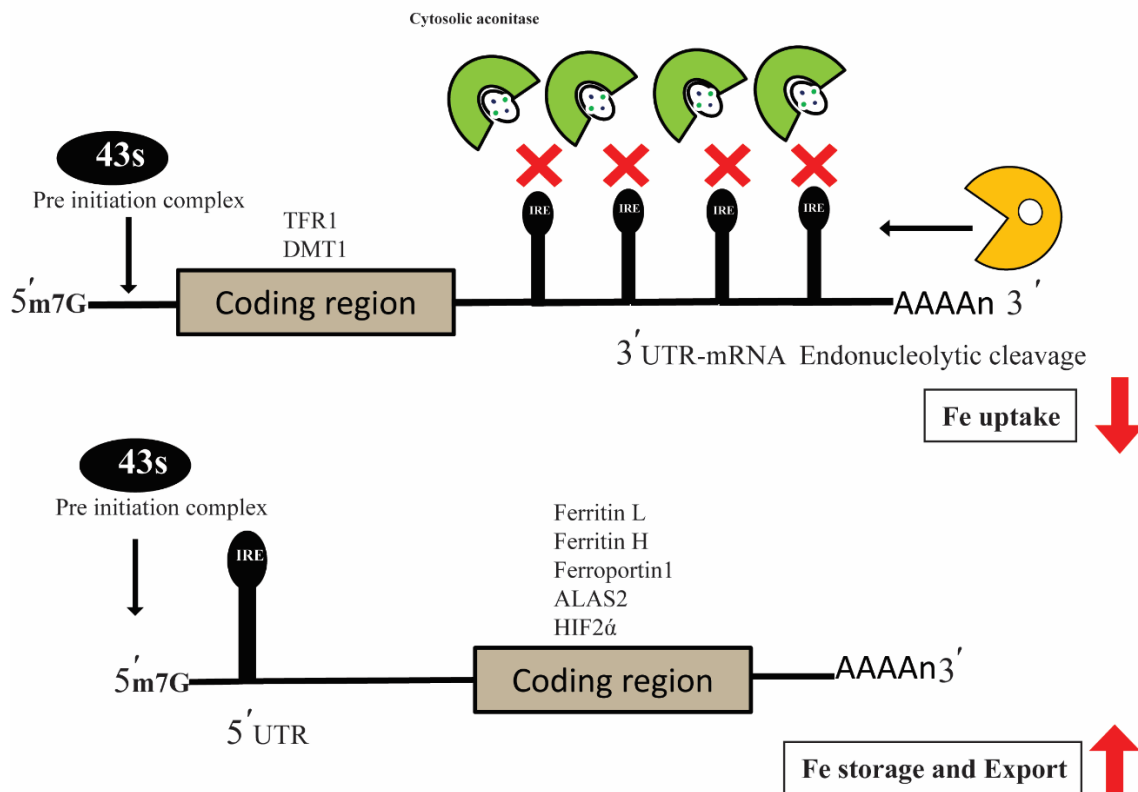
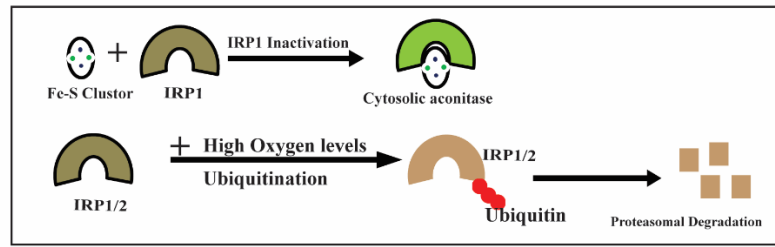


**Figure 1.4 IRE/IRP regulation of cellular iron metabolism during iron rich state.**

During iron repleted state IRPs associate with Fe-S cluster and function as cytosolic aconitase and lose the capacity to bind IREs at 3' end or 5' end. Due to this 3' UTR containing IREs undergoes nucleolytic degradation and no more iron uptake protein available. However, the 5' UTR containing IRE also fails to bind with IRPs which in turn favors the 43s pre-initiation complex binding and initiates translation of iron storage and export proteins. IRP= Iron regulatory protein; IRE=Iron regulatory element; UTR=Untranslated region; Fe-S cluster=Iron-Sulfur cluster

**1.2.3 Systemic iron metabolism:** Systemic regulators meticulously controls iron homeostasis throughout the body to prevent iron toxicity.<sup>1, 3</sup> Due to lack of an iron excretory mechanism in mammals, there must be effective communication between cells and organs to recycle and utilize the available iron.<sup>3</sup> Any loss of iron will be replaced by intestinal iron absorption from dietary sources.<sup>4</sup> The total body iron in adult male person is 3000 to 4000 mg and daily 20mg of iron required for erythropoiesis. Besides in the settings of hypoxia, inflammation, and infections the systemic iron homeostasis regulated differently.<sup>1</sup> Acute iron retention occurs during infections to prevent iron availability for microbial growth as part of host defense.

Hepcidin is a cysteine-rich key iron-regulatory peptide hormone plays an important role in systemic iron homeostasis.<sup>34, 41</sup> It belongs to defensin family member of innate immunity and hepatocytes are the major producers of hepcidin<sup>34, 41</sup> and it excreted through kidney cells.<sup>1</sup> Apart from hepatocytes, other cell types such as macrophages and adipocytes also express hepcidin.<sup>42, 43</sup> Excess iron up-regulates hepcidin expression, through hemojuvelin and bone morphogenetic protein signaling cascade.<sup>3</sup> Hepcidin is synthesized as an 84 amino acid prepropeptide, after proteolytic cleavage with furin generates the bioactive 25 amino acid hepcidin.<sup>3</sup> Hepcidin act as a central molecule in systemic iron homeostasis, by preventing excess iron entry from dietary sources and from reticuloendothelial macrophages. Hepcidin orchestrates iron levels in the body by targeting putative iron exporter called ferroportin. The mechanism of hepcidin action is to bind ferroportin, triggers its internalization, ubiquitination, and subsequent lysosomal degradation.<sup>34</sup> The regulation of hepcidin is very critical and

regulated by multiple factors such as systemic iron availability, hepatic iron stores, erythropoietic activity, hypoxia, inflammation, and infections.

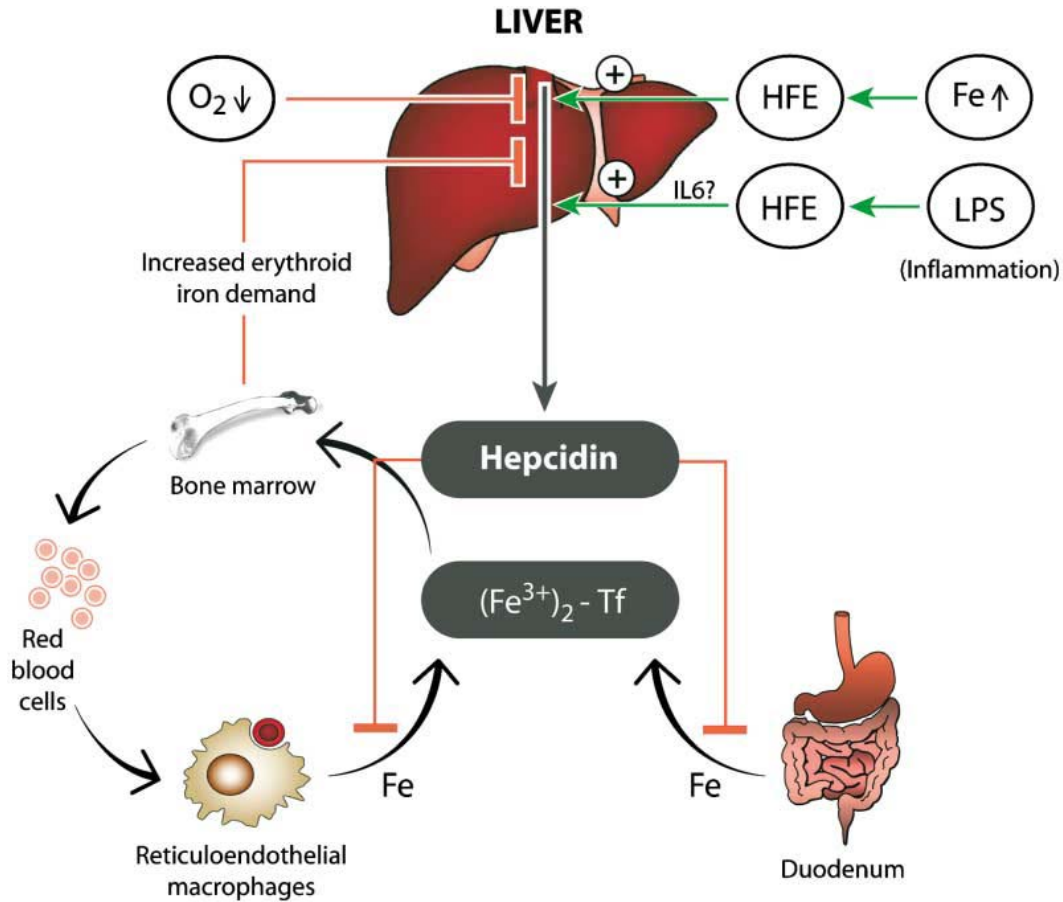


**Figure 1.5 Schematic presentation of systemic iron metabolism and its regulation.**

Hepcidin is a major iron hormone produced from liver controls systemic iron availability. It acts directly on ferroportin exporter present in reticuloendothelial macrophages and duodenal enterocytes and prevents systemic iron availability. Hepcidin also regulated systemic iron availability, infections, hypoxia and inflammation. HFE= High Fe; Fe=Iron; LPS=Lipopolysaccharide (Figure 1.5 is adapted from Fig 4. Balancing act: Molecular control of Mammalian iron metabolism)

### 1.3 Pathological conditions associated with iron-overload:

Uncontrolled gastrointestinal iron absorption from dietary sources and chronic blood transfusion leads excess iron accumulation in body and results into iron-overload. Iron-overload is a worldwide epidemic which has genetic as well as non-genetic causes. Iron-overload leads abnormal coloration of skin due to iron and in 1889 Von Recklinghausen observed this disease state named it as “hemochromatosis”.

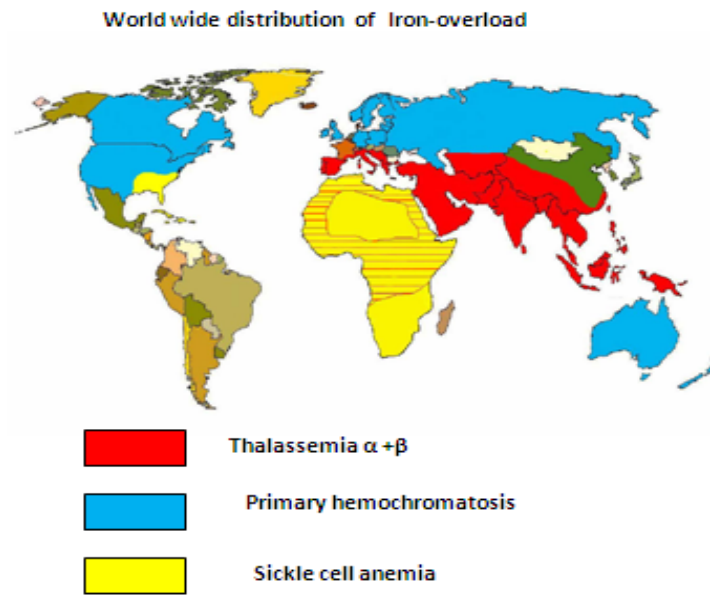


**Figure 1.6 Schematic presentation of worldwide distribution of Iron-overload diseases.** Prevalence of genetic and nongenetic iron-overload disease worldwide. Secondary iron-overload occurs due to hematological disorders such as  $\alpha, \beta$ -thalassemia, and sickle cell anemia distributed south-east Asian countries and in Africa respectively.  $\alpha, \beta$ -thalassemia represented in red colour and sickle cell anemia in yellow colour respectively. The hereditary hemochromatosis distributed Europe, Australia, and North America represented in blue colour.

**1.3.1 Primary hemochromatosis:** Increased gastrointestinal iron absorption leads to primary hemochromatosis which is an autosomal genetic disorder and also called as hereditary hemochromatosis.<sup>44, 45</sup> It is mostly found in Celtic descents (UK, Ireland

North Europe, and Australia), so it is also called as “Celtic disease. In primary hemochromatosis, the intestine absorbs too much of iron from the food due to abnormal iron metabolism.<sup>44, 45</sup> Based on the type of iron metabolic gene (HFE, HJV, TfR2, and FPN) mutated there are four different subtypes of primary hemochromatosis.

*a. Type-1 Primary hemochromatosis:* Classical type 1 primary hemochromatosis is an autosomal recessive disorder occurs due to Cys282Tyr (C282Y) and His63Asp (H63D) mutation in HFE (High Fe) gene located at chromosome 6.<sup>13, 44-47</sup> The C282Y mutations mostly limited to Northern European ancestry with allele frequency of about 10% and H63D mutation is limited to the Middle East and the Indian subcontinent with >5% allele frequency.<sup>44</sup> HFE, is a transmembrane protein with  $\beta$ -2 microglobulin domain belongs to class I-MHC family, abundantly found in liver and intestine and controls the gastrointestinal absorption by interact with other proteins on the cell surface to sense the amount of iron in the body via regulating hepcidin expression which is called as the master iron regulatory hormone.<sup>13, 48, 49</sup>

*b. Type-2 Primary hemochromatosis:* Also called as juvenile hemochromatosis and usually develops between ages of 15 to 30.<sup>3, 13, 50</sup> It shows an autosomal inheritance pattern and the gene involved in this type are HJV and HAMP gene, which encodes hemojuvelin and hepcidin protein respectively, which plays a central role in iron metabolism.<sup>50-52</sup> Hemojuvelin is a membrane bound protein and in humans, HJV is called as HFE2 gene or RGMc (Repulsive and Guidance Molecules).<sup>50, 52, 53</sup> HJV act as a bone morphogenetic protein co-receptor and regulate the expression of hepcidin and mutation in HJV produces decreased or inactivation of hepcidin production. Type 2 primary hemochromatosis is of two types, such as –Type 2A primary hemochromatosis

in which HJV is mutated and Type2B primary hemochromatosis in which hepcidin (HAMP) is mutated.

*c. Type-3 Primary hemochromatosis:* It is the non-classical type with an autosomal recessive hemochromatosis, occurs due to the mutations in the transferrin receptor2 (TfR2).<sup>14</sup> Transferrin Receptor 2 (TfR2) expressions are restricted to hepatocytes, duodenum, and erythroid precursors.<sup>7, 11, 12</sup> TfR1 and TfR2 receptors are expressed in hepatocytes of liver and enterocytes of the small intestine, especially in the duodenum. In Type 3 primary Iron-overload the TfR2 is mutated, and the major function of TfR2 is to sense the iron levels and regulate hepatic hepcidin secretion.<sup>13, 14</sup>

*d. Type-4 Primary hemochromatosis:* It is an autosomal dominant, non-classical type 4 primary hemochromatosis occurs due to a mutation in ferroportin, also called as Ferroportin disease<sup>13, 34, 38</sup>. Ferroportin also called as solute carrier family 40 iron-regulated transporter and regulated by hepcidin<sup>34</sup>, a specific mechanism called hepcidin-induced clathrin-mediated ferroportin internalization and ubiquitin-mediated degradation<sup>34, 38</sup>. Mutations in ferroportin at Y302F and K253A are resistant to clathrin-mediated ferroportin internalization and ubiquitin-mediated degradation respectively. In type 4 primary hemochromatosis ferroportin is mutated and this prevents resistant to internalization and ubiquitination of ferroportin by hepcidin results excess iron export. It was documented that Tyrosine (Tyr) amino acid phosphorylation at position 302 is very critical for internalization and mutation of this amino acid prevents internalization and a good example of such mutation is FerroportinY302F. Lysine (K) at position 253 required for efficient ferroportin degradation, and mutation at this amino acid position

may prevent ubiquitination and a good example of such mutation is ferroportin K253A mutants.<sup>13, 34, 38</sup>

**1.3.2 Secondary iron-overload:** Secondary iron-overload is acquired in nature and occurs due to repeated blood transfusions in the settings of ineffective erythropoietic activity and excess iron exposure. Typically patients with hemoglobinopathies (sickle cell disease, Thalassemia, sideroblastic anemias), congenital hemolytic anemias, myelodysplasia are associated with secondary iron-overload conditions.<sup>54-57</sup> Defective  $\alpha$ - and  $\beta$ -globin chains of hemoglobin exhibits ineffective erythropoiesis, which is the most common monogenetic disease in human and predominantly confined to Mediterranean region, Africa, Middle East, Indian subcontinent and South East Asia with estimated gene frequency of 3 to 10% but certain population has high as 30 to 40%.<sup>4, 7, 54-56</sup> Sickle cell anemia or sickle cell disease also another most common hematological disorder found in African ancestry due to presence of sickle hemoglobin (HbS). Survival of these patients (Thalassemia and Sickle cell anemia) requires repeated blood transfusion and this result into severe iron-overload. Besides thalassemia and Sickle cell disease (SCD) several other clinical pathologies associated with secondary iron-overload including myelodysplastic syndrome, sideroblastic anemia, acute myeloid leukemia, chronic renal failure and congenital dyserythropoietic anemia etc.

## 1.1 Table Diseases associated with iron-overload

Type	Inheritance	Affected organs	Molecular cause	Study
<b>Primary hemochromatosis</b>				
Type-1 Primary hemochromatosis	AR	Liver, Heart, Endocrine Glands	<i>HFE</i> C282Y; H63D	13, 44, 48
Type-2 Primary hemochromatosis ( <i>Juvenile hemochromatosis</i> )	AR	Liver, Heart, Endocrine Glands	<i>HJV</i> (hemojuvelin); subtype A <i>HAMP</i> (hepcidin); subtype B	3, 50, 53
Type-3 Primary hemochromatosis	AR	Liver, Heart, Endocrine Glands	<i>TfR2</i>	11, 12, 14
Type-4 Primary hemochromatosis	AD	Liver, Heart, Endocrine Glands, Macrophages	<i>FPN</i> (Ferroportin)	13, 34, 38
<b>Secondary Iron-overload</b>				
$\alpha$ -Thalassemia	AR	Liver, Heart, Pancreases, Pituitary gland	Decreased synthesis of $\alpha$ -globin chains	58, 59
$\beta$ -Thalassemia	AD	Liver, Heart, Pancreases, Pituitary gland	Decreased synthesis of $\beta$ -globin chains	54, 60, 61
SCD	AR/AD	Liver, Heart	Glu $\rightarrow$ Val $\beta$ -Globin gene	62-64
Sideroblastic Anemia	X-Linked AD/AR	Neurons, Heart, Mitochondria	Decreased synthesis of Heme	65, 66
CDA	AR (Type I) AD (Type II)	Liver, Heart, Endocrine Glands	Ineffective erythropoiesis	67
CRF	Acquired (Polygenic)		Oral and intravenous iron supplements	68, 69

AR= Autosomal Recessive; AD= Autosomal Dominant; HFE= High Fe, a major atypical class I Major histocompatibility protein family, heterodimerizes with  $\beta_2$ -Microglobulin, senses the iron levels and modulates hepcidin expression; HJV= Hemojuvelin, a bone morphogenetic protein co-receptor required for hepcidin expression; HAMP= Heparin binding EGF-like protein, master regulator of iron absorption from dietary sources; TfR2= Transferrin receptor 2; FPN=Ferroportin a major iron exporter; SCD=Sickle cell disease; Glu=Glutamic acid; Val= Valine; CDA=congenital dyserythropoietic anemia; CRF= Chronic renal failure; \*= Genes are indicated in italic fonts.

## **1.4 Iron-overload Cardiomyopathy.**

Cardiomyopathies represent a heterogeneous group of heart diseases, divided into primary (genetic, acquired or mixed) or secondary (infiltrative, toxic or inflammatory) origin, and literally, cardiomyopathy means heart muscle disease.<sup>70, 71</sup> Excess accumulation of iron in heart muscle leads to iron-overload cardiomyopathy; it could be due to genetic hemochromatosis or transfusional iron-overload, represents a growing clinical burden on an international scale.<sup>4, 46, 70, 72-76</sup>

### **1.4.1 Clinical description of iron-overload cardiomyopathy.**

Iron-overload cardiomyopathy is a newly recognized secondary form of cardiomyopathy and is often overlooked by cardiovascular specialists. Iron-overload cardiomyopathy is associated with excess accumulation of iron in cardiac muscle and a common cause of death worldwide with higher morbidity and mortality.<sup>75, 76</sup> Regardless of its origin, it is restrictive with prominent early diastolic dysfunction and as the disease progresses it leads to an end-stage dilated cardiomyopathy.<sup>72, 73, 75, 77</sup>

### **1.4.2 Pathophysiology of iron-overload cardiomyopathy.**

Iron absorption and transport are tightly regulated process to prevent iron-induced tissue damage and oxidative stress during iron-overload.<sup>1, 4</sup> Under physiological conditions iron is stored and transported into cardiomyocytes with the help of traditional iron transporters,<sup>1, 4</sup> however during iron-overloaded conditions, transferrin becomes saturated, which results in free iron accumulation called non-transferrin bound iron (NTBI).<sup>78</sup> The existence of NTBI during iron-overloaded condition was reported by Hershko *et.al*<sup>79</sup> This form of iron represents a significant fraction of iron which

transported through L/T-Type  $\text{Ca}^{2+}$  channels into cardiomyocytes and results cardiac iron-overload.<sup>77, 80, 81</sup> Cardiac iron-overload is a gradual process and gradual accumulation of non-transferrin bound iron is fatal. NTBI is toxic and highly reactive and readily available for Fenton-type reactions results in reactive oxygen species formation.<sup>78, 82</sup> In the absence of iron-overload, formation and toxic effects of free radicals is minimized by intrinsic anti-oxidant (enzymatic and non-enzymatic) systems<sup>4, 74, 77, 82, 83</sup>. When transferrin saturated with iron; excess free iron enters into body under some disease condition such as high intestinal iron absorption, repeated blood transfusions etc.<sup>84</sup>

NTBI is the major contributor to ROS-mediated myocardial oxidative stress.<sup>82, 84</sup> When NTBI elevated in cardiomyocytes leads free radical formation via Fenton-type reactions and excessive free radical generation leads to increased cellular damage includes-lipid peroxidation, DNA damage, protein modification and depletion of antioxidant reserves (**Figure 1.7**) etc.<sup>82, 85-87</sup> Increased accumulation of lipid peroxidation products (unsaturated-Malondialdehyde, hydroxyneononal and saturated-hexanal) combined with decreased antioxidant levels triggers loss of myocardial cellular integrity and cytotoxic reactions.<sup>88-90</sup> The accumulated lipid peroxidation aldehydes have adverse effects on numerous sub-cellular compartments such as lysosomes, Golgi complexes, mitochondria, and endoplasmic reticulum etc.<sup>87, 88</sup>

Iron induced free radical formation and oxidative stress has been well documented in several animal models as well as patients with genetic hemochromatosis, secondary iron-overload and chronic kidney disease.<sup>77, 83-86, 91</sup>

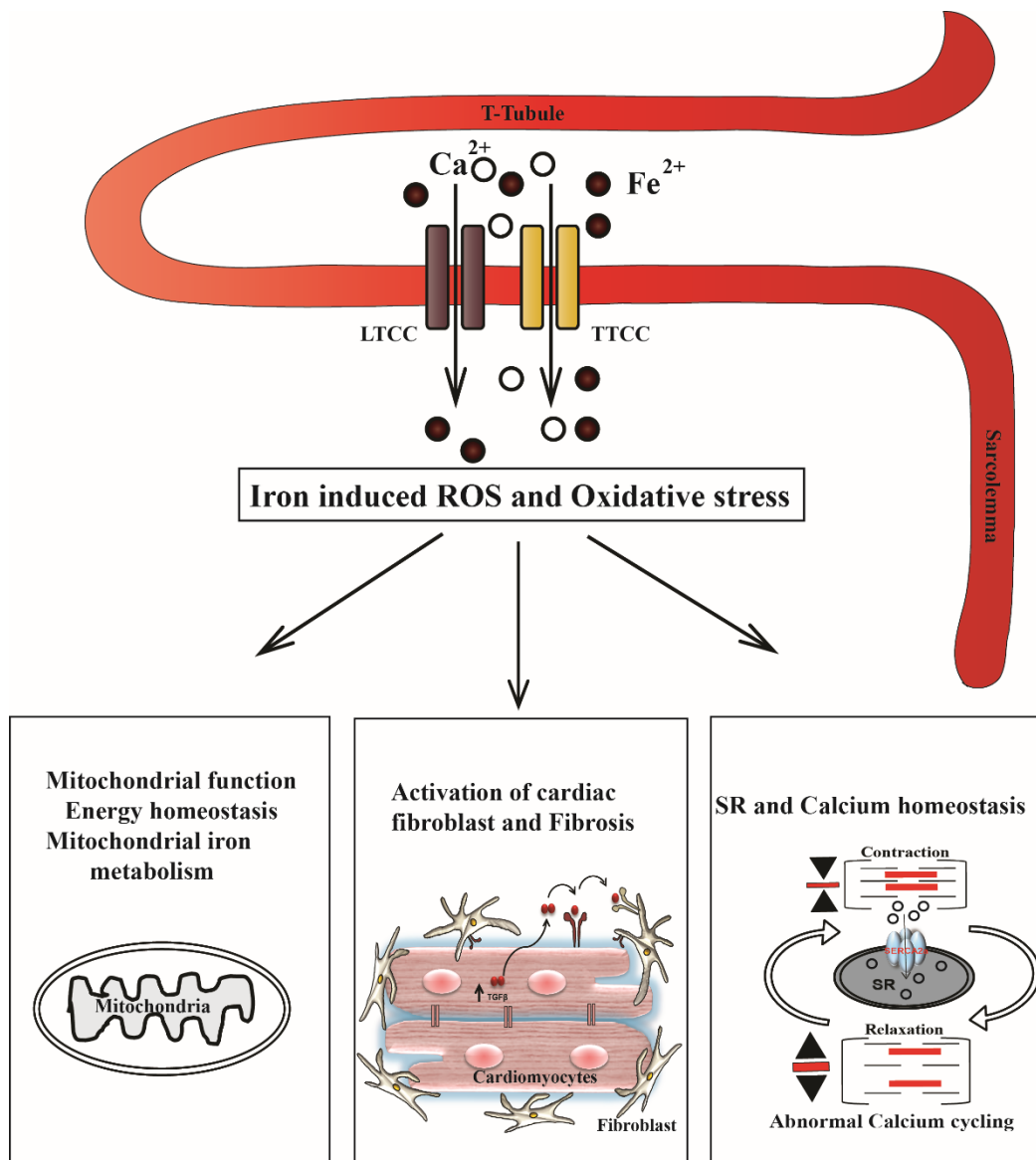


**Figure 1.7 Schematic presentation of Pathophysiology of iron-overload cardiomyopathy** During iron-overloaded condition, iron enters into cardiomyocytes through L/T-Type calcium channels. Inside cardiomyocyte non-transferrin bound iron accumulate and cause ROS formation and oxidative stress. Cardiac iron-overload leads altered calcium cycling and defective SERCA2a, fibroblast activation and myocardial fibrosis and abnormal mitochondrial function. LTCC= L-Type calcium channel; TTCC=T-Type calcium channel; ROS=Reactive oxygen species; SR= Sarcoplasmic reticulum; SERCA2a= Sarco-endoplasmic reticulum calcium ATPase.

In patients with hereditary primary hemochromatosis, manganese-superoxide dismutase (MnSOD) genotype affects the risk of developing iron-overload cardiomyopathy.<sup>92</sup> Iron induced oxidative stress is the key driver in the pathogenesis of iron-overload

cardiomyopathy, which might explain the beneficial effects of antioxidant therapy.<sup>83, 91,</sup>  
<sup>93</sup> Iron-overload cardiomyopathy also associated with abnormal mitochondrial function with mitochondrial iron-overload as seen in Friedreich's ataxia.<sup>82, 93-97</sup>

### **1.4.3 Role of gender in the pathogenesis of iron-overload cardiomyopathy.**

A Large number of reports in the literature showing sex-related differences in cardiovascular function exist in experimental animals and in humans, however, gender based differences in cardiac iron metabolism and cardiovascular function yet to determine. Many lines of evidence showed that males are highly susceptible to excess iron and cardiovascular diseases than females. Female iron-overload patients showed better survival, low frequency of heart failure and better clinical outcomes. The prevalence of iron overload mediated injury and clinical outcomes in female sex are better than male, it was reported that  $\beta$ -thalassemia female patients showed better clinical outcomes than  $\beta$ -thalassemia male patients that receive blood transfusions.<sup>98</sup> It was documented that sex steroids modulate iron metabolism at multiple levels (**Figure 1.8**). The gender-related difference does exist in the pathophysiology of cardiac diseases and sex-specific pathways play a key role in the cardioprotection observed in cardiomyopathies and heart failure in pre-clinical models and patients.<sup>99, 100</sup> The cardioprotective role of estrogen reported, functional estrogen receptors (ERs  $\alpha$  and  $\beta$ ) expressed in the myocardium.<sup>101, 102</sup>

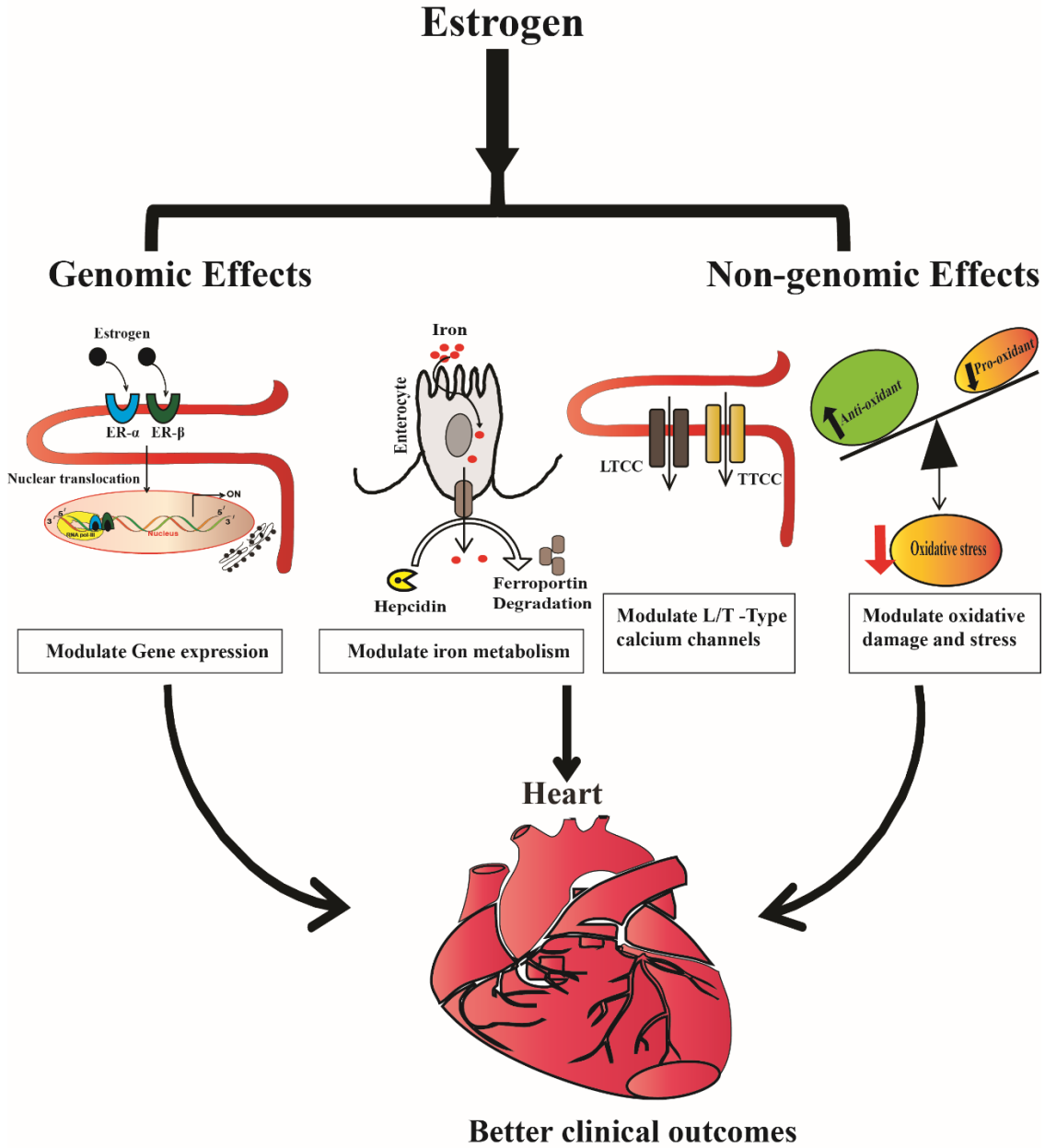


**Figure 1.8 Schematic presentation of estrogen effects in heart.** Genomic and non-genomic effects of estrogen. Genomic effects showed estrogen binds to ERs present on the cell membrane and this complex translocate into the nucleus, triggers activation of genes having ERE at their promotor regions. Estrogen also exerts multiple non-genomic effects, modulate iron metabolism via regulating hepcidin expression, a major iron hormone produced by the liver and it acts directly on ferroportin exporter present in duodenal enterocytes and prevents systemic iron availability, besides hepcidin also exerts antioxidant effects and prevents oxidative stress. ER= Estrogen receptor; LTCC=L-Type  $\text{Ca}^{2+}$  channels; TTCC=T-Type  $\text{Ca}^{2+}$  channels.

Estrogen exerts genomic and non-genomic effects.<sup>99, 103, 104</sup> Estrogen has several beneficial pleiotropic effects on the cardiovascular system. Estrogen receptors (ERs  $\alpha$  and  $\beta$ ) function as ligand-activated transcription factors and upon binding with estrogen translocate into nucleus and activate transcription of genes that have estrogen responsive elements (ERE), beside this estrogen also exert several non-genomic effects (**Figure 1.8**), includes modulation of L-Type  $\text{Ca}^{2+}$  channels and  $\text{Ca}^{2+}$  current, act acts as an antioxidant and prevent oxidative stress and also modulate iron absorption by regulating iron metabolic genes (hepcidin).

In addition, lack of estrogen leads to adverse pathophysiological cardiac remodeling and precipitates heart failure. Gender-related disparities in the regulation of iron metabolism may contribute to the differences in progression of iron-overload heart disease.

### **1.5 Hepatic iron-overload diseases:**

Abnormal iron metabolism associated with either iron-overload or iron deficiency.<sup>1, 3, 4, 7</sup> Liver diseases are prevalent with abnormal iron-overload, which has genetic and non-genetic causes.<sup>105</sup> Abnormal iron metabolism and hepatic iron-overload is a major cause of liver injury and in the development of chronic liver diseases. Iron-overload mediated liver disease leads to end-stage cirrhosis and/or hepatocellular carcinoma.<sup>105-108</sup> Body iron stores have a significant relationship with liver and liver is the main source of production of hepcidin, an iron regulatory hormone, and transferrin which keeps and transports iron without any toxic side effects.<sup>105</sup> Liver hepatocytes store the significantly large amount of iron in a safe and non-toxic form, however, liver

hepatocytes tightly regulate iron homeostasis by producing an iron regulatory hormone called hepcidin. Genetic loss of hepcidin or hemojuvelin, ferroportin or Transferrin receptors leads excess gastrointestinal iron absorption and hepatic iron-overload particularly with genetic hemochromatosis, secondary iron-overload and alcohol-related liver diseases.

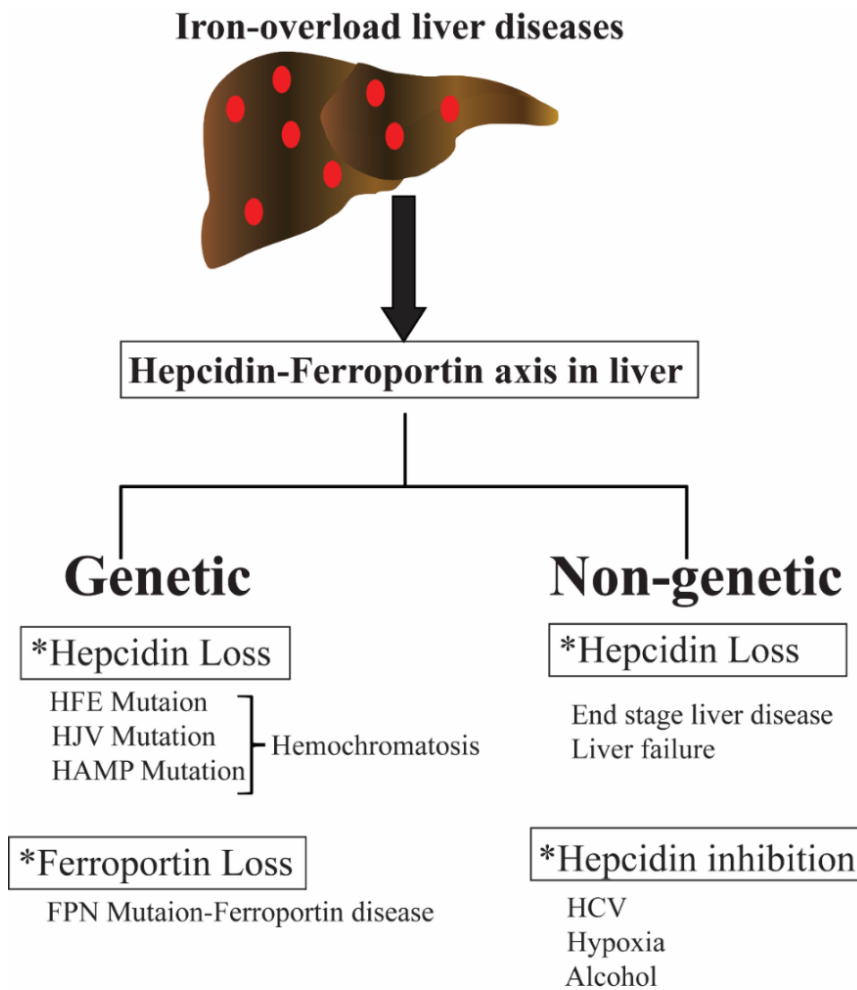


**Figure 1.9 Schematic presentation of Pathophysiology of iron-overload liver diseases.** Abnormal hepcidin-ferroportin axis leads iron-overload liver diseases. Hepcidin is a major iron hormone produced from liver and it acts directly on ferroportin exporter present in reticuloendothelial macrophages and duodenal enterocytes controls. Hepcidin loss or inhibition and

ferroportin loss associated with many genetic and non-genetic iron-overload liver diseases. HFE= High Fe; HAMP=Hepcidin gene; HJV=Hemojuvelin; FPN=Ferroportin

**1.6 Iron-induced oxidative stress:** Iron induced oxidative stress plays a fundamental role in the pathogenesis of iron-overload cardiomyopathy. Iron-overload in heart is a gradual process associated with accumulation of iron, transferrin saturation and non-transferrin bound iron formation. Under physiological conditions iron is stored and transported by a specific iron transporter called Transferrin into blood compartments, besides the effect of free radicals is minimized by a number of cellular enzymatic and non-enzymatic antioxidant systems.

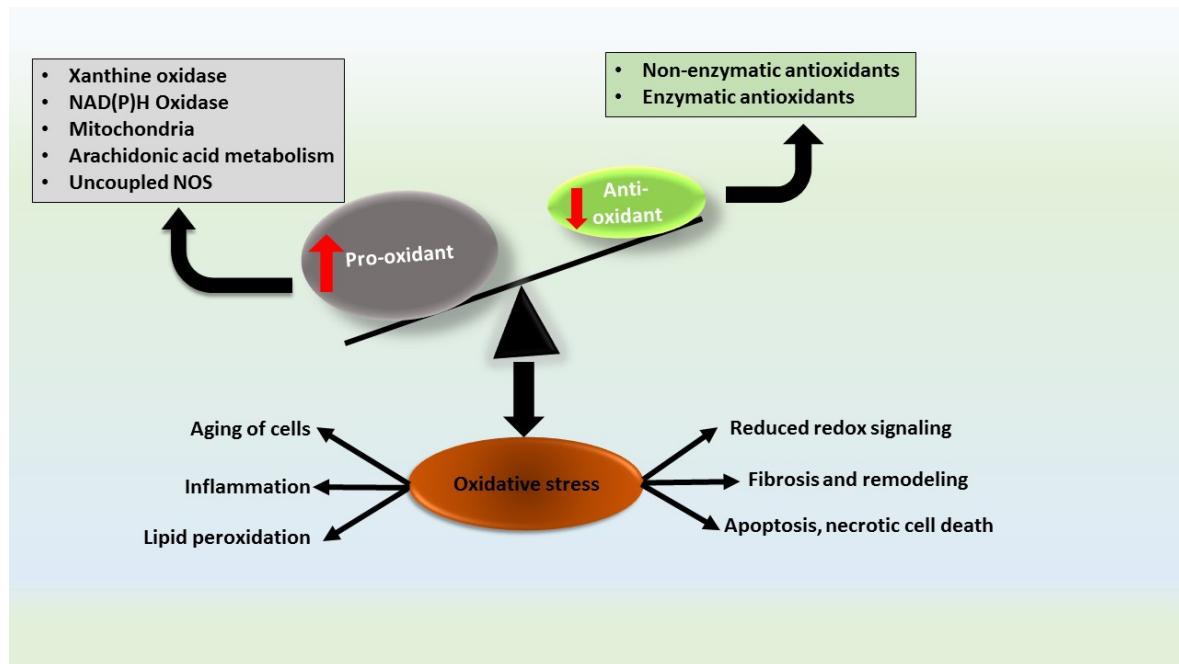
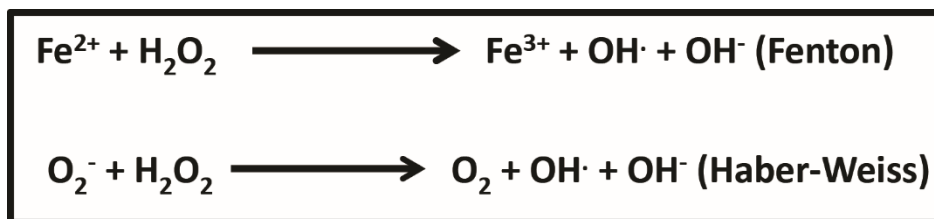


**Figure 1.10 Schematic presentation of oxidative stress and consequences.** During oxidative stress, the level of pro-oxidants raises and level of antioxidants goes down, and this imbalance is called oxidative stress. During a normal state, the effects of pro-oxidants are neutralized by inherent enzymatic and non-enzymatic antioxidants, however during iron induced oxidative stress, the levels of pro-oxidants raises and levels of antioxidants depleted results reduced redox signaling, cardiac remodeling, myocardial fibrosis, and lipid peroxidation.

**1.6.1 Pro-oxidants:** Oxidative stress represents a pathological state at which excess accumulation of pro-oxidants (reactive oxygen/nitrogen species) relative to antioxidants (intrinsic enzymatic and non-enzymatic) <sup>109, 110</sup> Pro-oxidants are the free radicals which have one or more unpaired electron in their outermost orbit, due to this they are chemically reactive in nature. The pro-oxidants majorly involve in cellular damage via lipid peroxidation, DNA damage, protein oxidation, cell death and necrosis. Major pro-oxidants are the reactive oxygen species (ROS) and reactive nitrogen species (RNS) and they play a potential detrimental role in the pathogenesis of oxidative stress, cardiac remodeling and heart failure (**Figure 2.0**).<sup>111</sup> ROS can be generated from different sub-cellular sources (**Figure 2.0**) and mitochondrial electron transport system (ETS) is the primary source of ROS beside this xanthine oxidase, NADPH oxidase, nitric oxidase synthase, arachidonic acid metabolism and autooxidation of catecholamines also generate ROS.<sup>109, 112-115</sup> Superoxide anion ( $O_2^{\cdot-}$ ), hydroxyl radical ( $\cdot OH$ ) and hydrogen peroxide ( $H_2O_2$ ) are highly unstable chemical species considered as reactive oxygen species (ROS). The hydroxyl radical is the most potent ROS which is generated following biochemical reactions: The Fenton reaction and the Haber-Weiss reaction as shown below.



In Fenton reaction,  $H_2O_2$  breakdown occurs by accepting an electron from metal ions such as ferrous iron ( $Fe^{2+}$ ). In the Haber-Weiss reaction, hydroxyl radical ( $\cdot OH$ ) is

formed from Superoxide anion ( $O_2^-$ ) and hydrogen peroxide ( $H_2O_2$ ). Metal ions such as iron play a key role in the formation of ROS via Fenton and Haber-Weiss reaction.<sup>113</sup> It was documented that approximately 5% of the total oxygen in the body during metabolism produce partially reduced oxygen species. Mitochondria produce ROS through a one electron transport to molecular  $O_2$  in the respiratory chain.<sup>116</sup> Heart consist a lot of mitochondria and under physiological condition and a small quantity of ROS generated, which is detoxified by intrinsic antioxidant systems, however, mitochondria from failing hearts produce more ROS with decreased mitochondrial complex activities .<sup>116</sup> Therefore mitochondrion is the main source of ROS in failing heart, and linking mitochondrial dysfunction and oxidative stress.<sup>117</sup>

**1.6.2 Antioxidants:** In order to prevent the cellular damage by pro-oxidants, cells associated with an inherent antioxidant defense system.<sup>118</sup> Antioxidants exert their effect through several mechanisms. In primary defense mechanism, the anti-oxidant compounds transforming the reactive pro-oxidants into less reactive compounds, whereas in secondary defense mechanism, the anti-oxidants trap or scavenge the harmful radicals.<sup>118-120</sup>

**1.6.2.1 Enzymatic antioxidants:** Endogenous enzymes play a central role in the primary defense mechanism to prevent cellular damage. Following antioxidant enzymes involved.

*a. Superoxide dismutase (SOD).* This enzyme represents the first line of defense against oxidative damage. SOD is responsible for converting superoxide radicals ( $O_2^-$ ) into cell reactive hydrogen peroxide ( $H_2O_2$ ).<sup>113</sup> There are three different types of SOD;

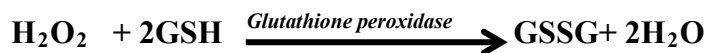
Manganese SOD (MnSOD or SOD2) present in the mitochondria, Copper-Zinc SOD (CuZnSOD or SOD1), present in the cytoplasm and Extra Cellular SOD (ECSOD) present in the extracellular matrix. The lack or inactivation of MnSOD results dilated cardiomyopathy and neonatal lethality.<sup>121</sup>



**b. Catalase (CAT).** The primary defense against hydrogen peroxide (H<sub>2</sub>O<sub>2</sub>) is mediated by the enzyme Catalase, which converts toxic hydrogen peroxide (H<sub>2</sub>O<sub>2</sub>) into the water and molecular oxygen.



**c. Glutathione peroxide (Gpx).** It is an important selenodependent enzyme abundantly present in the heart. Gpx catalyzes the reduction of hydrogen peroxide (H<sub>2</sub>O<sub>2</sub>) glutathione (GSH) dependent manner into glutathione disulfide (GSSG) and water. There are four isoforms of glutathione peroxidase enzyme.



**d. Glutathione Reductase.** The glutathione disulfide (GSSG) reduced back to glutathione with the help of glutathione reductase enzyme.



**e. Heme oxygenase.** A cytoprotective enzyme that degrades heme, excess accumulation of heme is toxic and heme is a potent pro-oxidant. Heme oxygenase has

two isoforms hemeoxygenase-1 (HO-1) and heme oxygenase-2 (HO-2).<sup>122-124</sup> Heme oxygenase is responsible for heme degradation into biliverdin, iron and carbon monoxide.<sup>125</sup> Heme oxygen-1 a 32kDa protein and is abundantly found in spleen, liver, and bone marrow<sup>124, 123</sup>, however, heme oxygen-2 a 36kDa protein and is highly expressed in testes, brain, endothelial cells and smooth muscle cells.<sup>123, 126</sup>

### **1.6.2.2 Non-enzymatic antioxidants:**

*a. Glutathione.* Glutathione tripeptide (glutamyl-cysteinyl-glycine) is an abundant cellular antioxidant produced in all kind of cells.<sup>127, 128</sup> Biochemically glutathione consists of three amino acids- cysteine, glycine, and glutamate.<sup>128</sup> Liver has a large amount of glutathione, which allows it to be a suitable detoxifying organ and consider as a reservoir of GSH. Glutathione is an essential component of bodies natural defense to prevent oxidative stress.<sup>129, 130</sup> Besides liver it also found in the heart to prevent oxidative damage. Reduced glutathione (GSH) contains a sulfhydryl (SH) group which allows it as a strong electron donor. It donates electron during oxidative stress to ROS and become oxidized, and two such oxidized molecules combine to form glutathione disulfide (GSSG) or oxidized glutathione.<sup>131</sup> GSH is an extremely important defense protein present in every cell to prevent oxidative damage.<sup>130</sup> It directly quenches reactive hydroxyl free radicals, other oxygen-centered free radicals.<sup>130</sup> GSH is a primary protectant of skin, lens, cornea, and retina against radiation damage and other biochemical foundations of P450 detoxification in the liver, kidneys, lungs, intestinal epithelia and other organs.<sup>130, 132 133, 134</sup>

GSH is synthesized by two closed linked enzymes that utilize ATP. First, L-cysteine and L-glutamate are combined by an enzyme called gamma-glutamyl cysteinyl synthetase. Second, GSH synthetase combines gamma-glutamylcysteine with glycine to form GSH. Fasting, malnutrition of proteins, or other dietary amino acid deficiencies limit GSH synthesis. Glutathione depletion has been linked with a number of diseases of oxidative stress. In the heart, 95% of glutathione exist in reduced form (GHS) and it undergoes redox cycling between reduced to oxidized and the redox ratio is a sensitive indicator of oxidative stress.<sup>129, 135</sup> A family of enzymes-glutathione reductase, glutathione peroxidase, and glutathione S-transferase use GSH as a co-factor.<sup>131</sup> Higher-order thiol cell systems, such as the metallothioneins (MT1 and MT2), thioredoxins and other redox regulator proteins are ultimately regulated by cellular GSH levels and the redox ratio.<sup>136</sup>

**b. Thioredoxin system.** A ubiquitous thiol containing redox regulating protein system and plays an important role in cellular processes. Thioredoxin system consists of three components named thioredoxin and (Trx), thioredoxin reductase (TrxR) and NADPH respectively.<sup>137</sup> Thioredoxins are ubiquitous proteins with oxidoreductase activity found in eukaryotic and prokaryotic systems.<sup>138</sup> Three different types of thioredoxin proteins named thioredoxin-1 (Trx1), thioredoxin-2 (Trx2) and spermatozoa thioredoxin (SpTrx1) present in cytosolic, mitochondrial compartments and spermatozoa respectively.<sup>137, 139-141</sup> Thioredoxin contains a conserved active site (Cys-Gly-Pro-Cys) as a redox center.

Thioredoxin exerts most of its antioxidant properties through thioredoxin peroxidase, which uses SH groups as reducing equivalents.

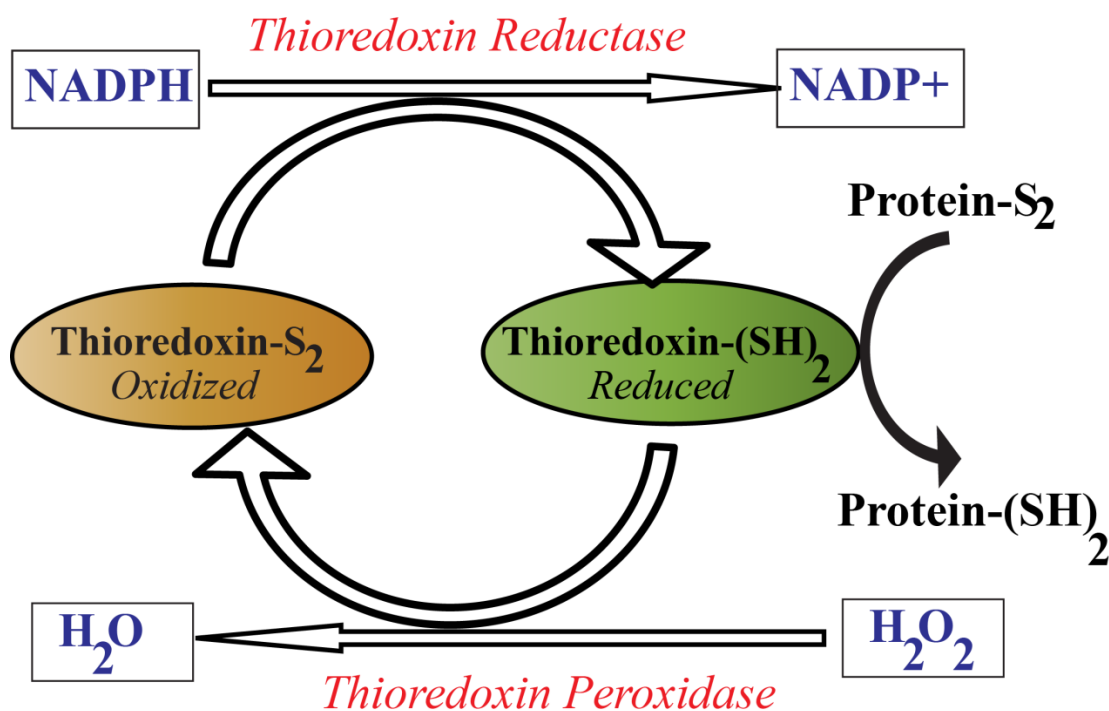


**Figure 1.11 Schematic presentation of thioredoxin system.** During oxidative stress, the level of pro-oxidants raises. Thioredoxin system prevents protein oxidation.

Thioredoxin system protects cell with multiple ways, Ejima *et al* reported that estrogen exerts its antioxidants effects to prevent H<sub>2</sub>O<sub>2</sub> toxicity via thioredoxin system.<sup>137, 142</sup> Das *et al* found that in lung endothelial cells the activation of Manganese superoxide dismutase (Mn-SOD) requires thioredoxin.<sup>143</sup> Thioredoxin also ubiquitously expressed in vascular smooth muscle cells (VSMCs),<sup>144</sup> however the regulation of thioredoxin is not by ROS instead regulated by H<sub>2</sub>O<sub>2</sub>, HO-1 and platelet-derived growth factor (PDGF).<sup>145</sup> Glutaredoxins (GRX) are glutathione incorporated thioredoxins. These are also a member of a family of thiol-disulfide oxidoreductases is a ubiquitously expressed small cytosolic protein that modulates redox states in a cell-specific manner.

## 1.7 Current therapies:

Iron-overload leads progressive iron accumulation in different body parts, early diagnosis and treatment should be required to prevent iron accumulation and end organ failure.<sup>74</sup> The current mainstay therapies for iron-overload patients were periodic manual whole blood phlebotomies and iron chelation therapy respectively.<sup>146, 147</sup> Erythrocytapheresis or red cell apheresis is also an alternative treatment method available,<sup>148-150</sup> which removes total body iron contents. Regular phlebotomies are considered to be the treatment of choice, due to simple, cheap and safe strategy to remove excess iron.<sup>151</sup> Phlebotomy therapy consists 3 phases. Initiated with induction phase, in which the 500cc blood removed weekly until the transferrin saturation value fallen below <50%. Followed by transition phase in which the iron levels dramatically reduced and the frequency of phlebotomies may change from once per weekly to once per monthly. During this phase body reached to a healthy iron range and last phase is the maintenance phase, in which the iron levels reach to satisfactory and healthy level. Phlebotomy procedure can reverse the cardiac dysfunction with iron-overload cardiomyopathy in hereditary hemochromatosis patients. Unfortunately, the genetic hemochromatosis patients are often diagnosed and treated only in an advanced state of iron-overload. Phlebotomy therapy is a slower procedure which may result in iron-induced severe oxidative stress which also needs close attention, besides repeated phlebotomies also associated with discomfort and lack of compatibility.

In patients with secondary iron-overload, iron chelation therapy is the standard therapy.<sup>54, 152, 153</sup> There are different kinds of iron chelators available such as oral iron chelators (deferiprone and deferasirox) and parenteral iron chelators (deferoxamine)

respectively. Chelation therapy has been shown to improved cardiac function in iron-overload patients without any arrhythmias.<sup>54, 152, 154, 155</sup> It was noticed that iron chelators effectively remove iron from different body parts and rapidly normalizes the serum iron levels and hepatic iron levels, while leaving myocardial iron content elevated because of the slower rate of clearance, which may increase the risk of severe oxidative stress and iron-overload cardiomyopathy.<sup>156</sup> However chelation therapies reduce the iron-overload clinical burden in heart, due to secondary iron-overload, but chelation therapy treatment strategy is cumbersome associated with toxic side effects and has limited clinical outcomes.<sup>54, 74, 155, 157, 158</sup>

In erythrocytapheresis or red cell apheresis, an alternative approach to phlebotomy removes at least twice as much iron. In this method erythrocytes are selectively removed from the whole blood, followed by reinfusion of leukocytes, platelets, and plasma to the patient.<sup>148, 149, 159</sup>

## **1.8 Proposed Therapies:**

Current therapies are not effectively reducing the clinical burden of iron-overload cardiomyopathy. Iron chelation therapy rapidly normalizes serum iron levels and liver iron, but slowly removing cardiac iron, which in turn promotes iron induced oxidative stress and cardiomyopathy disease progression. Iron induced oxidative stress is the key driver in the disease progression, due to a high degree of iron induced oxidative stress condition; antioxidant therapy should be a suitable rational therapy.

### **1.8.1 Antioxidant therapy**

However, current antioxidants are ineffective and unable to target particular intracellular compartments to reduce pro-oxidants (ROS/RNS) and some antioxidants converts into pro-oxidants during oxidative environment. Therefore, in order to effectively control iron-induced oxidative stress, a more comprehensive approach required.

It was shown that resveratrol a new natural antioxidant with pleiotropic beneficial effects inhibit heavy metal-induced oxidative stress and lipid peroxidation.<sup>160, 161</sup> Resveratrol is a natural polyphenol with phytoalexin properties, produced in plants in response to stress and also found in many natural foods (fruits, and vegetables).<sup>162, 163</sup> It was also shown that resveratrol modulates metabolic functions, anti-inflammatory and cardioprotective beneficial effects.<sup>162-164</sup> Many lines of evidence showed that resveratrol protects against obesity, type2 diabetes, beside improves mitochondrial function and biogenesis by PGC-1 $\alpha$  induction.<sup>165</sup> PGC-1 $\alpha$  is a master regulator of mitochondrial biogenesis.

## Pleiotropic Cardiovascular and hepatic benefits of resveratrol

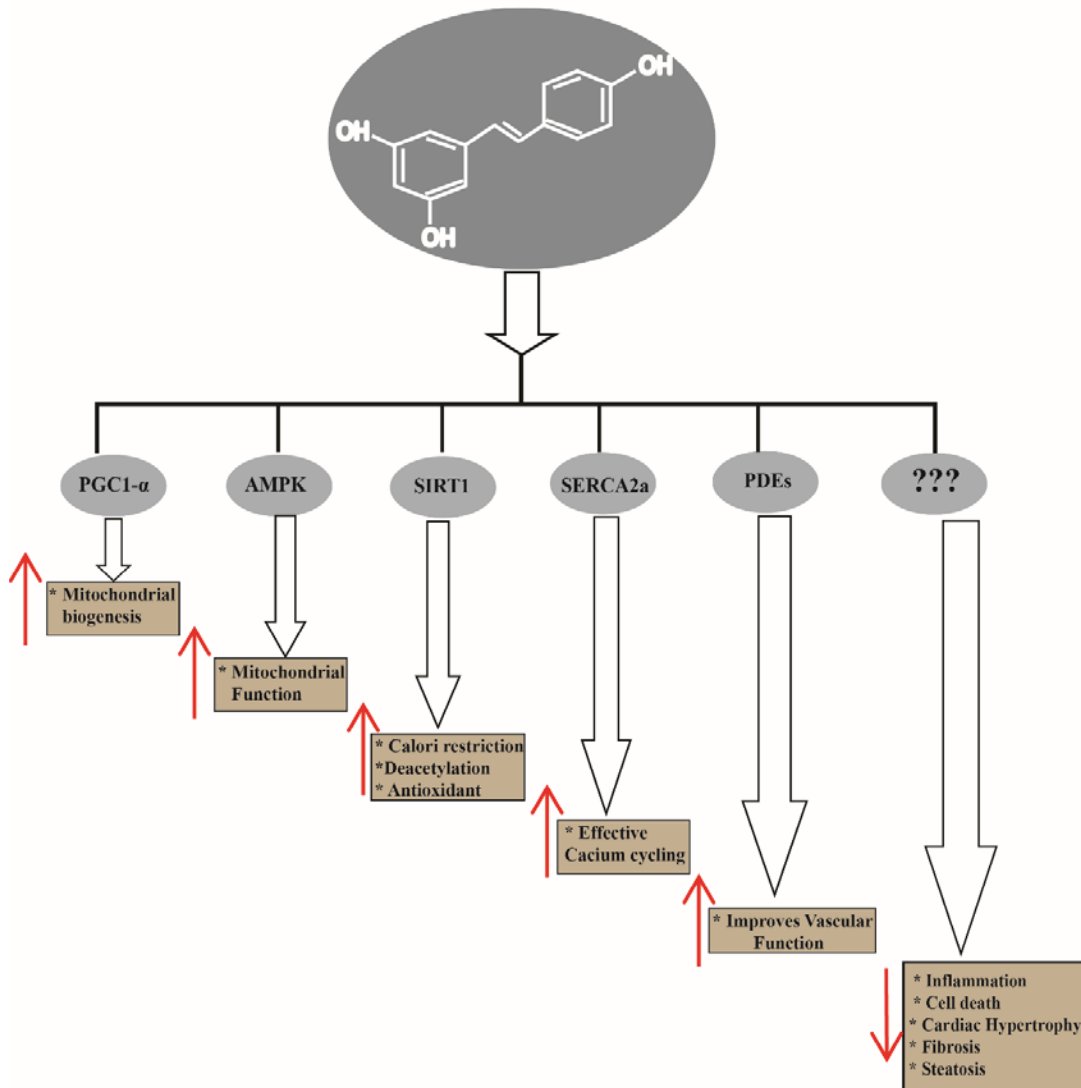


**Figure 1.12 Schematic presentation of cardiovascular and hepatic benefits of resveratrol therapy.**

Resveratrol is a pleiotropic natural polyphenol. It exerts multiple pharmacological benefits, activation of PGC1- $\alpha$  favors mitochondrial biogenesis, activation of AMPK, SIRT1 allows many cardioprotective and hepatoprotective benefits. Resveratrol act as a metabolic modulator in calorie restriction, anti-aging molecule, increases antioxidant levels in the cell. It prevents calcium cycling defects by upregulating the levels of SERCA2a. It act as anti-fibrotic agent, prevents cardiac hypertrophy, cell death, and inflammation. Resveratrol also improves vascular function by increasing NO production and inhibits PDEs so maintains the level of cAMP concentrations. PGC1- $\alpha$  = peroxisome proliferator-activated receptor c coactivator 1- $\alpha$ ; AMPK= AMP Activating Protein Kinase; SIRT1=Sirtuin1; SERCA2a=Sarco-endoplasmic reticulum calcium ATPase; PDEs= Phosphodiasteraes;cAMP= Cyclic AMP.

Resveratrol exerts its physiological effects by improves mitochondrial function, and modulates glucose metabolism by activating indirectly AMP-Activated protein kinase (AMPK) and AMPK activation has been shown to modulate metabolism by decreasing fat accumulation, increasing glucose tolerance, and insulin sensitivity etc.<sup>162, 166-168</sup> It was also reported that resveratrol activates SIRT1 upon AMPK activation(**Figure 1.13**)<sup>169-171</sup> The activity of AMPK requires two AMPK kinases named LKB1 and calcium-calmodulin dependent kinase, which phosphorylates AMPK.<sup>167</sup> Activation of AMPK increases the levels of NAD<sup>+</sup> which in turn activate SIRT1 (**Figure 1.13**).<sup>170, 172</sup> Activated SIRT1 deacetylates Sirtuin substrates.<sup>170</sup> Resveratrol also shown to improve liver function by decreasing liver triglyceride formation, inflammation, cell death and oxidative stress.<sup>173</sup> Activated AMPK and activated SIRT1, inhibit sterol regulatory element binding protein1 (SREBP1), a major transcription factor required for triglyceride synthesis and it was also shown to promote steatosis formation and end stage liver cirrhosis in liver (**Figure 1.13**).<sup>162, 174-176</sup> Resveratrol also improves SERCA2a transcript and protein levels, in cardiomyocytes and shown to improve calcium cycling defects.<sup>91, 177</sup> Beside cardiac and hepatic beneficial effects it also showed vascular effects, resveratrol shown to inhibit phosphodiesterase (PDEs), and the enzymes that hydrolyses cAMP / cGMP into AMP/GMP respectively but nor adenylyl cyclase (AC) and guanylyl cyclase (GC) activity<sup>178</sup> and improves vascular function by increasing the nitric oxide (NO) production, reduce hypertension, atherosclerosis of blood vessels etc.

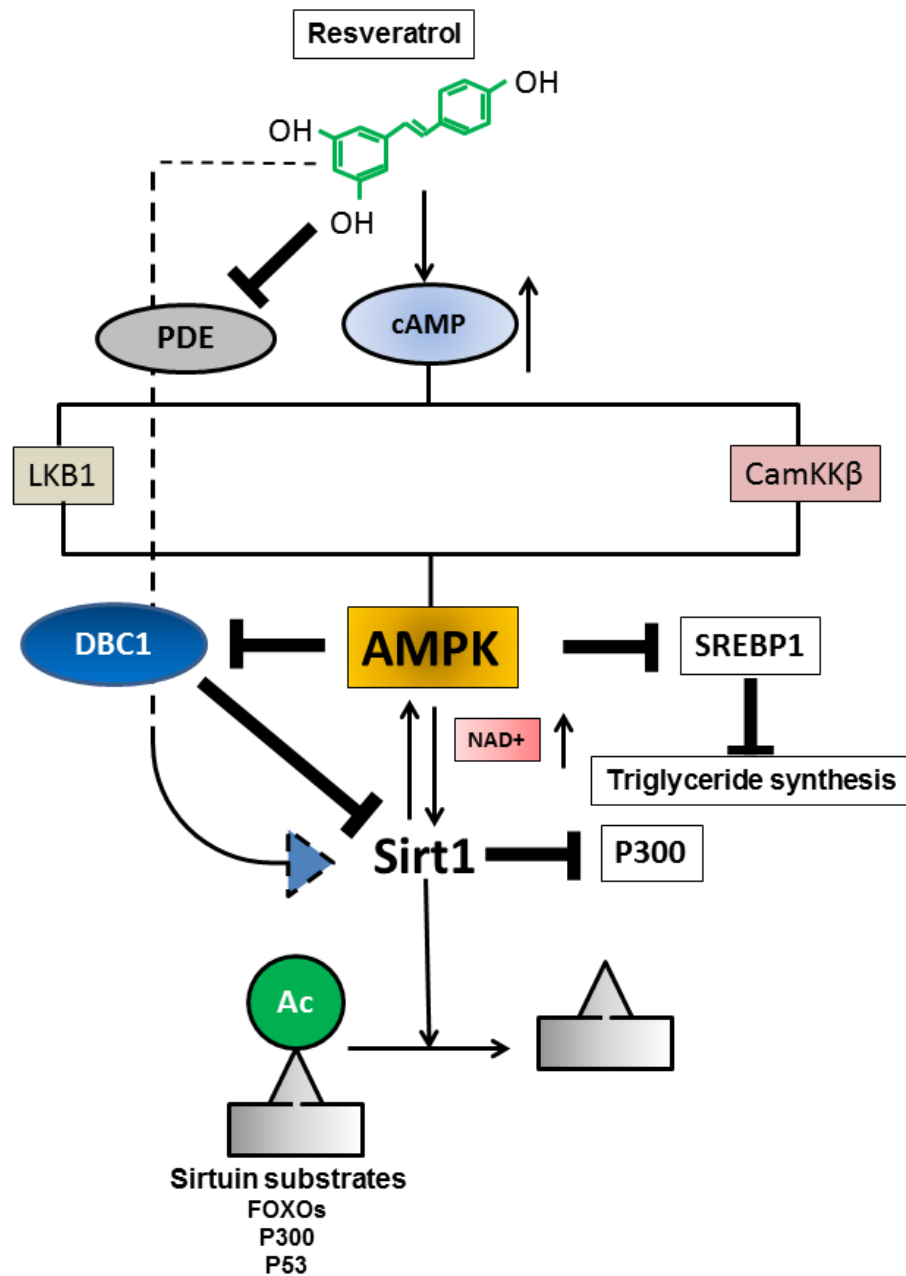


**Figure 1.13 Schematic presentation how resveartrol regulates AMPK and SIRT1.**

Resveratrol activate AMPK and SIRT1 directly as well indirect, Low concentration of resveratrol direct activator of SIRT1 and high concentration resveratrol indirectly activate SIRT1 via AMPK. AMPK is activated by other up stream kinases such as LKB1 and CamKKβ. Acivated AMPK modulate energy metabolism. LKB1=Liver kinase B1; AMPK=AMP activated protein kinase; SIRT1=Sirtuin1; SREBP1=Sterol regulatory element binding protein1; PDE=Phosphodiasterases; CamKKβ=Calmodulin kinase kinase beta.

## 1.8.2 Resveratrol in clinical trials

Preclinical studies with animal models showed significant beneficial effects of resveratrol.<sup>179-186</sup> The safety and effectiveness of resveratrol in various preclinical murine models are promising.<sup>184, 187, 188</sup> A randomized double-blinded, placebo-controlled clinical trial in hypertension patients treated with resveratrol showed improved outcomes.<sup>189</sup> In stable coronary artery disease patient's chronic administration of resveratrol showed increased serum adiponectin with reduced inflammation and atherothrombotic signaling.<sup>190</sup> Supplementation of 500 mg of resveratrol to patients with non-alcoholic fatty liver disease showed reduced serum ALT and hepatic steatosis.<sup>191</sup> Much progress has been done in our understanding of resveratrol biology, however, the molecular targets, how they exert its therapeutic action yet to be found out.<sup>188</sup> The precise mechanism of resveratrol is highly interconnected and still controversial. Translating the beneficial effects of resveratrol into clinical trial studies are bit challenging and several clinical trials with resveratrol showed inconsistency results.<sup>192</sup> The main reason is that low bioavailability of resveratrol and humans are heterogeneous in which patients to patients the resveratrol bioavailability and pharmacokinetics varies.<sup>192</sup> Beside this resveratrol upon absorption in the intestine rapidly metabolized into glucuronide and sulfate conjugates. The metabolites of resveratrol mask the biological activity of the parent molecule, which makes more difficult to determine the proper dose response needed in humans.<sup>193</sup> There are several strategies developed to increase the bioavailability of resveratrol, such as 1) resveratrol analogs 2) metabolite inhibitors of resveratrol and 3) agents to improve the stability of resveratrol.

There is increasing needs for alternative strategies to prevent cardiovascular disorder in this regard resveratrol may be a potential adjuvant therapy to prevent heart failure.

### 1.8.3 Amlodipine (L-Type Calcium Channel Blocker)

L-Type calcium channels are voltage-gated calcium channels, plays an important role in the contractile properties of heart muscle, skeletal muscle, and vascular smooth muscle cells and in neurons.<sup>194-199</sup> L-Type calcium channel consists of  $\alpha_1$ ,  $\alpha_2/\delta$ , and  $\beta$  heterotetrameric of polypeptides chains.<sup>200, 201</sup> The  $\alpha_1$  subunit is the major pore forming unit and consist of four homologous motifs I-IV and further consists of six transmembrane alpha helices.<sup>201</sup> The  $Ca_v1$  gene family consists of  $Ca_v1.1$ ,  $Ca_v1.2$ , and  $Ca_v1.3$  which plays a major role in pore formation.<sup>195, 202</sup>

L-Type calcium channel blockers are the frequently used medicine in clinical practice of cardiovascular diseases and introduced in the year of 1960.<sup>202, 203</sup> There are three groups of L-Type calcium channel blockers or L-Type calcium channel antagonists such as dihydropyridines (DHP) (example-nifedipine, amlodipine), benzothiazepine (example-diltiazem) and phenylalkalamine (example-verapamil).<sup>202, 204</sup> The first generation dihydropyridine, nifedipine a LTCC blocker and is a potent vasodilator as well as it also prevents heart rhythm abnormalities along with blocking pore of LTCC, however, it has short half-life.<sup>204, 205</sup> To increase the selectivity and short half-life of nifedipine, the physicochemical and pharmacodynamic properties modified and second-generation dihydropyridine CCBs developed, example- nimodipine.<sup>205</sup> A third generation dihydropyridine CCBs also has also been developed and amlodipine is one of third generation dihydropyridine CCBs with pleiotropic cardiovascular protective effects (**Figure 1.14**).<sup>204</sup>

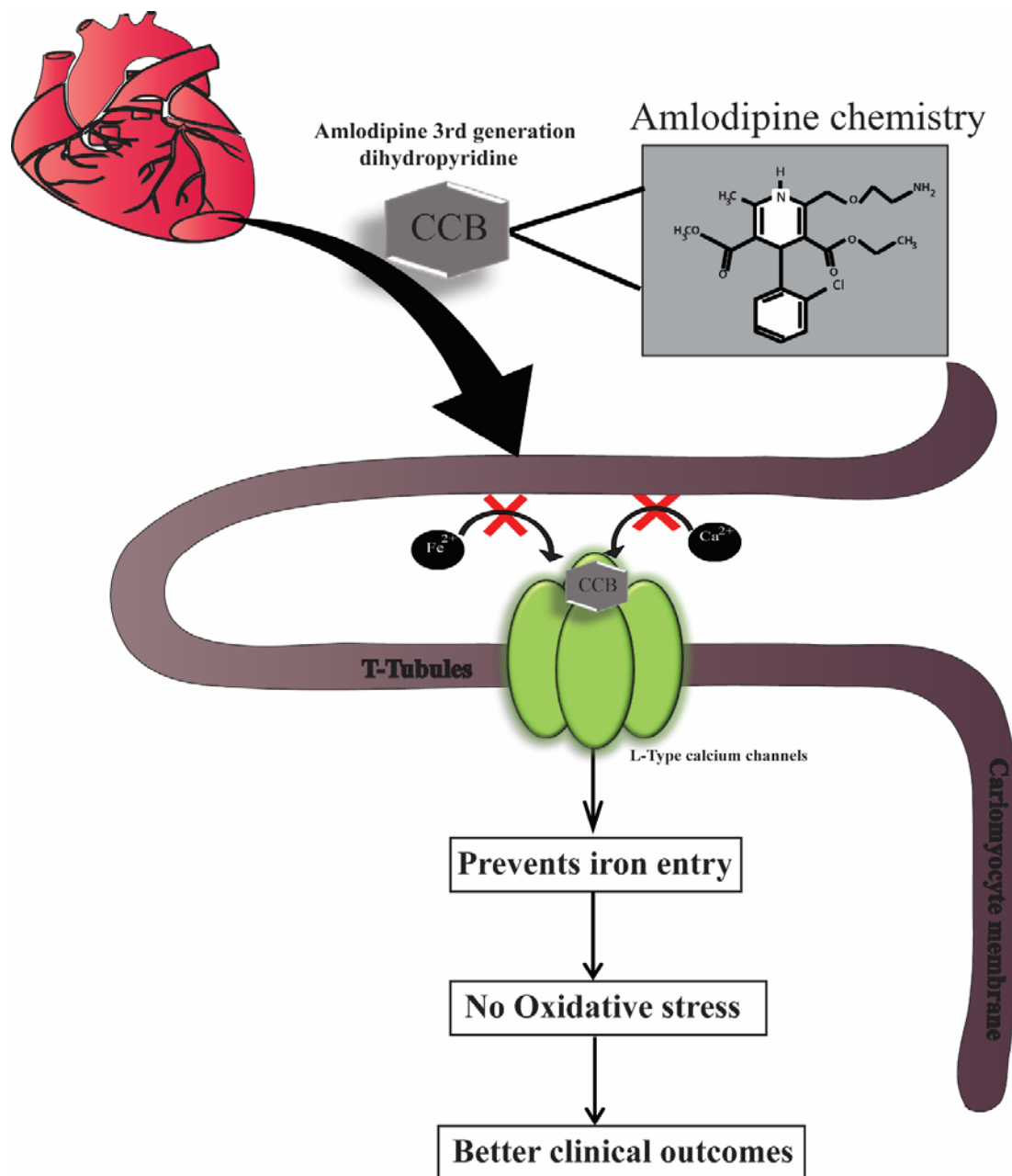


**Figure 1.14 Schematic presentation of cardiovascular benefits of amlodipine calcium channel blocker therapy.** Amlodipine calcium channel blocker is a pleiotropic third generation dihydropyridine. It exerts multiple pharmacological benefits, at cardiac and vascular effects. In iron-overload cardiomyopathy, iron enters into heart cells via L-Type calcium channels and amlodipine blocks L-Type calcium channels and prevents iron entry as well as iron induced oxidative stress with overall beneficial effects. CCB = calcium channel blocker.

Due to the presence of a basic amino functional group, amlodipine is positively charged at physiological  $P^H$ .<sup>206</sup> Dihydropyridines (DHPs) are hydrophobic in nature, which favors them to gain access to the receptor site at the time of channel inactivation.<sup>196, 202</sup> In contrast, verapamil a phenylalkalamine calcium channel blocker negatively charged at physiological  $P^H$  and binds to the inner sarcolemmal surface.<sup>196, 202</sup> Verapamil blocks, L-Type calcium channels only when it is in the open state (require voltage pulse). It was shown that L/T Type calcium channels are the major transporters of redox iron into cardiomyocytes during iron-overloaded conditions.<sup>77, 80</sup> By blocking these channels, we can prevent iron entry into cardiomyocytes. So L-Type Calcium Channel Blocker (CCBs) opens up another new possibility to prevent or reduce the clinical burden of iron-overload cardiomyopathy. We propose a combination of antioxidants and L-Type Calcium Channel Blocker (CCBs) therapy represents a new rational therapy to target iron induced oxidative stress and blocking further iron entry.

## 1.9 Hypothesis and Objectives

*We hypothesize that iron induced oxidative stress is a major risk factor in the pathogenesis of heart and liver diseases during iron-overloaded condition.*

*Resveratrol treatment can rescue/prevent iron-overload cardiomyopathy and iron-overload liver diseases possibly by:*

- \* Reducing iron induced oxidative stress in the heart and liver.*
- \* Reducing myocardial and hepatic fibrosis.*
- \* Correcting  $Ca^{2+}$  cycling defects in the heart.*
- \* Reducing hepatic inflammation, steatosis and lipotoxicity.*

The main objectives are as follows:

- 1) To understand the fundamental mechanism of iron-overload cardiomyopathy and therapeutic effects of resveratrol in acquired and genetic murine models of iron-overload at early and chronic stage.**
- 2) To understand the advanced stage of iron-overload cardiomyopathy and therapeutic effects of resveratrol in aged genetic murine models iron-overload.**
- 3) To understand the fundamental mechanism of hepatic iron-overload and therapeutic effects of resveratrol in acquired and genetic murine models of iron-overload at early, chronic and advanced disease stage.**
- 4) To understand the gender basis of iron-overload cardiomyopathy in male and female murine models of iron-overload.**

# CHAPTER TWO

## OVERVIEW OF RESEARCH PROTOCOLS

**2.1 Iron-overload animal models:** There are different murine models available to study iron-overload pathophysiology. Both acquired and genetic iron-overload murine models are available, which recapitulates secondary iron-overload and genetic hemochromatosis. In my research, I used C57BL6 strain wild type mice and of S129 strain HJVKO mice. HJVKO mice are deficient in hemojuvelin protein which acts as a co-receptor for BMPs and modulates the expression of an iron regulatory hormone called hepcidin. Hepcidin regulates gastrointestinal iron absorption and impaired hepcidin leads irregular iron absorption from high iron dietary sources.

**2.2 Experimental Animal Protocols.** Wild type (WT) male and female C57BL6 mice (from Jackson Laboratory, Bar ME) of 10-12 weeks and male and female HJV knockout mice (*HVJ<sup>-/-</sup>*) (kindly provided by Dr. Nancy C. Andrews, Duke University) bred in-house at the University of Alberta Health Sciences Laboratory Animal Services housing facility. All experiments were performed in accordance with University of Alberta institutional guidelines which conformed to guidelines published by the Canadian Council on Animal Care and the Guide for the Care and Use of Laboratory Animals published by the US National Institutes of Health (revised 2011). WT mice were subjected to iron/placebo-injection protocol whereas HJV knockout mice (*HVJ<sup>-/-</sup>*; *HJVKO*) were treated with high iron diet (Prolab<sup>®</sup>RHM 3000 with iron 380 ppm) respectively.

The wild type mice are injected iron dextran intraperitoneally to make them iron-overload, which closely recapitulates secondary iron-overload conditions. In wild type

mice we have two different time points: **Early stage:** 5 mg/25 gm body weight of iron dextran (from sigma) or placebo (5% of dextrose with phenol) i.p injected on a 5day/week schedule for a total duration of 4 weeks to WT male C57BL6 mice and **Chronic stage:** 5 mg/25 gm body weight of iron-dextran i.p. was injected on a 5 day/week schedule for total duration of 4 weeks followed by 1.25 mg/25 gm body weight for 8 more weeks in WT male C57BL6 mice.

The HJVKO mice are treated with high iron diet high iron diet (Prolab<sup>®</sup>RHM 3000 with iron 380 ppm) to make them iron-overload, which closely recapitulates genetic iron-overload conditions or genetic hemochromatosis. In HJVKO mice we have two different time points: **Chronic stage:** In this HJVKO mice are treated with high iron diet for 6 months and **advanced stage:** In this HJVKO mice were treated with high iron diet for 12 months.

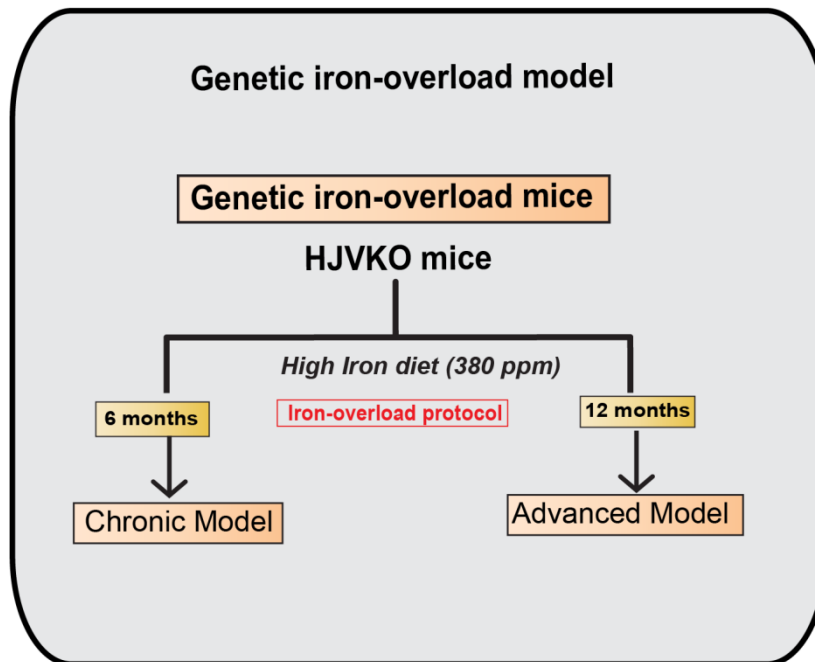
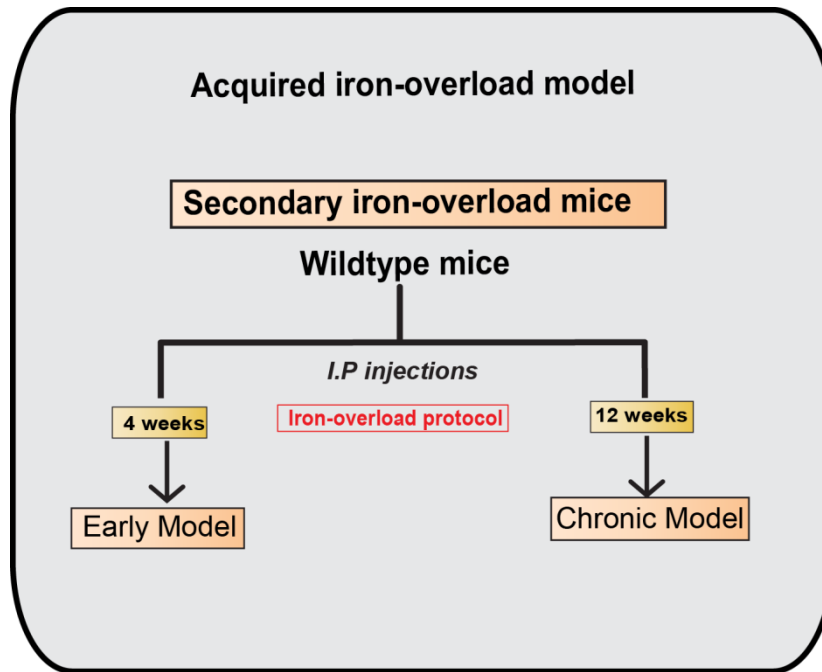


**Figure 2.1 Overview of animal models and research protocol.** The upper pannel represents the acquired murine model and the lower pannel represents the genetic murine model.

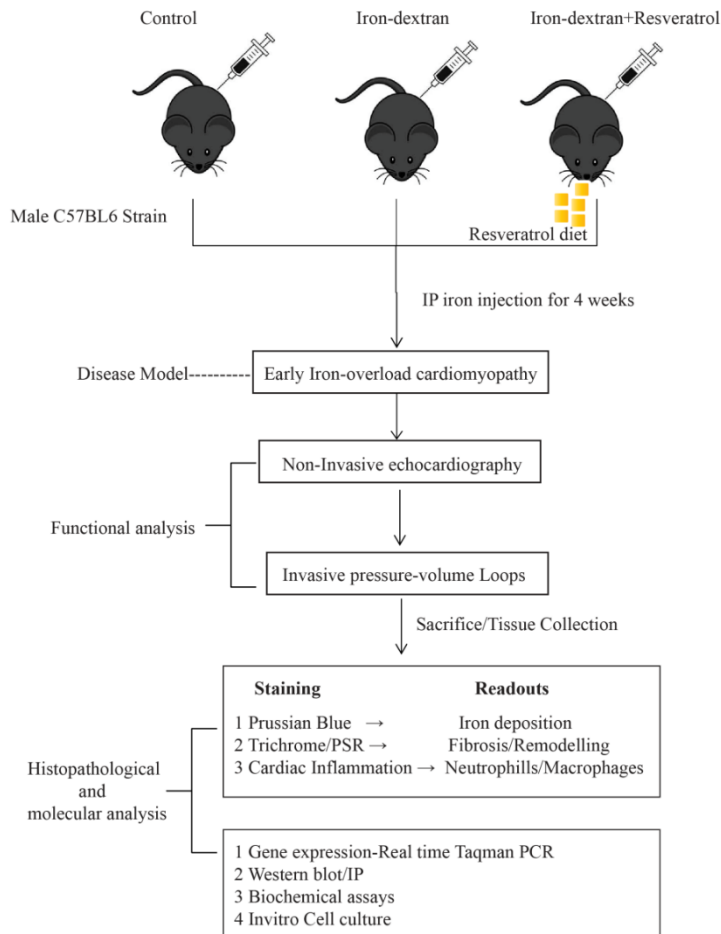
### **2.3 Sample size, Power of study and choice of statistical method.**

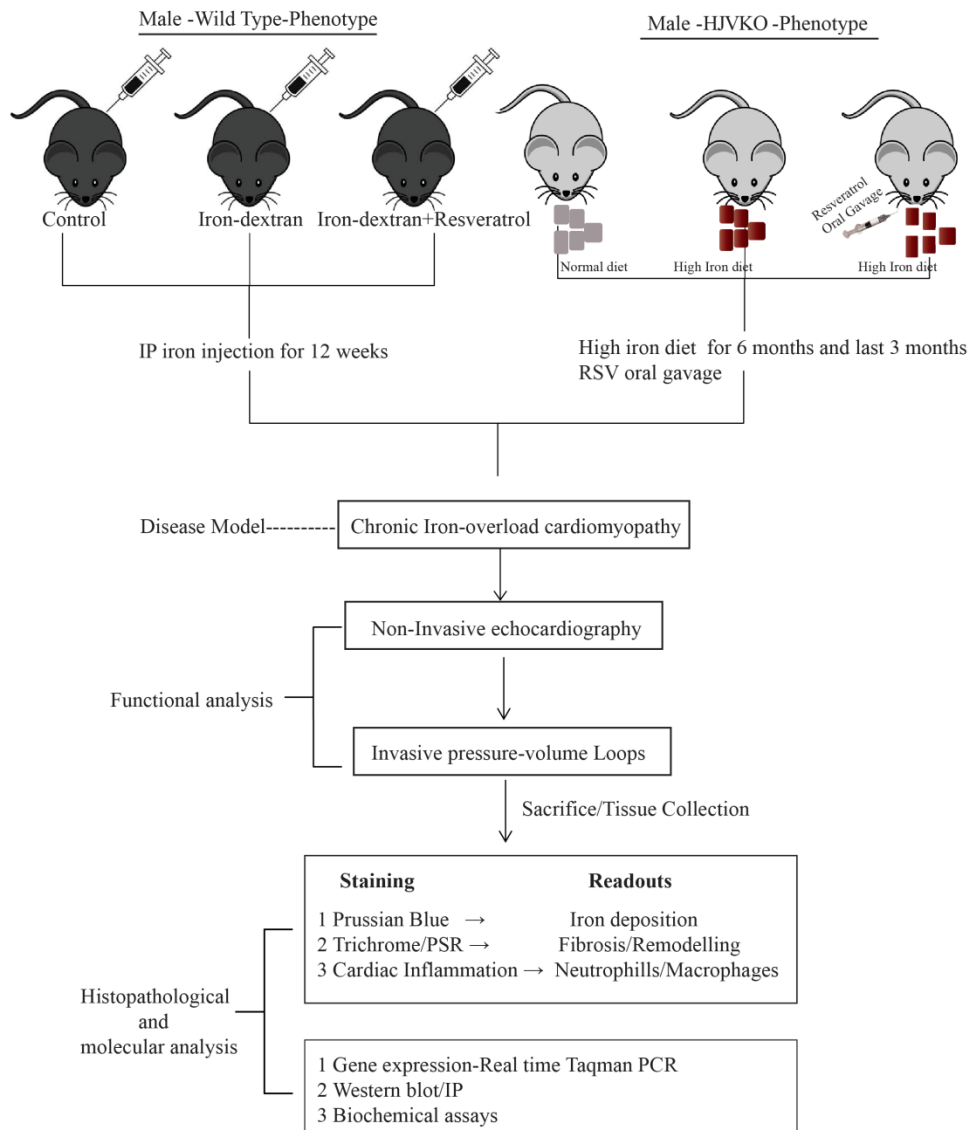
Sample is a small fraction of universe and is the best parameter to study universe. To generate precise results in biomedical science, an adequate sample size is highly important.<sup>207</sup> If the sample size is too small it will not give valid results similarly a larger sample size further results misuse of money and manpower.<sup>207</sup> Hence, appropriate sample size will be highly necessary to produce precise results.<sup>208-210</sup> We used animals n=10 to 12 per group for *in vivo* work and for *in vitro* myocyte and fibroblast work at least from n=3 hearts and recording was made from 5-10 cells thereby achieving a final sample size of 15-20, based on previously published research work.<sup>77, 83</sup>

Power of study is very important to calculate sample size calculation.<sup>210</sup> Power is calculated by subtracting beta error (type-II error) from 1 (Power=1- $\beta$ ). This is highly important to know whether study had enough power to pick up the difference if it existed. We considered power of our study as 80% as shown in most biomedical studies.<sup>210</sup>

All statistical analyses were performed using SPSS 19 software and the averaged values are presented as mean  $\pm$  SEM. Student's t-test is used to compare between two groups. For comparing three or more sets of data we used multi-talented method called as analysis of variance (ANOVA). We used one-way ANOVA and two-way ANOVA based on the type of study.

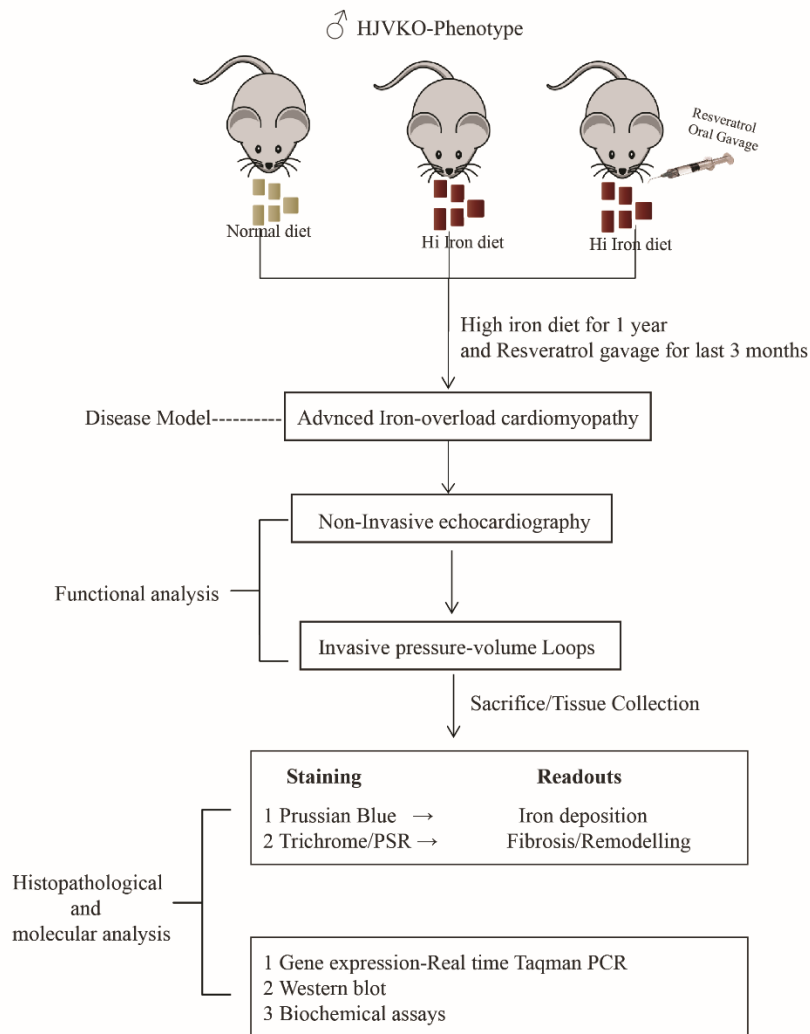
## Study 1 (Chapter 3): Iron-overload injury and cardiomyopathy in acquired and genetic models is prevented by resveratrol therapy





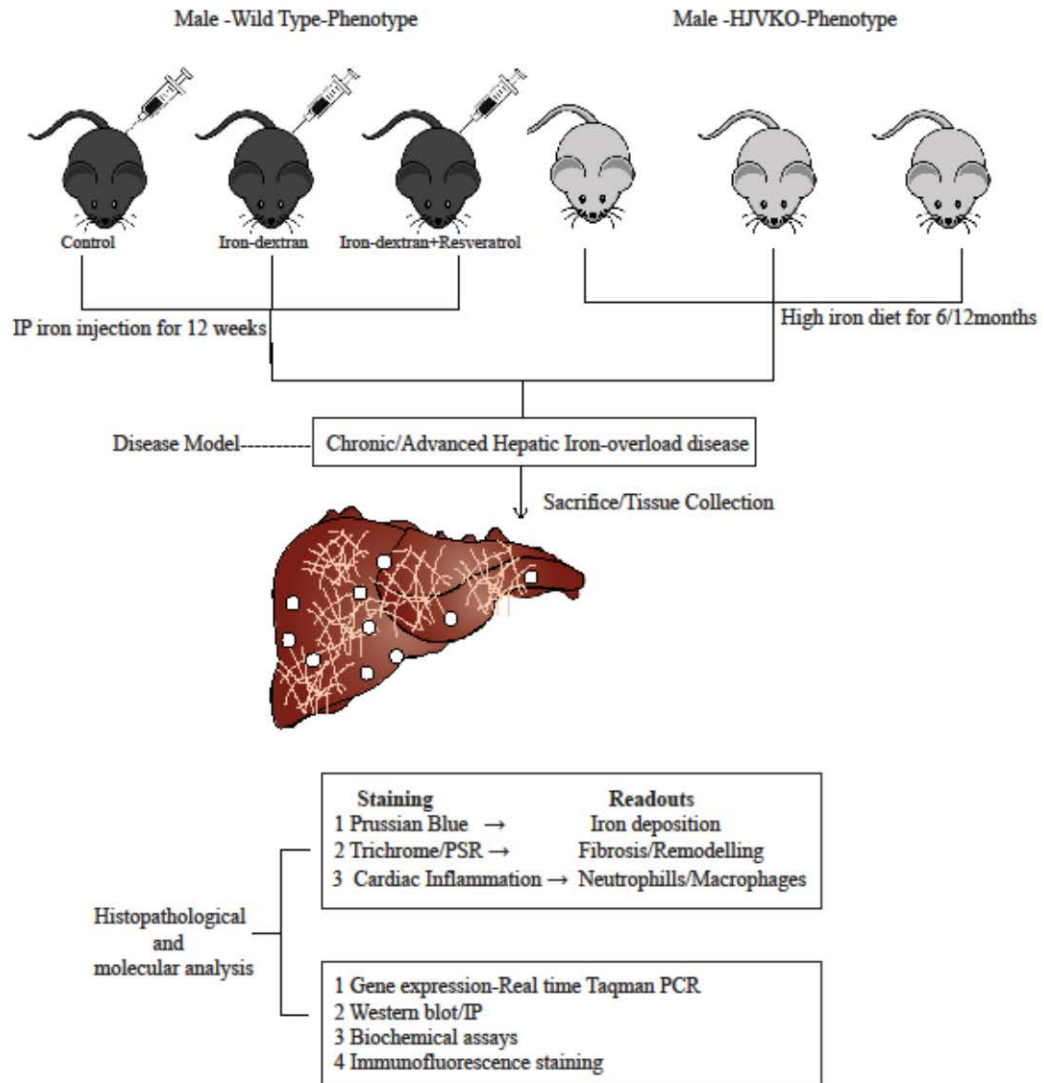
**For detailed Material and Methods..... Please see Chapter-3**

## Study 2 (Chapter 4): Iron-overload cardiomyopathy in aged Juvenile hemochromatosis genetic murine model is rescued by resveratrol



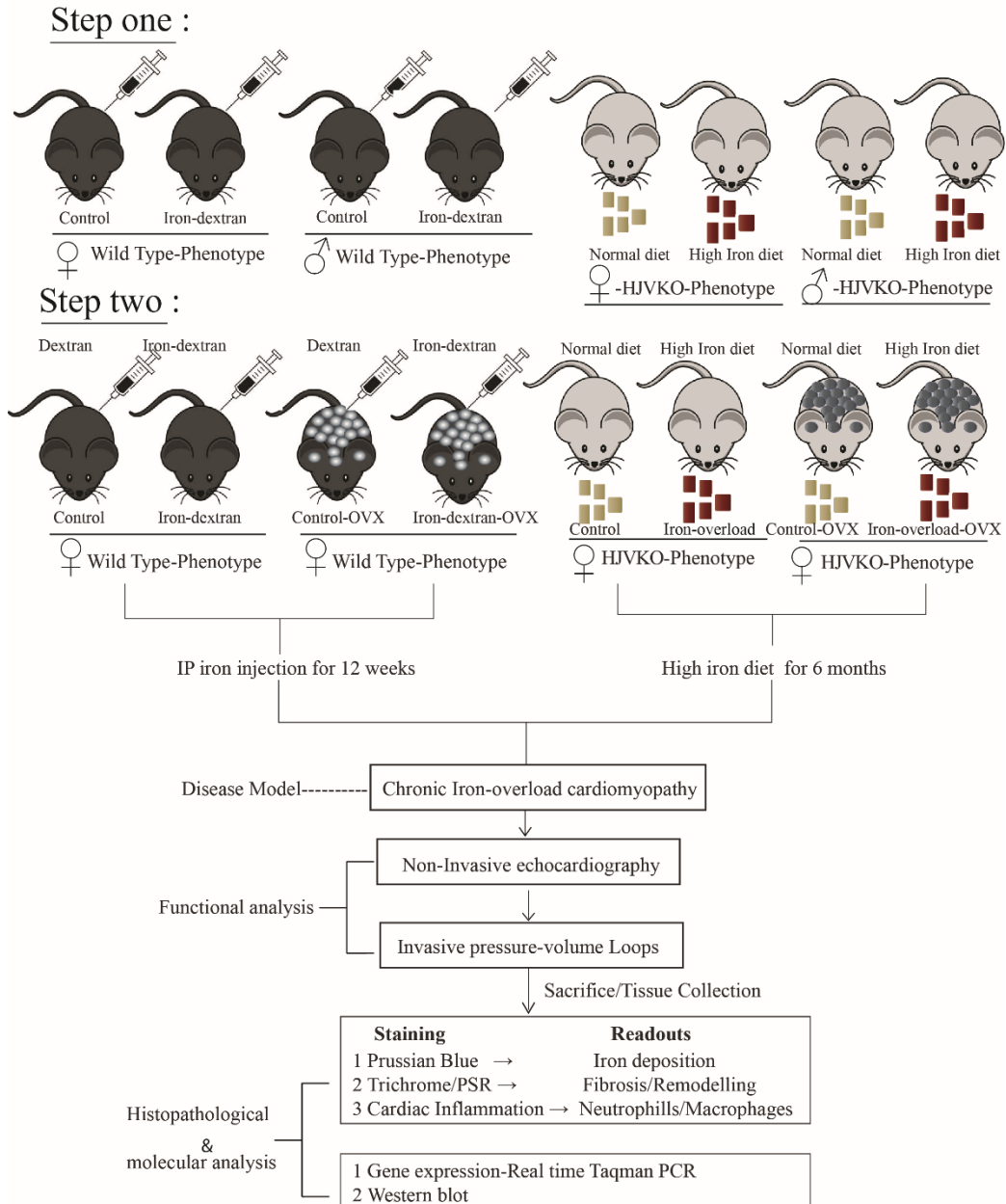
For detailed Material and Methods..... Please see Chapter-4

## Study3 (Chapter 5): Resveratrol mediates therapeutic hepatic effects in acquired and genetic murine models of iron-overload



For detailed Material and Methods..... Please see Chapter-5

## Study 3 (Chapter 6): Females are protected from iron-overload cardiomyopathy independent of iron metabolism: key role of oxidative stress



For detailed Material and Methods..... Please see Chapter-6

# **CHAPTER THREE**

## **Iron-overload injury and cardiomyopathy in acquired and genetic models is attenuated by resveratrol therapy**

Subhash K. Das<sup>1,2</sup>, Wang Wang<sup>2,3</sup>, Pavel Zhabyeyev<sup>1,2</sup>, Ratnadeep Basu<sup>1,2</sup>, Brent McLean<sup>2,3</sup>, Dong Fan<sup>2,3</sup>, Nirmal Parajuli<sup>1,2</sup>, Jessica DesAulniers<sup>1,2</sup>, Vaibhav B. Patel<sup>1,2</sup>, Roger J. Hajjar<sup>4</sup>, Jason R. B. Dyck<sup>5</sup>, Zamaneh Kassiri<sup>2,3</sup>, and Gavin Y. Oudit<sup>1,2</sup>

<sup>1</sup>Division of Cardiology, Department of Medicine, <sup>2</sup>Mazankowski Alberta Heart Institute,

<sup>3</sup>Department of Physiology, University of Alberta, <sup>4</sup>Mount Sinai School of Medicine, New York, <sup>5</sup>Departments of Pediatrics and Pharmacology, University of Alberta, Edmonton, Canada,

**A modified version of this chapter has been published in *Nature Scientific***

***Reports*, 2015 Dec 7; 5:18132.**

### 3.1 Abstract

Iron-overload cardiomyopathy is a prevalent cause of heart failure on a worldwide basis and is a major cause of mortality and morbidity in patients with secondary iron-overload and genetic hemochromatosis. We investigated the therapeutic effects of resveratrol in acquired and genetic models of iron-overload cardiomyopathy. Murine iron-overload models showed cardiac iron-overload, increased oxidative stress, altered  $\text{Ca}^{2+}$  homeostasis and myocardial fibrosis resulting in heart disease. Iron-overload increased nuclear and acetylated levels of FOXO1 with corresponding inverse changes in SIRT1 levels in the heart corrected by resveratrol therapy. Resveratrol reduced the pathological remodeling and improved cardiac function in murine models of acquired and genetic iron-overload at varying stages of iron-overload. Echocardiography and hemodynamic analysis revealed a complete normalization of iron-overload mediated diastolic and systolic dysfunction in response to resveratrol therapy. Myocardial SERCA2a levels were reduced in iron-overloaded hearts and resveratrol therapy restored SERCA2a levels and corrected altered  $\text{Ca}^{2+}$  homeostasis. Iron-mediated pro-oxidant and pro-fibrotic effects in human and murine cardiomyocytes and cardiofibroblasts were suppressed by resveratrol which correlated with a reduction in iron-induced myocardial oxidative stress and myocardial fibrosis. Resveratrol represents a clinically and economically feasible therapeutic intervention to reduce the global burden from iron-overload cardiomyopathy at early and chronic stages of iron-overload.

**Keywords:** iron-overload, heart failure, oxidative stress, fibrosis, cardiomyopathy, heart disease, resveratrol

### 3.2 Introduction

Iron-overload is driven by hemochromatosis and secondary iron-overload conditions.<sup>4, 6, 13, 46, 60, 74</sup> Thalassemia, sickle cell anemia and hemochromatosis are among the most frequently inherited disorders worldwide.<sup>13, 55, 57</sup> The prevalence and global clinical burden of iron-overload is increasing with epidemic proportions but therapy remains limited.<sup>74, 211</sup> Iron-overload cardiomyopathy is the most common cause of mortality in patients with secondary iron-overload and is a major co-morbidity in patients with genetic hemochromatosis.<sup>45, 47, 54, 60, 74, 152, 154, 212</sup> Altered iron homeostasis allows uncontrolled iron entry and deposition in different organs including the heart leading to progressive tissue damage and end-organ failure.<sup>1, 47</sup> Excess entry of iron leads to transferrin saturation and non-transferrin bound iron (NTBI) accumulation in iron-overload conditions.<sup>1, 213</sup> Iron-induced oxidative stress plays a fundamental role in the pathogenesis of iron-overload mediated heart disease.<sup>77, 83, 94</sup> The formation of labile NTBI alters the pro-oxidant/antioxidant balance leading to a pro-oxidant state with increased free radical production, oxidative stress, and cellular damage.<sup>83, 84, 214</sup> Current antioxidants are ineffective because of failure to target the correct intracellular compartment of reactive oxygen species in the setting of iron-overload and some antioxidants such as ascorbic acid can be readily converted into a free radical pro-oxidant.<sup>82, 215</sup>

The basic molecular mechanism of iron-overload cardiomyopathy has not been elucidated and strategies to treat this global epidemic are limited. Iron-overload in humans leads to an advanced cardiomyopathy<sup>54, 60, 74, 152, 154</sup>, and the development and validation of pre-clinical models of iron-overload cardiomyopathy are important for the

discovery of new therapies.<sup>51, 77, 216</sup> We identified the SIRT1/FOXO1 axis as a key pathway involved in iron-overload. Resveratrol is a natural polyphenolic flavonoid with a unique ability to activate SIRT1 and has key pleiotropic and anti-oxidant properties.<sup>165, 217-220</sup> We used dietary supplementation with resveratrol to rescue the heart disease in murine models of secondary iron-overload and genetic hemochromatosis. We also demonstrated that iron-mediated pathological effects on human cardiomyocytes and cardiofibroblasts were prevented by resveratrol. Collectively, our results strongly suggest that resveratrol is a useful therapy to reduce the global burden of iron-overload cardiomyopathy.

### 3.3 Materials and Methods

**Experimental Animal Protocols.** Wild type (WT) male C57BL6 mice (from Jackson Laboratory, Bar ME) of 10-12 weeks and male HJV knockout mice (*HVJ<sup>-/-</sup>*) (kindly provided by Dr. Nancy C. Andrews, Duke University) bred in-house at the University of Alberta Health Sciences Laboratory Animal Services housing facility. WT mice were subjected to iron/placebo-injection protocol whereas HJV knockout mice (*HVJ<sup>-/-</sup>*; *HJVKO*) were treated with high iron diet (Prolab<sup>®</sup>RHM 3000 with iron 380 ppm) respectively. All experiments were performed in accordance with institutional guidelines, Canadian Council on Animal Care and the Guide for the Care and Use of Laboratory Animals published by the US National Institutes of Health (revised 2011). The iron-overload regimens used in this study corresponded to early and chronic stages of iron-overload:

1. **Early stage:** 5 mg of iron dextran per 25 g body weight (Sigma-Aldrich, Saint Louis, MO) or placebo (5% of dextrose with phenol) injected i.p. on a 5 day/week schedule for

a total duration of 4 weeks to WT male C57BL6 mice, to study the early stage of iron-overload.<sup>77</sup> We also treated these early iron-overload mice with resveratrol enriched chow diet (Modified AIN-93G Dyets, Inc., Bethlehem, PA.) corresponding to a daily dose of 320 mg/kg<sup>179</sup> for 6 weeks started at 2 weeks prior to iron injection.

**2. Chronic stage:** 5 mg of iron dextran per 25 g body weight injected i.p. on a 5 day/week schedule for the total duration of 4 weeks followed by 1.25 mg/25 g body weight for 8 more weeks in WT male C57BL6 mice. We used dietary resveratrol supplementation (Modified AIN-93G Diets, Inc., Bethlehem, PA) corresponding to a daily dose of 320 mg/kg<sup>179</sup> in wildtype mice started at 2 weeks prior to iron injections for a total duration of 14 weeks. We also used a chronic protocol in 4 weeks old HJVKO mice by feeding them with a high iron diet (Prolab<sup>®</sup>RHM 3000 with iron 380 ppm) for 6 months. We also examined the effects of resveratrol (trans-resveratrol synthetic >99% pure, Lalilab Inc. Durham), on the iron-overloaded HJVKO mice by daily oral gavage (240 mg/kg/day) for 2 months starting at 4 months of age. The iron-injection protocols in WT mice was used as a model of acquired iron-overload<sup>77, 83</sup> and the HJVKO mice were used as a genetic model of hemochromatosis<sup>51</sup>.

**Adenoviral SERCA2 gene delivery *in vivo*.** After 3 weeks of early iron-overload, mice were randomized to receive either adeno-associated virus expressing SERCA2a (AAV-9 SERCA2a, n=10) at  $1 \times 10^{12}$  gcp/ $\mu$ l or adeno-associated virus expressing GFP (AAV-9 GFP, n=5) at  $5 \times 10^{11}$  gcp/ $\mu$ l. The viral constructs were injected by single bolus tail vein injection method as described.<sup>221, 222</sup> and the mice were carefully monitored for one week and their cardiac function was assessed by non-invasive echocardiography.

**Echocardiography.** Transthoracic echocardiography was performed on early, chronic and advanced stages of iron-overload phenotype mice with the Vevo770 high resolution imaging system equipped with a 30-MHz transducer (Visual Sonic Vevo 770) by using 0.8% isoflurane.<sup>223, 224</sup> Both diastolic as well as systolic, cardiac function parameters are recorded and analyzed. Systolic function was assessed using B-mode and M-mode images of Echocardiography. M-mode images were obtained for measurements of left ventricular (LV) wall thickness, LV end-diastolic diameter (LVEDD), and LV end-systolic diameter (LVESD) (measures of LV dilation). LV fractional shortening (FS) and LV ejection fraction (EF) were calculated using the following equations:  $FS (\%) = (LVEDD - LVESD / LVEDD) \times 100$  and  $EF (\%) = (LVEDV - LVESV / LVEDV) \times 100$ . Diastolic function was assessed using pulsed-wave Doppler imaging of the trans-mitral filling pattern with the early trans-mitral filling wave (E-wave) followed by the late filling wave due to atrial contraction (A-wave). Isovolumetric relaxation time (IVRT) was calculated as the time from the closure of the aortic valve to initiation of the E-wave. The deceleration time of the E-wave (DT) was determined by measuring the time needed for the down-slope of the peak of the E-wave to reach the baseline while the rate of E-wave deceleration rate (EWDR) was calculated as the E-wave divided by the DT. Tissue Doppler imaging (TDI) represents a novel and validated technique to assess systolic and diastolic function, with a reduction in  $E'$  and an elevation in  $E/E'$  being considered as valid markers of elevated LV filling pressure and diastolic dysfunction. TDI was carried out at the inferolateral region in the radial short axis at the base of the LV with the assessment of peak annular systolic ( $S'$ ), early diastolic ( $E'$ ), and late diastolic ( $A'$ ) myocardial velocities as described previously.<sup>225</sup>

**Invasive hemodynamic analysis.** We performed PV loop analysis by using 1.2F Scisense catheter connected to an amplifier (TCP-500 Scisense Inc.).<sup>226</sup> Mice were anesthetized by using isoflurane (1-1.5%) and are maintained at 37<sup>0</sup>C by using a heating pad. An incision was made in the right common carotid artery and the catheter was carefully inserted into the incision and the catheter was advanced through the aortic valve and placed into the LV chamber. The position of the catheter was monitored by pressure along with the magnitude and phase using ADvantage pressure volume system (Scisense Inc., London, Canada) and iworx (iWorx Systems Inc., Dover, USA) data acquisition system connected to the catheter. Initially, the catheter position was set in the LV to obtain the magnitude difference of more than 200 $\mu$ S along with a physiological pressure-volume loop shape. After the magnitude was accomplished in the desired range, the phase was adjusted to 4-8 with slightly adjusting the position of the catheter in the LV where phase represents the conductivity imparted by the LV tissue. Once, the desired range for magnitude and phase was achieved, baseline scan was performed to derive volume using Baan's equation and pressure-volume loop was obtained using the LabScribe2 software (version 2.347000). Following baseline PV measurements, transient inferior vena cava occlusion was performed through the diaphragm to obtain the alteration in venous return to derive end-diastolic pressure volume relationships; transient infra-renal aorta occlusion was used to derive the end-systolic pressure volume relationship. Load-dependent and load-independent indices of LV functions were derived. By making and plotting the instantaneous values of pressure and volume at different time points, we determined the ESP, EDP, ESV and EDV in mmHg and  $\mu$ L respectively. Heart rate was estimated beat-to-beat cycle length.

The  $SV = EDV - ESV$ ,  $CO = SV \times HR$ ,  $EF\% = SV / EDV$ , the SW is the area under a PV-Loop and was normalized by dividing with EDV to obtain preload recruitable stroke work (PRSW) which is also a load independent parameter.  $+dP/dt_{(max)}$ , and  $-dP/dt_{(min)}$  are the first derivative of pressure with respect to time and we also took their ratio ( $-dP/dt_{(min)} / +dP/dt_{(max)}$ ) to show a better index of relaxation phase,  $\tau$  (tau)-the time constant of monoexponential pressure decay during isovolumic relaxation, the preload-independent  $+dP/dt_{(max)}$ , also called the Starling's contractile index (SCI) was calculated by dividing  $+dP/dt_{(max)} / EDV$ , which is a better index of myocardial contractility. Systolic and diastolic cardiac performances were also assessed by the end-systolic pressure volume relationship (ESPVR) and end-diastolic pressure volume relationship (EDPVR), respectively.

**Histology.** Mice were anesthetized, hearts were removed and arrested in diastole by using 1M KCl, fixed with 10% buffered formalin and embedded in paraffin. Five  $\mu m$  thin sections were stained with Prussian blue, picro-Sirius red (PSR) and trichrome stain for morphometric analysis. Briefly, The 5  $\mu m$  tissue sections were deparaffinized in xylene and alcohol grades, then rehydrated in water and subjected to respective staining protocol as described previously.<sup>77, 83, 226</sup> The deposition of iron was visualized as blue depositions using bright field microscope. Fibrosis pattern was evaluated by using PSR staining followed by visualization under Olympus IX81 microscope and image analysis using MetaMorph software.

**Immunofluorescence.** Immunofluorescence (IF) was performed on 5-10 $\mu m$  thick formalin fixed and OCT embedded sections from heart and liver. Briefly, formalin fixed paraffin embedded sections were deparaffinized in xylene and alcohol grades,

then rehydrated in water and subjected to respective antigen retrieval procedures followed by blocking with blocking buffer (1% BSA in 1X PBS) for 1 hour. Similarly, the OCT embedded sections were fixed with 4% paraformaldehyde for 20 min and rehydrated in 1X PBS for 30 minutes. Then the paraformaldehyde fixed OCT sections are permeabilized with 0.25% Triton-X-100 for 15 minutes followed by blocking with blocking buffer (1% BSA in 1X PBS) for 1 hour. They were then incubated with primary antibody against rat anti-mouse neutrophil (Serotec:MCA771GA), rat anti-mouse F4/80 (Serotec:MCA497GA), mouse anti-nitrotyrosine (Santa Cruz), mouse anti-4-HNE (Abcam), Rabbit-anti-FOXO1 (Cell Signaling-2880), rabbit anti-collagen-I (Abcam-ab84956), Mouse anti-Sirt1 (Cell Signaling-8469), mouse-anti-alpha-sarcomeric actin (Abcam#ab-28052), rat-anti-mouse-CD-4 (BDPharmingen™:550954), and rat-anti-mouse-CD-8 (BDPharmingen™ : 550281) over night in a humidified chamber at 4<sup>0</sup>C. Sections were incubated with different fluorophore conjugated secondary antibodies (Invitrogen USA) respectively as described previously.<sup>224, 226, 227</sup>

The adult murine and human cardiac fibroblasts and cardiomyocytes after their respective treatment were washed several times with PBS and fixed with 4% paraformaldehyde for 20 minutes, both cardiomyocytes and cardiac fibroblasts were then permeabilized with 0.25% Triton-X100 in PBS for 5 minutes, followed by incubation with 1% bovine serum albumin. The cardiac fibroblasts were then incubated with mixture of primary antibodies against alpha-smooth muscle actin(Abcam-5694) (1:100), vimentin (1:1000), FOXO1(Cell Signaling-2880) (1:100), anti-collagen-I (Abcam-ab84956), (1:300) and SIRT1(Cell Signaling-8469) (1:100) overnight at 4<sup>0</sup>C and the cardiomyocytes were incubated separately with Nitrotyrosine (Santa Cruz),

(1:400), 4-HNE (Abcam) (1:600) primary antibodies at 4<sup>0</sup>C overnight. Both cultured cell types were incubated with a mixture of different fluorophore conjugated secondary antibodies for 1 hour at 37<sup>0</sup>C (Invitrogen). Above mentioned tissue sections as well cells were washed with 1X PBS, three times for 5 minutes each, in between each step, after mounting with Prolong Gold antifade mounting medium with DAPI and some sections without DAPI (Invitrogen). The stained sections, as well as cells, were visualized under a fluorescence microscope (Olympus IX81) and quantified by using MetaMorph software as described previously.<sup>224, 226</sup>

**Dihydroethidium and Phalloidin fluorescence staining.** Dihydroethidium (DHE) is an ROS detection fluorescent dye which produces an excess fluorescent signal in the presence of ROS. Phalloidin stabilizes the F-actin and fluorophore conjugated Phalloidin can be used to stains the cytoskeletal F-actin. We performed dihydroethidium fluorescent staining on 15µm thick LV, liver frozen sections and also in cultured adult murine and human single cell cardiomyocytes. OCT-embedded cryosections were incubated with the 1X hanks balanced salt solution (HBSS) with calcium and magnesium at 37<sup>0</sup>C for 5 min, followed by incubation with 20µM DHE fluorescent dye in 1X HBSS for 30 min at 37<sup>0</sup>C. For the cultured murine and adult human cardiomyocyte were incubated for 30 min with 20µM DHE and then washed with 1X HBSS. For F-actin staining the cultured adult, human cardiomyocytes were fixed in 4% paraformaldehyde, permeabilized with 0.1% Triton X-100 in Dulbecco's phosphate buffered saline (DPBS) and incubated with Alexa Fluor 488 conjugated phalloidin in 1% BSA for 30 minutes at room temperature. The sections were then mounted using Prolong gold antifade mounting medium with DAPI. The sections were

washed three times with DPBS in between each step. The tissue sections and cultured cardiomyocyte dishes were wrapped with foil to minimize light exposure and visualized under Olympus IX81 fluorescent microscope and quantified by using MetaMorph software.

**Tissue iron levels.** 20 mg frozen tissue from LV tissues were subjected to inductive coupled plasma resonance mass spectrometry to quantify tissue iron level in the Trace Metals Laboratory, London, Western Ontario.<sup>77, 83</sup> The samples were analyzed in triplicate and the average values are used.

**Measurement of lipid peroxidation.** The levels of malondialdehyde (MDA), an indicator of lipid peroxidation, were measured in myocardial and hepatic tissues (100-150mg) by using a commercially available kit (Bioxytech® MDA-586™ assay kit cat#21044, OxiResearch, Percipio Biosciences Inc. Los Angeles, CA U.S.A).<sup>228, 229</sup> Briefly, tissue samples were homogenized in potassium phosphate extraction (KPE) buffer pH 7.5 (0.1M potassium phosphate, 5mM EDTA, 0.1% Triton X-100 and 0.6% sulfosalicylic acids) containing 5mM BHT. The samples were allowed to react with N-methyl-2-phenylindole (NMPI) in the acidic pH at 45°C for 1 hour. The clear supernatant was then collected and read in at 586 nm using a plate reader (Spectramax M5, Molecular Devices, and Sunnyvale, CA). MDA levels were estimated using a standard curve derived using 0.5 to 4.0 µM of standard MDA.

**Taqman real-time PCR.** mRNA expression levels were studied in iron-overload hearts, by real-time PCR using Taqman primers and probes (**Table 3.1 of primers and probes listed below**). Total RNA was extracted from flash frozen LV-tissue and

hepatic tissue by using TRIzol RNA extraction method.<sup>223</sup> Beside tissues RNA also extracted from cultured murine and human adult cardiomyocyte and fibroblast by using above mentioned method. 1µg of RNA was subjected to reverse transcription to synthesize cDNA. Real-time PCR was performed with 5µl of suitable cDNA dilutions from unknown and standard (brain cDNA), 8µl Taqman master mix (includes-primers + Probes) were loaded on white 384 Light cycler®480 multi-well plates supplied from Roche with 18s rRNA as an internal control. Samples were loaded in triplicate and the data was analyzed by Light cycler® 480 systems from Roche.

**Table 3.1.** List of TaqMan Primers and Probes.

Gene	Type	Sequence
ANF	Forward: Reverse: Probe:	5'-GGA GGA GAA GAT GCC GGT AGA-3' 5'-GCT TCC TCA GTC TGC TCA CTC A-3' 5'-FAM-TGA GGT CAT GCC CCC GCA GG-TAMRA-3'
BNP	Forward: Reverse: Probe:	5'-CTG CTG GAG CTG ATA AGA GA-3' 5'-TGC CCA AAG CAG CTT GAG AT-3' 5'-FAM-CTC AAG GCA GCA CCC TCC GGG-TAMRA-3'
β- MHC	Forward: Reverse: Probe:	5'-GTGCCA AGG GCC TGA ATG AG-3' 5'-GCA AAG GCT CCA GGT CTG A-3' 5'-FAM-ATC TTG TGC TAC CCA GCT CTA A-TAMRA-3'
IL-6	Forward: Reverse: Probe:	5'-ACAACCACGGCCTTCCTACTT-3' 5'-CACGATTTCCCAGAGAACATGTG-3' 5'-FAM-TTCACAGAGGATACCACTCCCAACAGACCT-TAMRA-3'
IL-1β	Forward: Reverse: Probe:	5'-AACCTGCTGGTGTGTGACGTTT-3' 5'-CAGCACGAGGCTTTTTTGTGT-3' 5'- FAM-TTAGACAGCTGCACTACAGGCTCCGAGATG-TAMRA-3'
TNF-α	Forward: Reverse: Probe:	5'- ACAAGGCTGCCCGACTAC-3' 5'- TTTCTCTGGTATGAGATAGCAAATC-3' 5'-FAM-TGCTCCTCACCCACACCGTCAGC-TAMRA-3'
Pro-Collagen-I	Forward: Reverse: Probe:	5'- CTTACCTACAGCACCTTGTG-3' 5'-TGACTGTCTTGCCCCAAGTTC-3' 5'-FAM-CTGCACGAGTCACACC-TAMRA-3'

Pro-Collagen-III	Forward: Reverse: Probe	5'- TGCCTTTGCGATGACATAATCTG -3' 5'- AATGGGATCTCTGGGTTGGG-3' 5'-FAM- ATGAGGAGCCACTAGACT-TAMRA-3'
TGF-β	Forward: Reverse: Probe	5'- CCTGCAAGACCATCGACATG-3' 5'- ACAGGATCTGGCCACGGAT-3' 5'-FAM-CTGGTCAAACGGAAGCGCATCGAA-TAMRA-3'
SOD1	Premix	Mm01700393_g1*
CAT	Premix	Mn00437992_m1*
Hmox-1	Premix	Mn00516005_m1*
Trfc(Transferrin R)	premix	Mm00441941_m1*
HJV(Hemojuvelin)	Premix	Mm00510148_s1
FPN1(Ferroportin)	Premix	Mm00489837_m1*
HAMP1(Hepcidin1)	Premix	Mm00519025_m1
HAMP2(Hepcidin2)	Premix	Mm00842044_g1*
Ftl1(Ferritin-L)	Premix	Mm03030144_g1
Fth1(Ferritin-H)	Premix	Mm00085707_g1
ATP2A2(SERCA2A)	Premix	Mm01201431_m1
ATP2A2(hSERCA2A)	Premix	Hs00544877_m1
Col1A1(Human Pro-Collagen-I)	Premix	Hs00164004_m1
Col3A1(Human Pro-Collagen-III)	Premix	Hs00943809_m1
ACTA2 (Human α-SMA)	Premix	Hs00426835_g1
Human TGF-β	Forward: Reverse: Probe:	5'-GTGACAGCAGGGATAACACACTG-3' 5'-CATGAATGGTGGCCAGGTC-3' 5'-FAM-ACATCAACGGGTTCACTACCGGC-TAMRA-3'
HPRT	Forward: Reverse: Probe	5'- AGCTTGCTGGTGAAAAGGAC-3' 5'- CAACTTGCGCTCATCTTAGG-3' 5'-FAM-CAACAAAGTCTGGCCTGTATCCAAC-TAMRA-3'
18S rRNA	Premix	Mm03928990_g1*
Human 18S rRNA		Catalogue#4308329

**Measurement of Glutathione levels (GSH/GSSG).** Myocardial reduced (GSH) as well as oxidized glutathione (GSSG) levels were measured as described previously.<sup>77, 128</sup>

**Western blot.** Protein lysates (30-100µg) from flash frozen LV and liver tissue were resolved on 8%, 15% sodium dodecyl sulphate-poly acrylamide gel electrophoresis (SDS-PAGE) then transferred to PVDF membranes using a Trans-blot cell (Bio-Rad laboratories, Hercules CA USA) as previously described.<sup>223</sup> The membranes were blocked with 5% milk, incubated with respective primary antibodies including SERCA2a, NCX1 (Thermo scientific), Collagen-I and Collagen-III, Sirtuin-1, FOXO1, total and phospho (threonine-172) AMPK (Cell signaling Inc) and subsequently incubated with HRP conjugated secondary antibodies respectively.<sup>179, 230, 231</sup> Blots were scanned and quantified by using ImageQuant LAS 4000 (GE Healthcare, Biosciences).

**Immunoprecipitation (IP).** Immunoprecipitation was performed with slight modification as described previously.<sup>226, 230, 232</sup> Total protein lysate (100-200 µg) from flash frozen LV tissue were incubated with 5 µg of anti-acetyl-Lysine (Millipore #05-515) overnight at 4<sup>0</sup>C with a gentle rock. The immune complex was captured by adding 50µl protein A/G Plus-agarose beads (Sc-2003) with gentle rocking for 6 hours at 4<sup>0</sup>C. After that tubes were centrifuged at 12000g for 3 minutes and the supernatants were discarded. The pellets were gently washed with ice-cold 1X PBS and resuspended the immune complex in 60µl of 2X Laemmli sample buffer and resolved on 8% sodium dodecyl sulphate-poly acrylamide gel electrophoresis (SDS-PAGE) then transferred to PVDF membranes using a Trans-blot cell (Bio-Rad laboratories, Hercules CA USA).

**Nuclear and cytosolic protein fractionation.** Nuclear fractionation was performed as previously described with modifications.<sup>226</sup> Briefly, LV tissues were homogenized in hypotonic lysis buffer (10 mM K-HEPES (pH 7.9), 1.5 mM MgCl<sub>2</sub>, 10mM KCl, 1 mM DTT, 0.2 mM Na<sub>3</sub>VO<sub>4</sub>, 1X protease inhibitor cocktail (Calbiochem), 1X phosphatase

inhibitors (Sigma and Calbiochem). The total homogenate was centrifuged at 100 g for 5 minutes to collect unbroken tissues. The supernatant was then centrifuged at 2,000 g for 10 minutes to precipitate crude nuclei from the cell membrane and cytosolic proteins (second supernatant). The second supernatant was further centrifuged at 100,000 g for 90 minutes to separate soluble cytosolic proteins (third supernatant) from membrane pellet. The crude nuclear fraction was resuspended in hypotonic lysis buffer supplemented with 2.4M sucrose, and then layered on top of a 2.4M sucrose cushion and purified by centrifugation at 100,000 g for 90 minutes. Following ultracentrifugation, the purified nuclear pellet was resuspended in storage buffer (20 mM Na-HEPES (pH 7.9), 0.42 M NaCl, 1.5 mM MgCl<sub>2</sub>, 0.2 mM EDTA, 0.2 mM EGTA, 0.5 mM PMSF, 0.5 mM DTT, 25% Glycerol, 1 x protease and phosphatase inhibitors). 30µg of nuclear protein from LV was subjected to Nrf2 (Abcam ab53019) and FOXO1 (Cell Signaling-2880) immuno-blotting. The purity of nuclear and cytosolic fractions was verified by using Histone H3 (Cell Signaling; nuclear marker) and GAPDH (Santa Cruz; cytosolic marker).

**Isolation and culture of adult murine cardiomyocytes.** Adult murine left ventricular (LV) cardiomyocytes were isolated as previously described.<sup>233</sup> (S)-(-)-Blebbistatin(1-phenyl-1,2,3,4-tetrahydro-4-hydroxypyrrolo[2,3-b]-7-methylquinolin-4-one) (25µM) from Toronto Research Chemicals was used to inhibit myocyte contractility by selective inhibition of ATPase activity of myosin-II as previously reported.<sup>234</sup> Briefly, mice were injected with 0.2 mL of 100 IU/mL heparin for 15 min and then anesthetized using 2% isoflurane (1 L/min oxygen flow rate) provided through a nose cone. After opening the chest cavity, the heart was quickly excised, cannulated, and attached to

perfusion system. Following 3-min perfusion with perfusion buffer (containing in mmol/L: 120 NaCl, 14.7 KCl, 1.2 KH<sub>2</sub>PO<sub>4</sub>, 10 HEPES, 1.2 MgSO<sub>4</sub>, 10 NaHCO<sub>3</sub>, 10 taurine, 20 glucose; pH 7.0), the heart was digested with 2.4 mg/mL collagenase type 2 (Worthington) for 7-8 min. After sufficient digestion, the ventricles were removed, dissociated using forceps and transfer pipettes, and resuspended in storage buffer (perfusion buffer pH 7.4 with 0.1% bovine serum albumin) for use in Ca<sup>2+</sup> transient measurements. Alternately, for the culture of myocytes, all steps after perfusion were performed in a laminar flow culture hood. Dissociated myocytes were pelleted (20g for 3min) and resuspended in perfusion buffer containing 10% FBS and 12.5μM Ca<sup>2+</sup>. Sequential Ca<sup>2+</sup> reintroduction was performed at 5min intervals to raise Ca<sup>2+</sup> levels to 100μM, 400μM and finally 900μM. Myocytes were then pelleted (20g for 3min) and resuspended in Minimal Essential Media (Sigma, M4780) containing 10% FBS and Penicillin-Streptomycin (Gibco, 15140) and plated on laminin coated dishes. After 2hrs to allow attachment of viable myocytes, media was changed to serum free media for 12 hours with ferric ammonium citrate (FAC, Sigma, St. Louis, Mo, USA) at 145.6μg/ml (equal to 20μg/ml iron, 1μg Fe=7.28μg FAC) in the absence or presence of resveratrol (22.8 mg/ml).<sup>235, 236</sup>

**Isolation and culture of adult murine cardiofibroblasts.** The standard method of cardiac fibroblast isolation and culture from adult murine left ventricle was done as previously described.<sup>233</sup> Briefly, 10 weeks old mice were injected with 0.05 mL of 1000USP/mL heparin for 15 min and then anesthetized. Then the heart was quickly excised and perfused at a constant speed (4ml/min) within 45s, and digested with collagenase type 2 (Worthington). After digestion, the ventricles were removed,

dissociated using forceps and transfer pipettes in stopping buffer (10% FBS perfusion buffer). Cardiomyocytes were collected by centrifugation at 20g for 3 min. The supernatant containing cardiac fibroblasts were centrifuged at 1500 rpm for 5 min to harvest the fibroblasts, and then the fibroblasts were plated onto a 10 cm culture dish in DMEM with 10% FBS, and then cultured at 37°C in a 5% CO<sub>2</sub> incubator. At the second passage, cardiac fibroblasts were seeded onto collagen type I-treated 6-well BioFlex culture plates (Flexcell Int. Corp.). Cardiac fibroblasts were serum-deprived for 24 hours and then cyclically stretched at 10% elongation 1Hz with ferric ammonium citrate (FAC, Sigma, St. Louis, Mo, USA) 145.6µg/ml (equal to 20µg/ml iron, 1µg Fe=7.28µg FAC) and resveratrol (22.8 mg/ml) for 24 hours.

**Isolation of adult human cardiomyocytes and cardiofibroblast.** Non-failing donor human cardiomyocytes and cardiofibroblasts were similarly isolated, with the following modification: approximately 1 gram of tissue from the LV free wall of healthy donor hearts was chopped into small pieces with forceps, followed by digestion in 100mL collagenase buffer<sup>233, 237, 238</sup> with the addition of (S)-(-)-Blebbistatin (25µM) at 37°C and mixed with a magnetic stir bar. After 20 minutes, stirring was periodically stopped to allow large chunks to settle. The supernatant was then centrifuged (20g for 3 minutes) to pellet the cardiomyocytes and simultaneously harvest the cardiac fibroblast<sup>239</sup> from the supernatant, and the remaining digestion buffer was returned to the digestion beaker and stirring continued. This was repeated periodically 3-4 times, ended after a total digestion time of approximately 60 minutes. Ca<sup>2+</sup> reintroduction and plating were then performed as previously described.<sup>233, 237, 238</sup> The supernatant containing cardiac fibroblasts were centrifuged at 1500 rpm for 5 min to harvest the

fibroblasts, and then the fibroblasts were plated onto a 10 cm culture dish in DMEM with 10% FBS, and then cultured at 37°C in a 5% CO<sub>2</sub> incubator. Following a similar protocol for the murine cardiomyocytes and cardiofibroblasts, cells were treated with ferric ammonium citrate (FAC, Sigma, St. Louis, Mo, USA) at 145.6µg/ml (equal to 20µg/ml iron, 1µg Fe=7.28µg FAC) in the absence or presence of resveratrol (22.8 mg/ml).<sup>235, 236</sup>

**Recording of Ca<sup>2+</sup> transients from isolated cardiomyocytes.** An aliquot of isolated cardiomyocytes was placed in a conical tube with storage solution containing 2µmol/l FURA2-AM and 0.04% pluronic acid and incubated at 35 °C. After 15 min, the solution was carefully aspirated and replaced with storage solution, and cells were incubated at 35 °C for another 15 min. Following this, cells were collected from the bottom of the tube, transferred to a glass-bottomed recording chamber on top of an inverted microscope (Olympus IX71), and allowed to settle for 5-6 min. Cells were superfused at a rate of 1.5-2 mL/min with modified Tyrode's solution (containing in mmol/L: 135 NaCl, 5.4 KCl, 1.2 CaCl<sub>2</sub>, 1 MgCl<sub>2</sub>, 1 NaH<sub>2</sub>PO<sub>4</sub>, 10 Taurine, 10 HEPES, 10 glucose; pH 7.4 with NaOH). The perfusion solutions were heated to in bath temperature of 35-36°C using the in-line heater (SH-27B, Harvard Apparatus) controlled by an automatic temperature controller (TC-324B, Harvard Apparatus). Quiescent rod-shaped cardiomyocytes with clear striations were selected for the study. Platinum wire electrodes were placed near the cell just outside of the microscope view at 400X magnification. Cardiomyocytes were paced with 3-4 V (50% above threshold) and pulse duration of 2.5ms using S48 stimulator (Grass Technology). Fluorescence signal was recorded at 510-nm emission frequency using ratiometric fluorometer D-104

(Photon Technology International) in response to excitation frequencies of 340 and 380 nm injected via 40X objective (UAPO 40X3/340, Olympus). Excitation frequencies were alternated 200 per second. Fluorescence in response to excitations was recorded for the 60s and stored on the hard drive for offline analysis. The 60-s recording (sweep) consisted of 5-s baseline (no electrical stimulation) and 55-s stimulation at 1 Hz (i.e., 55 pulses in total). 5 to 10 sweeps with in-between rest (no stimulation) of 2 min were recorded per cardiomyocyte. At the end of the sweep series for a cardiomyocyte, background signal was recorded for adjustment during analysis. Signal from 1-2 myocytes were recorded from one loading cycle. Sweeps showing a stable regular response to electrical stimulation were selected for analysis. Analysis consisted of signal processing to reduce noise in the signal and measurement of parameters of interest (diastolic  $\text{Ca}^{2+}$  or CaD, systolic  $\text{Ca}^{2+}$  or CaS, the amplitude of the transient or  $\Delta\text{Ca}$  (CaS-CaD), and the time constant of the transient or  $\tau$ ). Signal processing consisted of (i) background adjustment and (ii) averaging of fluorescence signal for stimulation pulses from 20th to 55th within the train. These operations were performed separately for F340 (fluorescence in response to excitation at 340 nm) and F380 (fluorescence in response to excitation at 380 nm). After that, the signal was expressed as F340/F380 to estimate intracellular  $\text{Ca}^{2+}$  concentration. F340/F380 trace was fitted from 100 to 999 ms post-electrical stimulation with monoexponential function to obtain time constant ( $\tau$ ) and diastolic  $\text{Ca}^{2+}$  (CaD), which was defined as a value of monoexponential fit function at 1000 ms (since the fitted trace is an average of steady-state response to electrical stimulation, end-value of a transient is equivalent to the pre-stimulation value of the next transient). Systolic  $\text{Ca}^{2+}$  was defined as a maximum of

F340/F380 trace. To minimize the contribution of the residual noise, the 5-point adjacent average was calculated prior finding the maximum. Calculations were performed in Origin 8.5 (OriginLab) using Lab Talk custom-made scripts.

**Statistical Analysis:** All data were statistically analyzed by using the SPSS Statistics 19 software and the averaged values are presented as mean  $\pm$  SEM. One-way or two-way ANOVA was used for data analysis followed by multiple comparison testing using the Tukey's test.

### 3.4 Results

#### **A key role of SIRT1/FOXO1 pathway in iron-overload induced myocardial injury**

We investigated the molecular basis of iron-induced myocardial injury and focused on the SIRT1/FOXO-1 pathway and the modulation by resveratrol therapy in early iron-overloaded WT mice. Forkhead box-O (FoxOs) and Nrf2 transcription factors transduce a wide range of extracellular signals while FOXO1 is regulated by SIRT1.<sup>230</sup> While Nrf2 levels were unchanged, total nuclear and acetylated FOXO1 levels increased in response to iron-overload which was markedly suppressed by resveratrol with corresponding inverse changes in SIRT1 levels (**Figure 3.1A-C**). Immunofluorescence staining in cultured and stretched cardiofibroblasts exposed to iron showed reduced SIRT1 levels which were restored by resveratrol and co-localized with FOXO1 (**Figure 3.1D**). Resveratrol therapy also increased phosphorylation of AMPK, a key mediator of its beneficial action<sup>169, 174</sup> in the iron-overloaded myocardium (**Figure 3.1E**). We next used a specific and potent SIRT1 activator, SRT1720, to critically examine the role of the SIRT1 pathway in iron-mediated injury. Isolated adult murine cardiomyocytes showed a strong pro-oxidant response to exposure to iron based on superoxide (dihydroethidium, DHE), aldehyde (4-hydroxynonenal, 4-HNE) and nitrotyrosine levels which were markedly suppressed by SRT1720 (**Figure 3.1F**). These results provide instrumental evidence for a critical role of the SIRT1-FOXO1 axis in iron-mediated myocardial injury and in mediating resveratrol protective effects in iron-overload cardiomyopathy.

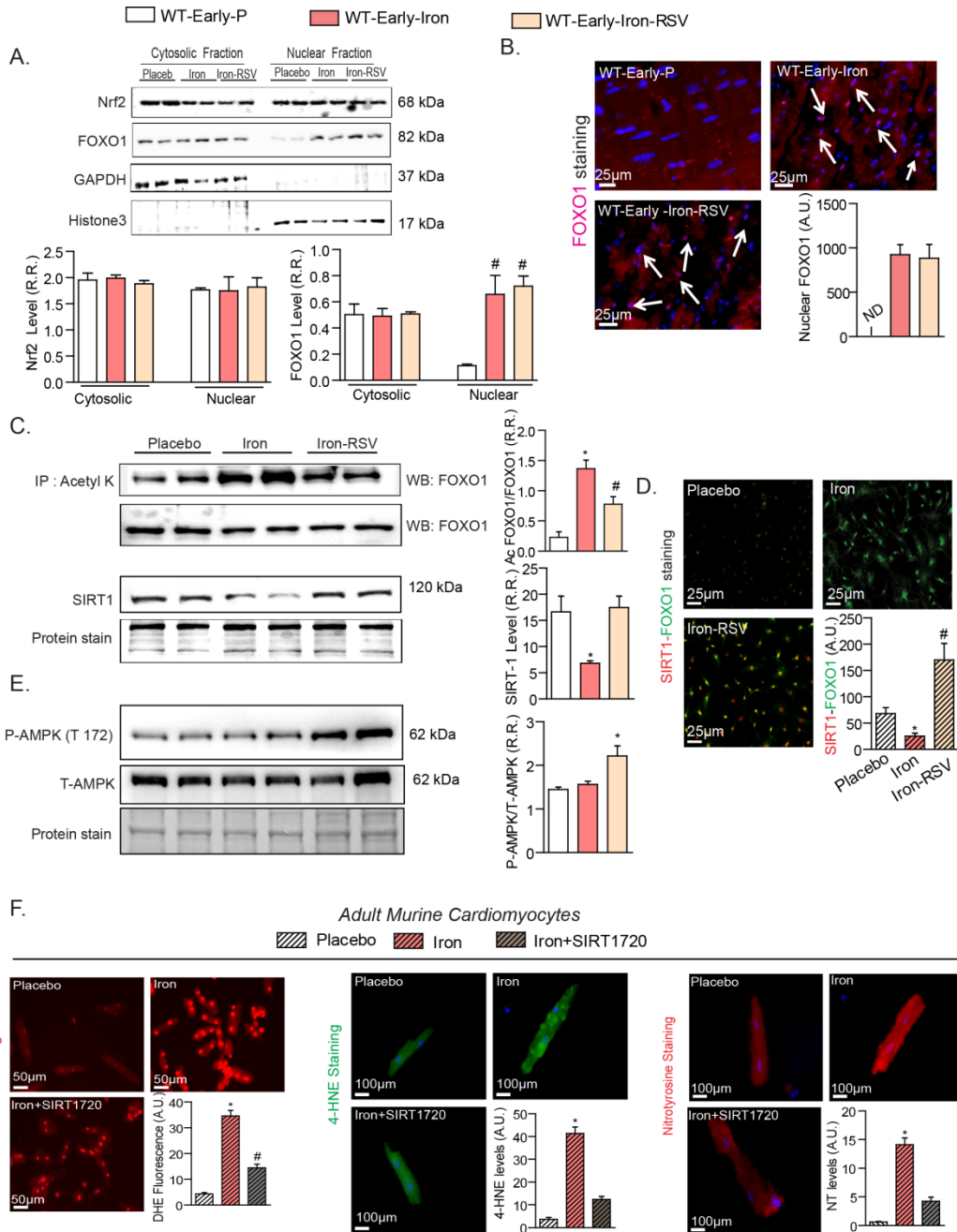


**Figure 3.1. Iron-overload alters myocardial SIRT1/FOXO1 signaling which is restored by resveratrol.** (A-B) Western blot analysis and quantification of two major transcriptional factors, Nrf2 and FOXO1, showing no change in Nrf2 levels but increased nuclear levels of FOXO1 in early iron-overloaded hearts (A) with immunofluorescence staining in myocardial tissue with early iron-overload confirming increased nuclear FOXO1 levels as illustrated by the white arrows (B). (C-D) Immunoprecipitated cardiac acetylated FOXO1 increased in response to iron-overload which was markedly suppressed by resveratrol (RSV) with corresponding inverse changes in SIRT1 levels (C) while immunofluorescence staining for FOXO1 (green) and SIRT1 (red) in cultured and stretched murine LV cardiomyoblasts showing that in response iron exposure nuclear FOXO1 increased with reduced SIRT1 levels, while resveratrol (100  $\mu$ M) prevents the loss of SIRT1 without affecting the increased total FOXO1 levels (D). Resveratrol therapy increased the phosphorylation of AMPK (threonine-172) in the iron-overloaded myocardium (E). SIRT1 activator, SRT1720 (1  $\mu$ M), prevents iron-induced oxidative

stress in cardiomyocytes based on dihydroethidium (DHE) staining for superoxide levels, 4-hydroxynonenal (4-HNE) and nitrotyrosine immunofluorescence (F). R.R.=relative ratio; A.U.=arbitrary unit. n=3 repeats from n=2 hearts. \*p<0.05 compared with all other groups; #p<0.05 compared with the placebo group.

### **Downregulation of SERCA2a in early iron-overload cardiomyopathy: impact of SERCA2a gene and resveratrol therapies**

We explored the mechanism of iron-induced heart disease at an early stage of acquired iron-overload in WT mice which displayed clear evidence of iron injury as reflected by myocardial accumulation of iron (**Figure 3.2A**) and the increased and decreased expression of iron metabolic genes, ferritin L/H and ferroportin, and transferrin receptor 1, respectively (**Figure 3.2B**). The myocardial injury in early iron-overload was associated with diastolic dysfunction driven by impaired myocardial relaxation as shown by echocardiographic assessment using transmitral Doppler flow and tissue Doppler imaging and invasive pressure-volume loop analysis (**Figure 3.2C-D; Tables 3.2 and 3.3**) without myocardial fibrosis (**Figure 3.2.1A-B**) and myocardial inflammation (**Figure 3.2.1C-D**). Resveratrol suppressed the expression of myocardial disease markers, ANF, BNP and  $\beta$ -MHC (**Figure 3.2E**) in early iron-overload which correlated with correction of iron-overload induced diastolic dysfunction (**Figure 3.2C-D; Tables 3.2 and 3.3**) without affecting myocardial iron levels (**Figure 3.2A-B**).

These results identify an abnormality of the cardiomyocytes in early iron-overload which correlated with a significant reduction in myocardial SERCA2a levels (**Figure 3.2.2A**). Importantly, *in vivo* adenoviral gene delivery of *Serca2a* to mice with iron-overload cardiomyopathy restored SERCA2a levels in the heart (**Figure 3.2.2A-B**) resulting in complete correction of diastolic dysfunction (**Figure 3.2.2C**). Interestingly, resveratrol increased SERCA2a levels (**Figure 3.2.2D**) which correlated with

resveratrol mediated reversal of iron-induced downregulation of *Serca2a* mRNA in murine and human cardiomyocytes (**Figure 3.2.2E**). Increased sodium-calcium exchanger level, another key feature of heart disease, was also normalized by resveratrol therapy (**Figure 3.2.2F**). Our results highlight a key role of altered  $\text{Ca}^{2+}$  regulatory proteins in iron-overload cardiomyopathy and, therefore, we examined whole cell  $\text{Ca}^{2+}$  transients in isolated cardiomyocytes from early iron-overloaded mice. Importantly,  $\text{Ca}^{2+}$  transients were prolonged in isolated ventricular iron-overloaded cardiomyocytes and normalized by SERCA2 gene therapy and resveratrol (**Figure 3.2.2H**) which correlated with restoration of normal diastolic function and reversal of disease markers. Our results illustrate the key role of abnormal  $\text{Ca}^{2+}$  cycling driven by reduced SERCA2a levels in iron-overload cardiomyopathy with resveratrol having a profound corrective effect on SERCA2a levels,  $\text{Ca}^{2+}$  cycling, and cardiac dysfunction.

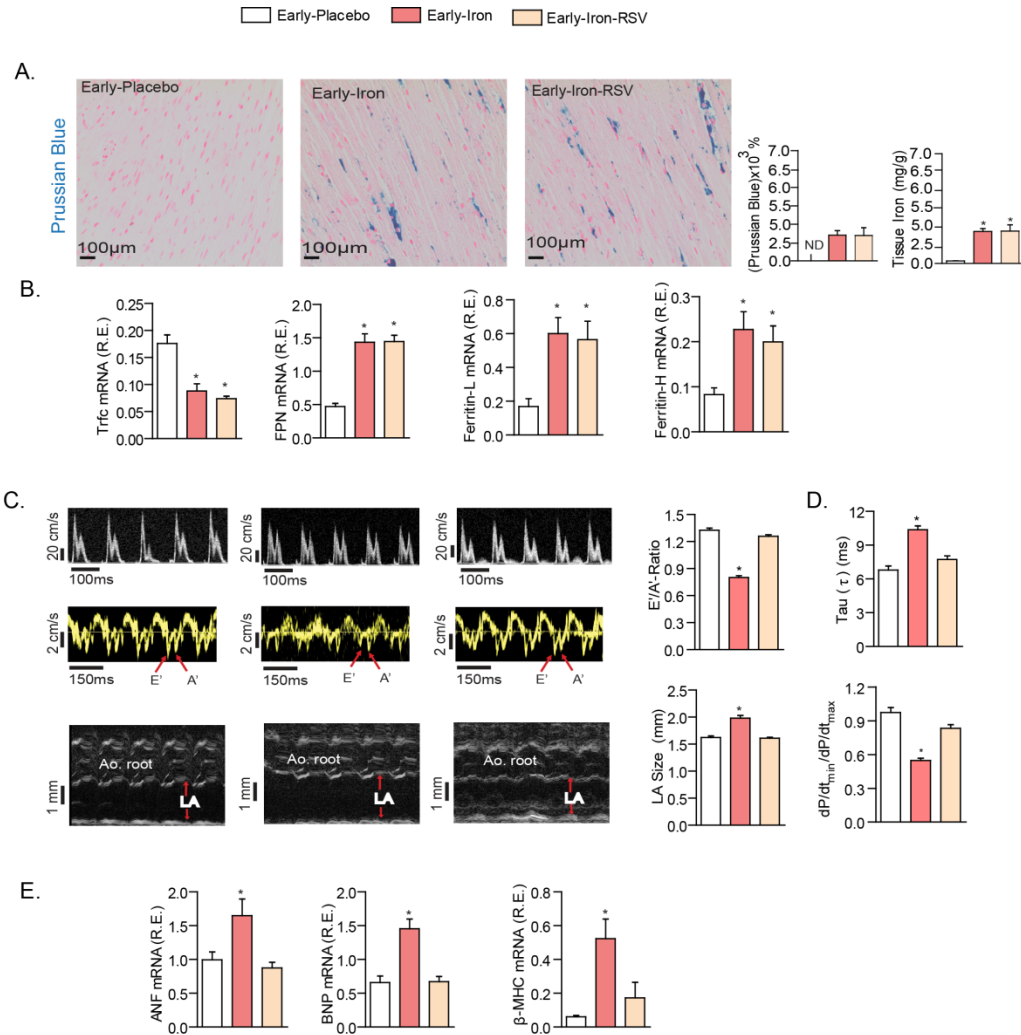


**Figure 3.2 Pathological myocardial remodeling and diastolic dysfunction in early iron-overload is completely rescued by resveratrol therapy independent of myocardial iron-deposition.** Prussian blue staining and quantification of iron deposition in early iron-overloaded mice showing myocardial iron-overload (A) and altered expression of iron metabolic genes, transferrin receptor 1 (Trfc), ferroportin (FPN), and ferritin light (L) and heavy (H) chain (B). Resveratrol did not affect myocardial iron deposition or the expression iron metabolism genes (A-B). Echocardiographic assessment of heart function illustrated by transmitral filling pattern (top panel), tissue Doppler (middle panel) and left atrial (LA) size (bottom panel) (C) showing adverse remodeling and diastolic dysfunction in early iron-overloaded wildtype mice. The invasive hemodynamic measurement revealed impaired myocardial relaxation as the primary functional abnormality (D). Resveratrol (RSV) treatment normalized the diastolic dysfunction (C-D) and the expression of myocardial disease markers (E). E'=early tissue Doppler velocity; A'=tissue Doppler due to atrial contraction; LA=left atrial; Tau=LV relaxation time constant; dP/dt=rate of change in LV pressure; ANF=atrial natriuretic factor; BNP=brain natriuretic peptide; β-MHC=beta-myosin heavy chain. n=8 for gene expression analysis; n=6 for placebo and n=8 for iron-treated groups. ND=not detected; \*p<0.05 compared with the placebo group.

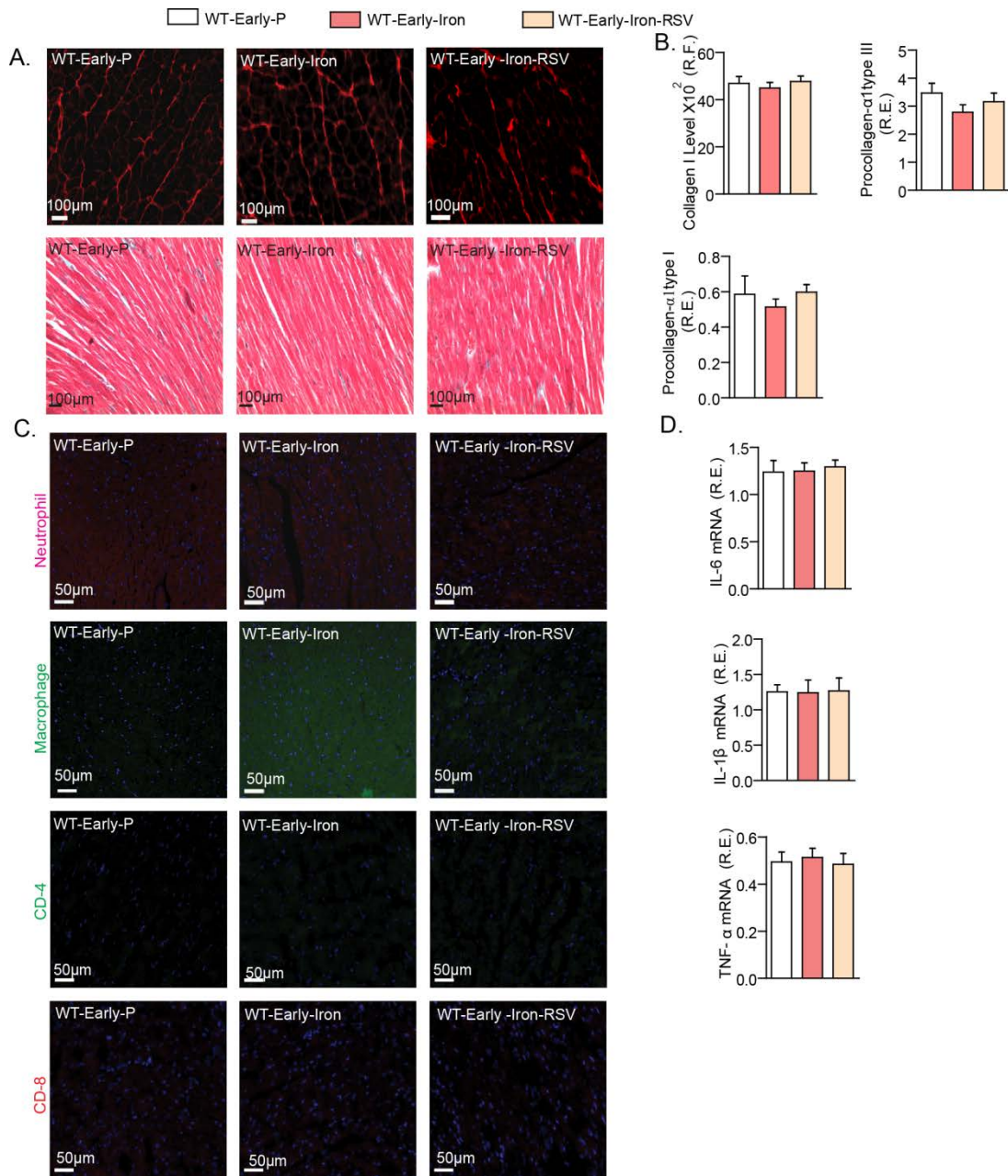


**Figure 3.2.1 Early iron-overload cardiomyopathy is not associated with any fibrosis or inflammation** (A-B) Picosirius Red (Upper panel) and Trichrome (bottom panel) (A) and collagen quantification and expression analysis of pro-collagen I  $\alpha$ 1 and pro-collagen III  $\alpha$ 1 (B) showing a lack of myocardial fibrosis in early iron-overloaded hearts. Immunohistochemical staining for neutrophil, macrophage, CD4, CD8 positive lymphocytes (C) and gene expression analysis of pro-inflammatory cytokines (D) showing a lack of myocardial inflammation in early iron-overloaded hearts. IL-6=Interleukin 6; IL-1 $\beta$ = Interleukin-1 $\beta$ ; TNF- $\alpha$ =Tumor necrosis factor- $\alpha$ . n=6 for placebo and n=8 for iron-overloaded groups.

**Table 3.2** Echocardiographic assessment of cardiac function in early iron-overloaded male WT mice

	WT+Placebo	WT+Iron	WT+Iron+Resveratrol
n	8	12	12
HR (bpm)	491±12	439±19*	463±15
E-wave (mm/s)	715±34	651±33	672±31
A-wave (mm/s)	443±17	498±18*	422±23
E/A Ratio	1.61±0.09	1.3±0.08*	1.59±0.11
IVRT (ms)	13.4±0.4	16.9±0.9*	14.1±0.3
DT (ms)	21.4±1.8	28.9±2.1*	23.5±2.4
EWDR (mm/s <sup>2</sup> )	33.4±2.1	22.5±3.4*	28.5±2.5
E' (mm/s)	31.8±3.2	24.3±2.6*	32.2±1.9
A' (mm/s)	23.6±2.1	30.2±2.3*	25.6±1.7
E' /A'	1.35±0.06	0.8±0.05*	1.26±0.05
LA Size (mm)	1.62±0.06	1.98±0.11*	1.61±0.07
E/E' (Filling pressure)	22.48±11	26.79±13	22.86±16
LVEDD (mm)	3.79±0.07	3.56±0.08	3.68±0.07
LVESD (mm)	2.54±0.06	2.35±0.07	2.41±0.06
LVFS (%)	33±1.8	34±2.2	34.5±1.9
LVEF (%)	63.1±2.2	62.9±3.3	64.1±2.1
VCFc (circ/s)	6.24±0.18	6.17±0.28	6.53±0.27
LVPWT (mm)	0.66±0.07	0.65±0.06	0.69±0.04

HR=heart rate; E=early trans-mitral filling wave; A=atrial trans-mitral filling wave; E'=early tissue Doppler velocity; A'=tissue Doppler due to atrial contraction; DT=deceleration time; IVRT=isovolumetric relaxation time; EWDR=E-wave deceleration rate; LA=left atrium; LVEDD= left ventricular end diastolic dimension; LVESD=left ventricular end systolic dimension; LVFS=left ventricular fractional shortening; LVEF=left ventricular ejection fraction; VCFc=velocity of circumferential fiber shortening; LVPWT=left ventricular posterior wall thickness; \*p<0.05 compared with all other groups.

**Table 3.3** Pressure-Volume loop assessment of cardiac function in early iron-overloaded WT mice

Parameters	WT+Placebo	WT+Iron	WT+Iron+Resveratrol
n	6	8	8
HR (bpm)	554±11	424±10*	509±14
EDP (mmHg)	2.6±0.5	7.1±0.91	3.5±0.5
ESP (mmHg)	105±3.4	78.9±5.1*	93±3.8
EDV(μl)	30±1.6	27.4±2.9	30.95±3.9
ESV (μl)	5.3±1.3	3.7±1.5	6.9±1.7
SV(μl)	25.6±0.9	23.8±3.5	23±2.6
CO (ml/min)	12.9±0.33	10.6±1.2	10.8±0.9
<b>Systolic indexes</b>			
EF (%)	83.6±3.1	84.3±5.9	79±5.4
dP/dt <sub>max</sub> (mmHg/s)	10120±204	9397±332	10440±525
SW (mJoules)	0.41±0.018	0.32±0.031	0.35±0.037
PRSW (mJoules/μl)	0.0134±0.02	0.0120±0.012	0.0120±0.09
dP/dt <sub>max</sub> /EDV(mmHg/s/μl)	333±13	318±32	307.0±23
ESPVR (mmHg/μl)	1.97±0.5	2.1±0.3	2.08±0.3
<b>Diastolic indexes</b>			
dP/dt <sub>min</sub> (mmHg/s)	9675±560	5140 ±250*	8426±207
τ (Weiss) (ms)	6.0±0.4	10.6±0.3*	6.45±0.5
τ (Glantz) (ms)	6.8±0.4	10.4±0.4*	7.8±0.4
EDPVR (mmHg/μl)	0.013±0.003	0.081±0.006*	0.017±0.002

HR=heart rate; EDP=end diastolic pressure; ESP=end systolic pressure; EDV=end diastolic volume; ESV=end systolic volume; SV=stroke volume; CO=cardiac output; EF=ejection fraction; dP/dt=rate of change in LV pressure; SW=stroke work; dP/dt<sub>max</sub>/EDV= Starling's contractile index; Tau (τ)= LV relaxation time constant; Ees=end-systolic elastance; EDPVR= end-diastolic pressure-volume relationship; \*p<0.05 compared with all other groups.

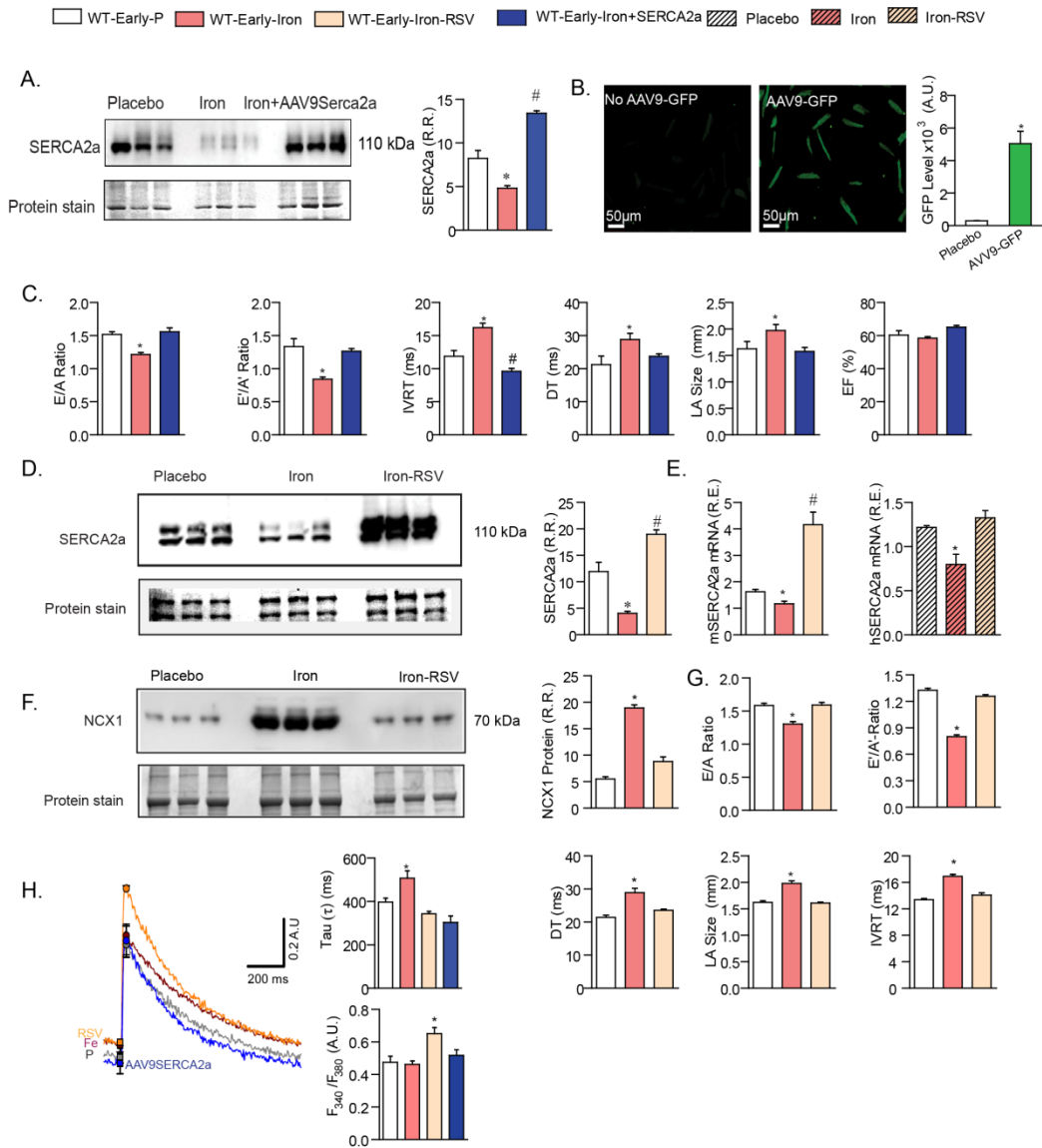


**Figure 3.2.2. Early iron-overload cardiomyopathy is driven by downregulation of SERCA2a: rescue with the adenoviral transfer of SERCA2a and resveratrol.** (A-B) Western blot analysis and quantification shows a marked decreased in myocardial SERCA2a level (A) which was prevented by *in vivo* adeno-viral gene therapy (AAV9) confirmed in isolated adult ventricular cardiomyocytes following *in vivo* AAV9 delivery of green fluorescent protein (GFP) showing a high yield of efficient gene delivery to the heart (B). Assessment of diastolic function using transthoracic echocardiography showing *in vivo* gene delivery of SERCA2 normalized the diastolic dysfunction associated with early iron-overload (C). (D-E) Western blot analysis revealed a dramatic corrective action of resveratrol (RSV) on the reduced SERCA2a levels (D) which correlated with the ability of resveratrol (RSV) to prevent iron-induced downregulation of *Serca2a* mRNA expression in mouse (m) and human (h) LV cardiomyocytes (E). (F) Western blot analysis of sodium-calcium exchanger-1 (NCX-1) showing increased levels in early iron-overload which was normalized in response to resveratrol. (G) Functional assessment of heart function showing diastolic dysfunction in early iron-overloaded wildtype mice was completely normalized by resveratrol therapy. (H) Ca<sup>2+</sup> transients in ventricular cardiomyocytes showing elevated diastolic Ca<sup>2+</sup> levels and prolongation of Ca<sup>2+</sup> decay, and correction by SERCA2a gene therapy and resveratrol. R.R.=relative ratio; R.E.=relative expression; E=early LV transmitral filling velocity; A=LV transmitral filling due to atrial contraction; DT=deceleration time; LA=left atrial; EF=ejection fraction. E<sup>2</sup>=early

tissue Doppler velocity; A'=tissue Doppler due to atrial contraction; IVRT=isovolumetric relaxation time. n=8-12 for functional studies; n=8 for expression analysis and n=3-4 for Western blot analysis. \*p<0.05 compared with all other groups; #p<0.05 compared with the placebo group.

### **Resveratrol suppressed iron-induced increased oxidative stress in cardiomyocytes and in the myocardium of murine iron-overload models**

Iron-mediated Fenton reaction leads to the formation of free radicals.<sup>77, 83, 94</sup> We isolated healthy human left ventricular cardiomyocytes and showed that exposure to iron triggered oxidative stress with increased superoxide (dihydroethidium, DHE), aldehyde (4-hydroxynonenal, 4-HNE) and nitrotyrosine levels (**Figure 3.3A-B**) which reflect reactive oxygen species, lipid peroxidation, and reactive nitrogen species, respectively. Resveratrol completely prevented the iron-mediated oxidative stress on human ventricular cardiomyocytes demonstrating its potent anti-oxidant properties (**Figure 3.3A-B**). We used a similar approach in murine ventricular cardiomyocytes and showed a conserved antioxidant response of resveratrol against iron-mediated oxidative stress (**Figure 3.3C-D**). We next investigated the *in vivo* antioxidant effects of resveratrol in murine models of iron-overload. In addition to early iron-overload, we also used a chronic acquired iron-overload model in WT mice<sup>77, 83</sup>, and importantly, we generated a chronic genetic hemochromatosis model by aging HJVKO mice fed an iron-enriched diet. Our acquired and genetic murine models of chronic iron-overload clearly demonstrated myocardial iron accumulation and altered expression of genes involved in myocardial iron homeostasis characterized by increased expression of ferritin L/H and ferroportin and decreased expression of transferrin receptor 1 (**Figure 3.3.1**). *In vivo* analysis of early and chronic acquired and genetic murine models of

iron-overload using DHE fluorescence, 4-HNE and nitrotyrosine immunostaining showed a strong increase in myocardial oxidative stress which was markedly decreased in response to resveratrol therapy (**Figure 3.3.2**). Biochemical assessment of myocardial oxidative stress showed increased oxidized glutathione (GSSG) coupled with decreased reduced glutathione (GSH) and redox ratio (**Figure 3.3.3A**) along with the generation of the lipid peroxidation product, malondialdehyde (MDA) (**Figure 3.3.3B**), consistent with iron-mediated myocardial oxidative stress. Resveratrol mediated activation of the SIRT 1 pathway<sup>165, 217, 230</sup> normalized iron-induced oxidative stress in early and chronic iron-overloaded WT hearts and chronic iron-overloaded HJVKO hearts illustrated by reduced levels of free radicals, lipid peroxidation products and increased GSH levels (**Figure 3.3.2A-D; Figure 3.3.3A-B**) which correlated with increased expression of key antioxidant genes, catalase, superoxide dismutase 1 and heme oxygenase 1 (**Figure 3.3.3C**). These results illustrate a key antioxidant effect of resveratrol against iron-induced oxidative stress at the cellular and myocardial level.

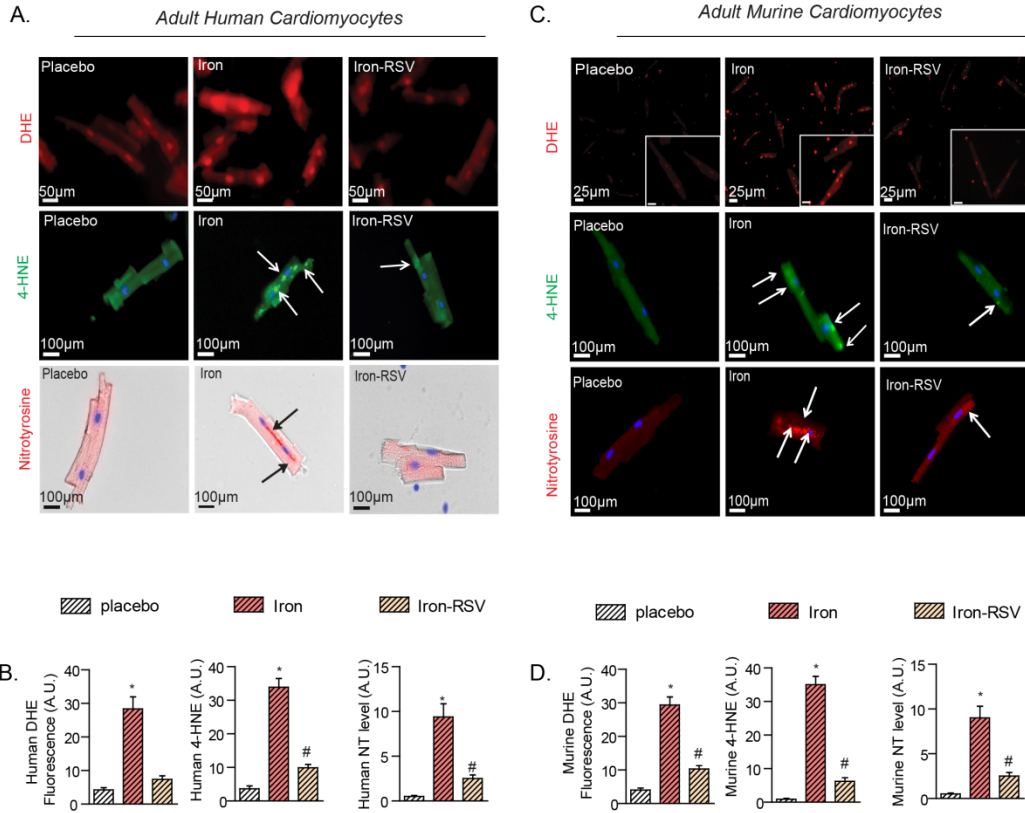


**Figure 3.3 Iron-induced pro-oxidant effects in human and murine cardiomyocytes and in murine models of iron-overload are prevented by resveratrol.** (A-B) Isolated adult LV human cardiomyocytes display a pronounced pro-oxidant phenotype after exposure to iron with increased dihydroethidium (DHE) staining for superoxide levels (top), 4-hydroxynonenal (4-HNE) immunofluorescence (middle), nitrotyrosine (NT) immunofluorescence (bottom) (A) and quantification of oxidative stress (B), while resveratrol (RSV; 100  $\mu$ M) markedly suppressed iron-induced cellular oxidative stress. (C-D) Murine LV cardiomyocytes mirrored similar responses to iron as seen in human LV cardiomyocytes and iron-mediated cellular oxidative stress as illustrated by increased DHE staining, 4-HNE and nitrotyrosine immunofluorescence (C) and quantification of oxidative stress (D) was markedly suppressed by treatment with RSV. DHE fluorescence is predominantly nuclear while 4-HNE and nitrotyrosine immunofluorescence are more diffuse and highlighted by the white arrows. n=4 for immunofluorescence analysis; n=8 for biochemical and gene expression analysis. \*p<0.05 compared with all other groups; #p<0.05 compared with the placebo group.

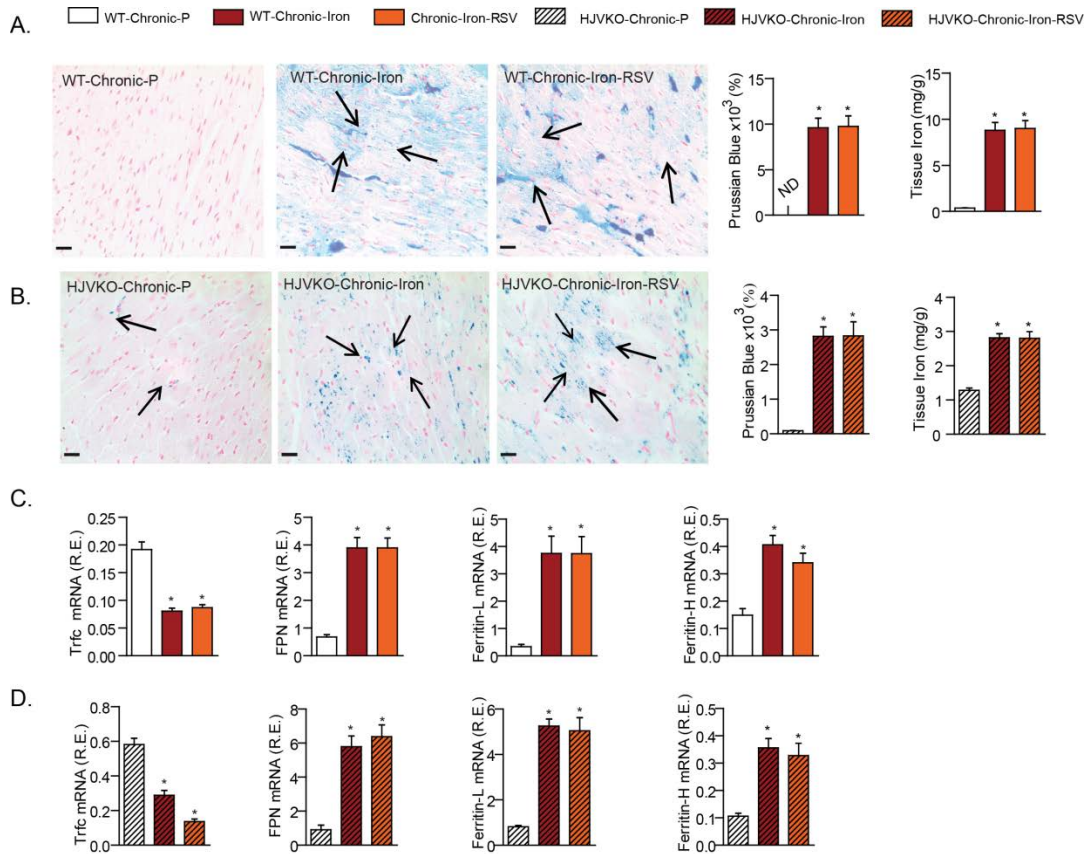


**Figure 3.3.1 Iron metabolism in wild type and hemojuvelin knockout mice. (A-B)**

Prussian Blue staining with quantification of myocardial iron levels in the hearts of chronically iron-overloaded wild type (A) and hemojuvelin knockout (B) showing myocardial iron-overload with resveratrol (RSV) having no effect on the degree of myocardial iron-overload. Myocardial gene expression analysis revealed that the heart was clearly sensitized to chronic iron injury as reflected in the altered iron metabolic gene expression in wild type (C) and HJVKO (D). Resveratrol did not alter the expression pattern of these iron metabolism genes. n=6 for placebo and n=8 for iron-treated groups. ND=not detected; \*p< 0.05 compared with the placebo group.

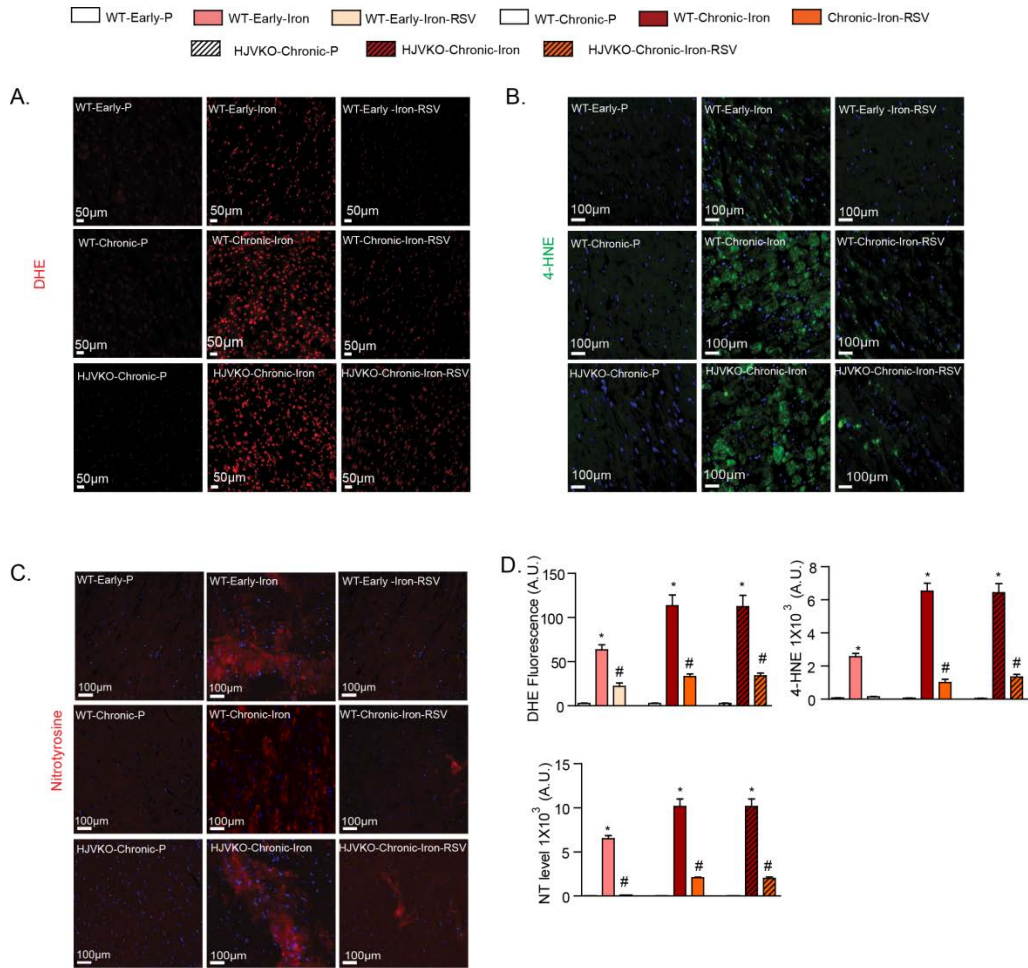


**Figure 3.3.2. Iron-induced oxidative stress in early and chronic murine models of iron-overload is prevented by resveratrol.** Dihydroethidium fluorescence, (A) 4-hydroxynonenal (4-HNE) (B) and nitrotyrosine (NT) (C) immunostaining confirmed increased myocardial oxidative stress in murine models of iron-overload and respective quantifications(D). Staining clearly showed the therapeutic effects of resveratrol. A.U.=arbitrary unit; n=4 for immunofluorescence analysis. \*p<0.05 compared with all other groups

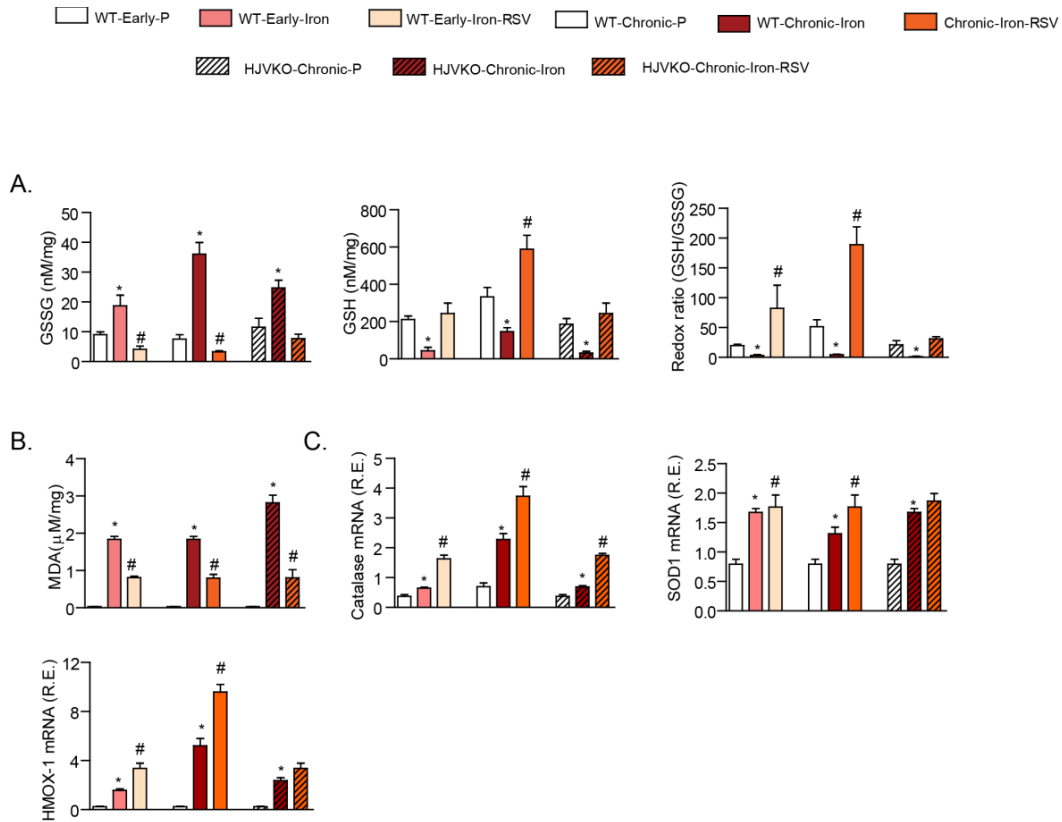


**Figure 3.3.3. Iron-induced oxidative stress in early and chronic murine models of iron-overload is prevented by resveratrol.** (A) Myocardial levels of reduced glutathione (GSH), oxidized glutathione (GSSG) and the redox ratio, and the myocardial lipid peroxidation product, malondialdehyde (MDA) (B) were altered demonstrating biochemical evidence of increased oxidative damage and reduced antioxidant reserve in early and chronic iron-overloaded hearts, markedly corrected by oral resveratrol therapy. (C) Resveratrol potentiated the upregulation of key antioxidant enzymes, catalase (CAT), superoxide dismutase 1 (SOD1) and heme oxygenase 1 (HMOX1), in early and chronic iron-overloaded hearts. R.E. relative expression; LV=left ventricle; n=8 for biochemical and expression analyses. \*p<0.05 compared with all other groups; #p<0.05 compared with the placebo group.

## **Resveratrol prevents pro-fibrotic effects in murine and human cardiofibroblasts, and iron-induced myocardial fibrosis and cardiac dysfunction**

We next examined the pro-fibrotic effects of iron and the therapeutic potential of resveratrol. To enhance the translational impact of our findings, we investigated the impact of iron on human ventricular cardiofibroblasts subjected to cyclical stretching to simulate the cardiac cycle. Exposure to iron transformed human ventricular cardiofibroblasts into an activated myofibroblast phenotype characterized by increased levels of alpha-smooth muscle actin ( $\alpha$ SMA) and collagen I, and increased expression of pro-collagen I and III, transforming growth factor beta (TGF $\beta$ ) and  $\alpha$ SMA (**Figure 3.4A-C**). Similarly, in murine ventricular cardiofibroblasts, iron-mediated pro-fibrotic gene expression changes and the increase in collagen I and III levels as also observed in murine ventricular fibroblasts (**Figure 3.4D-F**). Immunohistochemical staining for collagen I confirmed a pro-fibrotic effect of iron in human cardiofibroblasts (**Figure 3.4G**). Resveratrol prevented iron-induced activation of human and murine cardiofibroblasts illustrated by normalization of pro-fibrotic gene expression and  $\alpha$ SMA and collagen I levels (**Figure 3.4A-G**). These phenotypic changes in cardiofibroblasts are consistent with the restoration of normal SIRT1 levels coupled with co-localization with FOXO1 in these cells (**Figure 3.1D**).

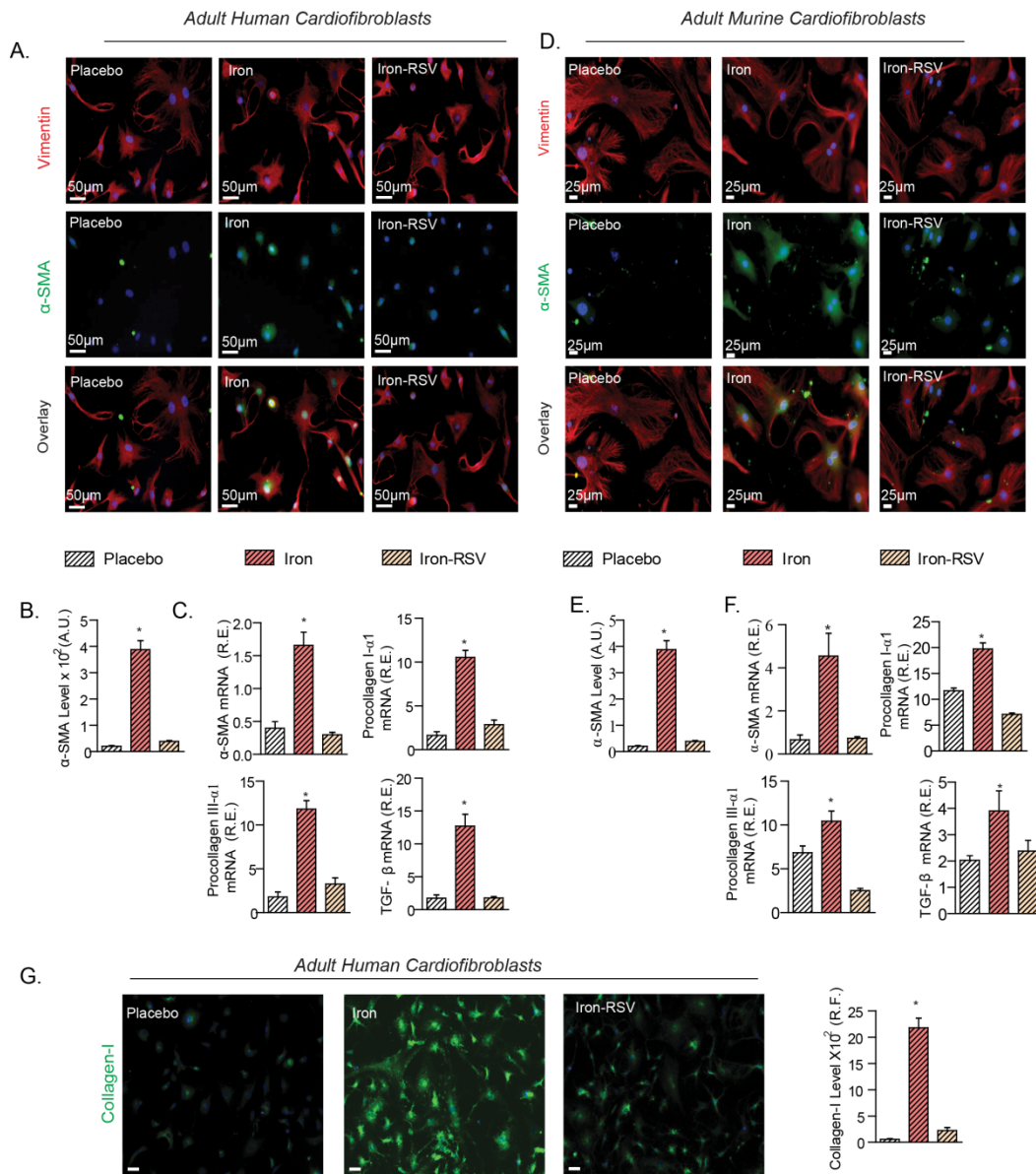


**Figure 3.4 Iron-induced profibrotic effects in human and murine cardiofibroblasts are suppressed by resveratrol.** (A-C) Cultured and cyclically stretched adult human LV cardiofibroblasts mounted a pro-fibrotic response to exposure to iron (20  $\mu\text{g}/\text{ml}$ ) resulting in increased immunostaining for alpha-smooth muscle actin ( $\alpha\text{-SMA}$ ) (A-B), and mRNA expression of  $\alpha\text{-SMA}$ , TGF $\beta$ 1, pro-collagen type III $\alpha$ 1, and pro-collagen type I $\alpha$ 1 (C) which was prevented by resveratrol (RSV; 100  $\mu\text{M}$ ). (D-F) Murine LV cardiofibroblasts cultured and cyclically stretched showed a similar pro-fibrotic response when exposed to iron (20  $\mu\text{g}/\text{ml}$ ) with increased levels of alpha-smooth muscle actin ( $\alpha\text{-SMA}$ ) (D-E) and upregulation of the expression of pro-fibrotic genes, pro-collagen I $\alpha$ 1 and III $\alpha$ 1,  $\alpha\text{-SMA}$ , TGF $\beta$ 1, was normalized in response to resveratrol (RSV) (100  $\mu\text{M}$ ) (F). (G) Human cardiofibroblasts also showed increased collagen I levels in response to iron (20  $\mu\text{g}/\text{ml}$ ) which was largely prevented by resveratrol treatment. A.U.=arbitrary unit; R.E.=relative expression; R.F.=relative fraction;  $\alpha\text{-SMA}$ =alpha smooth muscle actin; TGF $\beta$ 1=transforming growth factor beta1; n=4 for immunofluorescence analysis; n=8 for expression analysis. \*p<0.05 compared with all other groups

Chronic iron-overload *in vivo* resulted in marked increase in myocardial interstitial and perivascular fibrosis (**Figure 3.4.1A-C**), along with increased pro-collagen I and III mRNA and with increased collagen I and III levels protein levels (**Figure 3.4.1D-E**) in the absence of myocardial inflammation (**Figure 3.4.2A-C**). Resveratrol therapy resulted in marked suppression of myocardial fibrosis *in vivo*, consistent with its *in vitro* anti-fibrotic effects. Interestingly, increased expression of myocardial disease markers, ANF, BNP and  $\beta$ -MHC were also all rescued by resveratrol treatment in chronic iron-overloaded wildtype and HJVKO hearts (**Figure 3.4.1F**). These results are consistent with a primary and direct pro-fibrotic effect of iron-overload on cardiofibroblasts as the primary trigger of the increased myocardial fibrosis in chronic iron-overload. Importantly, the functional analysis showed that the severe diastolic dysfunction in chronic iron-overload hearts was completely rescued by resveratrol therapy based on echocardiography (**Figure 3.4.3A-C; Tables 3.4-3.5**) and invasive pressure-volume loop hemodynamic analysis (**Figure 3.4.3D-E; Tables 3.6-3.7**). In particular, end-diastolic pressure volume relationship, a relatively load-independent index of myocardial stiffness, was markedly increased in response to chronic iron-overload and corrected by resveratrol therapy (**Figure 3.4.3D-E; Tables 3.6-3.7**). Our results demonstrate that chronic iron-overload results in increased myocardial fibrosis as a key driver of heart disease and resveratrol mediates a pronounced therapeutic effect against iron-induced pro-fibrotic effects.

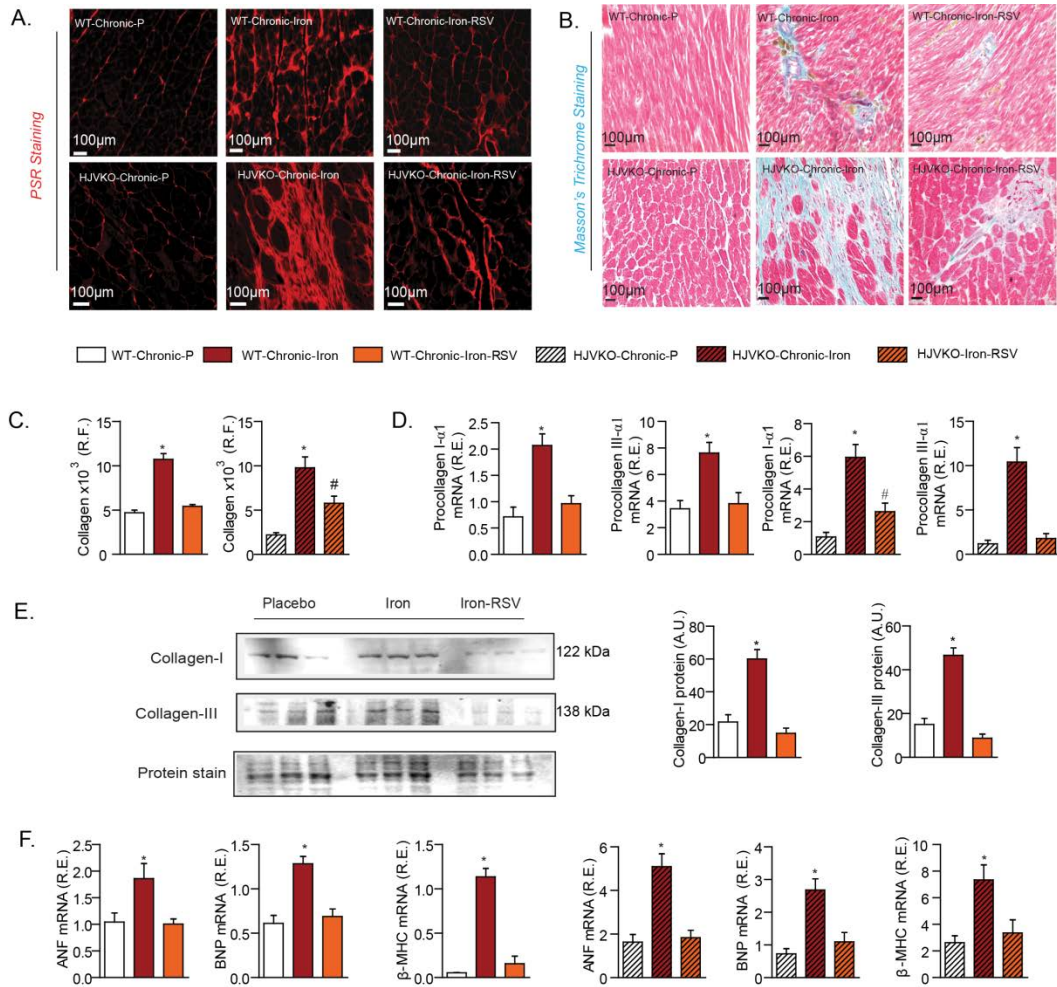


**Figure 3.4.1. Increased myocardial fibrosis associated with chronic iron-overload cardiomyopathy is completely rescued by resveratrol therapy.** (A-C) Histological assessment of myocardial fibrosis using picro-sirius red (PSR) (A) and Masson's trichrome (B) staining and quantification of fibrosis (C) revealed increased myocardial interstitial and perivascular fibrosis in the chronic iron-overloaded hearts. Expression analysis of myocardial pro-collagen I $\alpha$ 1 and pro-collagen III $\alpha$ 1 (D) and Western blot analysis of myocardial collagen I and collagen III levels (E) in chronic iron-overloaded hearts revealed increased levels consistent with a pro-fibrotic state. Resveratrol therapy prevented the increased in myocardial fibrosis based on histological, gene expression and Western blot analysis (A-E). Expression analysis of myocardial disease markers in chronic iron-overload models showing a complete normalization of the expression of disease markers in response to resveratrol therapy (F). A.U.=arbitrary unit; R.E.=relative expression; R.F.=relative fraction; ANF=atrial natriuretic factor; BNP=brain natriuretic peptide;  $\beta$ -MHC=beta-myosin heavy chain. n=4 for histological analyses; n=6 for Western blot and n=8 for expression analyses. \*p<0.05 compared with all other groups; #p<0.05 compared with the placebo group.

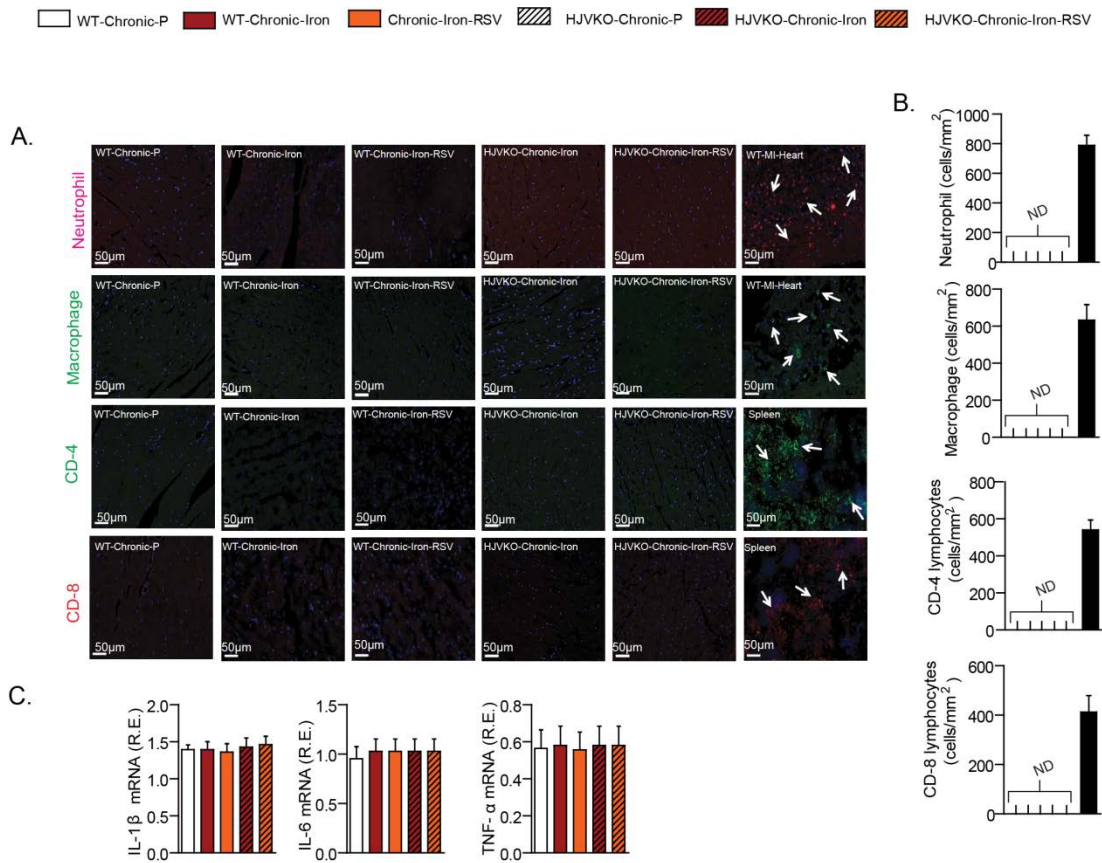


**Figure 3.4.2. Lack of inflammation associated with chronic iron-overload cardiomyopathy . (A-C)** Histological assessment of myocardial inflammation (A) and quantification of inflammation (B) Expression analysis of myocardial inflammatory disease markers in chronic iron-overload models showing a lack of inflammation (C) A.U.=arbitrary unit; R.E.=relative expression; histological analyses and n=8 for expression analyses. \*p<0.05 compared with all other groups; #p<0.05 compared with the placebo group.

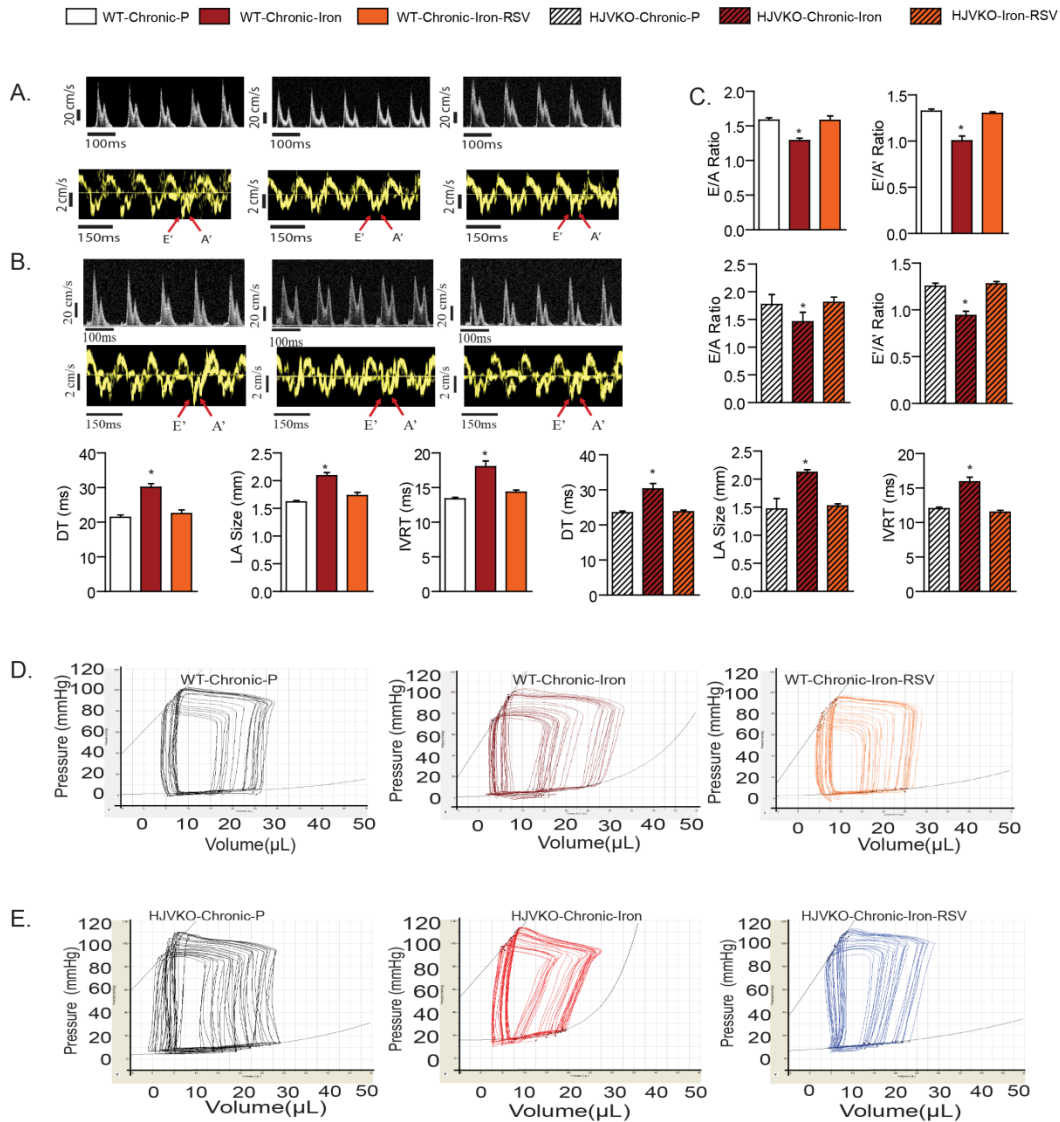


**Figure 3.4.3 Resveratrol therapy completely rescued the cardiac dysfunction in chronic iron-overloaded wildtype and hemojuvelin knockout mice.** Echocardiographic assessment of heart function with transmittal filling pattern (top panel) and tissue Doppler (bottom panel) illustrating diastolic dysfunction in chronic iron-overloaded wild-type mice (A) and hemojuvelin knockout (HJVKO) mice (B) and quantification (C) of the echocardiographic assessment showing diastolic dysfunction. Resveratrol (RSV) treatment completely normalized the diastolic dysfunction in wildtype and HJVKO models of chronic iron-overload (A-C). Invasive hemodynamic assessment illustrated by representative pressure-volume tracings confirming load-independent diastolic dysfunction in chronic iron-overloaded wildtype mice (D) and HJVKO mice (E). E=early LV transmittal filling velocity; A=LV transmittal filling due to atrial contraction; E'=early tissue Doppler velocity; A'=tissue Doppler due to atrial contraction; DT=deceleration time; LA=left atrial; IVRT=isovolumetric relaxation time. n=8 for the placebo groups and n=10-12 for the iron-treated groups. \*p<0.05 compared with all other groups; #p<0.05 compared with the placebo group.

**Table 3.4.** Echocardiographic assessment of cardiac function in chronically iron-overloaded male WT mice

	WT+Placebo	WT+Iron	WT+Iron+Resveratrol
n	8	12	12
HR (bpm)	493±13	397±10*	441±14 <sup>#</sup>
E-wave (mm/s)	706±34	628±33	713±26
A-wave (mm/s)	438±17	375±13*	451±26
E/A Ratio	1.61±0.09	1.67±0.11	1.58±0.11
IVRT (ms)	13.8±0.4	18.2±0.9*	14.3±0.3
DT (ms)	21.9±2.1	30.1±1.8*	22.5±2.2
EWDR (mm/s <sup>2</sup> )	32.2±2.1	20.9±2.7*	31.7±2.4
E' (mm/s)	30.4±2.5	22.7±1.6*	34±2.7
A' (mm/s)	24.3±1.9	22.8±1.4	25.8±2.1
E'/A' Ratio	1.25±0.06	1±0.05*	1.31±0.07
LA Size (mm)	1.62±0.05	2.09±0.07*	1.73±0.06
LVEDD (mm)	3.92±0.06	2.49±0.05	2.44±0.05
LVESD (mm)	2.53±0.06	2.49±0.05	2.44±0.05
LVFS (%)	35.5±1.7	35.1±2.3	37.9±1.8
LVEF (%)	64.1±2.4	63.7±3.1	66.1±2.3
VCF <sub>c</sub>	6.31±0.15	6.37±0.23	6.42±0.24
LVPWT (mm)	0.71±0.05	0.69±0.06	0.7±0.06

HR=heart rate; E=early trans-mitral filling wave; A=atrial trans-mitral filling wave; E'=early tissue Doppler velocity; A'=tissue Doppler due to atrial contraction; DT=deceleration time; IVRT=isovolumetric relaxation time; EWDR=E-wave deceleration rate; LA=left atrium; LVEDD= left ventricular end diastolic dimension; LVESD=left ventricular end systolic dimension; LVFS=left ventricular fractional shortening; LVEF=left ventricular ejection fraction; VCF<sub>c</sub>=velocity of circumferential fiber shortening; LVPWT=left ventricular posterior wall thickness; \*p<0.05 compared with all other groups; #p<0.05 compared with the WT+Iron group.

**Table 3.5** Echocardiographic assessment of cardiac function in chronically iron-overloaded male HJV knockout mice

	HJVKO+Vehicle	HJVKO+Iron+Placebo	HJVKO+Iron+Resveratrol
n	8	12	12
HR (bpm)	461±15	453±11	441±14
E-wave (mm/s)	636±31	679±39	587±20
A-wave (mm/s)	363±19	526±26*	331±23
E/A Ratio	1.75±0.09	1.29±0.12*	1.77±0.11
IVRT (ms)	12.8±0.5	13.5±0.8	11.8±0.6
DT (ms)	23.4±2.3	30.4±2.2*	23.8±1.9
EWDR (mm/s <sup>2</sup> )	27.2±2.2	22.3±2.4*	24.6±2.3
E' (mm/s)	31.4±2.6	26±1.2	26.1±1.3
A' (mm/s)	25±1.5	27.8±1.8	20.5±0.8
E' /A'	1.25±0.06	0.94±0.05	1.27±0.09
LA Size (mm)	1.47±0.07	2.12±0.08*	1.53±0.07
LVEDD (mm)	3.81±0.08	3.99±0.14	3.74±0.09
LVESD (mm)	2.47±0.07	2.61±0.08	2.43±0.06
LVFS (%)	35.3±1.8	34.6±2.2	35.1±2.1
LVEF (%)	62.9±2.3	63.9±3	64.3±2.6
VCFc (circ/s)	6.39±0.14	6.44±0.21	6.52±0.24
LVPWT (mm)	0.71±0.05	0.96±0.05*	0.7±0.04
HW/TL (gm/mm)	0.075 ± 0.007	0.13 ± 0.015*	0.095 ± 0.013

HR=heart rate; E=early trans-mitral filling wave; A=atrial trans-mitral filling wave; E'=early tissue Doppler velocity; A'=tissue Doppler due to atrial contraction; DT=deceleration time; IVRT=isovolumetric relaxation time; EWDR=E-wave deceleration rate; LA=left atrium; LVEDD= left ventricular end diastolic dimension; LVESD=left ventricular end systolic dimension; LVFS=left ventricular fractional shortening; LVEF=left ventricular ejection fraction; VCFc=velocity of circumferential fiber shortening; LVPWT=left ventricular posterior wall thickness; \*p<0.05 compared with all other groups; #p<0.05 compared with other HJVKO groups.

**Table 3.6** Pressure-Volume loop assessment of cardiac function in chronically iron-overloaded male WT mice

Parameters	WT+Placebo	WT+Iron	WT+Iron+Resveratrol
n	6	8	8
HR (bpm)	540±2.9	398±7.5*	474.1±19
EDP (mmHg)	2.9±0.4	12±0.9*	7.1±0.4
ESP (mmHg)	88±1.3	96±1.5*	87±2.9
EDV(μl)	25±1.0	26.7±2.0	25.7±1.3
ESV (μl)	6.9±0.8	6.6±0.8	7.2±0.9
SV(μl)	17.9±0.4	18.1±1.8	18.08±1.2
CO (ml/min)	9.8±0.3	7.7±0.7*	9.4±0.9
<b>Systolic indexes</b>			
EF (%)	73.9±2.2	70.1±2.6	71.9±3.7
dP/dt <sub>max</sub> (mmHg/s)	8849±110	8633±172	8373±301
SW (mJoules)	0.27±0.009	0.26±0.021	0.27±0.03
PRSW (mJoules/μl)	0.011±0.008	0.010±0.11	0.011±0.023
dP/dt <sub>max</sub> /EDV(mmHg/s/μl)	342±22	340±36	363±31
ESPVR (mmHg/μl)	3.3±0.6	3.6±0.5	3.6±0.6
<b>Diastolic indexes</b>			
dP/dt <sub>min</sub> (mmHg/s)	7900±309	6693±83.17*	7415±363.7
τ (Weiss) (ms)	6.2±0.095	7.7±0.19*	6.7±0.39
τ (Glantz) (ms)	8.8±0.36	11.21±0.38*	8.5±0.42
EDPVR (mmHg/μl)	0.021±0.008	0.082±0.019*	0.039± 0.013

HR=heart rate; EDP=end diastolic pressure; ESP=end systolic pressure; EDV=end diastolic volume; ESV=end systolic volume; SV=stroke volume; CO=cardiac output; EF=ejection fraction; dP/dt=rate of change in LV pressure; SW=stroke work; dP/dt<sub>max</sub>/EDV= Starling's contractile index; Tau (τ)= LV relaxation time constant; Ees=end-systolic elastance; EDPVR= end-diastolic pressure-volume relationship; \*p<0.05 compared with all other groups.

**Table 3.7** Pressure-Volume loop assessment of cardiac function in chronically iron-overloaded male HJV knockout mice

Parameters	HJVKO+Vehicle	HJVKO+Iron+Placebo	HJVKO+Iron+Resveratrol
n	6	8	8
HR (bpm)	431±8	426±9	443±14
EDP (mmHg)	9.86±1.43	16.2±1.95*	8.86±1.53
ESP (mmHg)	103±6.1	106.7±7.4	110.3±6.3
EDV(μl)	22.5±2.8	24.7±2.6	23.7±2.2
ESV (μl)	4.36±1.72	4.7±1.38	4.12±0.72
SV(μl)	18.2±1.7	20±1.9	19.9±2.1
CO (ml/min)	8.67±0.22	8.52±0.26	8.84±0.23
<b>Systolic indexes</b>			
EF (%)	79.1±3.8	80.4±5.3	83.7±5.1
dP/dt <sub>max</sub> (mmHg/s)	9637±135	9201±149	9781±172
SW (m Joules)	0.341±0.062	0.382±0.049	0.393±0.056
PRSW (m Joules/μl)	0.016±0.023	0.016±0.019	0.017±0.026
dP/dt <sub>max</sub> /EDV (mmHg/s/μl)	428±31	372±45	413±37
ESPVR (mmHg/μl)	3.14±0.35	3.08±0.29	3.75±0.32
<b>Diastolic indexes</b>			
dP/dt <sub>min</sub> (mmHg/s)	8003±177	8228±156	8740±303
τ (Weiss) (ms)	7.11±0.65	9.72±0.41*	7.22±0.46
τ (Glantz) (ms)	9.23±0.41	13.7±0.32*	9.49±0.49
EDPVR (mmHg/μl)	0.017±0.006	0.112±0.013*	0.014±0.005

HR=heart rate; EDP=end diastolic pressure; ESP=end systolic pressure; EDV=end diastolic volume; ESV=end systolic volume; SV=stroke volume; CO=cardiac output; EF=ejection fraction; dP/dt=rate of change in LV pressure; SW=stroke work; dP/dt<sub>max</sub>/EDV= Starling's contractile index; Tau (τ)= LV relaxation time constant; Ees=end-systolic elastance; EDPVR= end-diastolic pressure-volume relationship; \*p<0.05 compared with all other groups.

### 3.5 Discussion

Therapeutic options for iron-overload cardiomyopathy are limited and there is a clear and urgent need for better therapies to curtail its high degree of mortality and morbidity.<sup>57, 60, 74</sup> Our acquired and genetic murine models of iron-overload recapitulate essential features of clinical iron-overload and its associated heart disease. The therapeutic effects of resveratrol prevented and rescued iron-induced oxidative stress and profibrotic effects in both acquired and genetic models of iron-overload at early and chronic stages of iron-overload cardiomyopathy. Notably, iron-induced oxidative stress in human cardiomyocytes and cardiofibroblasts was completely prevented by resveratrol directly supporting a possible therapeutic effect in patients with iron-overload. We showed that resveratrol therapy prevents and rescues the iron-induced pathological events including  $\text{Ca}^{2+}$  dysregulation, oxidative stress and myocardial fibrosis. Hemojuvelin knockout (HJVKO) mice, a pre-clinical model of juvenile hemochromatosis (type 2 primary hemochromatosis)<sup>13, 51</sup>, are resistant to iron-induced end-organ pathology<sup>51, 53</sup> requiring the use of an iron-enriched diet and aging in order to elucidate significant heart disease. The myocardial iron levels obtained in our murine models (2.5-10 mg/g LV dry weight) are similar to myocardial iron levels (3.5-9.2 mg/g dry LV weight) reported in patients with iron-overload cardiomyopathy and heart failure<sup>76</sup>. In HJVKO mice, resveratrol therapy was used following 3 months of iron-overload providing further evidence that resveratrol therapeutic effects are not blunted by pre-existing iron-overload.

We identified the SIRT1/FOXO1 pathway as clearly altered in the heart in response to iron-overload and resveratrol is a natural polyphenol with a unique ability to activate

SIRT1 and has key anti-oxidant properties. Deacetylation of FOXOs by SIRT1 protects cellular function during stress conditions and SIRT1 deacetylates FOXO1 and facilitates its nuclear translocation<sup>230</sup>. Resveratrol is a natural polyphenol with antioxidant and metabolic properties due partly to its ability to activate SIRT1<sup>165, 217, 219, 220, 240</sup>. SIRT1 deacetylates a variety of proteins and regulates genomic integrity, inflammatory responses, mitochondrial function and stress resistance<sup>217, 218</sup>. Resveratrol therapy resulted in reduced acetylation of myocardial nuclear FOXO1 in response to iron-overload providing a key molecular basis for resveratrol therapeutic action. The altered redox state of iron-overload coupled with the redox-sensitivity of SIRT1 deacetylase activity likely created a unique environment whereby the therapeutic effects of resveratrol are enhanced. We used high doses of oral resveratrol therapy (240-320 mg/kg body weight) in our *in vivo* experiments to ensure adequate bioavailability. Resveratrol used at 300 mg per kg body weight showed no detrimental effects in rats<sup>241</sup> and a dose of 320 mg per kg was associated with protection from pressure-overload induced heart failure in mice<sup>179</sup>. Given the detrimental effects of iron-overload on mitochondrial function<sup>94</sup> therapeutic effects of resveratrol on mitochondria possibly via AMPK activation<sup>174</sup> may also contribute to its beneficial effects in iron-overload cardiomyopathy. Moreover, our experimental design cannot distinguish between resveratrol therapeutic effects via SIRT1 modulation versus a direct antioxidant action.

Heart disease is a characteristic feature of iron-overload and is associated with diastolic dysfunction and a late-stage dilated cardiomyopathy.<sup>60, 74, 77</sup> Diastolic function depends on two major components, active relaxation and passive stiffness of the myocardium.

We showed that early stage of iron-overload induced selective diastolic dysfunction with reduced *Serca2a* mRNA and protein levels leading to abnormal  $\text{Ca}^{2+}$  cycling. SERCA2a is the dominant mediator of  $\text{Ca}^{2+}$  re-uptake and reduced SERCA2a function impairs myocardial relaxation leading to diastolic dysfunction<sup>221, 222</sup>, a phenotype similar to the early iron-overloaded hearts. Importantly, adenoviral gene therapy mediated correction of SERCA2a normalized the abnormal  $\text{Ca}^{2+}$  cycling and diastolic dysfunction. Iron-induced suppression of SERCA2 expression in murine and human cardiomyocytes was prevented by resveratrol resulting in the preservation of SERCA2a protein levels, restoration of normal diastolic function and alleviation of heart disease in early iron-overloaded hearts. Oxidative stress has been linked to decreased SERCA2a activity(Ref-40) with a key role of the SUMOylation pathway.<sup>242, 243</sup> While both N-acetylcysteine (NAC) and RSV are well-known antioxidants, their mechanisms of action on preserving SERCA2a function are different. N-acetylcysteine prevents oxidative damage to SERCA2a<sup>244</sup> likely by modulating reduced glutathione levels while we have shown that RSV increased SERCA2a mRNA and protein levels. In contrast to early iron-overload, chronic iron-overloaded hearts displayed marked adverse remodeling of the extracellular matrix with increased interstitial and perivascular fibrosis leading to diastolic dysfunction characterized by increased passive myocardial stiffness. Resveratrol had a marked anti-fibrotic effect in cultured murine and human cardiofibroblasts and prevented myocardial fibrosis and heart disease in both acquired and genetic models of chronic iron-overload. Iron-induced oxidative stress depletes the intrinsic antioxidant capacity and leads to the formation of aggressive free radicals which impair normal cellular function. Iron-overload is

associated with oxidative stress and lipid peroxidation which is a key driver of the progression of end-organ injury.<sup>77, 83</sup> The potentiation of the increased expression of antioxidant genes in response to RSV therapy likely contributed to the enhanced antioxidant response in the setting of iron-overload.

### **3.6 Conclusion:**

In summary, our murine models of acquired and genetic iron-overload resulted in iron-overload cardiomyopathy with resveratrol supplementation having multiple beneficial effects. Further experimental work is needed to establish a proper dose-response relationship with resveratrol and the impact of concomitant iron-chelation therapy. We propose that dietary intake of resveratrol represents a readily available and economically feasible therapy to prevent the progression of iron-induced injury and reduce the global clinical burden of iron-overload cardiomyopathy.

# CHAPTER FOUR

**Advanced iron-overload cardiomyopathy in a genetic murine model  
is rescued by resveratrol therapy.**

Subhash K. Das<sup>1,2</sup>, Pavel Zhabyeyev<sup>1,2</sup>, Ratnadeep Basu<sup>1,2</sup>, Vaibhav B. Patel<sup>1,2</sup>, Jason R. B.  
Dyck<sup>5</sup>, Zamaneh Kassiri<sup>2,3</sup>, and Gavin Y. Oudit<sup>1,2</sup>

<sup>1</sup>Division of Cardiology, Department of Medicine, <sup>2</sup>Mazankowski Alberta Heart Institute,  
<sup>3</sup>Department of Physiology, University of Alberta, <sup>5</sup>Departments of Pediatrics and  
Pharmacology, University of Alberta, Edmonton, Canada

Running Title: Iron-overload cardiomyopathy is rescued by resveratrol

**Keywords:** iron-overload, heart failure, oxidative stress, fibrosis, cardiomyopathy, heart disease,

**A modified version of this chapter has been submitted for reviewing to**

***Circulation heart failure* journal**

## 4.1 Abstract

**Background:** Iron-overload cardiomyopathy is a worldwide epidemic and is a major co-morbidity in patients with genetic hemochromatosis. The prevalence of hereditary hemochromatosis is increasing epidemic levels and Juvenile hemochromatosis is an autosomal iron metabolic disorder associated with a progressive increase in body iron stores in different body parts such as heart, liver. We investigated the therapeutic effects of resveratrol in aged genetic models of iron-overload cardiomyopathy.

**Methods and Results:** We treated male hemojuvelin knockout mice at the age of 4 weeks until they were 1 year with high iron diet (Prolab<sup>®</sup>RHM 3000 with iron 380 ppm). Aged hemojuvelin knockout murine models of genetic iron-overload showed cardiac iron-overload, increased oxidative stress, and myocardial fibrosis resulting in heart disease. Our aging studies with the hemojuvelin knockout (HJVKO) mice revealed progressive heart disease resulting in advanced iron-overload cardiomyopathy and recapitulates iron-overload cardiomyopathy in humans. Echocardiography and invasive pressure-volume loop analysis revealed a complete normalization of iron-overload mediated diastolic and systolic dysfunction in response to resveratrol therapy. Myocardial SERCA2a levels were reduced in iron-overloaded hearts and resveratrol therapy restored SERCA2a levels, besides we also found AMPK activation upon resveratrol administration. Iron-mediated oxidative stress and myocardial fibrosis were suppressed by resveratrol treatment.

**Conclusions:** Resveratrol represents a feasible therapeutic intervention to reduce the global burden from iron-overload cardiomyopathy at advanced stages of iron-overload.

## 4.2 Introduction

The prevalence of hereditary hemochromatosis is increasing to epidemic levels.<sup>3, 4, 7, 45, 46</sup> Juvenile hemochromatosis is a type 2 primary hemochromatosis with an autosomal iron metabolic disorder associated with a progressive increase in iron stores in different body parts such as heart, liver, and endocrine glands, due to a mutation in hemojuvelin, a bone morphogenetic co-receptor protein required for hepcidin expression.<sup>1, 3, 13, 50, 52, 53, 72</sup> Hepcidin acts as a major regulator of systemic iron homeostasis and prevents excess gastrointestinal iron absorption.<sup>17, 41, 46</sup> Type 2 primary hemochromatosis associated with reduced hepcidin expression, results in irregular gastrointestinal iron absorption that leads to iron-overload pathophysiology.<sup>149</sup> It is well documented that during iron-overloaded conditions L- and T-type calcium channels of cardiomyocytes allow iron to enter and that results in abnormal cardiac iron metabolism and cardiac iron-overload.<sup>32, 70, 75, 77, 80</sup> Excess cardiac iron produces transferrin saturation and non-transferrin bound iron (NTBI) formation in heart.<sup>78, 79, 245</sup> NTBI is highly toxic and leads to oxidative free radical formation via Fenton chemistry.<sup>78, 82</sup>

Iron-induced myocardial oxidative stress is a key driver in the progression of iron-overload cardiomyopathy pathogenesis.<sup>70, 74, 82, 83</sup> Progressive myocardial iron retention is associated with diastolic dysfunction at an early stage,<sup>91</sup> however as time progresses, leads to end stage dilated cardiomyopathy with diastolic and systolic dysfunction.<sup>72, 74, 246</sup> However, a pre-clinical model recapitulating iron-overload cardiomyopathy in human is lacking. We used the male HJVKO murine model which recapitulates type 2 primary hemochromatosis, and we aged these mice with dietary iron-overload to understand the

fundamental basis of iron-overload cardiomyopathy and suitable therapy with resveratrol as treatment.

Our results demonstrate that myocardial oxidative stress, fibrosis, and calcium cycling defects drive severe cardiomyopathy with diastolic and systolic dysfunction during the advanced stage of iron-overload. Resveratrol antioxidant supplementation reduces iron induced myocardial oxidative stress and rescues the progression of heart failure. Resveratrol dietary supplement presents a potential therapeutic intervention to reduce advanced iron-overload cardiomyopathy.

### **4.3 Methods**

**Experimental Animal Protocols.** Male HJV knockout mice (*HVJ<sup>-/-</sup>*) (kindly provided by Dr. Nancy C. Andrews, Duke University) were bred in-house at the University of Alberta Health Sciences Laboratory Animal Services housing facility. We performed advanced iron overload protocol by feeding 4 weeks old HJVKO mice with high iron diet<sup>51</sup> (Prolab<sup>®</sup>RHM 3000 with iron 380 ppm) until they were 1 year old. We also examined the effects of resveratrol on the 1-year-old iron-overloaded HJVKO mice by daily oral gavage (240 mg/kg/day) for three months starting at 9 months of age.<sup>91</sup> Resveratrol was dissolved in 5.4% ethanol/corn oil.<sup>247-249</sup> The placebo control groups received 5.4% ethanol/corn oil.

**Echocardiography and Invasive Hemodynamic analysis.** Transthoracic echocardiography was performed at early, chronic and advanced stages of iron-overload phenotype mice with the Vevo770 high resolution imaging system equipped with a 30-MHz transducer (Visual Sonic Vevo 770) by using 0.8% isoflurane.<sup>91, 179, 223, 226, 250</sup> PV loop analysis was done by using 1.2F Scisense catheter connected to an amplifier (TCP-500

Scisense Inc.) as previously described.<sup>91, 226</sup> Following baseline PV measurements, transient inferior vena cava occlusion was performed to obtain the alteration in venous return to derive end-diastolic pressure volume relationship; transient infra-renal aorta occlusion was used to derive the end-systolic pressure volume relationship.<sup>91, 226</sup>

**Quantitative Magnetic Resonance.** The body composition (fat mass, lean mass, free water and total water) was assessed by using an Echo MRI-900 (Echo Medical Systems, Houston, TX), as described previously.<sup>250, 251</sup>

**Histology.** Mice were anesthetized, and the hearts (arrested in diastole by using 1M KCl) were removed and fixed in 10% buffered formalin, and embedded in paraffin. 5- $\mu$ m thin sections were stained with Prussian blue, picro-Sirius red (PSR) and trichrome stain for morphometric analysis. The 5- $\mu$ m tissue sections were deparaffinized in xylene and alcohol grades, then rehydrated in water and subjected to respective staining protocol as described previously.<sup>77, 83, 91, 226</sup> Iron-depositions were visualized as blue depositions using bright field microscope. Fibrosis pattern was evaluated by using PSR staining followed by visualization under Olympus IX81 microscope and image analysis using MetaMorph software.<sup>91, 226</sup>

**Immunofluorescence.** Immunofluorescence (IF) was performed on 5- $\mu$ m thick formalin fixed and OCT embedded heart sections. Briefly, formalin fixed paraffin embedded sections were subjected to deparaffinization and respective antigen retrieval procedures followed by blocking with blocking buffer (1% BSA in 1X PBS) for 1 hr. Similarly, OCT embedded sections were fixed with 4% paraformaldehyde for 20 min and rehydrated in 1X PBS for 30 min. Sections were then incubated with primary antibody against rat anti-mouse neutrophil (Serotec), rat anti-mouse F4/80 (Serotec), mouse anti-nitrotyrosine (Santa Cruz),

mouse anti-4-HNE (Abcam), overnight in a humidified chamber at 4<sup>0</sup>C. Sections were incubated with different fluorophore conjugated secondary antibodies (Invitrogen USA) as described previously.<sup>91</sup>

**Measurement of Lipid Peroxidation and Glutathione levels (GSH/GSSG).** The levels of malondialdehyde (MDA), an indicator of lipid peroxidation, were measured in myocardial tissue (100-150mg) by using a commercially available kit (Bioxytech, MDA-586TM assay, Oxis International Inc., Foster City, CA. Myocardial reduced (GSH) as well as oxidized glutathione (GSSG) levels were measured as described previously.<sup>91, 128, 228</sup>

**Tissue Iron Levels.** 20 mg frozen tissue from LV were subjected to inductive coupled plasma resonance mass spectrometry to quantify tissue iron level in the Trace Metals Laboratory, London, Western Ontario. The samples were analyzed in triplicate and the average values are used.<sup>77, 83, 91</sup>

**Taqman real-time PCR.** mRNA expression levels were studied in iron-overload hearts and cells, by real-time PCR using Taqman primers and probes (see **Table 4.1** for primers and probes). Total RNA was extracted from flash frozen LV-tissue by using TRIzol RNA extraction method.<sup>91, 223, 226</sup> 1µg of RNA was subjected to reverse transcription to synthesize cDNA. Samples were loaded in triplicate and the data was analyzed by Light cycler® 480 systems from Roche.

**Table 4.1 List of TaqMan Primers and Probes**

Gene	Type	Sequence
ANF	Forward: Reverse: Probe:	5'-GGA GGA GAA GAT GCC GGT AGA-3' 5'-GCT TCC TCA GTC TGC TCA CTC A-3' 5'-FAM-TGA GGT CAT GCC CCC GCA GG-TAMRA-3'
BNP	Forward: Reverse: Probe:	5'-CTG CTG GAG CTG ATA AGA GA-3' 5'-TGC CCA AAG CAG CTT GAG AT-3' 5'-FAM-CTC AAG GCA GCA CCC TCC GGG-TAMRA-3'
β- MHC	Forward: Reverse: Probe:	5'-GTGCCA AGG GCC TGA ATG AG-3' 5'-GCA AAG GCT CCA GGT CTG A-3' 5'-FAM-ATC TTG TGC TAC CCA GCT CTA A-TAMRA-3'
Pro-Collagen-I	Forward: Reverse: Probe:	5'- CTTCACCTACAGCACCCTTGTG-3' 5'-TGACTGTCTTGCCCAAGTTC-3' 5'-FAM-CTGCACGAGTCACACC-TAMRA-3'
Pro-Collagen-III	Forward: Reverse: Probe	5'- TGTCCTTTGCGATGACATAATCTG -3' 5'- AATGGGATCTCTGGGTTGGG-3' 5'-FAM- ATGAGGAGCCACTAGACT-TAMRA-3'
Trfc(Transferrin R)	premix	Mm00441941_m1*
HJV(Hemojuvelin)	Premix	Mm00510148_s1
FPN1(Ferroportin)	Premix	Mm00489837_m1*
HAMP1(Hepcidin1)	Premix	Mm00519025_m1
Ftl1(Ferritin-L)	Premix	Mm03030144_g1
Fth1(Ferritin-H)	Premix	Mm00085707_g1
18S rRNA	Premix	Mm03928990_g1*

**Western blot analysis:** Western analysis was performed on flash frozen LV tissue samples as previously described.<sup>91, 223, 226</sup> Briefly, we extracted protein from LV tissues using the following primary antibodies: SERCA2a, NCX1 (Thermo scientific), Akt-P<sup>Ser-473</sup>, Akt-P<sup>Thr-308</sup>, Total Akt (Cell Signaling), AMPK-P<sup>172</sup> and Total AMPK (Cell Signaling) and subsequently incubated with HRP conjugated secondary antibodies respectively.

**Statistical Analysis:** All data were statistically analyzed by using the SPSS Statistics 19 software and the averaged values are presented as mean ± SEM. One-way or two-way

ANOVA was used for data analysis followed by multiple comparison testing using the Tukey's test.

## **4.4 Results**

**Evidence of abnormal cardiac iron metabolism in an aged murine model of genetic hemochromatosis.** Due to lack of suitable pre-clinical murine model which recapitulates human iron-overload cardiomyopathy, we took HJVKO male mice, which closely recapitulate type 2 primary hemochromatosis, and we aged these mice coupled with high iron diet for 1 year, and studied the effects of resveratrol therapy by treating mice for last 3 months (**Figure 4.1A**). Treatment with high iron diet showed significant cardiac iron deposition confirmed by Prussian blue histological staining and quantification (**Figure 4.1B**). Total myocardial tissue iron (**Figure 4.1C**) also measured by inductive coupled plasma resonance spectroscopy, which clearly confirmed excess deposition of iron cardiac tissues. We also assessed the iron metabolic gene expression and our data showed defective hemojuvelin expression, a co-receptor for hepcidin expression and due to defective hemojuvelin, leads altered hepcidin-ferroportin axis along with other iron metabolic genes (**Figure 4.1D**). Due to defective hepcidin expression, an iron regulatory hormone results in irregular iron absorption and iron-overload in the body, this, in turn, favors myocardial iron uptake via L/T-Type calcium channels, and results in cardiac iron-overload (**Figure 4.1A-D**). Resveratrol treatment does not show any impact on reducing the levels of iron in the tissues (**Figure 4.1A-D**).

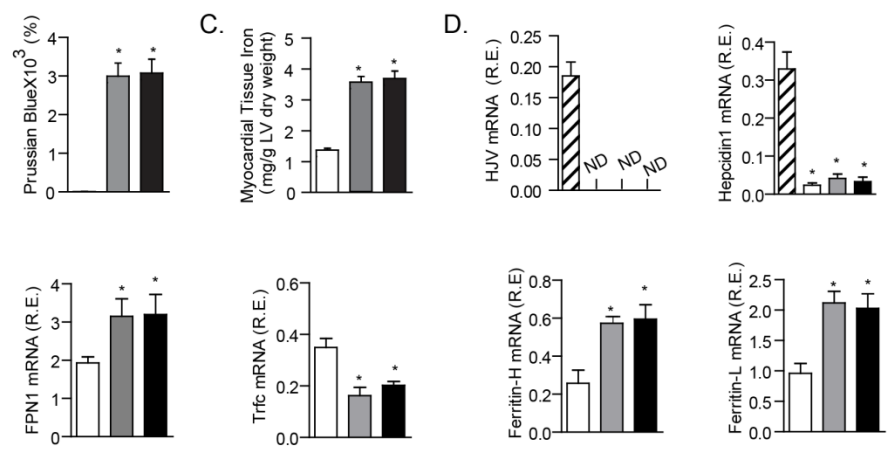
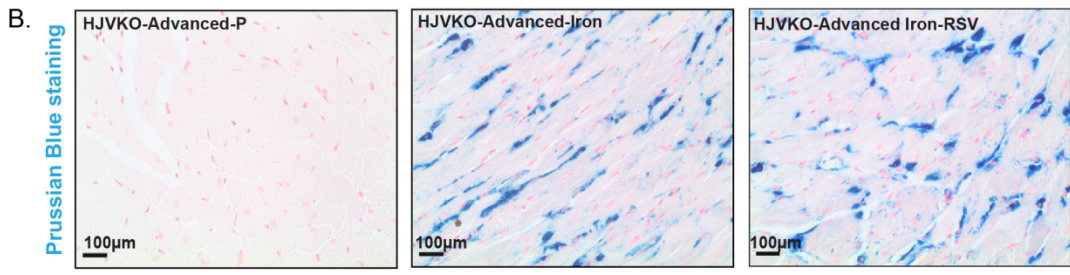
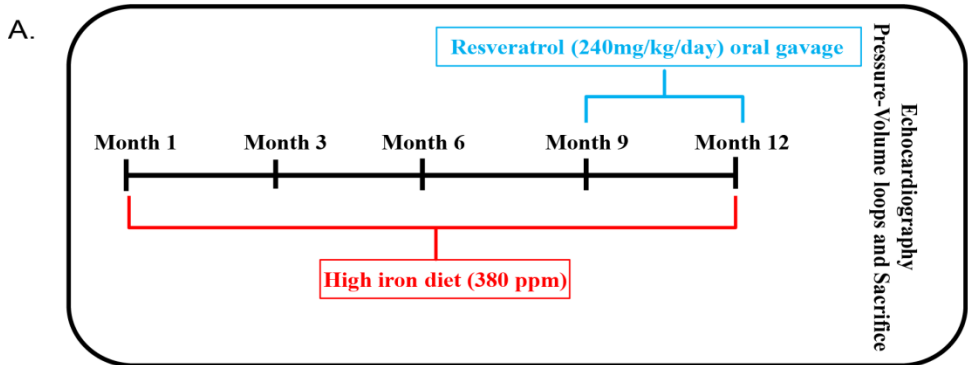


**Figure 4.1 Abnormal iron metabolism in murine models of aged genetic hemochromatosis.** A schematic representation of study design along with initiation of resveratrol therapy to rescue advanced iron-overload cardiomyopathy (A). Prussian blue staining and quantification along with total myocardial tissue iron levels in advanced stage iron-overloaded mice (B-C) and altered expression of iron metabolic genes, hemojuvelin (HJV), ferroportin (FPN), transferrin receptor 1 (Trfc), and ferritin light (L) and heavy (H) chain (D). Resveratrol did not affect myocardial iron deposition or the expression iron metabolism genes (A-D). ND=not detected; \* $p < 0.05$  compared with the placebo group.

**Resveratrol therapy prevents advanced iron-overload cardiomyopathy and increases survival during the advanced stage.** Aging coupled with iron-overload associated with severe cardiomyopathy with diastolic and systolic dysfunction and resveratrol rescued iron-overload cardiomyopathy during advanced disease stage. The non-invasive echocardiographic assessment showed the presence of distinct diastolic dysfunction and systolic dysfunction, characterized by decreased  $E'/A'$  ratio, prolonged isovolumic relaxation time (IVRT) and deceleration time (DT) for diastolic parameters (**Figure 4.2A; Table 4.2**), and decreased systolic parameters: ejection fraction (EF) and fractional shortening (FS) (**Figure 4.2A; Table 4.2**). Invasive hemodynamics showed that an increased EDPVR, a load-independent parameter reflecting the stiffness of LV (Tau) (**Figure 4.2B; Table 4.2**) and decreased  $dP/dt_{max}/EDV$  (starling's contractile index), decreased ejection fraction and cardiac output (**Figure 4.2B; Table 4.2**). Resveratrol therapy normalized diastolic and systolic parameters, based on echocardiography and hemodynamic analysis.

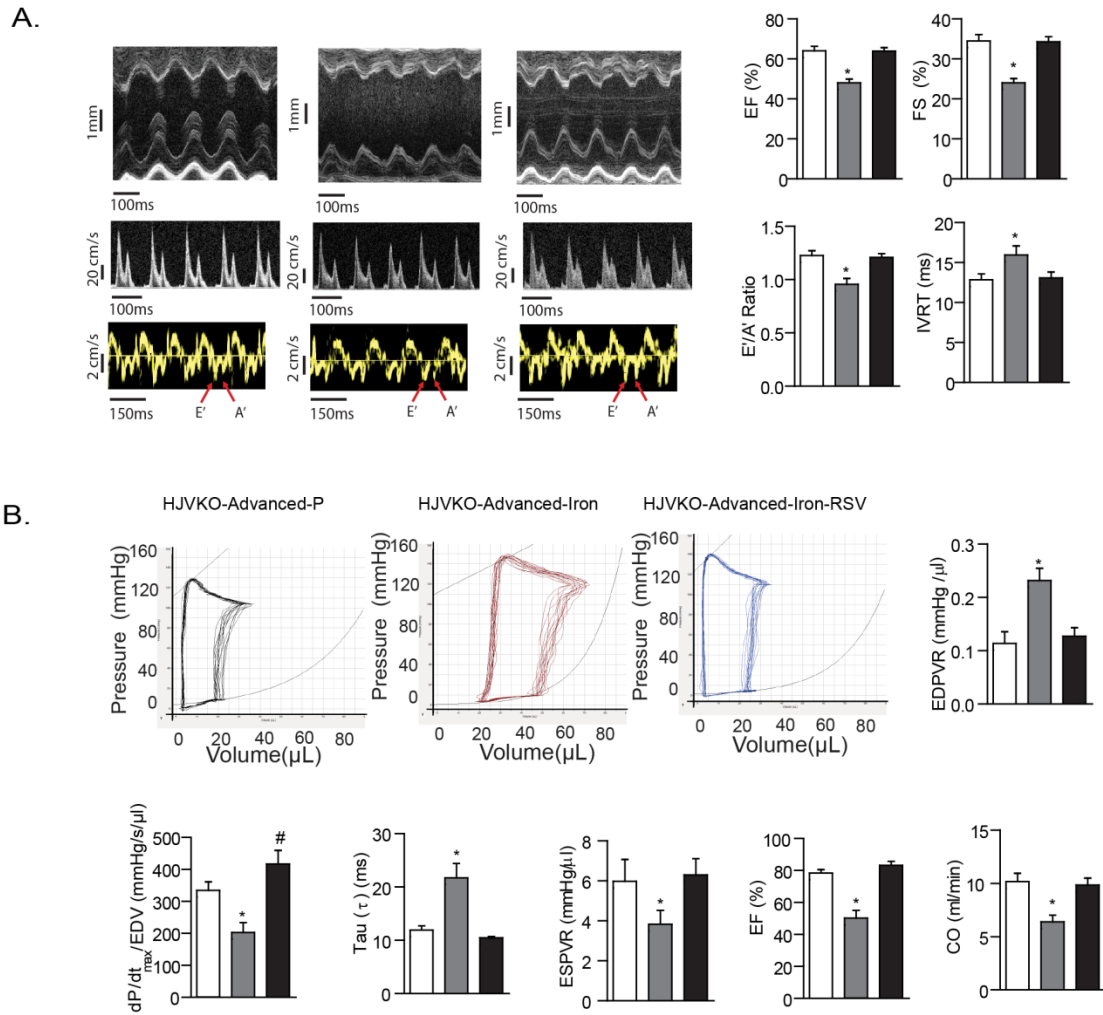
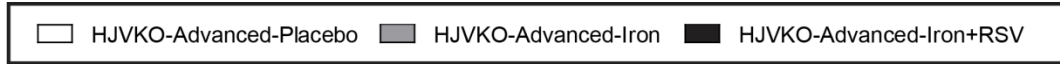


**Figure 4.2 Resveratrol therapy prevents the advanced cardiomyopathy in aged iron-overloaded hemojuvelin knockout mice.** Echocardiographic assessment of heart function with M-mode images (top panel), transmitral filling pattern (middle panel) and tissue Doppler (bottom panel) illustrating systolic and diastolic dysfunction in aged iron-overloaded hemojuvelin knockout (HJVKO) mice and quantification (A) of the echocardiographic assessment showing both systolic and diastolic dysfunction. Resveratrol (RSV) treatment completely normalized both systolic and diastolic dysfunction in aged HJVKO models of iron-overload (A). Invasive pressure-volume assessment illustrated by representative pressure-volume tracings confirming load-independent diastolic and systolic dysfunction in aged HJVKO models of iron-overload mice (B). EF= Ejection fraction; FS= Fractional shortening; E'=early tissue Doppler velocity; A'=tissue Doppler due to atrial contraction; IVRT=isovolumetric relaxation time. n=8 for the placebo groups and n=10-12 for the iron-treated groups. \*p<0.05 compared with all other groups; #p<0.05 compared with the placebo group.

**Table 4.2 Echocardiographic and Pressure-Volume assessment of cardiac function in advanced iron-overloaded male HJV KO mice at 1 yr of age**

	HJVKO+Vehicle	HJVKO+Iron+Placebo	HJVKO+Iron+Resveratrol
n	8	11	9
HR (bpm)	446±13	432.82±14.2	410±11
E-wave (mm/s)	680±47	682±36	631.55±18
A-wave (mm/s)	490±45	437±30	372±33
E/A Ratio	1.57±0.10	1.49±0.15	1.8±0.20
DT (ms)	24.9±1	32.8±2.14*	26.69±2.2
EWDR (mm/s <sup>2</sup> )	27.43±1.78	21.9±2.18*	24.7±2.01
E' (mm/s)	24.33±1.33	25.0±1.6	24.54±1.6
A' (mm/s)	20.08±1.5	26.51±1.5*	20.40±1.36
LA Size (mm)	1.92±0.08	2.2±0.06*	1.79±0.09
LVEDD (mm)	3.94±0.12	4.12±0.08	3.73±0.09
LVESD (mm)	2.59±0.13	3.13±0.08	2.45±0.07
VCFc (circ/s)	7.1±0.4	5.1±0.2	7.1±0.24
LVPWT (mm)	0.76±0.03	0.93±0.05	0.83±0.04
n	7	8	7
EDP (mmHg)	5.1±1.5	11.2±1.8*	3.7±0.9
ESP (mmHg)	118.9±4.9	137.9±3.38*	121.2±8.5
EDV(μl)	30.4±2.5	44.9±4.3*	24.2±1.5
ESV (μl)	6.7±1.1	22.2±4.9*	3.9±1.0
SV(μl)	23.6±1.8	15.7±0.8*	20.2±1.5
dP/dt <sub>max</sub> (mmHg/s)	9907.3±263	84204.9±685*	9922.2±847
dP/dt <sub>min</sub> (mmHg/s)	8362.3±385	7092.1±607*	8719.1±680
SW (mJoules)	0.41±0.03	0.47±0.03	0.36±1.0

HR=heart rate; E=early trans-mitral filling wave; A=atrial trans-mitral filling wave; E'=early tissue Doppler velocity; A'=tissue Doppler due to atrial contraction; LA=Left atrium; DT= deceleration time; LVEDD= left ventricular end diastolic dimension; LVESD= left ventricular end systolic dimension; VCFc = velocity of circumferential fiber shortening ; LVPWT= left ventricular posterior wall thickness; dP/dt=rate of change in LV pressure; EDP= end diastolic pressure; ESP=end systolic pressure; EDV=end diastolic volume; ESV=end systolic volume; SV=stroke volume ; EWRD= E wave deceleration rate.\*p<0.05 compared with all other groups.

In contrast to the early and chronic stage of iron-overload cardiomyopathy, advanced iron-overload cardiomyopathy resulted in severe cardiomyopathy, pathological cardiac hypertrophy with lower survival rate ~48% relative to placebo control mice, whereas

resveratrol antioxidant therapy significantly improved the survival rate in aged iron-overload mice ~76% (**Fig 3A**) during advanced iron-overload cardiomyopathy.

**Table 4.3 Echo-MRI assessment in iron-overloaded male HJV KO mice at 1 yr of age group**

	HJVKO+Vehicle	HJVKO+Iron	HJVKO+Iron+Resveratrol
n	6	9	6
Body weight	40.11 ± 0.9	43.71 ± 2.4	33.27 ± 1.4#
Total water	17.62 ± 0.3	18.83 ± 0.43	14.13 ± 0.31
Free water	0.21 ± 0.02	0.25 ± 0.03	0.20 ± 0.03
Fat mass	10.35 ± 0.77	11.87 ± 1.8	9.050 ± 1.1
Lean mass	25.76 ± 0.4	27.78 ± 0.7	20.93 ± 0.5

Heart weight to tibial length ratio and LV weight to tibial length ratio were significantly increased in iron-overloaded hearts and normalized in resveratrol-treated animals (**Figure 4.3B**). The liver weight to body weight ratio was also significantly increased in advanced iron-overload phenotype; resveratrol therapy did not affect liver to body weight ratio (**Figure 4.3B**). To further investigate the pathophysiology, we assessed the fetal gene expression, and we found ANF, BNP and  $\beta$ -MHC are significantly up-regulated during iron-overloaded cardiac pathology but normalized after resveratrol treatment (**Figure 4.3C**). The myocyte cross section area (MCSA), an indicator of myocardial hypertrophy, visualized by wheat germ agglutinin staining showed an increase in the iron-overload group and normalization in resveratrol treated groups (**Figure 4.3D**). Assessment of body composition by Echo MRI found no substantial differences in body composition in all groups (**Table 4.3**).

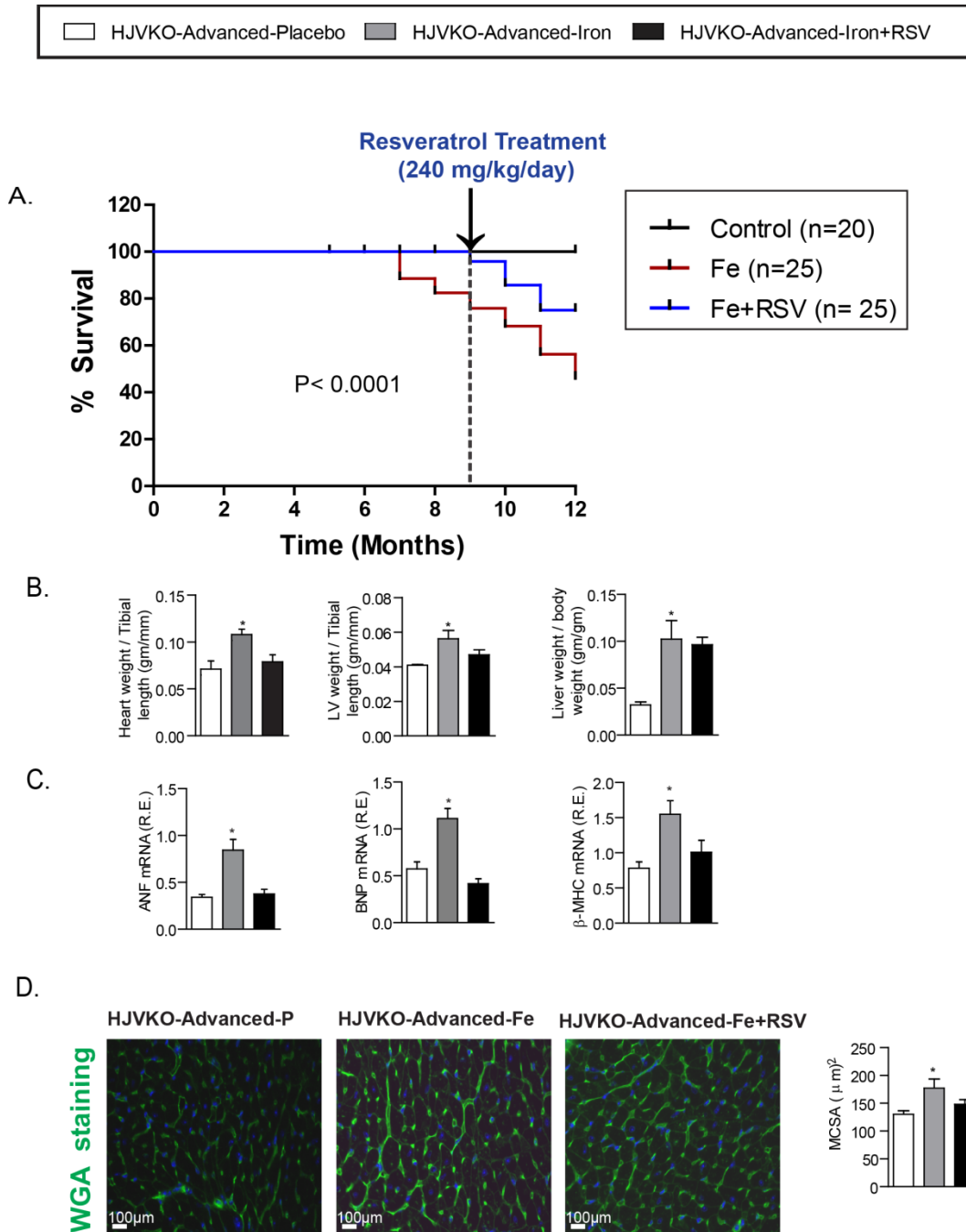


**Figure 4.3 Kaplan-Meier curves showing severe mortality in aged iron-overloaded HJVKO mice, salutary effects with resveratrol treatment.** Aged iron-overload mice showed decreased survival, (~48%), however, resveratrol (240mg/kg/day) treatment showed improved survival (~86%) in aged iron-overload HJVKO mice relative to 100% survival in the control group (A). Morphometric analysis showed increased heart weight to tibial length, increased LV weight to tibial length and increased liver weight to body weight, normalized with resveratrol treatment, however, unchanged in liver (B). Expression analysis of myocardial disease markers in advanced iron-overload models showing a complete normalization of the expression of disease markers in response to resveratrol therapy (C). WGA staining and quantification showed increased myocyte cross-sectional area in iron-

overloaded groups and complete normalization in response to resveratrol therapy (**D**). ANF=atrial natriuretic factor; BNP=brain natriuretic peptide;  $\beta$ -MHC=beta-myosin heavy chain. n=8 for gene expression analysis; n=6 for placebo and n=8 for iron-treated groups.

### **Resveratrol ameliorates myocardial fibrosis and calcium cycling defects at an advanced stage of iron-overload pathogenesis.**

We next assessed the myocardial fibrosis and calcium cycling defect proteins, which are the key drivers in the progression of cardiomyopathy.<sup>91, 164, 179, 223, 225</sup> Myocardial fibrosis is a characteristic feature of heart failure associated with diastolic and systolic dysfunction.<sup>223</sup>

We performed PSR staining to understand the cardiac fibrosis, we found massive interstitial fibrosis and we also quantified the fibrosis content and to confirm these we also performed Masson's trichrome staining (**Figure 4.4 A, B**). Gene expression analysis of pro-collagen I and III mRNA also significantly increased in aged iron-overload mice (**Figure 4.4 C**). Resveratrol therapy resulted in marked suppression of myocardial fibrosis and normalizes normalization of the pro-fibrotic gene expression (**Figure 4.4 A, B and C**).

Aged iron-overloaded heart resulted in decreased SERCA2a protein levels with a compensatory increase in NCX1 levels (**Figure 4.4 G-H**). Defective SERCA2a leads abnormal calcium cycling and this is the key driver in the progression of heart failure disease.<sup>91, 221, 225, 243</sup> Resveratrol therapy resulted in significant increase in SERCA2a protein levels accompanied by normalization of NCX1 levels (**Figure 4.4 G-H**). Similarly to early and chronic iron-overload phenotypes, advanced iron-overload exhibited no inflammation (**Figure 4.5 and 4.6**).

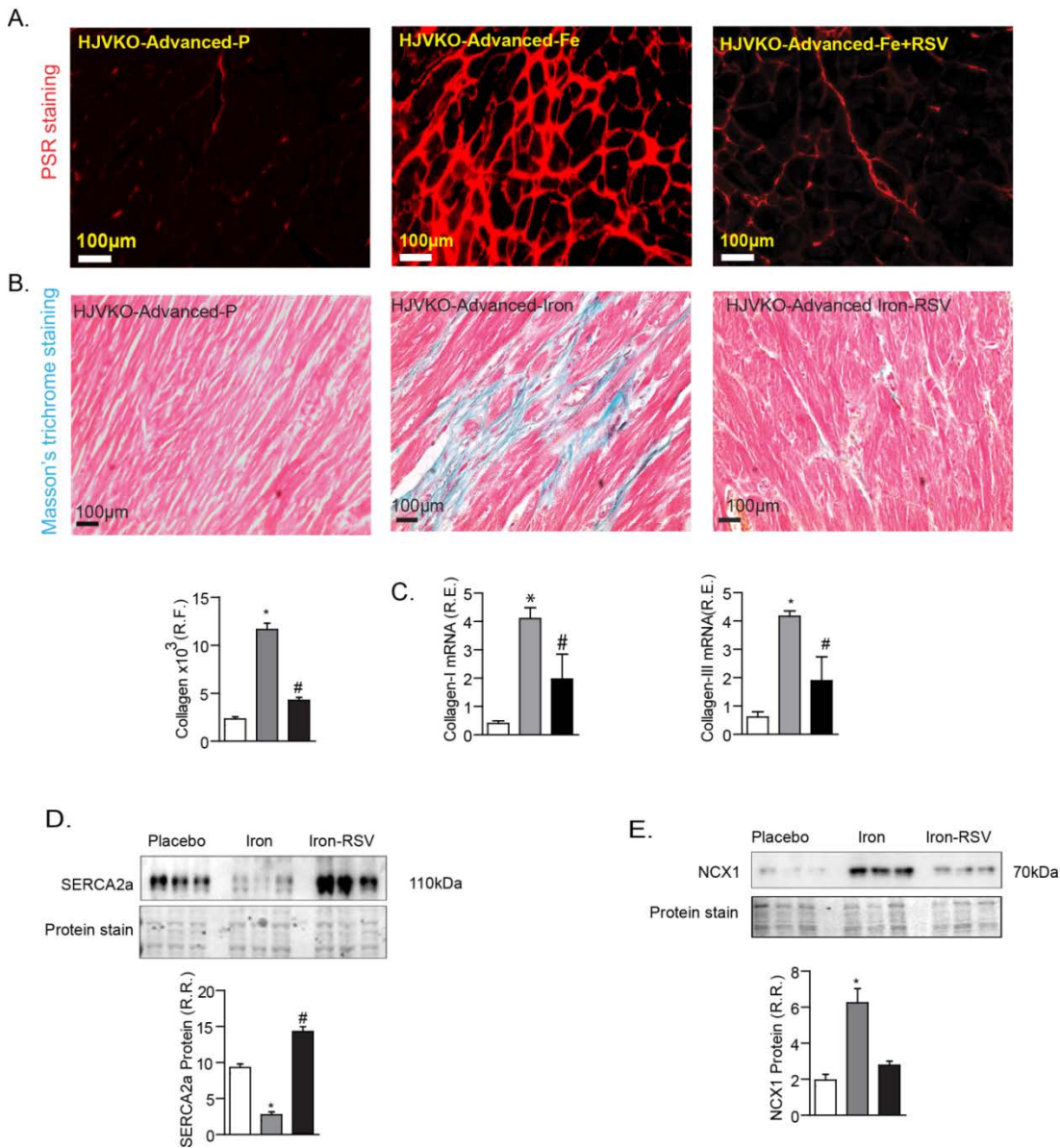
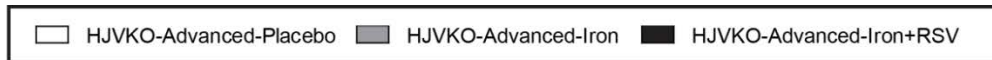


**Figure 4.4 Resveratrol therapy prevents myocardial fibrosis and defective calcium cycling proteins associated with advanced iron-overload cardiomyopathy. (A-C)**

Histological assessment of myocardial fibrosis using picro-sirius red (PSR) (A) and Masson's trichrome (B) staining and quantification of fibrosis, revealed increased myocardial interstitial fibrosis in the aged HJVKO iron-overloaded hearts and expression analysis of myocardial pro-collagen I $\alpha$ 1 and pro-collagen III $\alpha$ 1 (C) in advanced iron-overloaded hearts revealed the presence of severe myocardial fibrosis. Resveratrol therapy prevented the increased in myocardial fibrosis based on histological and gene expression analysis (A-C). Western blot analysis and quantification show a marked decreased in myocardial SERCA2a level (D) and a compensatory increase in NCX1 protein levels (E). Resveratrol therapy restored the levels of SERCA2a protein and compensatory normalization of NCX1 protein

levels(D-E). A.U.=arbitrary unit; R.R.=relative ratio. n=4 for histological analyses; n=6 for Western blot.  
 \*p<0.05 compared with all other groups; #p<0.05 compared with the placebo group.

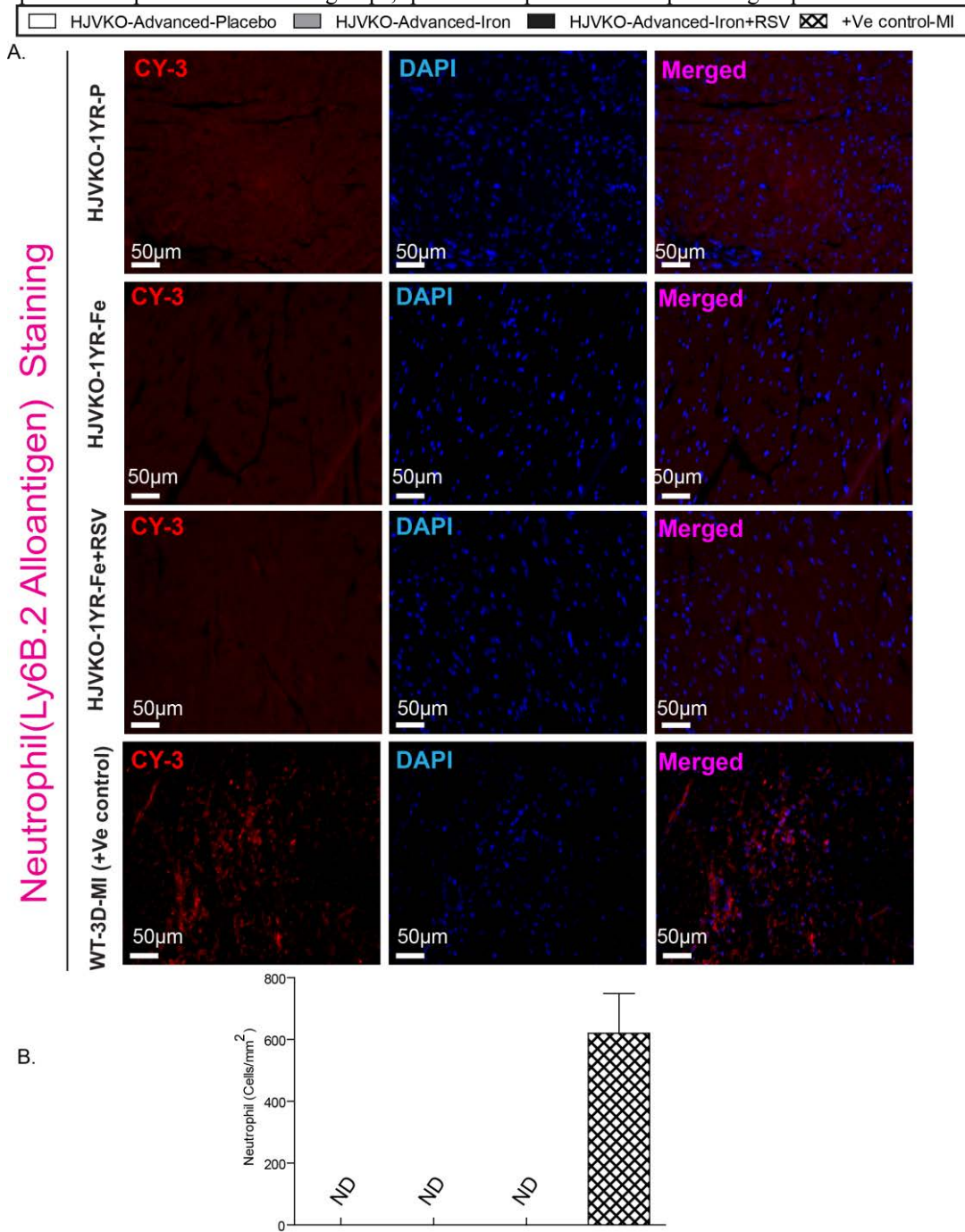
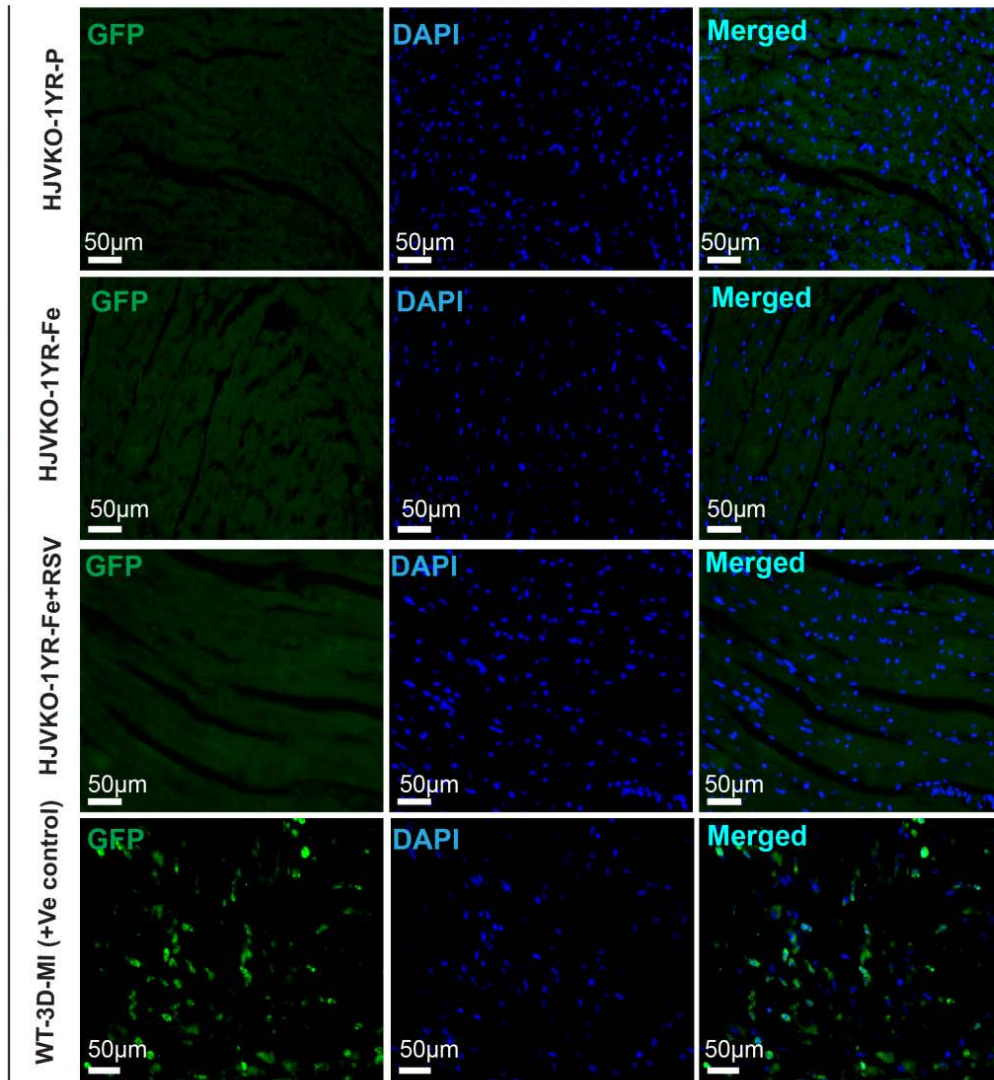


**Figure 4.5 Neutrophil inflammatory staining in advanced iron-overload cardiomyopathy.**(A-B) Immunohistological assessment of inflammation using Ly6B.2Alloantigen, neutrophil antibody (red), nuclear stain (blue) and merged with neutrophils (magenta) confirmed with WT-3D-MI as positive control (A) and quantification (B) n=4 for histological analyses.

HJVKO-Advanced-Placebo  
  HJVKO-Advanced-Iron  
  HJVKO-Advanced-Iron+RSV  
  +Ve control-MI

A.

Macrophage (F4/80) Staining



B.

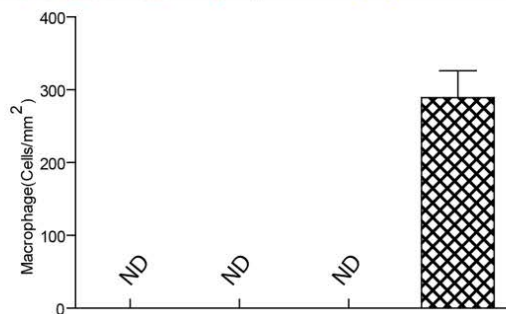


**Figure 4.6 Macrophage (F4/80) inflammatory staining in advanced iron-overload cardiomyopathy. (A-B)** Immuno-histological assessment of inflammation using F4/80, Macrophage (green), nuclear stain (blue) and merged with macrophages confirmed with WT-3D-MI as positive control (A) and quantification (B) n=4 for histological analyses.

**Iron induced oxidative stress is the key driver in the progression of advanced cardiomyopathy and normalized after resveratrol treatment.** Iron-overload is closely associated with Fenton chemistry to generate oxidative free radicals, and a key driver in the progression of iron induced oxidative damage.<sup>82, 157, 214</sup> We extensively characterized the myocardial oxidative stress in aged iron-overloaded murine models and evaluated the beneficial effects of resveratrol antioxidants. Lipid peroxidation is one of the major pathological features noticed during iron induced oxidative stress.<sup>74</sup> We found 4-HNE lipid peroxidation adducts in iron-overloaded myocardium (**Figure 5A**), we also biochemically measured the extent of lipid peroxidation, we found significantly higher levels of MDA, malondialdehyde another lipid peroxidation adduct produced as a results lipid peroxidation, and importantly, resveratrol therapy resulted in marked suppression of lipid peroxidation (**Figure 5 C**). We also looked peroxynitrite formation by nitrotyrosine immunostaining, and resveratrol administration showed a significant reduction in peroxynitrite formation (**Figure 5B**). Beside lipid peroxidation we also looked myocardial antioxidant reserves, a non-enzymatic intrinsic antioxidants named glutathione, and we found that iron-overload associated with significant decrease in reduced form of glutathione and increased accumulation of oxidized glutathione called glutathione disulfide levels, resveratrol antioxidant therapy significantly improved the reduced glutathione levels and decreased the levels of glutathione disulfide levels (**Figure 5D**). The oxidative stress response is known to modulate phosphorylation of Akt (PKB) and AMPK in cardiac tissue. We found that serine-473 phosphorylation of Akt was significantly reduced in the iron-overloaded group, whereas threonine-308 phosphorylation remained unchanged. Resveratrol treatment normalizes serine-473 phosphorylation and increased

phosphorylation of the threonine-308 (Figure 5E). Consistent with previous results, Phospho-AMP-Activated Protein Kinase (P-AMPK) levels were unchanged in the iron-overloaded group; however, resveratrol supplementation significantly increased P-AMPK levels (Figure 5F).

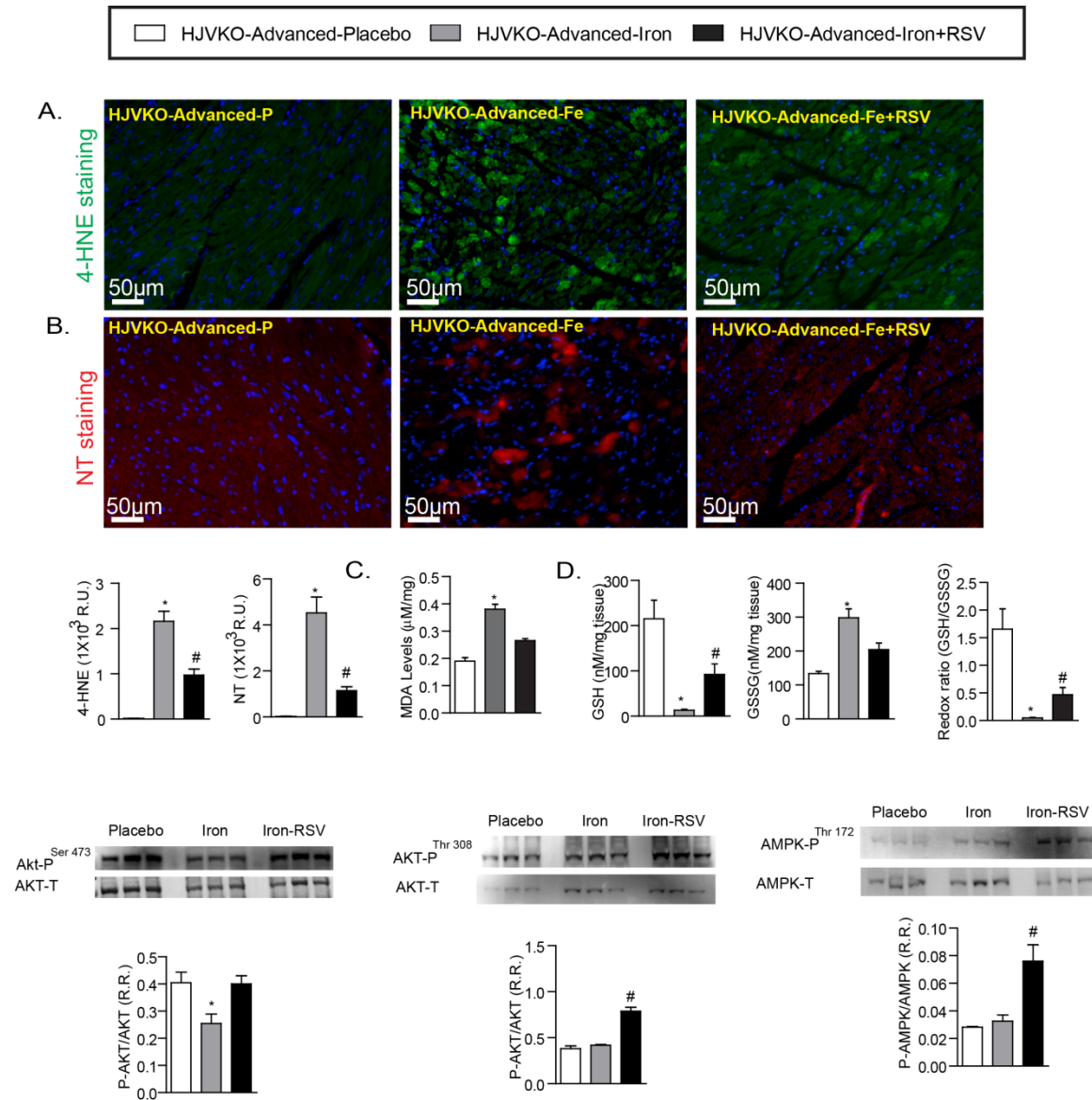


**Figure 4.7 Iron-induced oxidative stress in advanced murine models of iron-overload is prevented by resveratrol.** 4-hydroxynonenal (4-HNE) (A) and nitrotyrosine (NT) (B) and the myocardial lipid peroxidation product, malondialdehyde (MDA) confirmed increased myocardial lipid peroxidation in murine models of iron-overload and the therapeutic effects of resveratrol.(C. Myocardial levels of reduced glutathione (GSH), oxidized glutathione (GSSG) and the redox ratio, (D)

were altered demonstrating biochemical evidence of increased oxidative damage and reduced antioxidant reserve in advanced iron-overloaded hearts, markedly corrected by oral resveratrol therapy. **(D)** Signaling of AKT and AMPK also altered in aged HJVKO iron-overloaded mice, P-AKT Ser-473 levels were significantly reduced in iron-overload groups **(E)**, P-AKT-Thr-307 is unchanged **(F)** and P-AMPK levels unchanged in iron-overloaded hearts **(G)**. Resveratrol potentiated the upregulation of P-AKT and P-AMPK in advanced iron-overloaded hearts. R.U.=Relative unit; R.R. relative Ratio; LV=left ventricle; n=8 for biochemical. \*p<0.05 compared with all other groups; #p<0.05 compared with the placebo group.

## 4.5 Discussion

Iron-overload cardiomyopathy is a major cause of heart failure with the highest rate of morbidity and mortality. Clinical complications associated with this disorder are increasing in epidemic proportions in patients with primary hemochromatosis and secondary iron-overload with limited therapies.<sup>45, 106</sup> We recently showed that murine models of early and chronic acquired and genetic iron-overload cardiomyopathy are characterized by diastolic dysfunction with preserved ejection fraction that can be normalized by cardioprotective antioxidant therapy with resveratrol.<sup>91</sup> However, there is no a pre-clinical murine model which closely recapitulates genetic iron-overload cardiomyopathy that occurs in human.<sup>91, 149</sup> In this study, we elucidated the cardiac pathophysiology as a result of advanced iron-overload in preclinical aged murine models of genetic hemochromatosis and demonstrated the efficacy of resveratrol antioxidant therapy, in ameliorating the advanced cardiomyopathy with systolic and diastolic dysfunction. Our study is the first, to understand the advanced iron-overload cardiomyopathy in genetic iron-overload murine models importantly, we aged these mice coupled with dietary iron-overload, provided new insights into the disease pathogenesis and our murine model of iron-overload recapitulates type 2 primary hemochromatosis.

To investigate the potential new insights into the pathogenesis of advanced iron-overload cardiomyopathy and therapeutic effects of resveratrol, we established advanced

cardiomyopathy by treating HJVKO male mice with high iron diet (Prolab<sup>®</sup>RHM 3000 with iron 380 ppm) for 1 year and also tried to rescue with resveratrol (240 mg/kg/day) oral gavage. Interestingly, although resveratrol did not prevent or reduce cardiac iron levels, it markedly improved cardiac function (both systolic, diastolic) by preventing the progression of advanced cardiomyopathy. We evaluated the diastolic and systolic function in the aged iron-overload murine model by using a state-of-the-art echocardiographic and invasive pressure-volume loops techniques, and it was consistent with previous studies.<sup>91, 179, 225, 226, 250</sup> Resveratrol antioxidant therapy significantly reduced the end systolic and end- diastolic pressures and LA size. Systolic properties such as ejection fraction and fractional shortening from non-invasive echocardiography and ESPVR,  $dP/dt_{max}/EDV$  (load independent parameters) from invasive hemodynamics also significantly improved, after resveratrol treatment. In contrast, diastolic properties from echocardiography such as prolonged DT and IVRT, with decreased  $E'/A'$  ratio and diastolic parameters from pressure-volume loops such as increased EDPVR and prolonged Tau, significantly normalized after resveratrol treatment. Together, our functional data clearly shows that resveratrol improved diastolic and systolic properties, prevents impaired relaxation and reduces the myocardial stiffness along with improved contractility in the settings of advanced heart failure. Furthermore, resveratrol administration significantly improved survival rate in murine models of advanced iron-overload cardiomyopathy.

Myocardial remodeling, pathological hypertrophy and increased expression of fetal genes are the major contributor to the progression of advanced heart failure.<sup>179, 250</sup> Accordingly, prevention or suppression of pathological hypertrophy, cardiac remodeling, and fetal gene expressions are considered to be important therapeutic targets to stop the

progression of heart failure. Consistent with this, resveratrol therapy effectively normalized the progression of myocardial remodeling, cardiac hypertrophy and it also normalized the expression of fetal gene programming in the myocardium. Many lines of evidence have shown that resveratrol inhibits pathological hypertrophy and myocardial remodeling, predominantly by activating AMPK among other cardioprotective and metabolic benefits.<sup>168, 170, 179</sup> We also observed that resveratrol treatment increased the phosphorylation of AMPK to inhibit the progression of heart failure.

Myocardial fibrosis is also another key driver in the progression of advanced heart failure, which increases the myocardial stiffness that leads to decreased ventricular filling and greater end diastolic pressure.<sup>91, 179</sup> Interestingly, we found massive interstitial fibrosis with increased ventricular stiffness and greater end diastolic pressure in aged HJVKO mice in response to iron-overload. Resveratrol treatment significantly decreased myocardial fibrosis, which resulted in decreased ventricular stiffness and normalized end diastolic pressure. However, advanced iron-overload cardiomyopathy does not associate with any inflammation.

Advanced heart failure is also associated with significant reduction in SERCA2a mRNA and protein levels demonstrating defective calcium handling.<sup>91, 237</sup> We also found a decreased SERCA2a protein levels as a result of iron-overload cardiomyopathy with a compensatory increase in sodium-calcium exchanger protein. Furthermore, defective SERCA2a fail to reuptake  $\text{Ca}^{2+}$ , which in turn affects actin-myosin cross-bridge and also the myofilament  $\text{Ca}^{2+}$  sensitivity, which results in progression to heart failure. Interestingly resveratrol administration significantly improved SERCA2a protein levels and calcium cycling defects resulting in improved cardiac function.

A large number of studies showed that iron-induced oxidative stress is the key driver in the pathogenesis of iron-overload cardiomyopathy.<sup>77, 82, 91, 110, 214</sup> We also extensively characterized iron-induced oxidative stress in advanced iron-overload murine models. Consistent with previously published reports showing that cardiac iron-overload associated with oxidative stress and lipid peroxidation,<sup>75, 77, 83, 245</sup> we also observed elevated oxidative stress (decreased GSH levels) and increased lipid peroxidation (4-HNE and MDA levels) in advanced iron-overload cardiomyopathy. Furthermore, the lipid peroxidation end products are toxic in nature and cause cellular dysfunction mainly interferes with the excitation-contraction coupling properties of heart<sup>89</sup>. Consistent with this resveratrol administration significantly normalized oxidative stress and lipid peroxidation.

**4.6 Conclusions:** In summary, our novel HJVKO genetic iron-overload murine model showed advanced heart failure with systolic and diastolic dysfunction. Resveratrol supplementation significantly reduced the progression of iron induced oxidative damage and cardiac dysfunction. Although we have not likely identified all the molecular beneficial effects of resveratrol antioxidant therapy, however, our data showed that resveratrol can modulate iron-induced oxidative stress, improve SERCA2a and prevents pathological hypertrophy and fibrosis. Many studies confirmed the pleiotropic beneficial effects of resveratrol natural polyphenol without any toxic side effects and we propose that dietary intake resveratrol modulate the intrinsic antioxidant status and that may prove to be a useful intervention to prevent the progression of iron-induced cardiac dysfunction subsequently the clinical burden of global iron-overload.

# CHAPTER FIVE

## **Resveratrol mediates therapeutic hepatic effects in acquired and genetic murine models of iron-overload**

Subhash K. Das<sup>1,2</sup>, Jessica DesAulniers<sup>1,2</sup>, Jason R. B. Dyck<sup>5</sup>, Zamaneh Kassiri<sup>2,3</sup>,  
and Gavin Y. Oudit<sup>1,2</sup>

<sup>1</sup>Department of Medicine, <sup>4</sup>Department of Physiology, <sup>5</sup>Department of Pediatrics and  
Pharmacology, University of Alberta, Edmonton, Canada

**A modified version of this chapter has been published in *Liver International*,  
2016 Feb 16; 36(2):246-57.**

## 5.1 Abstract

**Background and Aims:** Abnormal iron metabolism and hepatic iron-overload is a major cause of liver injury and in the development of chronic liver diseases. Iron-overload mediated liver disease leads to end-stage cirrhosis and/or hepatocellular carcinoma.

**Methods:** Using a genetic hemochromatosis (hemojuvelin knockout mice) and non-genetic (secondary iron-overload) murine models of hepatic iron-overload we elucidated the mechanism of hepatic iron injury and the therapeutic effects of resveratrol.

**Results:** Hepatic iron-overload was associated with hepatosplenomegaly, increased oxidative stress, hepatic fibrosis, and inflammation, and a pro-apoptotic state which was markedly corrected by resveratrol therapy. Importantly our aging studies with the hemojuvelin knockout mice showed advanced liver disease in association with steatosis in the absence of a diabetic state which recapitulates the essential pathological features seen in clinical iron-overload. Chronic hepatic iron-overload showed increased nuclear localization of acetylated Forkhead fox-O-1 (FoxO1) transcription factor while resveratrol dietary intervention reversed the acetylation of FoxO1 in association with increased SIRT1 levels which together with its pleiotropic antioxidant properties are likely key mechanisms of its therapeutic action. Importantly, resveratrol treatment did not affect the degree of hepatic iron-overload but rather direct protects the liver from iron-mediated injury.

**Conclusions:** Our findings illustrate a novel and definitive therapeutic action of resveratrol and represent an economically feasible therapeutic intervention to treat hepatic iron-overload and liver disease.

**Keywords:** Iron-overload, liver disease, oxidative stress, resveratrol

## 5.2 Introduction

Abnormal iron homeostasis leads to end-organ injury and deleterious pathophysiological effects culminating in end-organ disease including liver fibrosis, cirrhosis and hepatocellular carcinoma.<sup>4, 6, 13, 106</sup> Liver stores significantly a large amount of iron in a safe and non-toxic form, however, liver hepatocytes tightly regulate iron homeostasis by producing an iron regulatory hormone called hepcidin.<sup>50</sup> Impaired iron metabolism found in many liver diseases particularly with genetic hemochromatosis, secondary iron-overload and alcohol-related liver diseases.<sup>252, 253</sup> Hereditary hemochromatosis associated with loss-of-function mutations in *HJV* or *HAMP* genes and produces a negligible amount of hepcidin, which drives uncontrolled iron uptake resulting in iron-overload<sup>6, 13, 51, 254, 255</sup>. Hepatic iron-overload results when transferrin is saturated and non-transferrin bound iron (NTBI) is formed which is highly reactive, toxic and triggers oxidative stress by producing reactive oxygen and nitrogen species.<sup>83, 106-108</sup>

While chelation therapy and phlebotomy can be effective against hepatic iron-overload and liver disease, there is ongoing effort to improve the therapeutic strategies against iron-overload. We first aimed to investigate the molecular and cellular basis of hepatic iron-overload pathogenesis and second to investigate the therapeutic effects of resveratrol. We report that Forkhead box-O 1(FOXO1) regulation is altered in iron-

overloaded livers and resveratrol act as a potent SIRT1 activator and modulates FOXO1 deacetylation which allows FOXO1 dependent anti-oxidant response during oxidative stress. Several lines of evidence suggested that resveratrol is a bioactive natural flavonoid with pleiotropic actions such as antioxidant, anti-inflammatory and anti-apoptotic.<sup>219, 220, 247</sup> We used resveratrol dietary intervention to prevent the liver disease in hepatic iron-overload murine models with secondary iron-overload and genetic hemochromatosis. Collectively, our results strongly suggest that resveratrol is a useful therapy to reduce the burden of hepatic iron-overload and liver disease.

### 5.3 Materials and Methods

**Experimental models of iron-overload.** Wild type (WT) male C57BL6 mice (from Jackson Laboratory, Bar ME) of 10-12 weeks and hemojuvelin knockout (HJVKO)<sup>51</sup> mice of 4 weeks are subjected to the iron-overload regimen. For wild type mice iron-dextran i.p. injected on a 5day/week schedule and for hemojuvelin knockout mice of 4 weeks are treated with high iron diet ((Prolab<sup>®</sup> RHM 3000-Iron diet; 380 mg iron/kg food). The iron-injection protocols in WT mice was used as a model of acquired iron-overload<sup>77, 83</sup> and the HJVKO mice were used as a genetic model of hemochromatosis.<sup>51</sup> The iron-overload regimens used in this study correspond to chronic and advanced stages of iron-overload:

1. **Chronic stage:** 5 mg/25 g body weight of iron-dextran i.p. was injected on a 5 day/week schedule for the total duration of 4 weeks followed by 1.25 mg/25 gm body weight for 8 more weeks in WT male C57BL6 mice.<sup>77, 83</sup> We used dietary resveratrol supplementation (Modified AIN-93G Diets, Inc., Bethlehem, PA) given at 320

mg/kg/day in wildtype mice for 14 weeks. We also used a chronic protocol in 4 weeks old HJVKO mice by feeding them with a high iron diet (Prolab<sup>®</sup>RHM 3000 with iron 380 ppm) for 6 months. We also examined the effects of resveratrol (trans-resveratrol synthetic >99% pure, Lalilab Inc. Durham), on the iron-overloaded HJVKO mice by daily oral gavage (240 mg/kg/day) for two months starting at 4 months of age.

2. **Advanced stage:** We also treated 4 weeks old HJVKO mice with high iron diet until they were 1 year old. We also examined the effects of resveratrol on the 1-year-old iron-overloaded HJVKO mice by daily oral gavage (240 mg/kg/day) for three months starting at 9 months of age. We dissolved resveratrol in 4% corn oil.<sup>248</sup> The placebo control groups received 4% corn oil.

**Histology, Immunofluorescence and Dihydroethidium fluorescence staining.** Livers were fixed with 10% buffered formalin, embedded in paraffin. 5µm thin sections and Prussian blue, H&E, picro-sirius red (PSR) and trichrome staining were performed. The stained sections were visualized by using bright field and fluorescent (Olympus IX81, MetaMorph software) microscope. Nitrotyrosine, 4-HNE, inflammatory (neutrophil, macrophage and CD-8) immune staining and FOXO1 staining performed respectively visualized under Olympus IX81 fluorescent microscope and quantified by using MetaMorph software as described previously. Dihydroethidium (DHE) is a reactive oxygen species (ROS) detection fluorescent dye which produces an excess fluorescent signal in the presence of ROS. We performed dihydroethidium fluorescence staining on 15µm thick liver frozen sections which were visualized using an Olympus IX81 fluorescent microscope and quantified by using the MetaMorph software.

**Terminal deoxynucleotidyl transferase-mediated dUTP nick-end labeling (TUNEL) assay.** 15 µm thick liver sections subjected to TUNEL staining and visualized using an Olympus IX81 fluorescent microscope as described previously.<sup>226</sup>

**Tissue iron levels.** 20 mg of frozen liver tissue were subjected to inductive coupled plasma resonance mass spectrometry to quantify hepatic iron levels (Trace Metals lab, London, Ontario).<sup>77, 83</sup>

**Measurement of lipid peroxidation and glutathione levels.** Malondialdehyde (MDA), an indicator of lipid peroxidation, was measured in liver tissue (100-150 mg) using a commercially available kit (Bioxytech<sup>®</sup> MDA-586<sup>™</sup> assay kit cat#21044, OxiResearch, Percipio Biosciences Inc. Los Angeles, CA U.S.A). Butylated hydroxytoluene (5 mM) was added during sample preparation to prevent further iron-induced lipid peroxidation product formation. Reduced (GSH) and oxidized (GSSG) glutathione levels were measured from liver tissues as described previously.<sup>83, 128</sup> 2-venyle pyridine (18.5 mM) was used to prevent the conversion of GSH to GSSG, samples were analyzed in triplicate and the average values were used.

**Measurement of liver tissue triglycerides and Oil Red-O staining.** Liver tissue triglyceride was measured using a commercially available kit (Wako LabAssay<sup>™</sup> Triglyceride) as described previously.<sup>250</sup> We performed oil red O (ORO) staining to detect lipid accumulation in liver tissues as described previously with minor modifications.<sup>256</sup>

**Oral Glucose Tolerance Testing.** Oral glucose tolerance test (OGTT) was performed to assess systemic insulin resistance as reported previously using an oral glucose load of 1.5 g/kg<sup>250</sup>

**Taqman real-time PCR and Western blot analyses.** mRNA expression levels were studied in iron-overload livers, by real-time PCR by using Taqman primers and probes (**Table 5.1**). Protein lysates from flash frozen liver tissue was processed and resolved on 8%, sodium dodecyl sulphate-poly acrylamide gel electrophoresis (SDS-PAGE) then transferred to PVDF membranes using a Trans-blot cell (Bio-Rad laboratories, Hercules CA USA) as previously described. The primary antibodies used included sirtuin-1, FOXO1, total and cleaved caspase-3 (Cell signaling) with their HRP-conjugated secondary antibodies respectively. Blots were scanned and quantified by using ImageQuant LAS 4000 (GE Health care, Biosciences)

**Table 5.1 :List of TaqMan probe and primer.**

Gene	Type	Sequence
IL-6	Forward: Reverse: Probe:	5'-ACAACCACGGCCTTCCCTACTT-3' 5'-CACGATTTCCCAGAGAACATGTG-3' 5'-FAM-TTCACAGAGGATACCACTCCCAACAGACCT-TAMRA-3'
IL-1 $\beta$	Forward: Reverse: Probe:	5'-AACCTGCTGGTGTGTGACGTTC-3' 5'-CAGCACGAGGCTTTTTTGTGTG-3' 5'- FAM-TTAGACAGCTGCACTACAGGCTCCGAGATG-TAMRA-3'
TNF- $\alpha$	Forward: Reverse: Probe:	5'- ACAAGGCTGCCCCGACTAC-3' 5'- TTTCTCCTGGTATGAGATAGCAAATC-3' 5'-FAM-TGCTCCTCACCCACACCGTCAGC-TAMRA-3'
Pro-Collagen-I	Forward: Reverse: Probe:	5'- CTTACCTACAGCACCCCTTGTG-3' 5'-TGACTGTCTTGCCCCAAGTTC-3' 5'-FAM-CTGCACGAGTCACACC-TAMRA-3'
Pro-Collagen-III	Forward: Reverse: Probe	5'- TGTCCCTTTCGATGACATAATCTG -3' 5'- AATGGGATCTCTGGGTTGGG-3' 5'-FAM- ATGAGGAGCCACTAGACT-TAMRA-3'
TGF- $\beta$	Forward: Reverse: Probe	5'- CCTGCAAGACCATCGACATG-3' 5'- ACAGGATCTGGCCACGGAT-3' 5'-FAM-CTGGTGAAACGGAAGCGCATCGAA-TAMRA-3'
TIMP1	Forward: Reverse: Probe:	5'-CATGGAAGCCTCTGTGGATATG-3' 5'-AAGCTGCAGGCACTGATGTG-3' 5'-FAM-CTCATCACGGGCCCGCTAAGGAAC-TAMRA-3'
TIMP3	Forward: Reverse: Probe:	5'-GGCCTCAATTACCGCTACCA-3' 5'-CTGATAGCCAGGGTACCCAAAA-3' 5'-FAM- TGCTACTACTTGCCCTGTTTTGTGACCTCCA-TAMRA-3'
SOD1	Premix	Mm01700393_g1*

CAT	Premix	Mn00437992_m1*
Trfc(Transferrin R)	premix	Mm00441941_m1*
HJV(Hemojuvelin)	Premix	Mm00510148_sl
FPN1(Ferroportin)	Premix	Mm00489837_m1*
HAMP1(Hepcidin1)	Premix	Mm00519025_m1
HAMP2(Hepcidin2)	Premix	Mm00842044_g1*
Ftl1(Ferritin-L)	Premix	Mm03030144_g1
Fth1(Ferritin-H)	Premix	Mm00085707_g1
HPRT	Forward: Reverse: Probe	5'- AGCTTGCTGGTGAAAAGGAC-3' 5'- CAACTTGCGCTCATCTTAGG-3' 5'-FAM-CAACAAAGTCTGGCCTGTATCCAAC-TAMRA-3'
18S rRNA	Premix	Mm03928990_g1*

**Immunoprecipitation.** Immunoprecipitation was performed with slight modification as described previously.<sup>226</sup> Total protein lysate (100-200 µg) from flash frozen liver tissue were incubated with 5 µg of anti-acetyl-Lysine (Millipore #05-515). The immune complex was captured by adding 50µl protein A/G Plus-agarose beads (Sc-2003) with gentle rocking for 6 hours at 4<sup>0</sup>C. After that tubes were centrifuged at 12000g for 3 minutes and the supernatants were discarded. The pellets were gently washed with ice-cold PBS and the immune complex resuspended in 60µl of 2X Laemmli sample buffer and resolved on 8% sodium dodecyl sulphate-poly acrylamide gel electrophoresis (SDS-PAGE) then transferred to PVDF membranes using a Trans-blot cell (Bio-Rad laboratories, Hercules CA USA).

**Nuclear and cytosolic protein extraction.** Nuclear fractionation was performed as previously described with slight modifications.<sup>226</sup> Briefly, liver tissues were homogenized in hypotonic lysis buffer (10 mM K-HEPES (pH 7.9), 1.5 mM MgCl<sub>2</sub>, 10mM KCl, 1 mM DTT, 0.2 mM Na<sub>3</sub>VO<sub>4</sub>, 1X protease inhibitor cocktail

(Calbiochem), 1X phosphatase inhibitors (Sigma and Calbiochem). The total homogenate was centrifuged at 100 g for 5 minutes to collect unbroken tissues. The supernatant was then centrifuged at 2,000 g for 10 minutes to precipitate crude nuclei from the cell membrane and cytosolic proteins (second supernatant). The second supernatant was further centrifuged at 100,000 g for 90 minutes to separate soluble cytosolic proteins (third supernatant) from membrane pellet. The crude nuclear fraction was re-suspended in hypotonic lysis buffer supplemented with 2.4 M sucrose, and then layered on top of a 2.4 M sucrose cushion and purified by centrifugation at 100,000 g for 90 min. Following ultracentrifugation, the purified nuclear pellet was re-suspended in storage buffer (20 mM Na-HEPES (pH 7.9), 0.42 M NaCl, 1.5 mM MgCl<sub>2</sub>, 0.2 mM EDTA, 0.2 mM EGTA, 0.5 mM PMSF, 0.5 mM DTT, 25% Glycerol, 1 x protease and phosphatase inhibitors). 30µg of nuclear protein and cytosolic protein from liver was subject to FOXO1 blotting. The purity of nuclear and cytosolic fractions was verified by using histone H3 (Cell Signaling; nuclear marker) and caspase-3 (Cell Signaling; cytosolic marker).

**Statistical Analysis.** All data were statistically analyzed by using the SPSS Statistics 19 software and the averaged values are presented as mean  $\pm$  SEM. One-way or two-way ANOVA was used for data analysis followed by multiple comparisons testing using the Tukey's test.

## **5.4 Results**

**Increased nuclear FOXO1 acetylation is the key contributor in the molecular pathogenesis of hepatic iron-overload which is reversed by resveratrol.** We first explored the signaling mechanisms associated with iron-mediated hepatic injury.

Deacetylation of FOXOs by SIRT1 protects cellular function during stress<sup>230</sup> and resveratrol is a natural polyphenol which can activate SIRT1<sup>165, 217, 230, 240</sup>. We performed FOXO1 immunofluorescence staining and confirmed the presence of nuclear FOXO1 during iron-induced oxidative stress in two distinct models of chronic hepatic iron-overload and was also unaffected by resveratrol treatment (**Figure. 5.1A**). Western blot analysis using nuclear and cytosolic fractions obtained from chronic iron-overloaded livers clearly showed increased levels of Forkhead box protein O1 (FOXO1) in the nuclear extract (**Figure. 5.1B**) with no change seen in response to resveratrol treatment. We next performed FOXO1 acetylation by immunoprecipitation and showed that iron-overloaded livers had significantly increased acetylated nuclear FOXO1 levels. Importantly, resveratrol supplementation markedly suppressed the acetylated FOXO1 levels (**Figure. 5.1C-D**). Consistent with these results, SIRT1 deacetylase protein levels was decreased in iron-overloaded livers and resveratrol supplementation restored SIRT1 to normal levels (**Figure. 5.1C-D**).

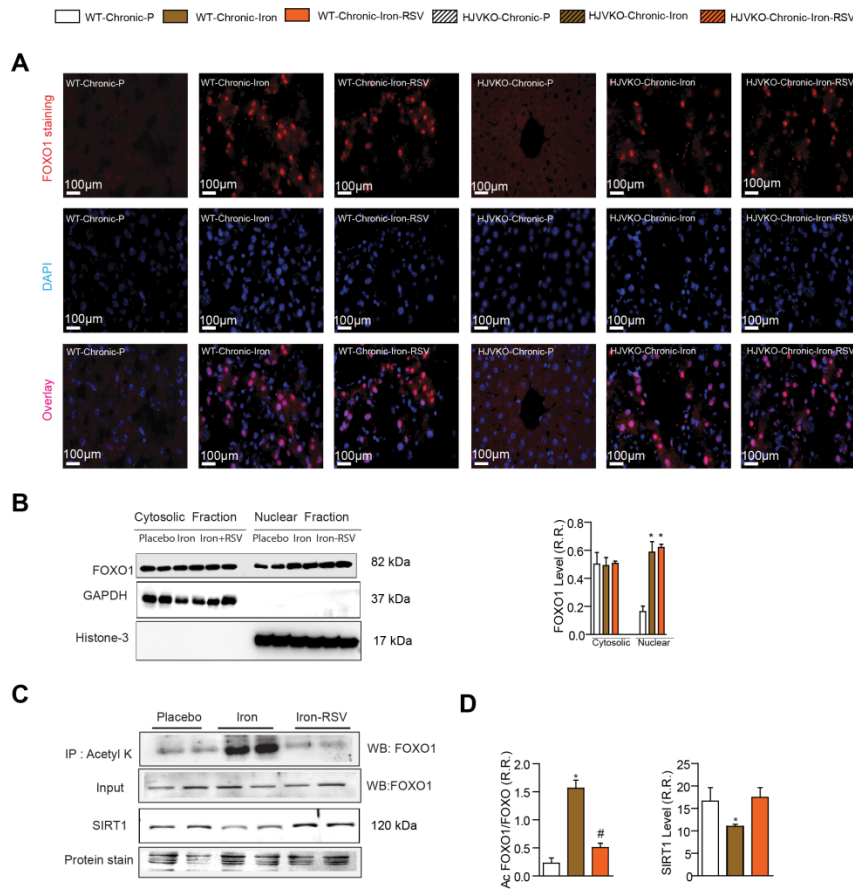


**Figure 5.1. Hepatic iron-overload increases nuclear FOXO1 acetylation which is restored by resveratrol.** (A) Immunofluorescence staining in hepatic iron-overload tissue confirming increased nuclear FOXO1 levels as illustrated by the merged images with nuclear FOXO1 levels and DAPI staining unaffected by resveratrol (RSV) treatment. (B) Western blot analysis and quantification of the major transcriptional factor, FOXO1, showing increased nuclear levels of FOXO1 in chronically iron-overloaded livers. (C-D) Western blot analysis and quantification showing increased acetylation of hepatic FOXO1 in response to iron-overload with decreased SIRT1 protein levels which were markedly ameliorated by the resveratrol (RSV) administration. A.U.= arbitrary unit; \* $p < 0.05$  compared with all other groups; # $p < 0.05$  compared with the placebo group.

**Chronic hepatic iron-overload alters iron metabolism and results in hepatic fibrosis: anti-fibrotic effects of resveratrol.** We established acquired and genetic murine models of chronic iron-overload and demonstrated hepatic iron-overload, as illustrated by Prussian blue staining and quantification of hepatic iron levels using inductive coupled plasma resonance spectroscopy (**Figure. 5.2A**), which was accompanied by hepatosplenomegaly ( **Figure. 5.2.1**). Iron metabolic gene expression analysis showed decreased expression of transferrin receptor 1 and increased expression of ferritin L/H, hemojuvelin, and hepcidin 1 and 2 in response to chronic iron-overload (**Figure. 5.2B**). The hepatic hemojuvelin (HJV)/hepcidin axis is altered in response to iron-overload while the HJVKO mice which lack HJV expression<sup>13, 51</sup> resulted in reduced hepcidin1 and hepcidin2 expression (**Figure. 5.2B**). These results provide important validation of our preclinical models of hepatic iron-overload. Importantly, resveratrol treatment did not affect the degree of hepatic iron-overload or the expression of key genes involved in iron metabolism (**Figure. 5.2A-B**).

Hepatic iron-overload in our pre-clinical models resulted in increased hepatic fibrosis as assessed by picro-Sirius red (PSR) and trichrome staining along with morphometric quantification (**Figure. 5.2C**). Consistent with these histological changes, expression analysis showed a marked upregulation of pro-fibrotic genes, pro-collagen I and III, TGF- $\beta$  and tissue inhibitor of metalloproteinases (TIMP), TIMP-1 and TIMP-3, in iron-overload liver tissues (**Figure. 5.2D**). We investigated the anti-fibrogenic effect of resveratrol dietary intervention in our chronic hepatic iron-overload models. Trichrome and PSR staining showed a significant reduction in hepatic fibrosis in resveratrol treated mice, which was consistent with the decreased hepatic expression

of the profibrotic genes in response to resveratrol (**Figure. 5.2C-D**). These results clearly demonstrate a seminal therapeutic effect of resveratrol on iron-overload mediated hepatic fibrosis independent of hepatic iron levels.

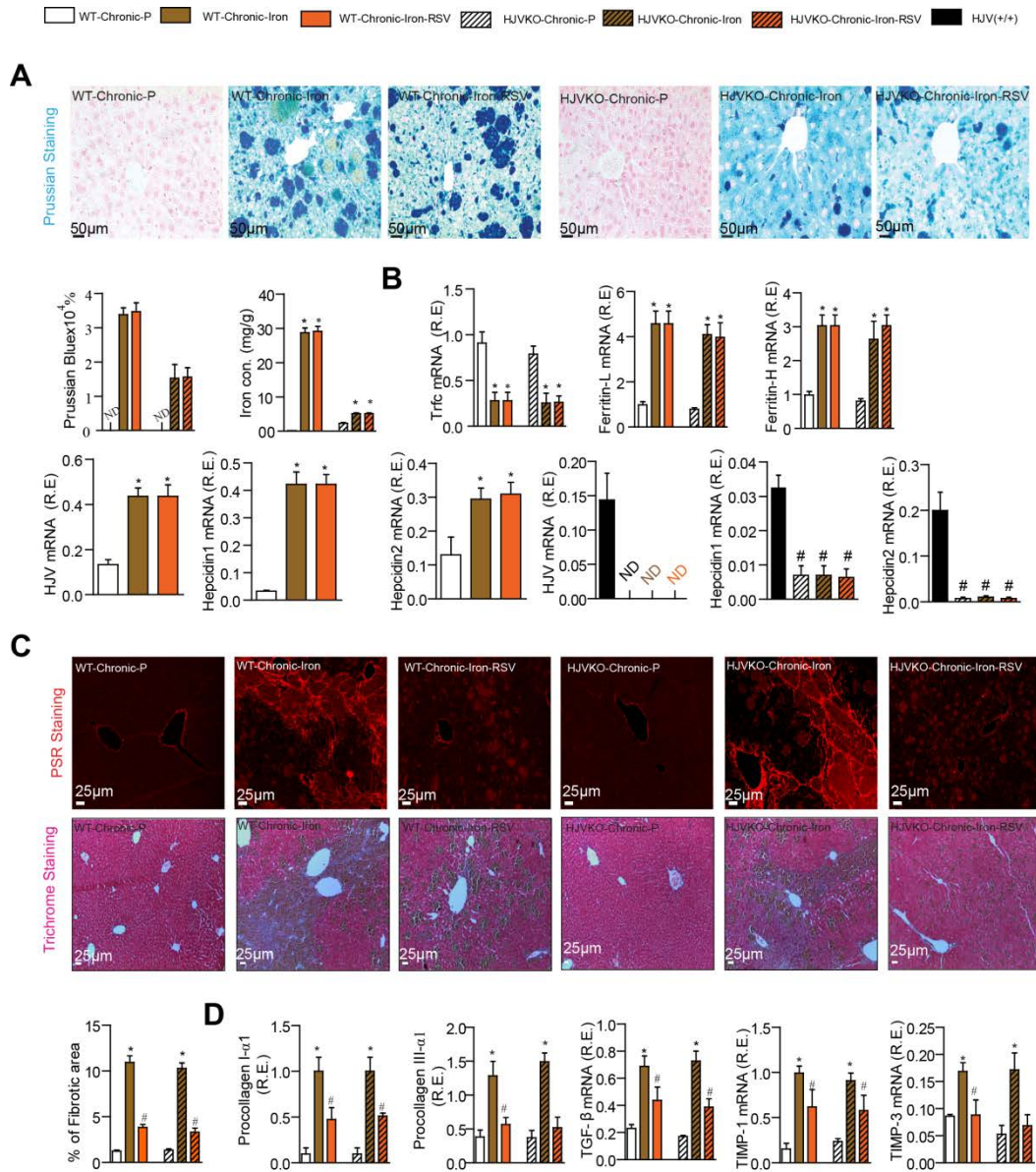


**Figure 5.2. Increased hepatic fibrosis, abnormal iron metabolism in chronic hepatic iron-overload is rescued by resveratrol therapy.** (A) Prussian blue staining of iron deposition in the livers of chronically iron-overloaded wildtype and hemojuvelin knockout (HJVKO) mice with quantification of hepatic iron levels. (B) Iron metabolic gene expression profile of transferrin receptor (*trfc*), ferritin light (ferritin-L) and heavy (ferritin-H) chains and hemojuvelin (HJV), showing hepatic iron-overload with resveratrol (RSV) having no effect on the degree of hepatic iron-overload. (C) Histological assessment of fibrosis using PSR and Trichrome staining. (D) Quantification of fibrotic area and expression of profibrotic genes (Procollagen I- $\alpha$ 1, Procollagen III- $\alpha$ 1, TGF- $\beta$  mRNA, TIMP-1 mRNA, and TIMP-3 mRNA).

hepatic fibrosis using picro-sirius red (PSR) and Mason's trichrome staining and quantification of fibrosis revealed increased hepatic fibrosis in the chronic iron-overloaded livers. (D) Expression analysis of hepatic pro-collagen I $\alpha$ 1, pro-collagen III $\alpha$ 1, transforming growth factor-beta (TGF- $\beta$ ), tissue inhibitor of metalloproteinases, TIMP1 and TIMP3 genes, in chronic iron-overloaded livers revealed increased levels consistent with a pro-fibrotic state. Resveratrol therapy prevented the increased in hepatic fibrosis based on histological changes and expression levels of the pro-fibrotic disease markers (C-D). R.F.=relative fraction; R.E.=relative expression; ND=not detected. n=4 for histological analyses; n=10 for iron levels; and n=8 for expression analyses. \*p<0.05 compared with all other groups; #p<0.05 compared with the placebo group.

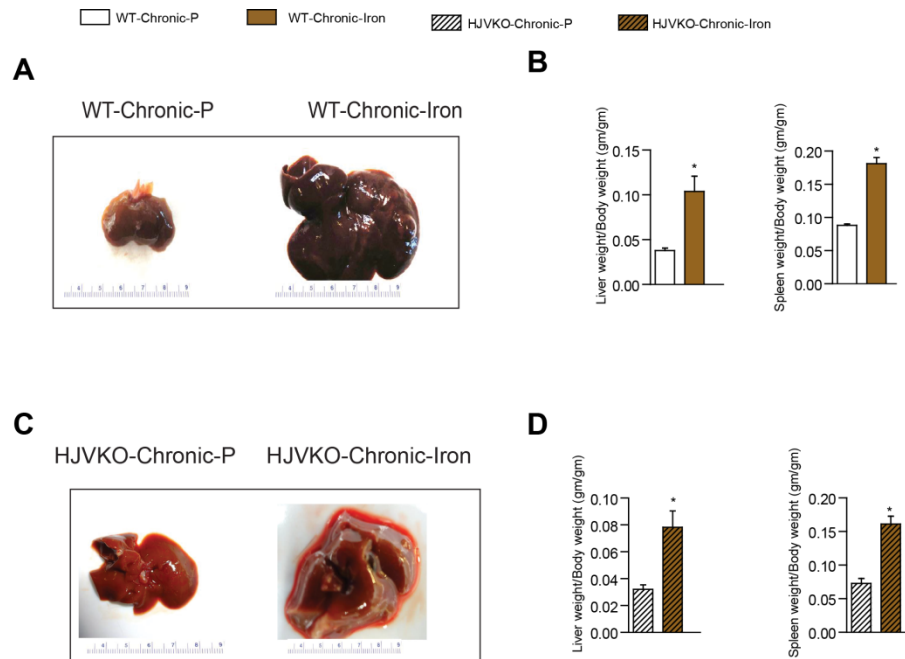


**Figure 5.2.1 Hepatic iron-overload is associated with hepatosplenomegaly.** Illustrative images showing increased liver weight in the chronic wildtype murine model (A) with increased liver and spleen weights corrected to body weight (B). Illustrative images showing increased liver weight in chronic hemojuvelin knockout (HJVKO) murine model (C) with increased liver and spleen weights corrected to body weights (D). n=8 per group; \*p<0.05 compared with all other groups; compared with the placebo group.

**Iron-induced oxidative stress and lipid peroxidation in the pathogenesis of chronic hepatic iron-overload: antioxidant effects of resveratrol.** Iron-induced free radicals are key mediators of hepatic oxidative stress and lipid peroxidation<sup>83, 107, 257</sup>. Chronic

iron-overload triggered increased oxidative stress in the liver characterized by increased dihydroethidium (DHE) fluorescence, 4-hydroxynonenal (4-HNE) and nitrotyrosine immunostaining confirming the presence of reactive free radicals (**Figure. 5.3A-B**). To further characterize the presence of oxidative stress in chronic iron-overloaded livers, we measured glutathione levels, which is a potent and abundant antioxidant system in the liver. Biochemical evaluation of hepatic oxidative stress revealed depletion of reduced glutathione (GSH), increased the formation of oxidized glutathione (GSSG) and a drastic reduction in the GSH/GSSG ratio, coupled with a marked generation of the lipid peroxidation product, malondialdehyde (MDA) (**Figure. 5.3C**). Chronic hepatic iron-overload markedly suppressed the expression of two key anti-oxidant genes, catalase and superoxide dismutase 1, which likely further exacerbates hepatic oxidative stress (**Figure. 5.3D**). We investigated the pharmacological effect of resveratrol on hepatic oxidative stress and lipid peroxidation under iron-overloaded conditions. Resveratrol completely prevented the iron-mediated oxidative stress in iron-overloaded wildtype and HJVKO murine models demonstrating a potent anti-oxidant effect. Dihydroethidium fluorescence, 4-HNE and nitrotyrosine immunostaining clearly confirmed a significant reduction of oxidative stress in mice treated with resveratrol (**Figure. 5.3A-B**). Resveratrol increased hepatic antioxidant GSH reserve, reduced the extent of lipid peroxidation and normalized the expression of the antioxidant genes, catalase and superoxide dismutase 1 (**Figure. 5.3C-D**). These data clearly demonstrate that iron-mediated oxidative stress in the liver is markedly reduced by resveratrol therapy based on fluorescence and immunostaining, biochemical and gene expression analyses.

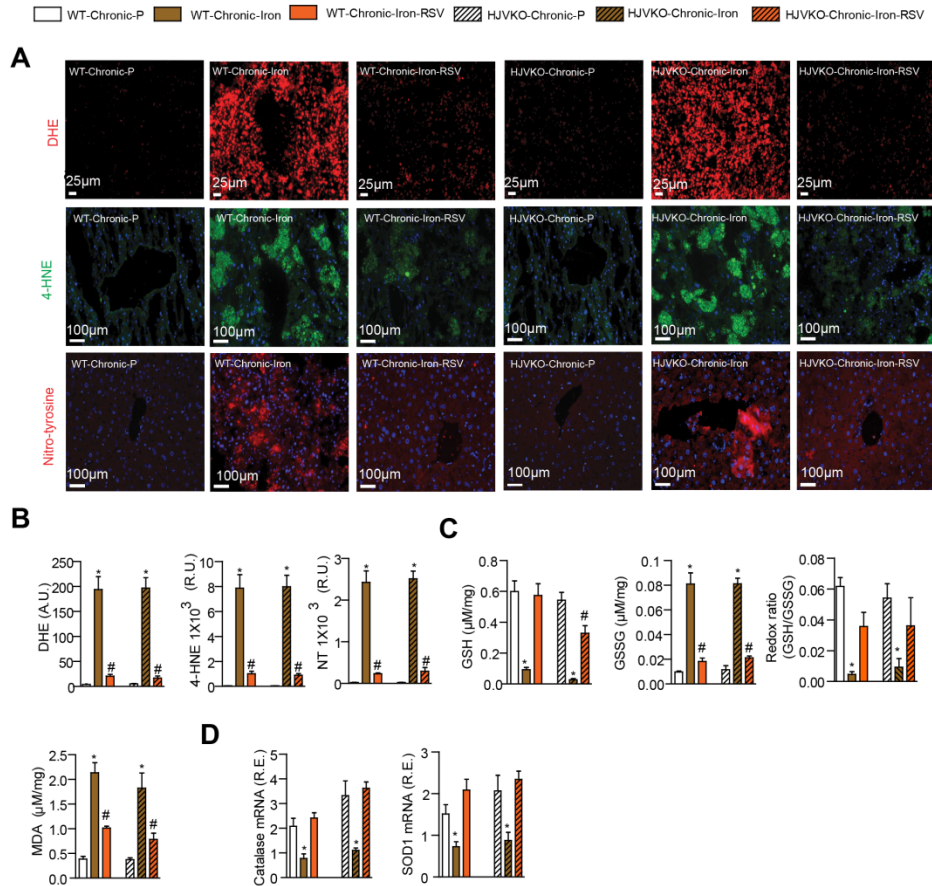


**Figure 5.3. Iron-induced oxidative stress in chronic hepatic iron-overload is suppressed by resveratrol therapy.** (A) Pronounced pro-oxidant hepatic phenotype with increased dihydroethidium (DHE) staining for superoxide levels (top), 4-hydroxynonenal (4-HNE) immunofluorescence (middle), nitrotyrosine (NT) immunofluorescence (bottom) and quantification of oxidative stress (B), with a marked suppression of iron-induced oxidative stress by resveratrol therapy. DHE fluorescence and is predominantly nuclear while 4-HNE and nitrotyrosine immunofluorescence are more diffuse. (C) Hepatic levels of reduced glutathione (GSH), oxidized glutathione (GSSG) and the redox ratio, and the hepatic lipid peroxidation product, malondialdehyde (MDA) were altered demonstrating biochemical evidence of increased oxidative damage and reduced antioxidant reserve in chronic hepatic iron-overload, markedly corrected by oral resveratrol therapy. (D) Resveratrol potentiated the upregulation of key antioxidant enzymes, catalase (CAT) and superoxide dismutase 1 (SOD1) in chronic hepatic iron-overloaded livers. A.U.=arbitrary unit; R.U.=relative unit; R.E.=relative expression; n=4 for immunofluorescence analysis; n=8 for biochemical and expression analyses. \*p<0.05 compared with all other groups; #p<0.05 compared with the placebo group.

**Resveratrol prevents the inflammatory and pro-apoptotic phenotype associated with chronic hepatic iron-overload.** Chronic hepatic injury can initiate a sequence of events resulting in chronic tissue inflammation and increased production of pro-inflammatory cytokines which further exacerbates liver injury and end-organ damage.<sup>258, 259</sup> We showed that hepatic iron-overload is associated with increased infiltration of neutrophils, macrophages and CD8-positive lymphocytes (**Figure. 5.4A**) and increased expression of pro-inflammatory cytokines, interleukin-6 (IL-6), interleukin-1beta (IL-1 $\beta$ ) and tumor necrosis factor-alpha (TNF- $\alpha$ ) (**Figure. 5.4B**). Increased hepatic inflammation correlated with greater susceptibility to apoptosis revealed by increased TUNEL-positive hepatocyte staining in wild-type and HJVKO chronic iron-overloaded mice (**Figure. 5.4C**) coupled with increased cleaved caspase-3 in chronic iron-overloaded livers (**Figure. 5.4D**). Resveratrol treatment resulted in a marked reduction in hepatic inflammation (**Figure, 5.4A-B**) and apoptotic cell death (**Figure. 5.4C-D**) in iron-overloaded wildtype and HJVKO mice.

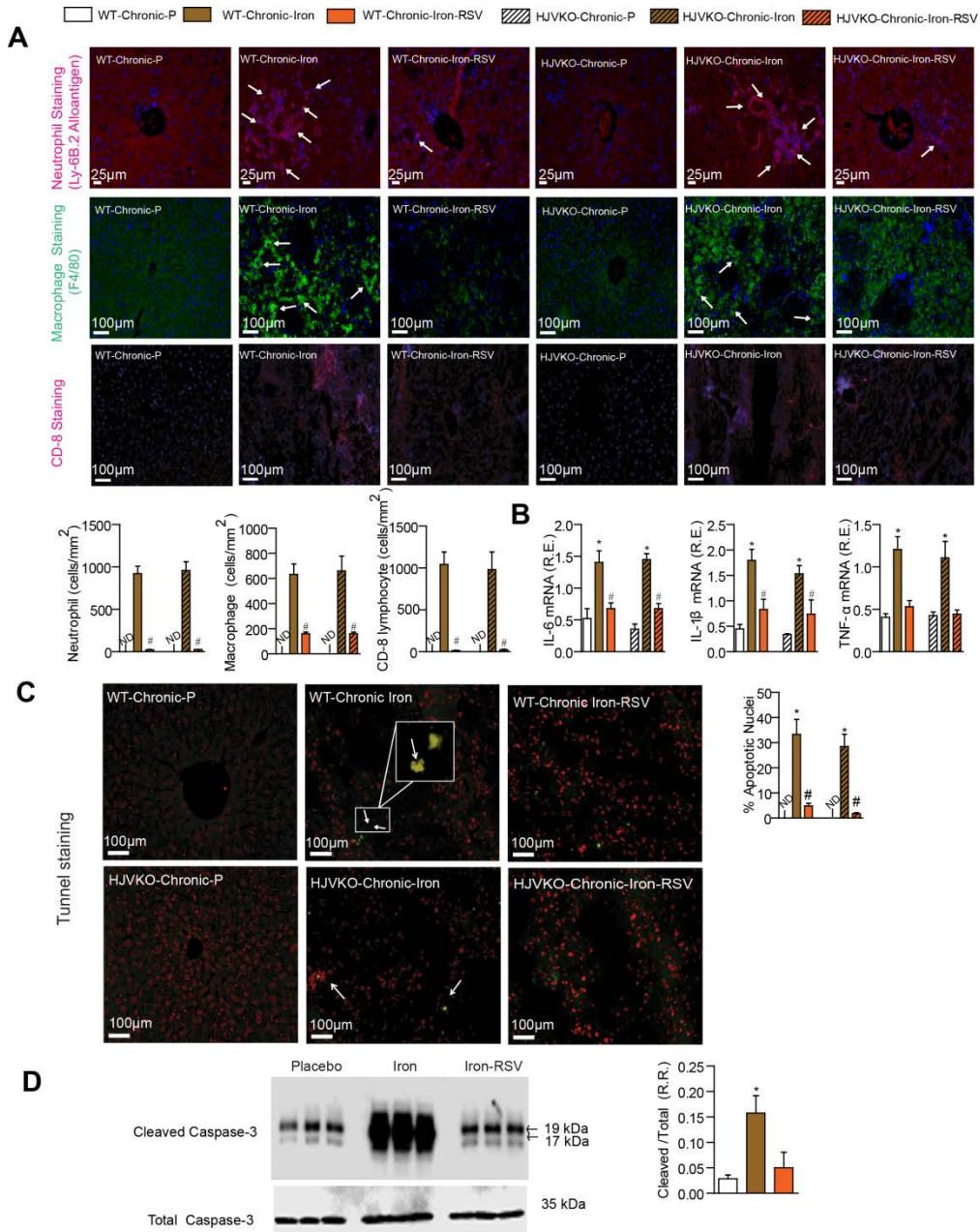


**Figure 5.4. Iron-induced hepatic inflammation and apoptosis in chronic hepatic iron-overload is suppressed by resveratrol.** (A) Immunostaining for neutrophil (top), macrophage (middle) and CD-8 positive lymphocyte (bottom) and quantification of inflammatory cells showing clear evidence of an increased inflammation in the liver prevented by resveratrol therapy. (B) Gene expression analysis of interleukin-6 (IL-6), interleukin-1beta (IL-1 $\beta$ ) and tumor necrosis factor-alpha (TNF- $\alpha$ ) showing a marked upregulation of pro-inflammatory genes in iron-overloaded livers which were prevented by resveratrol. (C) TUNEL staining and quantification in the livers of chronically iron-overloaded wildtype and hemojuvelin knockout (HJVKO) mice with quantification of hepatic apoptotic nuclei showing that resveratrol suppressed an iron-overload mediated increase in apoptosis in the liver. (D) Western blot analysis of cleaved/total caspase-3 confirmed a pro-apoptotic state in the chronic iron-overloaded liver which was rescued by resveratrol therapy. R.E.=relative expression; R.R.=relative ratio; ND=not detected; n=4 for histological analyses; n=8 for expression analysis; n=6 for Western blot. \*p<0.05 compared with all other groups; #p<0.05 compared with the placebo group.

**Therapeutic effects of resveratrol are maintained in advanced hepatic iron-overload.** Iron-overload is a chronic disease and, therefore, we aged HJVKO mice to one year of age while being fed an iron-enriched diet in order to examine progressive and cumulative hepatic iron-overload injury. Assessment of oxidative stress using DHE fluorescent and 4-HNE immunostaining showed markedly increased levels of reactive free radicals in the advanced hepatic iron-overload livers (**Figure. 5.5A**) coupled with increased oxidized glutathione (GSSG), decreased reduced glutathione (GSH) and redox ratio along with increased generation of MDA (**Figure. 5.5B**). Interestingly, the histopathological assessment showed that iron-overloaded one-year old HJVKO mice exhibited increased hepatic fibrosis (**Figure. 5.5C and Figure. 5.5E**), in association with marked hepatocyte vacuolation and hepatic steatosis (**Figure. 5.5D and Figure. 5.6A**) which was not present in chronic iron-overloaded livers ( **Figure. 5.6B-C**). Biochemical assessment of triglyceride levels confirmed a marked tissue accumulation of triglycerides in the liver (**Figure. 5.5D**) in the absence of a diabetic state but in association with chronic inflammation (**Figure. 5.7**). Resveratrol dietary intervention started at 9 months of age completely rescued the advanced iron-overloaded liver disease in association with normalization of the various histological and biochemical alterations proving that its therapeutic effects are persistent in advanced iron-overload (**Figure. 5A-D**).

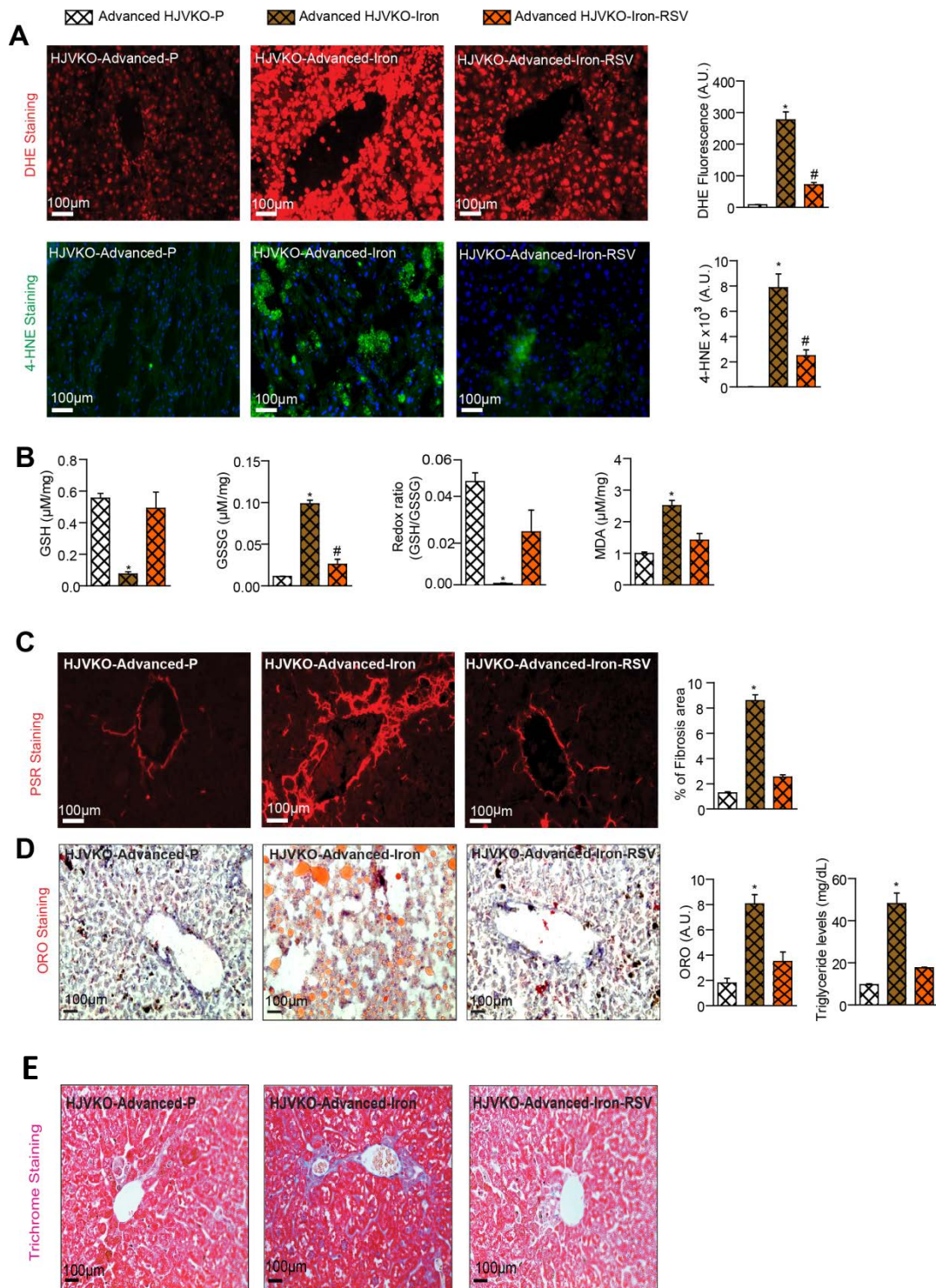


**Figure 5.5. Resveratrol therapy prevents iron-induced oxidative stress, fibrosis and steatosis at an advanced stage of hepatic iron-overload in aged hemojuvelin knockout mice.** (A) Iron-overload in aged hemojuvelin knockout (HJVKO) mice display a pronounced hepatic oxidative stress phenotype with increased dihydroethidium (DHE) staining for superoxide levels (A) and 4-hydroxynonenal (4-

HNE) immunofluorescence. (B) The biochemical assessment showed increased oxidized glutathione (GSSG), decreased levels of reduced glutathione (GSH) and the redox ratio, coupled with the increased generation of the lipid peroxidation product, malondialdehyde (MDA). Resveratrol therapy restored a normal redox state in the advanced iron-overloaded liver tissue (A-B). (C) Liver picosirius red (PSR) histopathological staining showing increased hepatic fibrosis markedly suppressed by resveratrol therapy. (D) Oil-O-Red (ORO) staining and biochemical assessment of hepatic triglycerides levels.(E) Masson's Trichrome staining showing the presence of hepatosteatosi and lipid accumulation in advanced iron-overload in HJVKO mice which was completely prevented by resveratrol therapy. ND=not detected; R.F.=relative fraction; A.U.=arbitrary unit. n=4 for histology analysis; n=8 for the biochemical analyses. \*p<0.05 compared with all other groups; #p<0.05 compared with the placebo group.

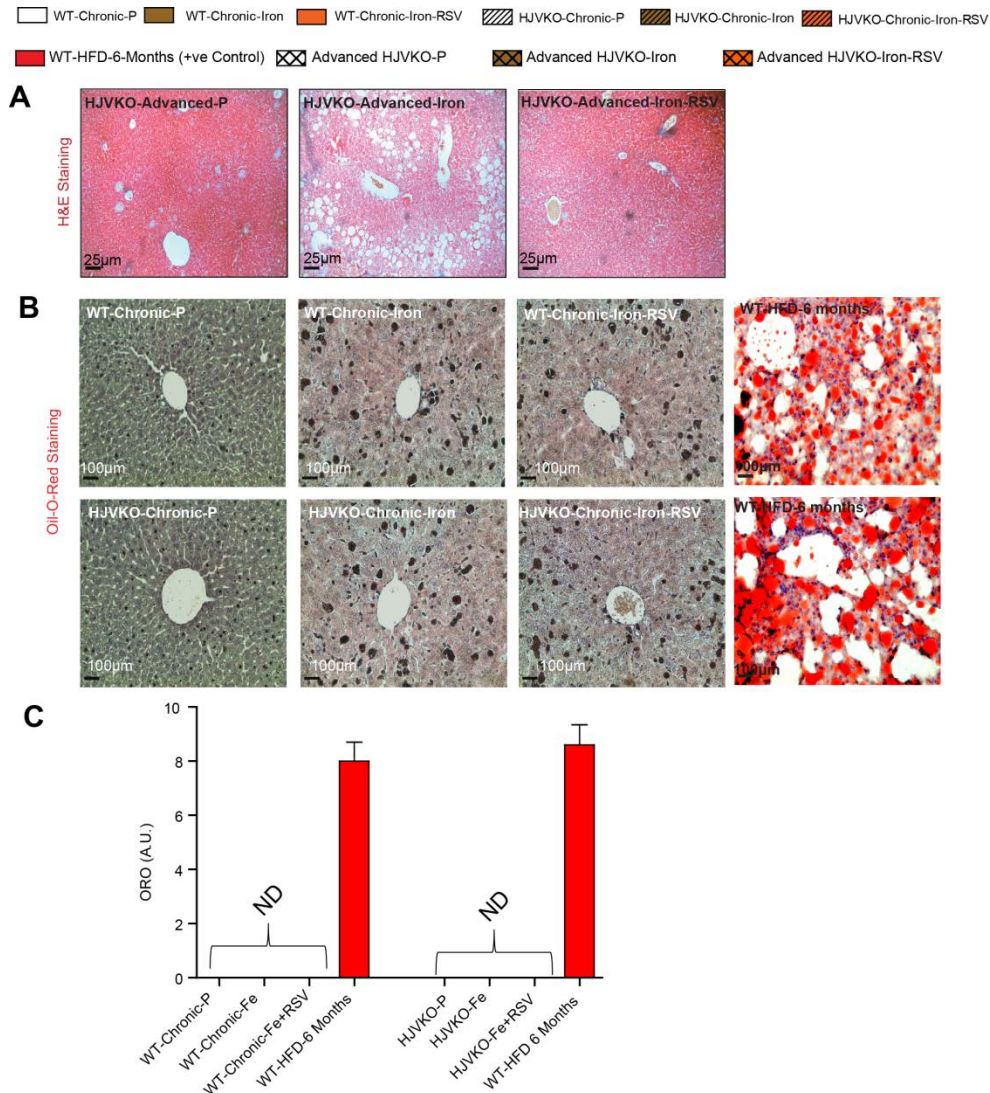


**Figure 5.6.** Hemotoxylin and eosin histopathological staining showing increased hepatic fibrosis and hepatocyte vacuolation in advanced iron-overloaded hemojuvelin knockout(HJVKO) livers markedly suppressed by resveratrol therapy (A).The absence of hepatosteatosi based on oil red O (ORO) staining (B) and morphometric quantification(C) in chronically iron-overloaded wildtype and HJVKO murine models. Positive control fatty livers were obtained from wild-type mice fed a 45% high-fat diet (HFD) for 6 months.

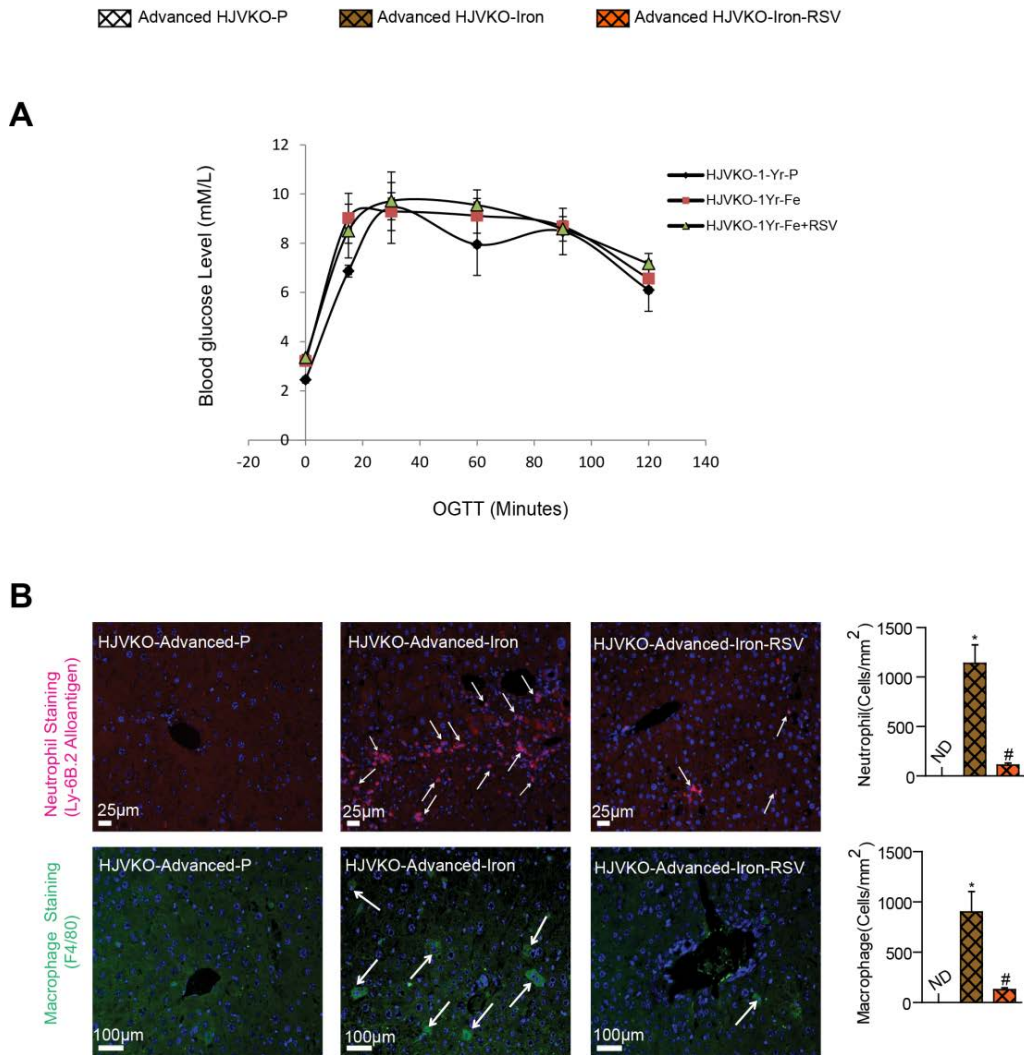


**Figure 5.7.** Oral glucose tolerance testing (1.5g/kg) showing normal fasting blood glucose levels with an equivalent response to glucose challenge in advanced iron-overloaded HJVKO mice (A). Hepatic inflammation in advanced iron-overloaded HJVKO livers characterized by the presence of increased inflammatory cells, neutrophils and macrophages (shown by white arrows), was markedly suppressed by resveratrol dietary (B)

## 5.5 Discussion

Advanced and chronic iron-induced oxidative stress is a major contributor to the progression of chronic liver diseases. Liver disease leading to end-stage cirrhosis and/or hepatocellular carcinoma due to iron-overload contributes to the morbidity and death in patients with iron-overload conditions.<sup>45, 106, 146, 147, 260</sup> Altered iron metabolism, iron-induced oxidative stress and lipid peroxidation have emerged as a unique and important mechanism by which iron can produce toxic effects resulting in hepatic dysfunction.<sup>83, 107, 257</sup> *In vivo* models of hepatic siderosis have provided a biochemical and histopathological basis for liver disease and represent a useful preclinical tool to examine novel therapies in iron-overload.<sup>108, 257, 261, 262</sup> We used both an acquired and genetic model of iron-overload including an advanced model of iron-overload to examine the therapeutic effects of resveratrol. The model of chronic iron-overload in wildtype mice has previously been validated to simulate acquired iron-overload.<sup>77, 83</sup> Our HJVKO mice were used to simulate both chronic and advanced iron-overload in a genetic hemochromatosis model,<sup>51, 263</sup> whereby the lack of the functional hemojuvelin protein downregulates hepcidin expression leading to abnormal iron homeostasis, uncontrolled gut absorption of iron, and iron-overload<sup>13, 254</sup> Importantly, the hepatic iron levels observed in our murine models is comparable to that observed in patients suffering from hemochromatosis and secondary iron-overload.<sup>53, 264, 265</sup>

We defined a pivotal therapeutic role of resveratrol on iron-mediated hepatic injury and liver disease. Histological, biochemical and molecular characterization demonstrated that our murine models mimicked many of the clinical features of iron-

overload. Chronic iron-overload in the liver resulted in increased acetylated FOXO1 nuclear levels which correlated with reduced SIRT1 levels and activity. The ability of resveratrol to modulate the SIRT1/FOXO1 axis is likely to play a major role in its therapeutic effects since classic anti-oxidant therapy using vitamin E in models of hepatic iron-overload has produced mixed results<sup>257, 262</sup>. The liver, in particular, has a high burden of oxidative stress and iron-induced oxidative stress further exacerbates the intrinsic antioxidant capacity and leads to formation of aggressive free radicals which impair normal cellular function leading to end-stage cirrhosis and liver disease.<sup>266</sup> Importantly, resveratrol supplementation did not affect the degree of iron-overload in the liver but rather provides protection from iron-mediated tissue injury. While resveratrol is a pleiotropic natural polyphenol with antioxidant capacity, reduced acetylation of FOXO1 leading to the increased expression of anti-oxidant genes has likely contributed to its therapeutic action in iron-loaded livers. The nuclear localization of FOXO1 transcription factor regulates metabolic and antioxidant gene expression while increased acetylated nuclear FOXO1 reduces the expression of key antioxidant enzymes and proteins<sup>230, 267</sup>. Given the detrimental effects of iron-overload on mitochondrial function<sup>94, 257</sup>, the therapeutic effects of resveratrol on mitochondria may also contribute to its beneficial effects in iron-overloaded liver disease.

Chronic hepatic iron-overload exacerbates hepatic fibrosis and iron induced hepatic remodeling, that leads to advanced liver disease and cirrhosis<sup>258, 266, 268, 269</sup>. Hepatocyte cell death and inflammation is the ultimate driver of liver disease progression and the development of advanced liver disease and has been linked to increased oxidative stress<sup>270, 271</sup>. Indeed, iron-induced oxidative stress and depletion of GSH can sensitize

hepatocytes to TNF- $\alpha$  induced apoptosis<sup>270</sup> Iron-mediated hepatocyte injury leads to permanent loss of hepatic parenchyma, associate with collagen deposition as a process of wound healing and overproduction and accumulation of different components of the extracellular matrix. Hepatic fibrosis is a major pathological feature of the chronic liver disease and new strategies are needed to target this key pathophysiological process in liver disease.<sup>258, 272, 273</sup> Our results are consistent with the beneficial effects of resveratrol on cultured rat hepatic stellate cells and Kupffer cells.<sup>274</sup> In addition, anti-oxidant treatment during experimental hepatic fibrosis arrests fibrogenesis mainly through inhibition of nonparenchymal cell proliferation induced by iron.<sup>262</sup>

We also used an advanced a pre-clinical genetic hemochromatosis in which these mice were subjected to iron-overload over a one-year period. Resveratrol rescued the liver disease in these experimental animals providing pivotal evidence that its therapeutic action is not curtailed in the setting of advanced liver disease.

**5.6 Conclusions:** In summary, our study provides the evidence that in murine models of chronic and advanced hepatic iron-overload, resveratrol therapy mediates salutary therapeutic effects and represents a potential therapy for liver disease in patients with iron-overload.

# CHAPTER SIX

# **Females are protected from iron-overload cardiomyopathy independent of iron metabolism: key role of oxidative stress**

Subhash K. Das<sup>1,2</sup>, Vaibhav B. Patel<sup>1,2</sup>, Ratnadeep Basu<sup>1,2</sup>, Wang Wang<sup>2,3</sup>, Jessica DesAulniers<sup>1,2</sup>, Zamaneh Kassiri<sup>2,3</sup> and Gavin Y. Oudit<sup>1,2,3</sup>

<sup>1</sup>Division of Cardiology, Department of Medicine, <sup>2</sup>Mazankowski Alberta Heart Institute,

<sup>3</sup>Department of Physiology, University of Alberta, University of Alberta, Edmonton, Canada,

**A modified version of this chapter has been submitted for reviewing to**

***Journal of American Heart Association***

## **6.1 Abstract**

Gender-based differences in cardiac function and iron metabolism exist in humans and experimental animals. Males are more susceptible to cardiomyopathies and heart failure in pre-clinical models and patients. However, whether similar differences are seen in iron-overload cardiomyopathy is poorly understood. Male and female wild-type and hemojuvelin-null (HJVKO) mice were injected and fed with high iron diet, respectively, to develop secondary iron-overload and genetic hemochromatosis. Female mice were completely protected from iron-overload cardiomyopathy while iron-overload resulted in marked diastolic dysfunction in male iron-overloaded mice based on echocardiographic and invasive pressure-volume analyses. Female mice demonstrated a marked suppression of iron-mediated oxidative stress and a lack of myocardial fibrosis despite the equivalent degree of myocardial iron deposition. Ovariectomized female mice with iron-overload exhibited essential pathophysiological features of iron-overload cardiomyopathy showing distinct diastolic and systolic dysfunction, severe myocardial fibrosis, increased myocardial oxidative stress and increased expression of cardiac disease markers. Ovariectomy prevented iron-induced upregulation of ferritin and decreased myocardial SERCA2a levels and increased NCX1 levels. The responses in wildtype and HJVKO female mice were remarkably similar highlighting a conserved mechanism of gender-dependent protection from iron-overload mediated cardiac injury. We conclude that male and female mice respond differently to iron-overload mediated effects on heart structure and function, and female gender is markedly protected from iron-overload cardiomyopathy. Ovariectomy in

female mice exacerbated iron-induced myocardial injury and precipitated severe cardiac dysfunction during iron-overload conditions.

**Keywords:** Iron-overload, oxidative stress, myocardial fibrosis, gender, heart failure, hemojuvelin and ovariectomy.

## 6.2 Introduction

Iron is an essential element in biological systems because of its ability to shuttle between two oxidative states, and plays a key role in cell metabolism and homeostasis. Excess iron (iron-overload) or lack of iron (iron-deficiency) are the two major pathophysiological states of abnormal iron metabolism.<sup>7, 13</sup> Under physiological conditions, iron transport is highly conserved and controlled by iron transporters including transferrin and its receptors via negative feedback regulatory mechanisms.<sup>1, 3</sup> However, in primary hemochromatosis and secondary iron-overload, iron metabolism is perturbed, which leads to chronic iron-overload and its associated morbidity and mortality.<sup>13, 152</sup> Iron-overload cardiomyopathy is the most common cause of mortality in patients with secondary iron-overload and is a major co-morbidity in patients with primary hemochromatosis.<sup>45, 54, 60, 74</sup> Uncontrolled iron absorption causes transferrin saturation and increased levels of non-transferrin bound iron, which is highly reactive, toxic and triggers oxidative stress.<sup>54</sup> Iron-induced oxidative stress is a key driver in the pathogenesis of myocardial tissue injury and progressive development of iron-overload cardiomyopathy.<sup>60, 77, 83</sup> Excess iron promotes oxidative stress via the Fenton reaction which plays a key pathogenic role in heart failure.<sup>83, 275</sup>

Gender-related difference does exist in the pathophysiology of cardiac diseases and sex-specific pathways play a key role in the cardioprotection observed in cardiomyopathies and heart failure in pre-clinical models and patients.<sup>276-279</sup> Estrogen has several beneficial pleiotropic effects on the cardiovascular system.<sup>280, 281</sup> Functional estrogen receptors are expressed in cardiomyocytes and cardiac fibroblasts<sup>101</sup> and via the activation of these receptors, beta-estradiol, attenuates cardiac hypertrophy, metabolic dysregulation and cardiac apoptosis.<sup>226, 282, 283</sup> In addition, lack of estrogen leads to adverse pathophysiological cardiac remodeling and precipitates heart failure.<sup>284, 285</sup> Gender-related disparities in the regulation of iron metabolism may contribute to the differences in progression of iron-overload heart disease.<sup>286, 287</sup> Moreover, women have lower iron stores which have been argued to confer protection in an iron-overloaded state.<sup>288, 289</sup> In this study, we investigated the gender-specific differences and mechanisms of iron-overload cardiomyopathy.

### **6.3 Materials and Methods**

**Experimental animal protocols.** Wildtype (WT; C57BL6/J) male and female mice (from Jackson Laboratory, Bar ME) and hemojuvelin null (HJV<sup>-/-</sup>; HJVKO) male and female mice kindly provided by Dr. Nancy C. Andrews, Duke University, were bred in-house at the University of Alberta Health Sciences Laboratory Animal Services housing facility. All experiments were performed in accordance with University of Alberta institutional guidelines which conformed to guidelines published by the Canadian Council on Animal Care and the Guide for the Care and Use of Laboratory Animals published by the US National Institutes of Health (revised 2011). Intraperitoneal iron

injections of 5 mg of iron dextran per 25 g body weight injected i.p. on a 5 day/week schedule for the total duration of 4 wk followed by 1.25 mg/25 g body weight for 8 more wk in WT C57BL6 mice generated the secondary iron-overload model.<sup>7, 74, 173, 275</sup> Treatment with high iron diet (Prolab<sup>®</sup> RHM 3000 with iron 380 ppm) to HJVKO mice for 6 months generated the murine model of genetic hemochromatosis.<sup>275, 281</sup>

**Ovariectomy surgery protocol.** Ten weeks old WT and HJVKO female mice are subjected to bilateral ovariectomy as described previously.<sup>283, 290-292</sup> Briefly, mice were anesthetized by using isoflurane (1-1.5%) and maintained at 37<sup>0</sup>C on a heating pad. A midline abdominal incision was made in the skin and muscle layer and the ovaries were identified and excised after ligation. Animals were carefully inspected after surgery. The removed ovaries were fixed in 10% buffered formalin and characterized by H&E staining to confirm complete removal of ovaries. Mice were used for experimental use starting at 2 weeks following recovery.

**Echocardiography.** Non-invasive transthoracic echocardiography was performed on anesthetized mice by using isoflurane (1-1.5%) as described previously.<sup>77, 225, 226, 250</sup> A Vevo 770 high-resolution imaging system equipped with a 30-MHz transducer (RMV-707B; VisualSonics, Toronto, Canada) was used and systolic and diastolic cardiac functions were analyzed. Systolic function was assessed using B-mode and M-mode images of Echocardiography. (Motion mode) M-mode images were obtained for measurements of left ventricular (LV) wall thickness, LV end-diastolic diameter (LVEDD), and LV end-systolic diameter (LVESD) (measures of LV dilation). LV fractional shortening (FS) and LV ejection fraction (EF) were calculated using the following equations:  $FS (\%) = (LVEDD - LVESD / LVEDD) \times 100$  and  $EF (\%) =$

$(LVEDV-LVESV/LVEDV) \times 100$ . Diastolic function was assessed using pulsed-wave Doppler imaging of the trans-mitral filling pattern with the early trans-mitral filling wave (E-wave) followed by the late filling wave due to atrial contraction (A-wave). Isovolumetric relaxation time (IVRT) was calculated as the time from the closure of the aortic valve to initiation of the E-wave. The deceleration time of the E-wave (DT) was determined by measuring the time needed for the down-slope of the peak of the E-wave to reach the baseline while the rate of E-wave deceleration rate (EWDR) was calculated as the E-wave divided by the DT. Tissue Doppler imaging (TDI) represents a novel and validated technique to assess systolic and diastolic function, with a reduction in  $E'$  and an elevation in  $E/E'$  being considered as valid markers of elevated LV filling pressure and diastolic dysfunction. TDI was carried out at the inferolateral region in the radial short axis at the base of the LV with the assessment of peak annular systolic ( $S'$ ), early diastolic ( $E'$ ), and late diastolic ( $A'$ ) myocardial velocities as described previously.<sup>77, 225,</sup>  
250

**Invasive hemodynamic analysis.** We performed invasive pressure-volume (PV) loop analysis by using 1.2F Scisense catheter connected to an amplifier (TCP-500 Scisense Inc.) Mice were anesthetized by using isoflurane (1-1.5%) and are maintained at 37<sup>0</sup>C by using a heating pad. An incision was made in the right common carotid artery and the catheter was carefully inserted into the incision and the catheter was advanced through the aortic valve and placed into the LV chamber. The position of the catheter was monitored by pressure along with the magnitude and phase using ADvantage pressure volume system (Scisense Inc., London, Canada) and iworx (iWorx Systems Inc., Dover, USA) data acquisition system connected to the catheter. Initially, the

catheter position was set in the LV to obtain the magnitude difference of more than 200 $\mu$ S along with a physiological pressure-volume loop shape. After the magnitude was accomplished in the desired range, the phase was adjusted to 4-8 with slightly adjusting the position of the catheter in the LV where phase represents the conductivity imparted by the LV tissue. Once, the desired range for magnitude and phase was achieved, baseline scan was performed to derive volume using Baan's equation and pressure-volume loop was obtained using the LabScribe2 software (version 2.347000). Following baseline PV measurements, transient inferior vena cava occlusion was performed through the diaphragm to obtain the alteration in venous return to derive end-diastolic pressure volume relationships; transient infra-renal aorta occlusion was used to derive the end-systolic pressure volume relationship. Load-dependent and load-independent indices of LV functions were derived. By making and plotting the instantaneous values of pressure and volume at different time points, we determined the ESP, EDP, ESV and EDV in mmHg and  $\mu$ L respectively. Heart rate was estimated beat-to-beat cycle length. The  $SV = EDV - ESV$ ,  $CO = SV \times HR$ ,  $EF\% = SV / EDV$ , the SW is the area under a PV-Loop and was normalized by dividing with EDV to obtain preload recruitable stroke work (PRSW) which is also a load independent parameter.  $+dP/dt_{(max)}$ , and  $-dP/dt_{(min)}$  are the first derivative of pressure with respect to time and we also took their ratio ( $-dP/dt_{(min)} / +dP/dt_{(max)}$ ) to show a better index of relaxation phase,  $\tau(\tau)$ -the time constant of monoexponential pressure decay during isovolumic relaxation, the preload-independent  $+dP/dt_{(max)}$ , also called the Starling's contractile index (SCI) was calculated by dividing  $+dP/dt_{(max)} / EDV$ , which is a better index of myocardial contractility. Systolic and diastolic cardiac performances were also assessed

by the end-systolic pressure volume relationship (ESPVR) and end-diastolic pressure volume relationship (EDPVR), respectively as described previously.<sup>91, 225, 226, 293</sup>

**Histology and Fluorescence Staining.** Mice hearts were removed and arrested in diastole by using 1M KCl, fixed in 10% buffered formalin, and embedded in paraffin. Five  $\mu\text{m}$  thin sections were used for Prussian blue, picro-sirius red (PSR) and Masson trichrome staining as described previously.<sup>91, 224, 226</sup> Briefly, tissue sections were deparaffinized in xylene and alcohol grades, then rehydrated in water and subjected to respective staining protocol as described previously.<sup>91</sup> The deposition of iron was visualized as blue depositions using bright field microscope. Myocardial collagen content was evaluated by using PSR staining followed by visualization under Olympus IX81 microscope and image analysis using MetaMorph software as described previously.<sup>223, 226, 294</sup> 4-Hydroxynonenal (4-HNE) immunofluorescence detected an important marker of iron induced lipid peroxidation as previously described.<sup>91</sup> We also performed dihydroethidium fluorescence staining on 15 $\mu\text{m}$  thick myocardial frozen sections as described previously.<sup>224, 284</sup> which were visualized using an Olympus IX81 fluorescent microscope and quantified using the MetaMorph software.

**Terminal deoxynucleotidyl transferase-mediated dUTP nick-end labeling (TUNEL) assay.** Five  $\mu\text{m}$  thick LV heart sections were subjected to TUNEL staining and visualized using an Olympus IX81 fluorescent microscope as described previously.<sup>91, 226</sup> Briefly OCT sections were fixed with 4% paraformaldehyde and then hydrated with 1XPBS at room temperature. Permeabilization followed by blocking with 1% BSA for 30 min and immediately incubated with DNA labeling solution for 1 hours at 37<sup>0</sup>C. After this rinsed with rinse buffer 2 times 5min each followed by anti-BrdU

incubation at 37<sup>0</sup>C for 1hour, and counter stained with propidium iodide for 30 min at 37<sup>0</sup>C then by rinsed 3 times properly and mounted with antifade and coverslip and visualized using an Olympus IX81 fluorescent microscope.

**Tissue iron levels.** 20 mg of frozen LV tissues were subjected to inductively coupled plasma resonance mass spectrometry to quantify tissue iron level in the Trace Metals Laboratory, London, Western Ontario as described previously.<sup>77, 83, 91</sup>

**Measurement of lipid peroxidation and glutathione.** Malondialdehyde (MDA), an indicator of lipid peroxidation, was measured in myocardial tissues (100-150mg) by using a commercially available kit (Bioxytech@ MDA-586TM, OxiResearch, Percipio Biosciences Inc., Los Angeles, CA) as described previously.<sup>91</sup> Briefly, tissue samples were homogenized in potassium phosphate extraction (KPE) buffer pH 7.5 (0.1M potassium phosphate, 5mM EDTA, 0.1% Triton X-100 and 0.6% sulfosalicylic acids) containing 5mM BHT. The samples were allowed to react with N-methyl-2-phenylindole (NMPI) in the acidic pH at 45°C for 1 hour. The clear supernatants were then collected and read in at 586 nm using a plate reader (Spectramax M5, Molecular Devices, and Sunnyvale, CA). MDA levels were estimated using a standard curve derived using 0.5 to 4.0 µM of standard MDA. Myocardial reduced glutathione (GSH) as well as oxidized glutathione (GSSG) levels was measured by using a plate reader (Spectramax M5, Molecular Devices, and Sunnyvale, CA) as described previously.<sup>91,</sup>

128

**Taqman real-time PCR.** Taqman real-time PCR for mRNA expression analysis was performed as previously described using the Taqman primers and probes as previously.<sup>91, 250</sup> Briefly, 5µl of suitable cDNA dilutions from unknown and standard

(brain cDNA) samples, 8µl Taqman master-mix (includes-primers + Probes) were loaded on white 384 Light cyclers®480 multi-well plates (Roche) with 18S rRNA as the internal control. Samples were loaded in triplicate and the data was analyzed using the Light cycler® 480 systems (Roche) as described previously.<sup>91, 250</sup>

**Western blot.** We homogenized flash frozen LV tissue by using Tissue Lyser II (Qiagen) with special lysis buffer (CelLytic™ M) from sigma supplemented with Protease/Phosphatase inhibitor cocktail from Roche as described previously.<sup>91, 226</sup>. Tissue lysates from was processed and resolved on 8%, sodium dodecyl sulphate-poly acrylamide gel electrophoresis (SDS-PAGE) and transferred to PVDF membranes using a Trans-blot cell (Bio-Rad laboratories, Hercules CA USA) as previously described.<sup>91, 226, 250</sup> Membranes were immunoblotted using primary antibodies against phospho-Akt and total-Akt (Cell signaling), SERCA2a and NCX1 (Thermo Scientific), and ferritin (Abcam) followed by blotting with their HRP-conjugated secondary antibodies. Blots were scanned and quantified by using ImageQuant LAS 4000 (GE Health care, Biosciences).

**Statistical Analysis.** Three or more groups with a single variable were compared using a one-way ANOVA with Neuman-Keuls post-hoc test. Two-way ANOVA was used for two groups with two subgroups. The analysis was performed using SPSS 19 software. Values are shown as mean±SEM, with significance indicated by \*p<0.05.

## 6.4 Results

**Gender difference in iron-overload induced heart disease.** Chronic iron injections in WT and high-iron diet in HJVKO murine models are well-established models of iron-overload recapitulating secondary iron-overload and genetic hemochromatosis,

respectively.<sup>51, 77, 83, 173</sup> Effects of iron-overload on cardiac function were assessed non-invasively by transthoracic echocardiography and invasively by pressure-volume loop analysis. Iron-overloaded male WT and HJVKO mice resulted in diastolic dysfunction with preserved ejection fraction characterized by decreased  $E'/A'$  ratio, prolonged isovolumic relaxation time (IVRT) and deceleration time (DT) (**Figure 6.1A-B; Tables 6.1 and 6.2**), increased exponential time constant of the decay in LV pressure during isovolumic relaxation (Tau) and decreased  $dP/dt_{max}/dP/dt_{min}$  ratio with no change in ejection fraction (**Figure 6.1C-D; Tables 6.1 and 6.2**). In contrast, female WT, as well as HJVKO mice, were protected against iron-overload induced diastolic dysfunction (**Figure 6.1A-D; Tables 6.1 and 6.2**). We next investigated the mechanism for the gender differences in iron-overload cardiomyopathy. Estrogen can modulate iron homeostasis by regulating hepcidin and ferroportin expression via an estrogen response element. Therefore, we assessed iron deposition in the heart and liver. Iron-overload resulted in an equivalent increase in a cardiac iron deposition as assessed by Prussian blue staining (**Figure 6.1E-F**) and quantified myocardial iron levels using inductively coupled plasma-resonance mass spectrometry (**Figure 6.1G-H**) in male and female hearts. Taqman real-time PCR analysis for ferritin, a ubiquitous intracellular iron storage protein, showed that ferritin light chain and heavy chain mRNA were higher in female WT and HJVKO hearts compared with male WT and HJVKO hearts in response to iron-overload (**Figure 6.1 I-J**) which was also seen at the protein level (**Figure 6.1K**). However, there was an equivalent increase in ferritin protein expression in iron-overloaded female and male HJVKO hearts (**Figure 6.1L**). These results clearly document a marked gender dichotomy in response to iron-overload whereby female

mice are clearly protected against iron-overload cardiomyopathy despite an equivalent degree of myocardial iron-deposition.

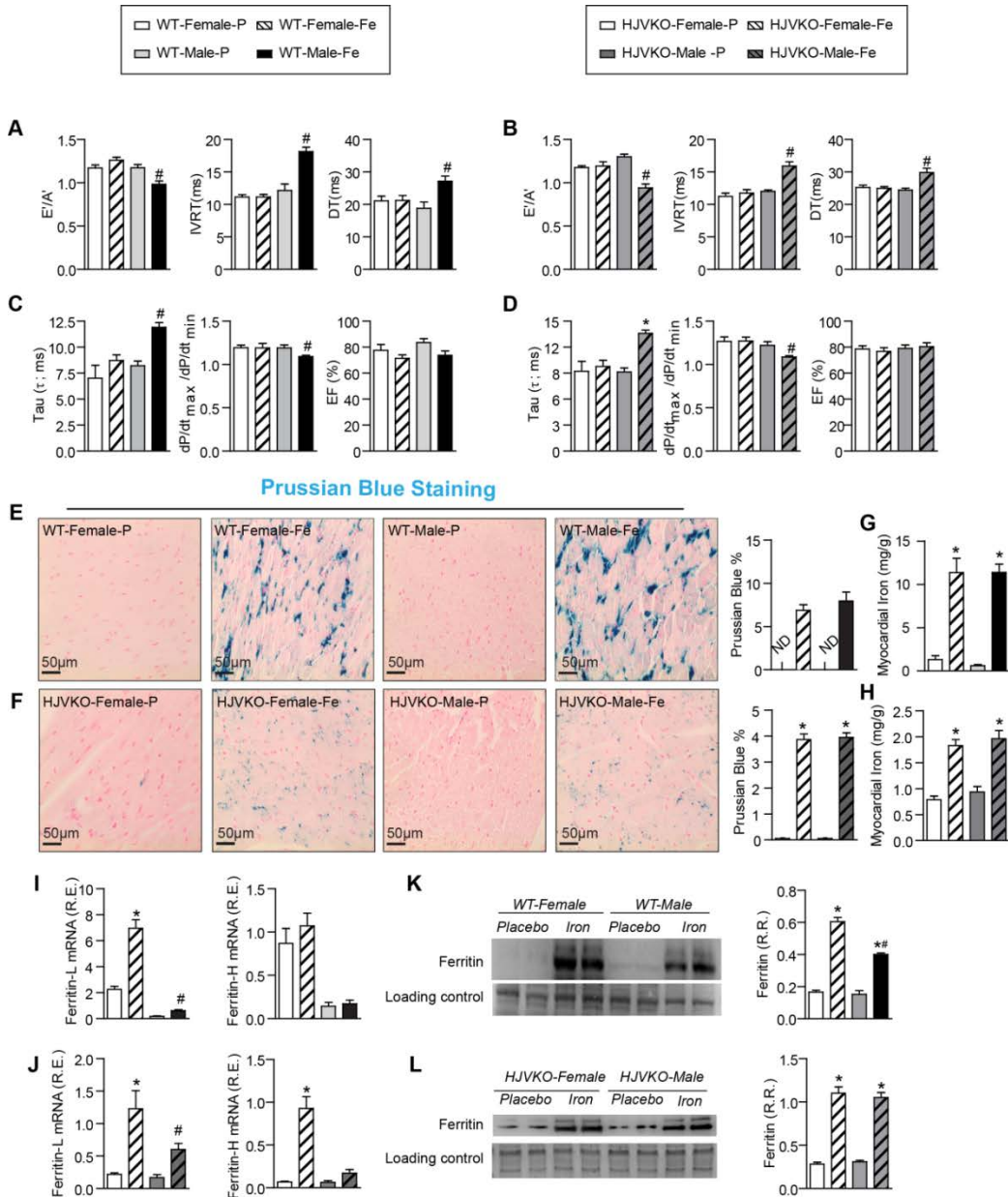


**Figure 6.1. Marked gender differences in iron-overload cardiomyopathy.** Non-invasive Echocardiographic assessment of heart function by tissue Doppler imaging and transmitral filling pattern and invasive hemodynamic assessment by PV loops in WT (A-B) and HJVKO mice (C-D) showing preserved cardiac function in female mice and heart failure with preserved ejection fraction in male mice in response to iron-overload. Representative Prussian blue staining images (E-F) and quantification of myocardial tissue iron levels (G-H) in WT and HJVKO mice showing equivalent cardiac iron depositions in male and female mice in response to iron-overload. Taqman real-time PCR analysis for Ferritin (L+H) mRNA expression and ferritin Western blot analysis in WT (I-J) and HJVKO mice (K-L) showing a lesser increase in ferritin expressions in male mice in response to iron-overload. R.R.=relative ratio; E'=early tissue Doppler velocity; A'=tissue Doppler due to atrial contraction; IVRT=isovolumetric

relaxation time; DT=Declaration time; EF=ejection fraction; ND=not detected. n=8-12 for functional studies; n=8 for gene expression analysis; n=4 for Western blot analysis. \*p<0.05 compared with the corresponding placebo group; #p<0.05 compared with the female iron-overload group.

**Table 6.1. Invasive Pressure-Volume (PV) loop assessment of cardiac function in iron-overloaded WT male and female mice.**

	WT-Male Placebo	WT-Male Iron	WT- Female Placebo	WT- Female Iron	WT-Female OVX- Placebo	WT-Female OVX-Iron
n	8	12	12	12	8	10
HR (bpm)	512±18	390±24*	508±22	503±24	469±27	407±30
LVEDP (mmHg)	2.9±0.4	12.9±0.9*	3.1±0.4	5.3±0.9	4.5±0.9	12.7±1.3#
LVESP (mmHg)	94±6.2	97±2.1	96±2.6	98±1.9	94±4.5	84±3.1
LVEDV(μl)	24.8±1.1	26.0±3.0	26.3±0.9	26.8±4.1	27.5±2.0	34.6±4.5
LVESV (μl)	6.8±0.9	7.1±0.9	6.9±0.9	6.8±0.7	4.8±1.3	15.2±0.9
SV(μl)	19.9±1.7	20.8±0.7	20.3±1.5	19.2±2.5	22.7±2.7	19.3±1.8#
EF (%)	80.2±3.6	80±3.1	77.2±3.9	71.7±4.9	84.8±3.2	55.7±5.1#
dP/dt <sub>max</sub> (mmHg/s)	8781±86	8538±232	8612±279	8612±279	8764±187	7923±322
SW (mJoules)	0.29±0.038	0.28±0.024	0.31±0.021	0.29±0.059	0.25±0.02	0.24±0.025
PRSW (mJoules/μl)	0.012±0.35	0.011±0.008	0.012±0.023	0.011±0.006	0.009±0.005	0.006±0.005
dP/dt <sub>max</sub> /EDV (mmHg/s/μl)	358±17	351 ±12	349±24	353±26	328±15	253±29#
ESPVR (mmHg/μl)	3.3±0.6	3.6±0.5	3.4±0.25	3.5±0.4	3.7±0.3	2.4±0.6#
τ (Glantz) (ms)	8.3±0.4	12.0±0.4*	7.1±1.2	8.8±0.5	9.8±0.9	12.2±0.7
EDPVR (mmHg/μl)	0.101±0.038	0.131±0.090*	0.105±0.016	0.109±0.012	0.118±0.01	0.141±0.023#

HR=heart rate; LVEDP=end diastolic pressure; LVESP=end systolic pressure; LVEDV=end diastolic volume; LVESV=end systolic volume; SV=stroke volume; EF=ejection fraction; dP/dt=rate of change in LV pressure; SW=stroke work; PRSW=pre-load recruitable stroke work; dP/dt<sub>max</sub>/EDV=Starling's contractile index; ESPVR=end-systolic pressure-volume relationship; Tau (τ)= LV relaxation time constant; EDPVR=end-diastolic pressure-volume relationship; \*p<0.05 compared with all other groups; #p<0.05 compared with the WT-female OVX placebo group.

**Table 6.2. Invasive Pressure-Volume (PV) loop assessment of cardiac function in iron-overloaded HJV knockout male and female mice.**

	HJVKO Male-P	HJVKO Male-Fe	HJVKO Female-P	HJVKO Female-Fe	HJVKO Female-OVX-P	HJVKO Female-OVX-Fe
n	8	12	12	8	8	12
HR (bpm)	431±8	426±9*	471±18	467±32 <sup>#</sup>	409±25	372±12
LVEDP (mmHg)	9.9±1.5	17.±2.0*	8.9±0.8	10.1±1.1	6.3±0.8	10.5±1.8 <sup>#</sup>
LVESP (mmHg)	103±6.1	107.±7.4	93±2.5	91±3.4	96±4.3	98±4.3
LVEDV(μl)	22.5±2.8	24.7±2.6	26.7±4.4	28.6±3.8	44.7±7.0	65.5±7.3
LVESV (μl)	4.36±1.72	4.7±1.38	6.1±1.1	5.8±0.9	12.2±3.2	34.1±1.5
SV(μl)	18.2±1.7	20±1.9	21±3.7	20±2.5	32.5±4.4	31.4±3.9
EF (%)	80.8±2.9	80.9±3.4	78.7±3.1	70±2.8	72.7±4.2	51.9±4.3 <sup>#</sup>
dP/dt <sub>max</sub> (mmHg/s)	9637±135	9201±149	8447±145	8367±128	9263±776	7089±477
SW (m Joules)	0.341±0.062	0.382±0.049	0.291±0.009	0.303±0.008	0.558±0.07	0.440±0.016
dP/dt <sub>max</sub> /EDV (mmHg/s/μl)	428±31	372±45	317±33	290±34	207±21	123±23
ESPVR (mmHg/μl)	3.14±0.35	3.08±0.29	3.53±0.39	3.55±0.36	3.48±1.1	2.01±0.34
τ (Glantz) (ms)	9.23±0.41	13.7±0.32*	9.29±1.1	9.87±0.66	10.7±0.72	12.73±1.3 <sup>#</sup>
EDPVR (mmHg/μl)	0.103±0.093	0.127±0.011*	0.095±0.009	0.091±0.014	0.110±0.04	0.147±0.004 <sup>#</sup>

HR=heart rate; LVEDP=LV end diastolic pressure; LVESP=LV end systolic pressure; LVEDV=LV end diastolic volume; LVESV=LV end systolic volume; SV=stroke volume; EF=ejection fraction; dP/dt=rate of change in LV pressure; SW=stroke work; PRSW=pre-load recruitable stroke work; dP/dt<sub>max</sub>/EDV=Starling's contractile index; ESPVR=end-systolic pressure-volume relationship; Tau (τ)=LV relaxation time constant; EDPVR= end-diastolic pressure-volume relationship; \*p<0.05 compared with all other groups; <sup>#</sup>p<0.05 compared with the HJVKO-female OVX placebo group.

**Female mice are protected against iron-overload mediated myocardial oxidative stress and myocardial fibrosis.** Iron-induced myocardial oxidative stress and lipid peroxidation coupled with reduced myocardial antioxidant reserves are major pathogenic processes in iron-overload cardiomyopathy.<sup>77, 83, 295, 296</sup> While male iron-overloaded hearts demonstrated a marked increase in oxidative stress, iron-overloaded female WT, and HJVKO hearts did not show increased oxidative stress (**Figure 6.2A-F**). Male WT and HJVKO iron-overloaded hearts displayed increased dihydroethidium (DHE) fluorescence and 4-hydroxynonenal (4-HNE) levels which were markedly suppressed in females (**Figure 6.2A-B**). The increased oxidative stress in male iron-overloaded hearts showed severely decreased reduced glutathione (GSH) levels, a key antioxidant reserve (**Figure 6.2C-D**), and increased malondialdehyde (MDA) levels, a marker of lipid peroxidation (**Figure 6.2E-F**). In contrast, female iron-overloaded hearts demonstrated a marked resistance to oxidative damage reflected in reduced glutathione (**Figure 6.2C-D**) and unchanged MDA (**Figure 6.2E-F**) levels. The expression of 2 key antioxidant enzymes, catalase and heme oxygenase-1 (HMOX1), and anti-oxidants, thioredoxin1 (TRX1) and metallothionein-1 (MT1), was evaluated. Baseline catalase expression was greater in female hearts but increased in male hearts (**Figure 6.2E-F**) while HMOX1 levels increased to a greater extent in female WT iron-overloaded hearts (**Figure 6.2G-H**). Expression of TRX1 and MT1 was greater in female compared to male hearts but while TRX1 expression did not change in response to iron-overload, MT1 expression increased equivalently (**Figure 6.2I-L**).

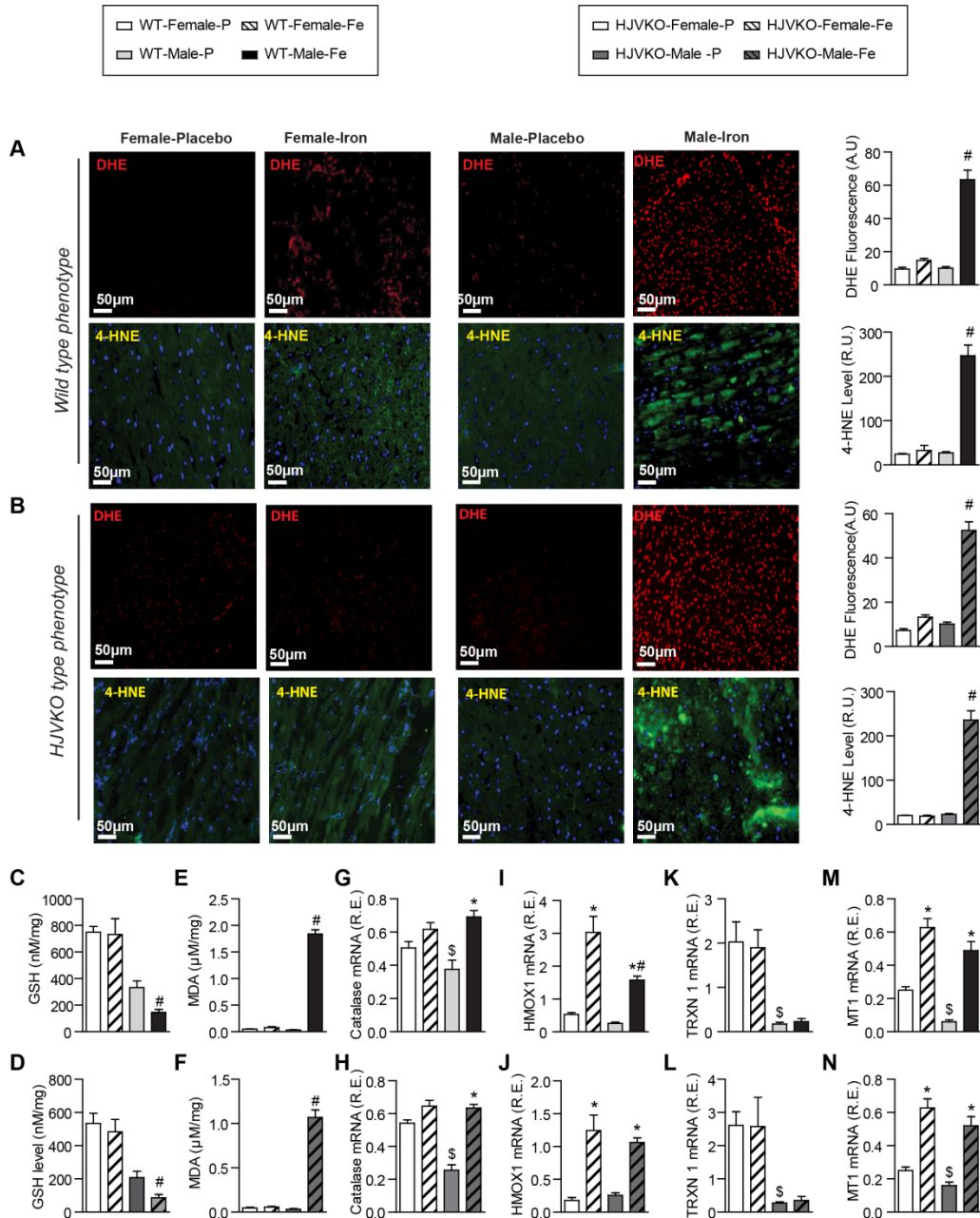


**Figure 6.2. Female mice are protected against iron-overload induced oxidative stress.** Representative dihydroethidium (DHE) fluorescence (red) and 4-hydroxynonenal (4-HNE) immunofluorescence (green) and quantification showing a relative lack of iron-induced myocardial oxidative stress in female WT (A) and HJVKO (B) mice, whereas iron-overload resulted in increased oxidative stress in male mice. Biochemical analysis of myocardial reduced glutathione (GSH) (C-D) and lipid peroxidation product, malondialdehyde (MDA) (E-F) levels in WT (C, E) and HJVKO hearts (D, F) showing increased oxidative stress in male mice in contrast to unchanged oxidative stress in female mice in response to iron-overload. Myocardial gene expression analysis using TaqMan real-time PCR showing gender-specific and iron-overloaded related alteration in the mRNA expression of catalase (E-F), heme oxygenase 1 (HMOX1) (G-H), thioredoxin 1 (TRX1) (I-J), and metallothionein 1 (MT1) (K-L) in WT and HJVKO mice, respectively. n=4 for histology; n=8 for gene expression and biochemical analyses. \*p<0.05 compared with the corresponding placebo group; #p<0.05 compared with the female iron-overload group; \$p<0.05 compared with the corresponding female placebo group.

We next assessed the extent of myocardial hypertrophy, fibrosis, and apoptosis, key pathological events in heart disease. Increased interstitial fibrosis is a characteristic feature of diastolic dysfunction. Iron-overload in male WT and HJVKO mice resulted in increased myocardial interstitial fibrosis as seen in the PSR staining and quantification of collagen content (**Figure 6.3A-B**). Myocardial fibrosis in male iron-overloaded mice was associated with increased mRNA expression of pro-collagen I and III (**Figure 6.3C-D**) and myocardial disease markers, ANF, BNP,  $\beta$ -MHC and  $\alpha$ -SkA (**Figure 6.3E-F**). Interestingly, female WT and HJVKO mice were protected against iron-overload mediated increase in myocardial fibrosis and the increased expression of collagen genes and disease markers (**Figure 6.3A-F**). Abnormalities in myocardial  $\text{Ca}^{2+}$  handling proteins has been linked to diastolic dysfunction.<sup>221, 225, 243</sup> However, we found no alteration in myocardial SERCA2a and NCX1 protein levels in male and female mice in response to iron-overload (**Figure 6.3G-H**). Both female and male mice did not show increased myocardial apoptotic cell death in response to iron-overload as shown by TUNEL staining (**Figure 6.4**). Our results collectively demonstrate that while male mice showed severe myocardial oxidative stress and fibrosis, female mice were markedly resistant to iron-overload mediated myocardial oxidative damage and fibrosis.

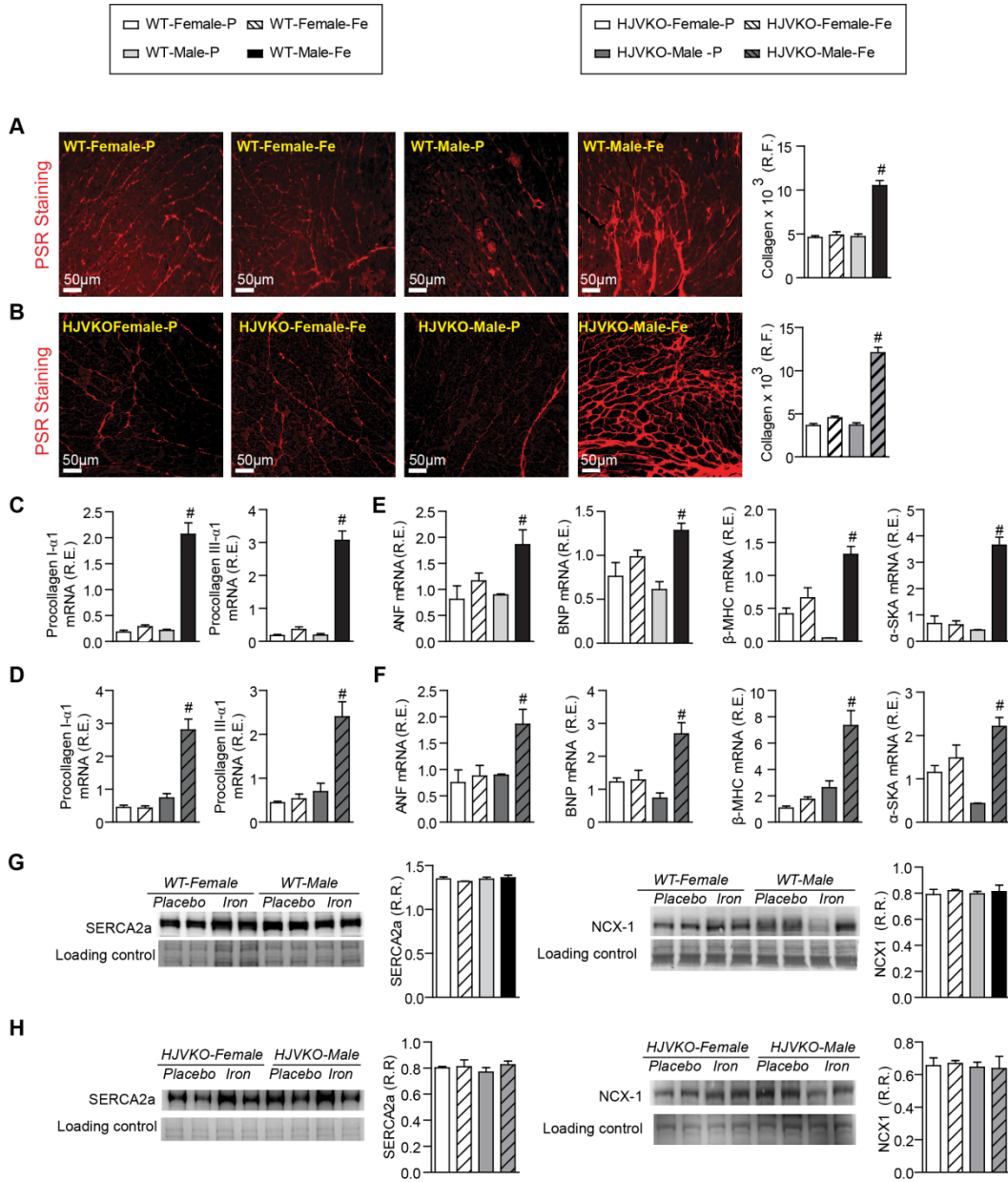


**Figure 6.3. Female mice are protected against iron-overload induced myocardial fibrosis and heart disease.** Representative picrosirius red (PSR) staining and quantification of myocardial fibrosis (A-B), and TaqMan real-time PCR expression analysis of procollagen type I $\alpha$ 1 and procollagen type III $\alpha$ 1 mRNA (C-D) in male and female WT and HJVKO mice showing a clear protection against iron-overload induced myocardial fibrosis in female mice. Expression analysis of cardiac disease markers, ANF, BNP and  $\beta$ -MHC and  $\alpha$ -SkA in WT (E) and HJVKO mice (F), showing a potential intrinsic cardioprotective effect against iron-overload cardiomyopathy in female mice. Western blot analyses in male and female WT and HJVKO mice showing no change in myocardial SERCA2a and NCX-1 levels in WT (G) and HJVKO (H) mice in response to iron-overload. R.F.=relative fraction; R.E.=relative expression; R.R.=relative ratio; ANF=atrial natriuretic factor; BNP=brain natriuretic peptide;  $\beta$ -MHC=beta-myosin heavy chain;  $\alpha$ -SkA=Alpha skeletal actin; SERCA2a=sarcoendoplasmic reticulum Ca<sup>2+</sup> ATPase; NCX-1=sodium-calcium exchanger-1. n=4 for histology and Western blot analyses; n=8 for gene expression analysis. #p<0.05 compared with the female iron-overload group.

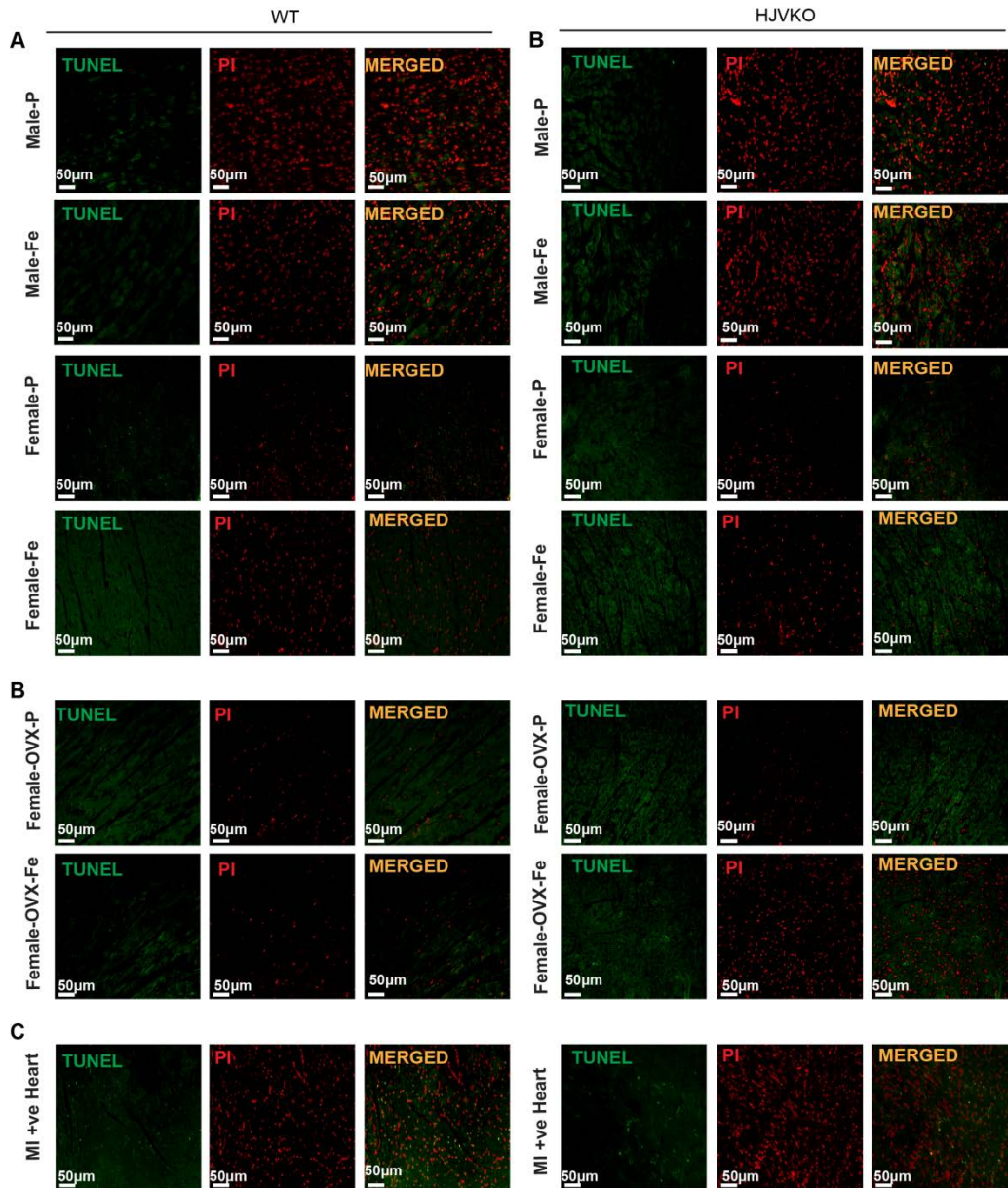


**Figure 6.4.** Lack of myocardial apoptosis in chronic iron-overloaded mice based on TUNNEL staining in WT (A) and HJVKO (B) female hearts. Positive TUNEL staining is shown using 3-day post-myocardial infarction murine hearts using the LAD ligation technique (C).

**Ovariectomy results in loss of protection and increased susceptibility to iron overload cardiomyopathy in female mice.** We observed the sex-specific phenotypes of iron-overload cardiomyopathy. To determine the effects of estrogen on the observed protection against iron overload cardiomyopathy in female mice, we performed

bilateral ovariectomy in WT and HJVKO female mice. Hematoxylin-eosin staining was performed to confirm the complete removal of the ovaries (**Figure 6.5**). Following a 2-wk recovery period, mice were then subjected to iron-overload. Importantly, OVX-WT female mice showed marked worsening of cardiac function in response to iron-overload resulting in heart failure with reduced ejection fraction compared with preserved cardiac function in sham-operated female mice (**Figure 6.6; Tables 6.1 and 6.2**). Ovariectomy in WT female mice exhibited diastolic dysfunction based on decreased  $E'/A'$  ratio, prolonged isovolumic relaxation time (IVRT) (**Figure 6.6A**), and increased LV end-diastolic pressure, prolonged LV relaxation time constant (Tau) (**Figure 6.6B**). Interestingly, loss of ovarian function precipitated systolic dysfunction as shown by the reduced ejection fraction, preload corrected  $dp/dt_{max}$  and end-systolic pressure volume relationship (**Figure 6.6C**). Representative pressure-volume loops illustrating diastolic and systolic function with LV dilation in OVX iron-overloaded female WT mice are shown in (**Figure 6.6D**). Ovariectomy in HJVKO female mice resulted in a similar pattern of cardiac dysfunction characterized by diastolic dysfunction (**Figure 6.6E-F**) and systolic dysfunction (**Figure 6.6G**) as illustrated by representative pressure-volume loops (**Figure 6.6H**).

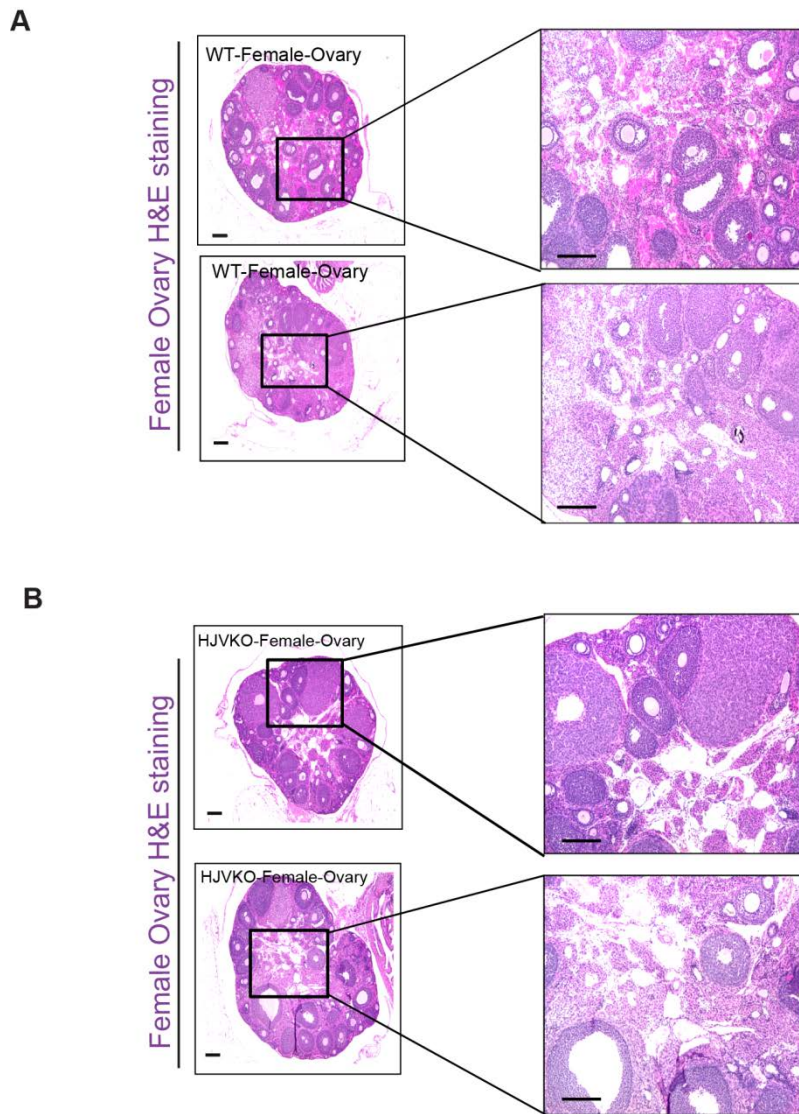


**Figure 6.5.** H&E staining of ovaries from ovariectomized WT (**A**) and HJVKO (**B**) mice.

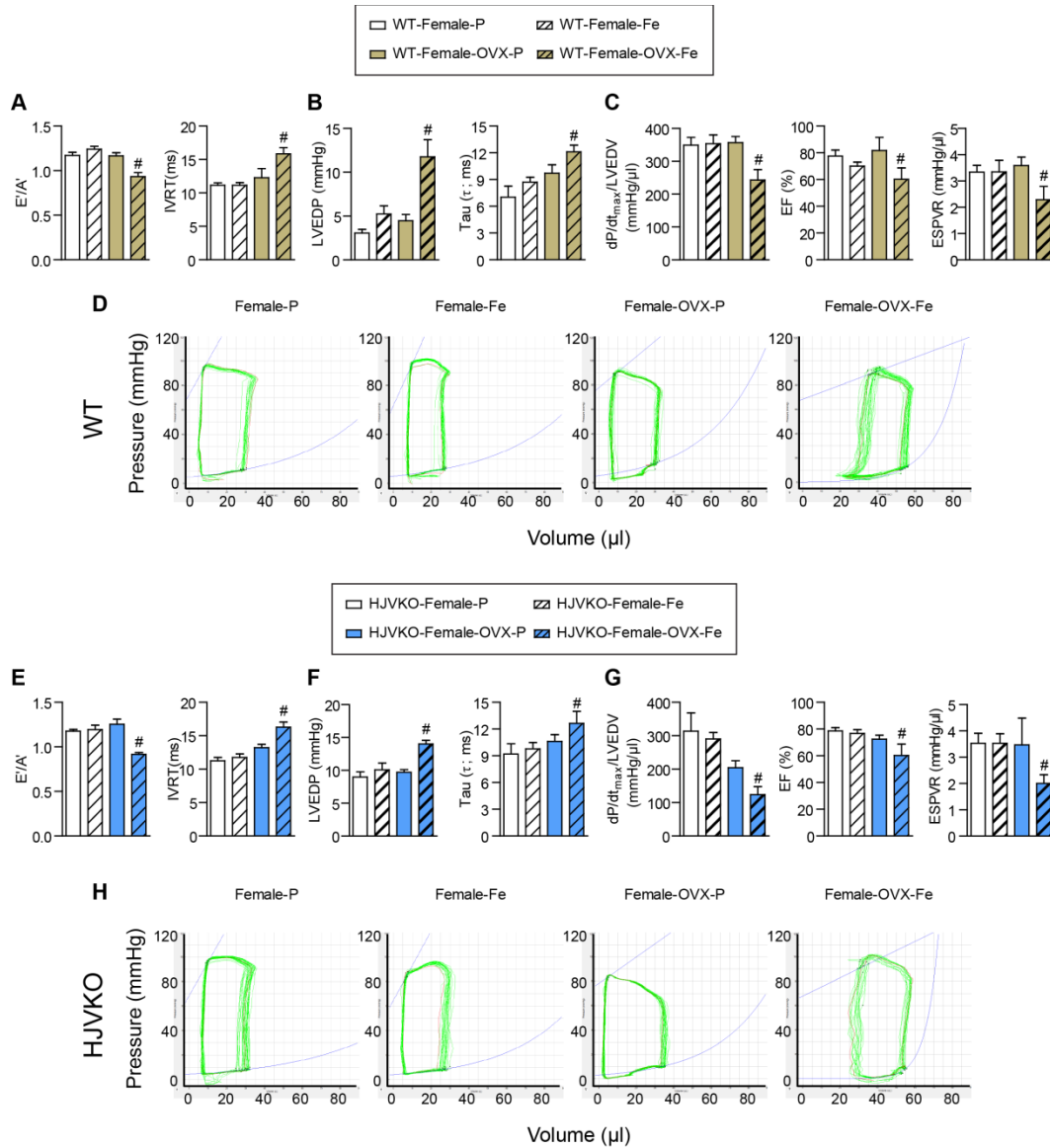


**Figure 6.6. Ovariectomy precipitates diastolic and systolic dysfunction in response to myocardial iron-overload.** Non-invasive echocardiographic assessment of heart function illustrated by tissue Doppler ( $E'/A'$ ) and transmitral filling (IVRT) (A), invasive hemodynamics illustrated by LVEDP and LV pressure exponential decay constant (Tau) (B) showing diastolic dysfunction in ovariectomized (OVX) WT females with iron-overload. Invasive hemodynamic assessment based on  $dP/dt_{max}/LVEDV$ , EF and ESPVR (C) showing systolic dysfunction in OVX WT female iron-overloaded mice. Representative pressure-volume loops illustrating diastolic and systolic dysfunction in OVX WT female iron-overloaded mice (D). Non-invasive echocardiographic assessment of heart function illustrated by tissue Doppler ( $E'/A'$ ) and transmitral filling (IVRT) (E), invasive hemodynamics illustrated by LVEDP and LV pressure exponential decay constant (Tau) (F) showing diastolic dysfunction in OVX HJVKO females with iron-overload. Invasive hemodynamic assessment based on  $dP/dt_{max}/LVEDV$ , EF and ESPVR (G) showing systolic dysfunction in OVX HJVKO female iron-overloaded mice. Representative pressure-volume loops illustrating diastolic and systolic dysfunction in OVX WT female iron-overloaded mice (H).  $E'$ =early tissue Doppler velocity;  $A'$ =tissue Doppler due to atrial contraction; IVRT=isovolumetric relaxation time; LVEDP=LV end-diastolic pressure; LVEDV=LV end-diastolic volume; EF=ejection fraction; ESPVR=end-systolic pressure volume relationship.  $n=8$  for placebo and  $n=10$  for iron-overload groups;  $\#p<0.05$  compared with the female iron-overload group.

To determine whether OVX has any effects on iron deposition, we characterized myocardial iron deposition in female mice by Prussian blue staining (**Figure 6.7A-B**) and inductively coupled plasma-resonance mass spectrometry (**Figure 6.7C-D**), which showed the degree of iron deposition was equivalent in OVX and sham-operated female mice in response to iron-overload. Ovariectomy inhibited iron-overload induced upregulation of myocardial ferritin mRNA (**Figure 6.7E-F**) and protein (**Figure 6.7G-H**) levels in WT and HJVKO female mice with an exception on ferritin light chain mRNA expression in HJVKO mice (**Figure 6.7F**). Signaling pathways are known to be gender-dependent and may modify the myocardial stress response.<sup>281</sup> We then assessed phosphorylation of Akt by Western blot analysis and found that phosphorylation (serine-473) of Akt remained unchanged in response to iron-overload in female mice and was unaffected by OVX (**Figure 6.7I-J**). Notably, OVX did not increase the susceptibility to apoptotic cell death in response to iron-overload as shown by TUNEL staining (**Figure 6.4**). Thus, OVX in female mice resulted in advanced iron-overload induced cardiac dysfunction, lack of upregulation of ferritin levels without a differential effect on myocardial iron deposition.

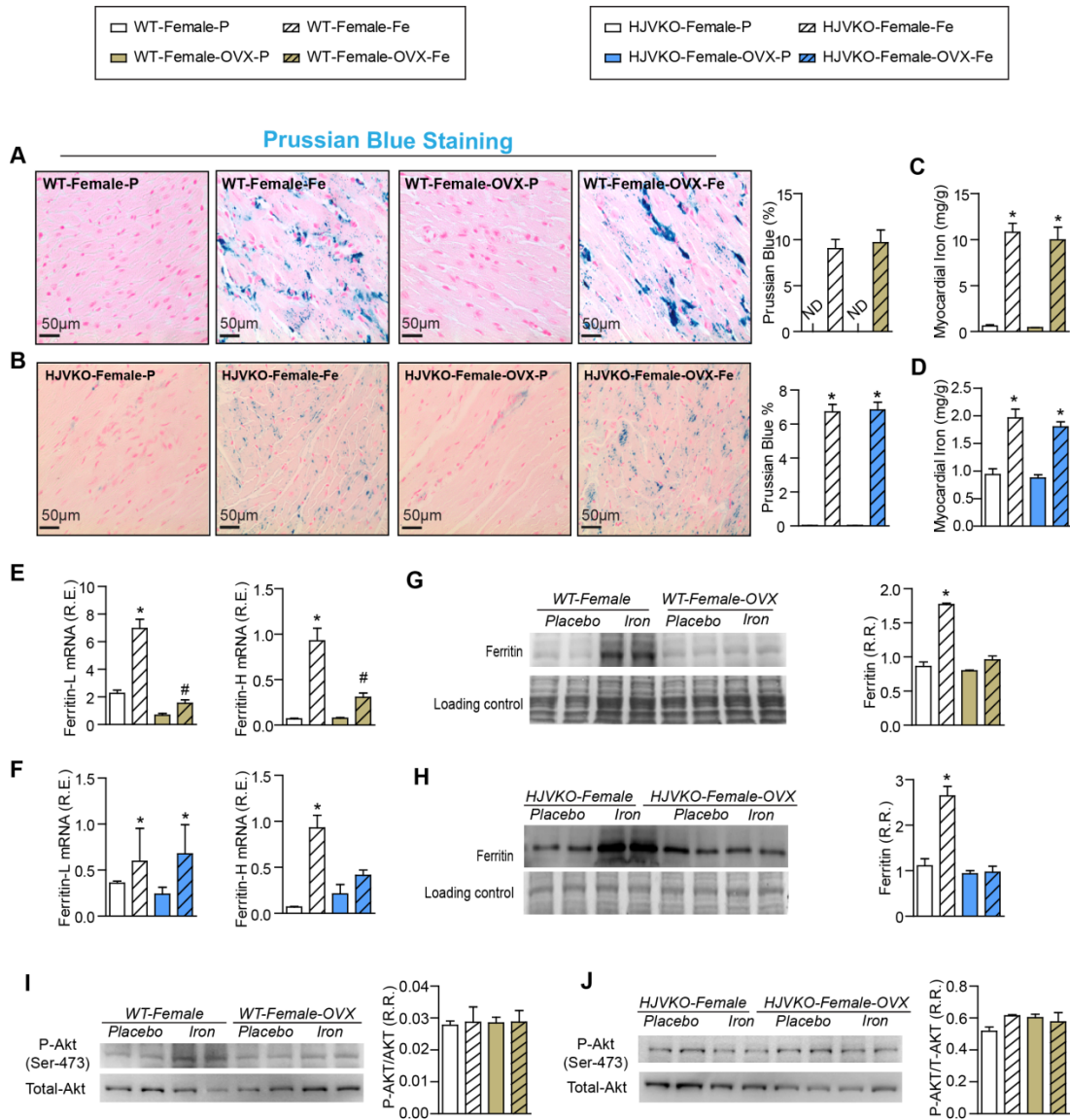


**Figure 6.7. Ovariectomy does not modulate myocardial iron deposition but suppressed the upregulation of ferritin expression.** Prussian blue staining (A-B) and quantification of myocardial tissue iron levels (C-D) in WT (A, C) and HJVKO (B, D) female hearts and in response to OVX confirming the presence of myocardial iron deposition without a differential response to OVX. (E-J) Gene expression of myocardial light (L) and heavy (H) ferritin using real-time PCR in WT and OVX female mice with iron-overload (E) and in HJVKO and OVX HJVKO females with iron-overload (F) showing a blunted upregulation of ferritin expression in OVX iron-overloaded hearts. Western blot analysis of myocardial ferritin levels in WT (G) and HJVKO (H) females in response to iron-overload showing a complete lack of an increase in myocardial ferritin in OVX mice. Western blot analysis of phospho-Akt/total-Akt in WT (I) and HJVKO (J) female hearts showing no change in myocardial phospho-Akt/PKB(Ser-473) level in response to OVX and iron-overload. ND=not detected; R.E.=relative expression; R.R.=relative ratio. n=8 for iron quantification and gene expression analysis; n=4 for histology and Western blot analysis. \*p<0.05 compared with the corresponding placebo group.

**Loss of antioxidant defense correlated with iron-overload mediated oxidative stress and heart disease in ovariectomized female mice.** To understand the contribution of estrogen to the intrinsic antioxidant defense capacity of female mice, we assessed myocardial oxidative stress, hypertrophy and fibrosis. Interestingly, we found that OVX resulted in loss of antioxidant defense seen in the WT and HJVKO female hearts resulting in greatly increased iron overload-induced myocardial oxidative stress, characterized by markedly increased DHE fluorescence and 4-HNE levels (**Figure 6.8A-B**), lowered reduced glutathione (**Figure 6.8C-D**), and increased MDA levels (**Figure 6.8E-F**). Gene expression analysis revealed decreased expression of catalase (**Figure 6.8G-H**) and HMOX1 (**Figure 6.8I-J**) following OVX and a lack of upregulation in response to iron-overload. Similarly, baseline expression of TRXN1 (**Figure 6.8K-L**) and MT1 (**Figure 6.8M-N**) was lowered in the OVX group and the iron-overload associated upregulation of MT1 was blunted (**Figure 6.8M-N**).

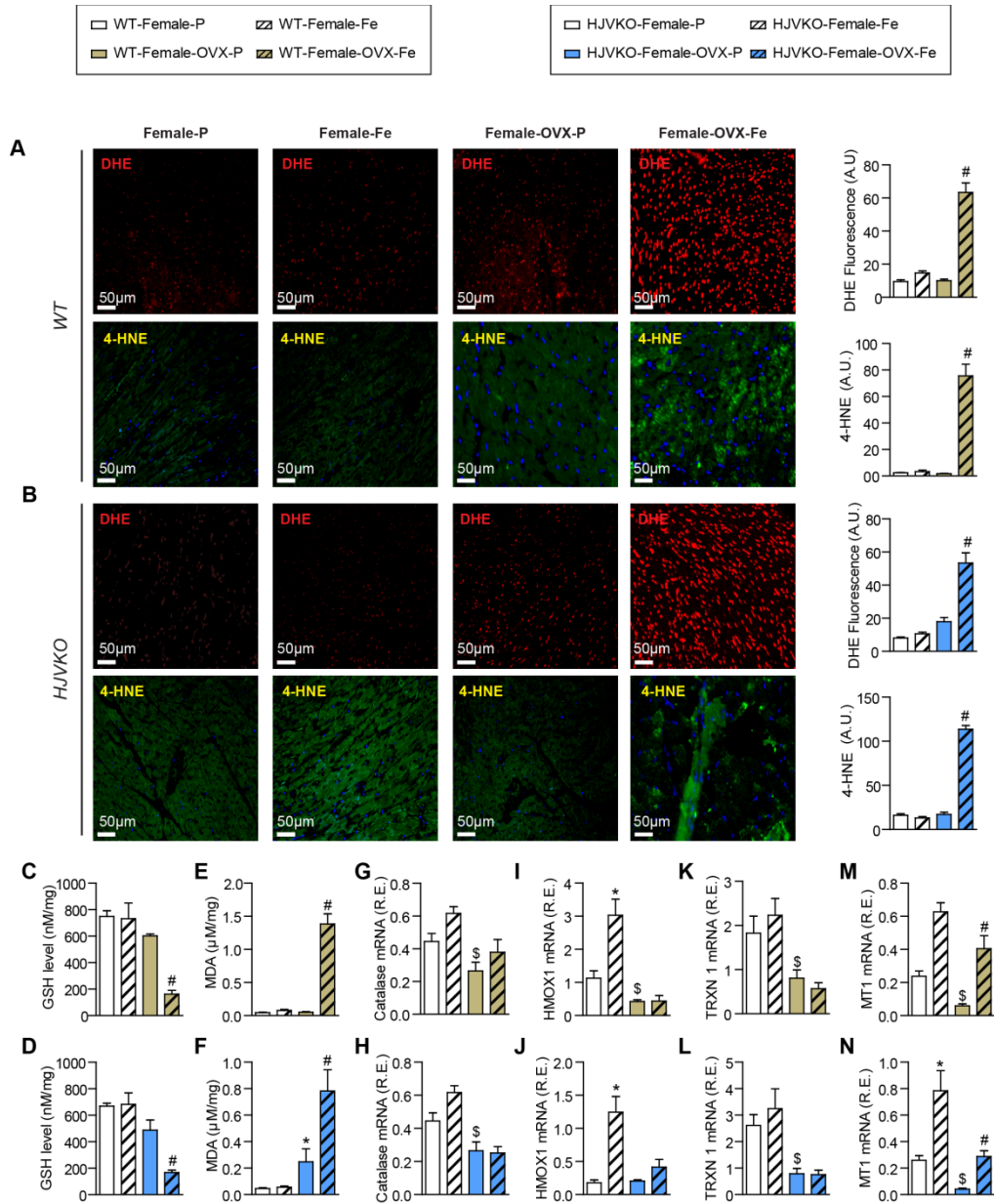


**Figure 6.8. Iron-overload induced myocardial oxidative stress is potentiated in ovariectomized female mice.** Increased iron-induced myocardial oxidative stress in OVX female gender with iron-overload detecting ROS by dihydroethidium (DHE) fluorescence (red) and 4-HNE immunofluorescence (green) in WT (A) and HJVKO (B) females in response to OVX and iron-overload. Biochemical analysis of myocardial reduced glutathione (GSH) (C-D) and lipid peroxidation product, malondialdehyde (MDA) (E-F) levels in female WT (C, E) and HJVKO hearts (D, F) clearly illustrating increased myocardial oxidative injury in OVX female iron-overloaded hearts. Gene expression analysis in hearts showing a marked downregulation in key antioxidant enzymes, catalase (G-H) and heme oxygenase 1 (HMOX1) (I-J), and anti-oxidant molecules, thioredoxin 1 (TRXN1) (K-L), and metallothionein 1 (MT1) (M-N) in WT and HJVKO mice, respectively, following OVX and a lack of upregulation of their expression following iron-overload. n=4 for histology analysis; n=8 for gene expression and biochemical analysis. \*p<0.05 compared with the corresponding placebo group; #p<0.05 compared with the female iron-overload group; §p<0.05 compared with the corresponding female placebo group.

Ovariectomy also promoted extreme susceptibility to myocardial interstitial fibrosis in WT and HJVKO female mice as shown by representative PSR staining and quantification of collagen content (**Figure 6.9A-B**) coupled with increased mRNA expressions of collagen I and III (**Figure 6.9C-D**). Pathological myocardial hypertrophy was exacerbated in iron-overloaded OVX WT and HJVKO females as illustrated by the increased expression of disease markers, ANF, BNP,  $\beta$ -MHC and  $\alpha$ -SkA (**Figure 6.9E-F**) and morphometric assessment showing increased LV weights (**Figure 6.9G-H**). Downregulation of SERCA2a and increased NCX1 levels have been linked to diastolic and systolic dysfunction.<sup>221, 225, 243, 297</sup> Importantly, OVX also resulted in decreased SERCA2a (**Figure 6.9I**) and increased NCX-1 (**Figure 6.9J**) protein levels in WT and HJVKO hearts in response to myocardial iron-overload. Loss of ovarian function resulted in iron-overload induced oxidative stress linked to increased myocardial fibrosis, pathological hypertrophy and altered  $\text{Ca}^{2+}$  regulatory proteins.

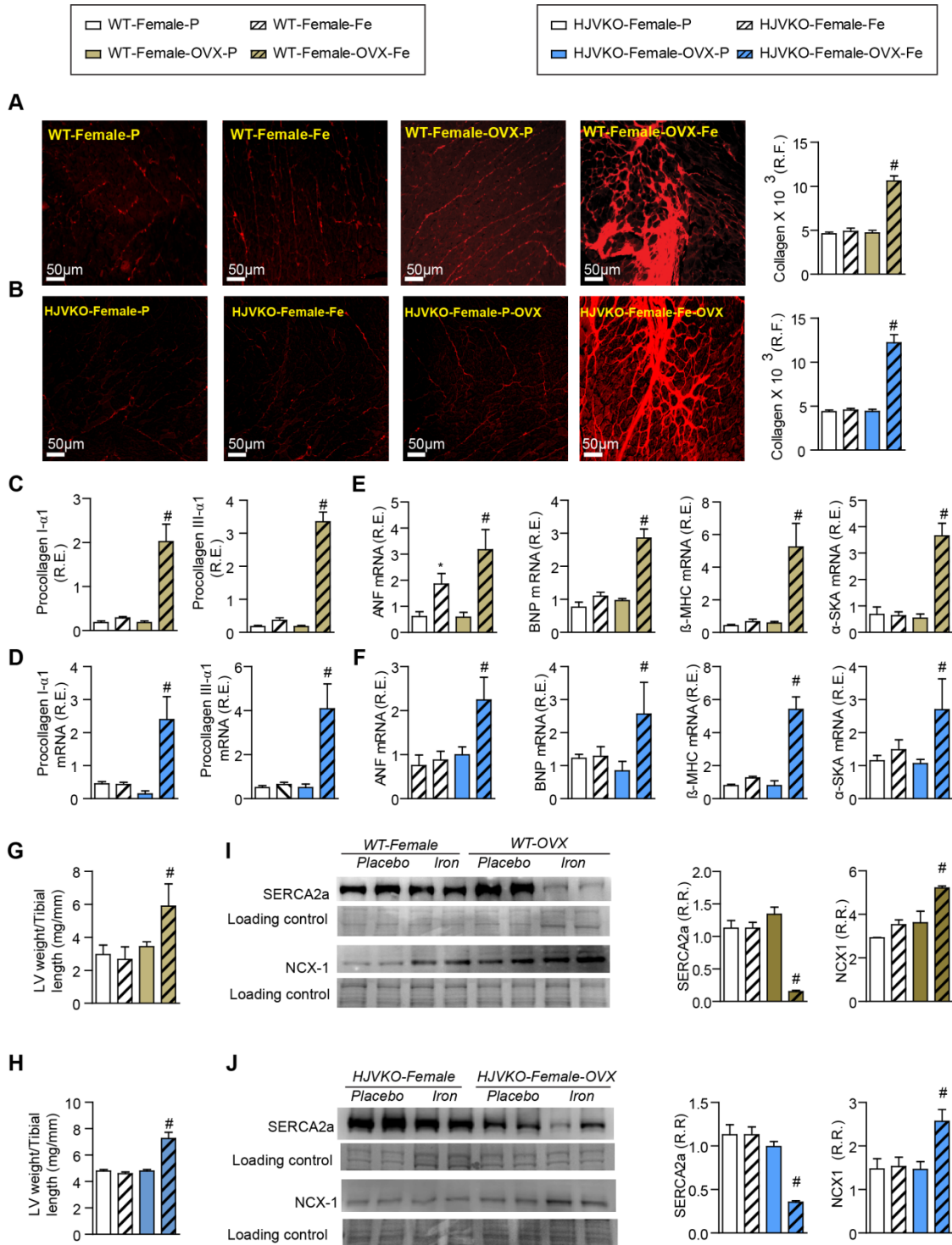


**Figure 6.9. Exacerbation of pathological myocardial remodeling in iron-overloaded ovariectomized female mice.** Picosirius red (PSR) staining and quantification of myocardial fibrosis (A-B) and gene expression of pro-collagen type Iα1 and pro-collagen type IIIα1 (C-D) in WT and HJVKO females clearly demonstrating that OVX potentiates iron-overload mediated myocardial fibrosis. Expression of disease markers, ANF, BNP, βMHC and α-SKA in WT (E) and HJVKO (F) mice illustrating pathological myocardial remodeling in iron-overloaded OVX female hearts. Morphometric assessment of

hypertrophy showing increased LV weights in iron-overloaded OVX female WT (**G**) and HJVKO (**H**) hearts. Western blot analysis and quantification clearly showed significant down regulation in myocardial SERCA2a and NCX1 levels in female WT (**I**) and HJVKO (**J**) iron-overloaded hearts following OVX. R.F.=relative fraction; R.E.=relative expression; R.R.=relative ratio; ANF=atrial natriuretic factor; BNP=brain natriuretic peptide;  $\beta$ -MHC=beta-myosin heavy chain;  $\alpha$ -SKA=Alpha skeletal actin; SERCA2a=sarcoplasmic reticulum  $\text{Ca}^{2+}$  ATPase; NCX1=sodium-calcium exchanger-1. n=8 for gene expression analysis; n=4 for histology and Western blot analyses. #p<0.05 compared with the female placebo group.

## 6.5 Discussion

Iron-overload cardiomyopathy remains an important cause of morbidity and mortality in patients with secondary iron-overload and primary hemochromatosis.<sup>45, 54, 60, 74</sup> In this study, we investigated gender-based differences in iron-overload cardiomyopathy in male and female WT and HJVKO mice. Our chronic acquired and genetic murine models of iron-overload recapitulate essential features of clinical iron-overload and its associated heart disease.<sup>51, 77, 83, 173</sup> While wildtype mice in C57Bl6 background can be resistant to iron-overload cardiomyopathy<sup>291</sup>, our murine models had prolonged iron-overload and we used the appropriate gender, age-matched and strain as appropriate controls. We showed that female acquired and genetic murine models were markedly resistant to iron-mediated cardiac injury based on functional, histological and molecular determinants of heart disease. Importantly, we evaluated cardiac function using non-invasive echocardiography and invasive pressure-volume loops and while iron-overloaded females showed normal cardiac function, iron-overloaded males exhibited diastolic dysfunction. In contrast, iron-overload in ovariectomized females resulted in advanced iron-overload cardiomyopathy characterized by both diastolic and systolic dysfunction. The phenotypic features and response to OVX were similar in both models highlighting a conserved mechanism for the gender-dependent cardiac remodeling in response to iron-overload.

Sexual dimorphism in terms of cardiovascular diseases and iron metabolism exist in humans as well as in experimental animals.<sup>281, 298, 299</sup> Several lines of evidence showed that estrogen exerts pleiotropic cardioprotective effects in well-established models of heart failure such as pressure-overload and myocardial infarction.<sup>278, 280, 281, 284, 285, 299</sup> Our study extends these observations and is the first study to demonstrate gender-specific differences in iron-overload induced heart disease. In humans gender differences are thought to be related to menstrual blood loss and lowered iron stores and serum ferritin in females compared to males.<sup>300</sup> In addition, regulation of iron metabolism is tightly controlled at a systemic level through hepcidin/ferroportin axis.<sup>1, 301</sup> and gonadal steroids can modulate iron metabolism such as estrogen-mediated suppression of hepcidin expression.<sup>298, 301</sup> Rodents have estrous cycles whereby there is no menstrual blood loss and, therefore, this cannot be evoked as a mechanism for the gender differences in iron-overload cardiomyopathy. Our assessment of iron deposition using both quantitative measures and histological staining did not demonstrate a difference in the degree of myocardial iron-overload in females compared to males and in response to OVX.

Instead, our data strongly suggest that the intrinsic response of the myocardial tissue to iron-induced injury is strongly modulated by gender. Excess iron promotes oxidative stress via the Fenton reaction and is the major pathogenic process in iron-overload cardiomyopathy.<sup>83, 275, 302</sup> Interestingly, we found that preserved ovarian function was associated with a marked antioxidant status in the heart and upregulation of myocardial ferritin levels. Female gender was clearly associated with blunting of iron-induced myocardial oxidative stress, lipid peroxidation product and increased intrinsic

antioxidant capacity. Conversely, OVX markedly exacerbated iron-overload induced myocardial oxidative stress. The ability to counteract iron-mediated oxidative stress is a key protective mechanism<sup>83, 91, 303</sup> and our results clearly demonstrate that estrogen-mediated differences in reactive oxygen species (ROS) production could account for some of the male–female differences in cardiovascular function and disease.<sup>281</sup> Several studies have suggested that female mitochondria generate less ROS<sup>304, 281</sup> and iron-induced mitochondrial ROS production may also have been curtailed in female hearts. Diastolic dysfunction correlated with increased myocardial fibrosis in the setting of increased myocardial oxidative stress possibly by activating the myocardial transforming growth factor beta signaling cascade.<sup>305, 306</sup> Importantly, systolic dysfunction in iron-overloaded OVX female mice was associated with marked reduction in SERCA2a and increased NCX-1 levels which represent a pivotal pathophysiological change in systolic heart failure.<sup>221, 297</sup>

**6.6 Conclusions:** Our results are consistent with the effects of female reproductive hormones on myocardial excitation-contraction coupling<sup>290</sup>. While we demonstrated decreased SERCA2 protein levels, oxidative post-translational modification of SERCA2a may have also directly contributed to the myocardial dysfunction.<sup>244, 307</sup> Our results clearly support the importance of directed anti-oxidant therapy for iron-overload cardiomyopathy.<sup>91</sup>

# CHAPTER SEVEN

## **Discussion and Future directions**

### **7.1 Discussion**

Iron is an essential element necessarily present in a number of molecular systems of the body and plays a key role in redox reactions because of its ability to shuttle between two oxidative states (reduced or oxidized).<sup>1, 3, 4, 8, 17</sup> Abnormal iron metabolism leads to cardiac and hepatic iron-overload disorders in an epidemic proportion.<sup>4, 91, 173, 260</sup> Abnormal iron absorption results in iron deposition in different organs of the body including the heart, liver and endocrine tissues.<sup>13, 74, 263</sup> Iron-overload heart and liver diseases are commonly observed in patients with genetic hemochromatosis and secondary iron-overload, which are a common cause of end organ failure and mortality worldwide basis.<sup>13</sup> Primary hemochromatosis is an autosomal recessive genetic disorder with gene a frequency of 10% in the Caucasian population. The risk of genetic iron-overload is prevalent in Celtic descents from Ireland, UK, North Europe, Australia, and Canada. Primary hemochromatosis has four different subtypes. Juvenile hemochromatosis (JH) is an aggressive form of type-2 primary hemochromatosis often leading to cardiomyopathy at an early stage of life. The risk of secondary iron-overload is still higher in patients who need chronic blood transfusions such as in thalassemia and sickle cell anemia (hemoglobinopathies), however, the risk of secondary iron-overload is very prevalent in the Middle East and South-East Asian populations. Iron-overload leads excess deposition of iron in different body parts, including heart, liver and endocrine glands.

Excess cardiac deposition in cardiac tissues develops iron overload cardiomyopathy a newly recognized cause of heart failure and is overlooked by cardiovascular

specialist, associated with early diastolic dysfunction with increased propensity for arrhythmias and a late-stage dilated cardiomyopathy. In addition to cardiomyopathy, it also associated with other comorbidities such as diabetes, pituitary dysfunction, and hypogonadism etc.<sup>308, 309</sup> Previous research confirmed that L/T-Type calcium channels are the major channels through which divalent form of iron ( $\text{Fe}^{2+}$ ) enters into cardiomyocytes and develops iron-overload cardiomyopathy.<sup>77, 80</sup> Excess body iron leads transferrin saturation and non-transferrin bound iron (NTBI) formation, which are highly reactive.<sup>245, 310</sup> The uptake of non-transferrin bound iron gradually bypasses the transferrin bound iron uptake mechanism and promotes a significant increase in the intracellular labile iron pool (LIP), which promotes the free radical formation and oxidative stress.<sup>152, 153, 311</sup> Hepatic iron deposition develops hepatic iron-overload culminating in end-organ disease including liver fibrosis, cirrhosis and hepatocellular carcinoma. The liver is one of the major organs which store a large amount of iron safely for cellular use. Hepcidin is an important iron regulatory hormone, produced majorly from liver hepatocytes and controls iron homeostasis. Impaired hepcidin expression or its inhibition leads irregular iron absorption and iron-overload. Defects in hepcidin-ferroportin axis are the major driver through which hepatic iron-overload occurs.

The global clinical burden of iron-overload cardiomyopathy and hepatic iron-overload is increasing worldwide and associated with genetic and non-genetic causes. Due to lack of an effective iron excretory mechanism, excess iron accumulation leads to the formation of highly reactive free radicals. These free radicals trigger oxidative stress, DNA damage, lipid peroxidation and, protein modifications.<sup>4, 260, 312</sup>

This iron-induced oxidative damage plays a key role in the pathophysiology of many disorders including iron-overload cardiomyopathy<sup>77, 83, 91</sup>, hepatic iron-overload disease<sup>107, 173, 252</sup>, Friedreich's ataxia associated cardiomyopathy,<sup>93, 94</sup> iron-overload endocrinopathies,<sup>313, 314</sup> neurodegenerative diseases,<sup>315</sup> bone diseases, ischemia-reperfusion injury and accelerated atherosclerosis.

Our recent studies established new insights into the pathogenesis of iron-overload mediated heart and liver diseases and novel therapeutic strategies to prevent this disorder. While increased oxidative stress is a well-documented biochemical change associated with iron injury, the fundamental mechanism of iron-overloaded mediated heart failure and liver disease is poorly understood. Current therapies such as iron chelation and phlebotomy therapies, unable to reduce the global burden of iron-overload cardiomyopathy, because these mainstay therapies fail to reduce iron induced oxidative stress, a key driver in the progression of iron-overload heart and liver diseases. Therefore, in order to effectively control iron-overload diseases, a more comprehensive approach required, such as antioxidant therapy should be a suitable rational therapy to prevent this worldwide epidemic.

***Evidence of cardiac and hepatic iron-overload:*** Previous research showed that iron enter into body through different routes and deposits in different organs such as liver, heart, and endocrine glands, and it was also reported that during iron-overloaded condition transferrin saturated and non-transferrin bound iron (NTBI) accumulates.<sup>7, 82, 105, 308</sup> Some of this redox active iron transported into cardiomyocytes via L/T-Type Calcium Channels and results into cardiac iron-overload, however, the transport mechanism differs in hepatocytes. We have shown cardiac and hepatic iron-overload

and deposition by using Prussian blue staining technique and tissue iron measurement were performed by inductive plasma resonance spectroscopy. We developed two murine models of iron-overload to understand the iron-overload heart and liver disease and our pre-clinical murine models, recapitulates genetic hemochromatosis and secondary iron-overload conditions respectively. Further we also extensively assessed the cardiac function by using non-invasive and invasive techniques. Our data clearly showed that excess iron deposition develops cardiomyopathy in hearts with diastolic dysfunction at an early stage of the disease and systolic dysfunction at an advanced stage. In addition, excess hepatic iron deposition leads liver failure, hepatocellular carcinoma and end stage liver cirrhosis. Current therapies are limited to prevent the global burden of iron-overload. We also looked new insights of the pathogenesis and novel therapeutic approaches to the prevent progression of cardiac and hepatic iron-overload disease.

***Pathophysiology of iron-overload cardiomyopathy:*** Excess iron in the heart leads transferrin saturation and non-transferrin bound iron (NTBI) formation, which is redox active. During iron-overloaded conditions the redox active iron ( $\text{Fe}^{2+}$ ) enters into cardiomyocytes through L/T-Type calcium channels results in iron-overload cardiomyopathy (**Figure 7.1 and Figure 7.4A**). The redox active iron available for a well-known reaction called Fenton's reaction and majorly favors the formation of hydroxyl (OH) radicals. These free radicals target different cellular targets and cause severe cellular damage (**Figure 7.1 and Figure 7.4A**). In healthy cells, the production of free radicals is minimized by intrinsic enzymatic and non-enzymatic antioxidant systems. During iron-overload excess redox, iron accumulation favors the generation of

free radicals results increased lipid peroxidation, protein oxidation, DNA damage and depletion of antioxidants. Cardiac iron-overload associated with decreased antioxidant reserves (reduced glutathione), increased lipid peroxidation products such as 4-hydroxynonenal (4-HNE), malondialdehyde (MDA). There is a clear evidence of iron-induced oxidative stress and lipid peroxidation in iron-overload cardiomyopathy showed in animal models and in patients with genetic hemochromatosis and secondary iron-overload. We extensively characterized the cardiac iron-overload pathophysiology in early chronic and advanced pre-clinical murine models.

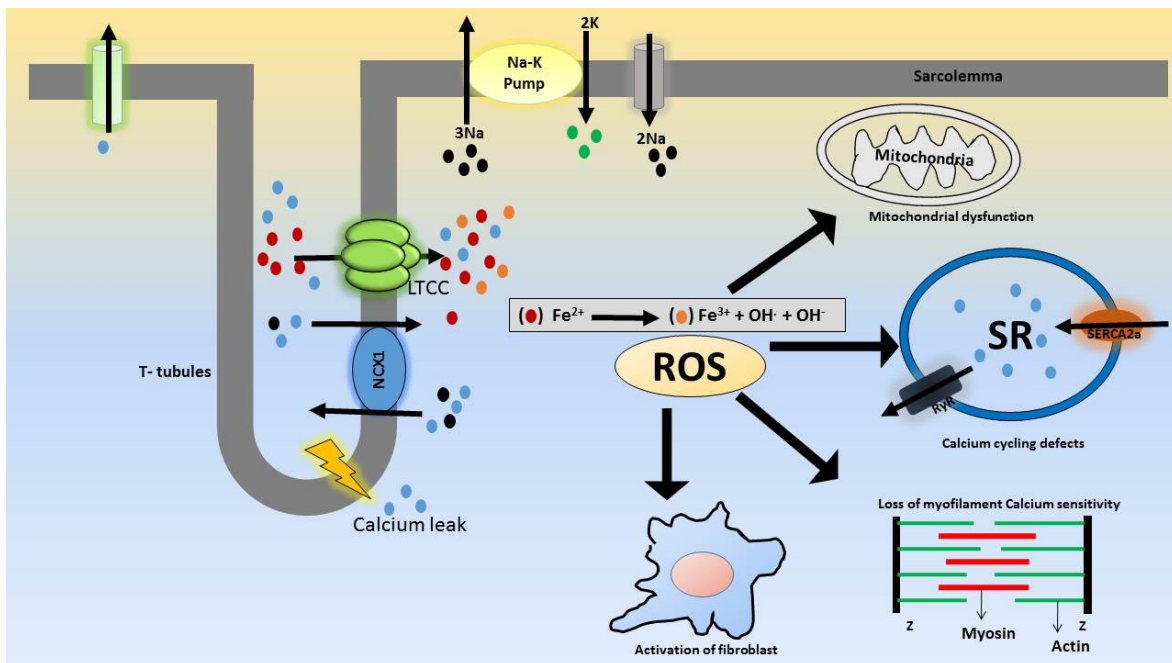


**Figure 7.1 Schematic presentation iron induced oxidative stress and cellular effects that lead to cardiomyopathy.** During iron-overload redox iron transports via L-Type calcium channels and participates in Fenton's chemistry, favors the formation of free radicals. These reactive oxygen species causes myocardial oxidative stress, targets mitochondria, SR calcium homeostasis, myofilament function and activation of fibroblast, all these pathological insults drive the iron-overload cardiomyopathy pathogenesis. LTCC= L-Type calcium channels, SR=Sarcoplasmic reticulum; SERCA2a=Sarcoplasmic reticulum calcium ATPase2a; NCX1=Sodium-calcium exchanger1; Na-K=Sodium-potassium pump; ROS=reactive oxygen species; RyR=Ryanodine receptor.

Our data clearly showed a marked increase in oxidative stress, and lipid peroxidation products with depleted antioxidant levels (reduced glutathione) (**Figure 7.1 and Figure 7.4A**).<sup>91</sup> Early stage of iron-overload associated with selective diastolic dysfunction with preserved ejection fraction and we noticed that active components of diastole are affected.<sup>91</sup> We found severe calcium cycling defects, with defective SERCA2a protein; however we didn't find any myocardial fibrosis in the early stage of iron-overload, interestingly SERCA2a adenoviral gene therapy completely prevented the development diastolic dysfunction, a key insight in the progression of diastolic dysfunction during early iron-overload cardiomyopathy. In contrast, resveratrol antioxidant therapy to iron-overloaded mice showed pleiotropic beneficial effects; resveratrol supplementation improved cardiac function by reducing oxidative damage (increased reduced glutathione levels), decreasing lipid peroxidation (reduced MDA, and 4-HNE products) and improved SERCA2a gene expression and protein levels. We also looked resveratrol action at molecular level in our early stage of iron-overload, resveratrol improved cardiac function by upregulating P-AMPK protein levels, besides we also found increased acetylation of FOXO1(decreased activity) with decreased SIRT1 protein levels, resveratrol treatment significantly improved the deacetylation (improved activity) of FOXO1 along with increased SIRT1 levels.

Interestingly chronic murine models of iron-overload associated with dose-dependent accumulation of iron and also showed diastolic dysfunction, however, the key driver of the pathogenesis is because of passive stiff component abnormality such as massive myocardial fibrosis with myocardial ECM remodeling and not because of active component abnormality. Like early stage iron-overload cardiomyopathy, we also

observed oxidative stress, lipid peroxidation, with massive fibrosis without any change in SERCA2a levels and inflammation. Interestingly resveratrol antioxidant therapy also showed reduced oxidative stress, reduced lipid peroxidation, and decreased fibrosis content.

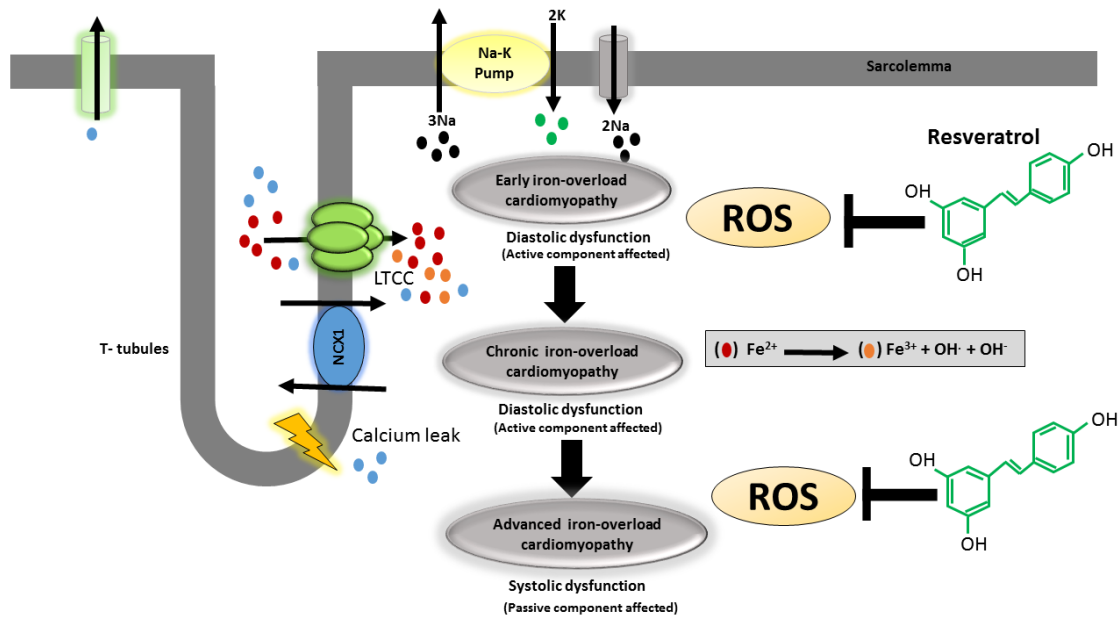


**Figure 7.2 Schematic presentation resveratrol therapeutic action in reducing iron induced oxidative stress and different stages of iron-overload cardiomyopathy.** During iron-overload redox iron transports via L-Type calcium channels and participates in Fenton's chemistry, favors the formation of free radicals. These reactive oxygen species causes myocardial oxidative stress, however, resveratrol antioxidant therapy prevents iron-induced oxidative stress and improves cardiac function in early, chronic and advanced disease states of iron-overload cardiomyopathy LTCCB= L-Type calcium channels, SR=Sarcoplasmic reticulum; SERCA2a=Sarcoplasmic reticulum calcium ATPase2a; NCX1=Sodium-calcium exchanger1; Na-K=Sodium-potassium pump; ROS=reactive oxygen species; RSV=resveratrol; RyR=Ryanodine receptor.

However, pre-clinical murine models which closely recapitulate human iron-overload cardiomyopathy are limited. To improve the translational prospect, we aged our murine models in association with iron-overload in the genetic iron-overload murine model, besides we also looked the therapeutic effects of resveratrol and these aged murine models called advanced stage. Interestingly we found severe

cardiomyopathy with diastolic and systolic dysfunction, with oxidative stress, lipid peroxidation, and massive fibrosis and reduced SERCA2a with calcium cycling defects. Resveratrol treatment showed significant improvement in cardiac function by reducing oxidative stress, lipid peroxidation, along with decreasing myocardial fibrosis and upregulating SERCA2a levels.

***Pathophysiology of hepatic iron-overload disease:*** Liver is a major organ of the body which stores a large amount of iron in a safe manner.<sup>105</sup> Abnormal iron metabolism leads to end-organ injury and deleterious pathophysiological effects culminating in end-organ disease including liver fibrosis, cirrhosis and hepatocellular carcinoma.<sup>13, 254, 263</sup> Liver tightly regulates iron-metabolism by secreting an iron regulatory hormone called hepcidin. Hepcidin deficiency in hemochromatosis disease conditions leads excess body iron due to irregular absorption of iron from dietary sources. Secondary iron-overload also associated with increased body iron due to chronic blood transfusions and excess iron deposits in the liver along with other organs. Hepatic iron-overload and the progression of liver failure are very common in genetic hemochromatosis and secondary iron-overload patients. Excess redox, iron accumulation in hepatocytes favors the generation of free radicals resulted in increased lipid peroxidation, protein oxidation, DNA damage and depletion of antioxidants (**Figure 7.3 and Figure 7.4B**). Many lines of evidence showed hepatic iron-overload associated with decreased antioxidant reserves (reduced glutathione), increased lipid peroxidation products such as 4-hydroxynonenal (4-HNE), malondialdehyde (MDA), along with inflammation, hepatic cell death in animal models and in patients with genetic hemochromatosis and

secondary iron-overload. The mainstay therapies are chelation and phlebotomy, however, these therapies are cumbersome and associated with toxic side effects.

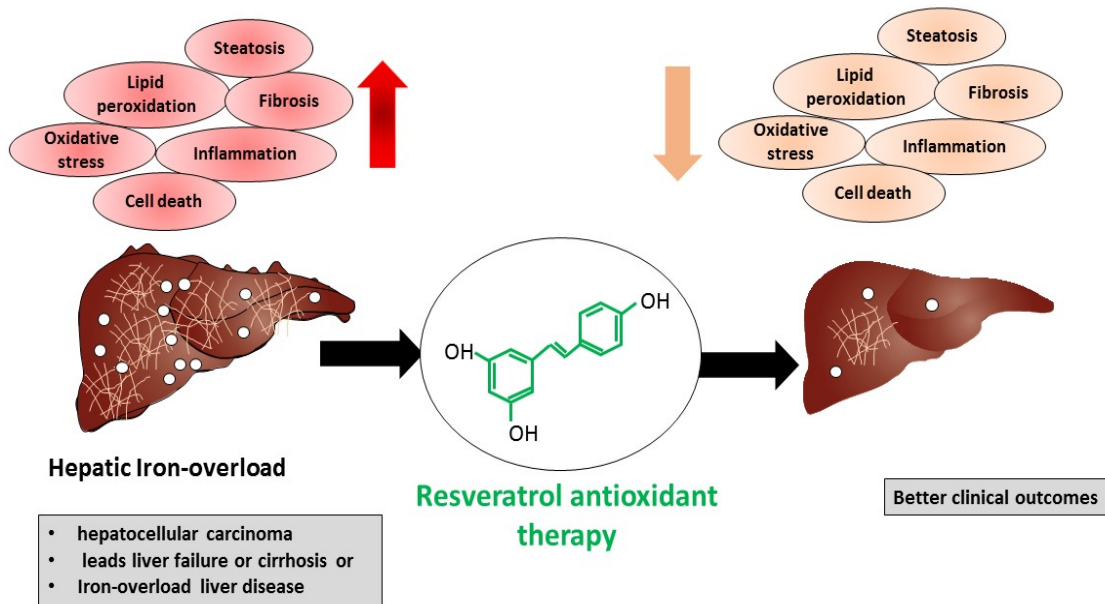


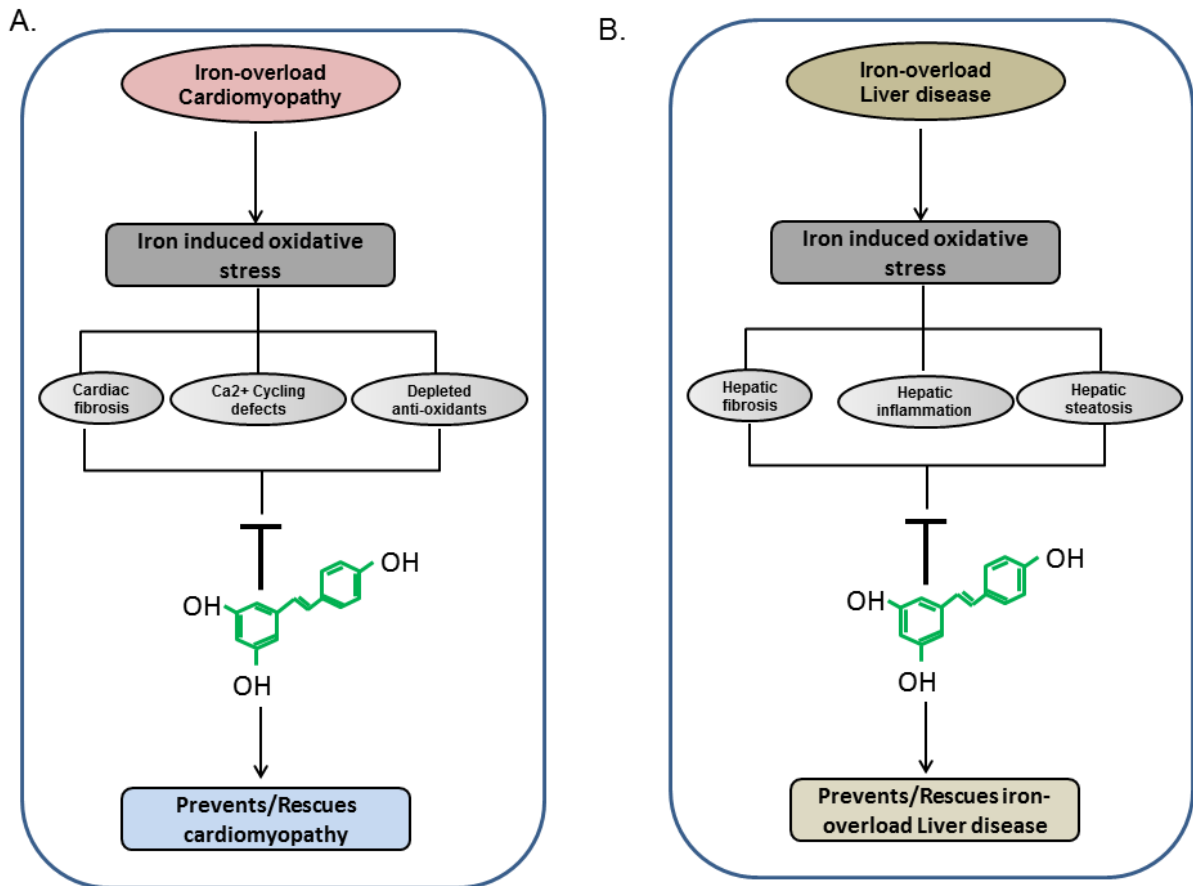
**Figure 7.3 Schematic presentation showing hepatoprotective benefits of resveratrol hepatic iron-overload.** Iron-overload in the liver associated with redox iron transports and, favors the formation of free radicals. These reactive oxygen species causes hepatic oxidative stress, lipid peroxidation, hepatic inflammation, cell death and steatosis promotes progression of hepatocellular carcinoma or cirrhosis or end stage liver disease. However, resveratrol antioxidant therapy prevents iron-induced oxidative stress, prevents lipid peroxidation, prevents fibrosis, reduces hepatic inflammation and improves liver function during hepatic iron-overload.

We extensively studied new insights of hepatic iron-overload pathophysiology in chronic and advanced pre-clinical murine models of iron-overload, and we found a dose-dependent accumulation of iron, hepatomegaly, hepatic fibrosis, hepatic inflammation, hepatic cell death and steatosis<sup>173</sup> (Figure 7.3 and Figure 7.4B). Iron-induced oxidative stress is a key driver in the progression of iron-overload liver diseases. We treated our chronic and advanced hepatic iron-overload phenotypes with resveratrol antioxidant, interestingly resveratrol supplementation reduced the oxidative

damage (increased reduced glutathione levels), and a significant reduction in hepatic lipid peroxidation (reduced MDA, and 4-HNE products), beside this iron induced inflammation, steatosis, and cell death also significantly reduced by resveratrol therapy.<sup>173</sup> Iron-overloaded liver at advanced stage leads increased triglyceride accumulation results in steatosis with fatty liver, however, resveratrol administration normalized the triglyceride levels and prevents steatosis with fatty liver (**Figure 7.3 and Figure 7.4B**). Although we did not investigate a complete panel of the molecular effects of resveratrol, interestingly we found increased hepatic acetylation of FOXO1 (decreased activity) with decreased SIRT1 protein levels during hepatic iron-overload, resveratrol treatment significantly reduced the acetylation of hepatic FOXO1 along with increased SIRT1 levels.

***Gender based differences in iron-overload cardiomyopathy:*** Sex-based differences in cardiac function and iron metabolism exist in nature.<sup>316-318</sup> Many lines of evidence showed that the clinical burden of type-1 primary hemochromatosis is significantly less in women,<sup>319</sup> besides, males are highly susceptible to excess iron than female which resulted in the development of heart disease, however, the basic molecular pathophysiology poorly understood.<sup>301</sup> We elucidated new insights of gender based differences in acquired and genetic murine models of iron-overload (**Figure 7.4C**). We showed that female acquired and genetic murine models were markedly resistant to iron-mediated cardiovascular injury based on functional, histological and molecular determinants of heart disease. Importantly, we evaluated cardiac function using non-invasive echocardiography and invasive pressure-volume loops and while iron-overloaded females showed normal cardiac function, iron-overloaded males exhibited

diastolic dysfunction. Interestingly, we found that iron-induced oxidative stress is the key driver in the progression of iron induced heart failure.<sup>82</sup> In contrast, iron-overload in ovariectomized females resulted in advanced iron-overload cardiomyopathy characterized by both diastolic and systolic dysfunction. We also found iron-induced oxidative stress in ovariectomized females with iron-overload, clearly shows the anti-oxidant effects of the female sex hormone estrogen (**Figure 7.4C**).<sup>142</sup> The phenotypic features and response to OVX were similar in both models highlighting a conserved mechanism for the gender-dependent cardiac remodeling in response to iron-overload.



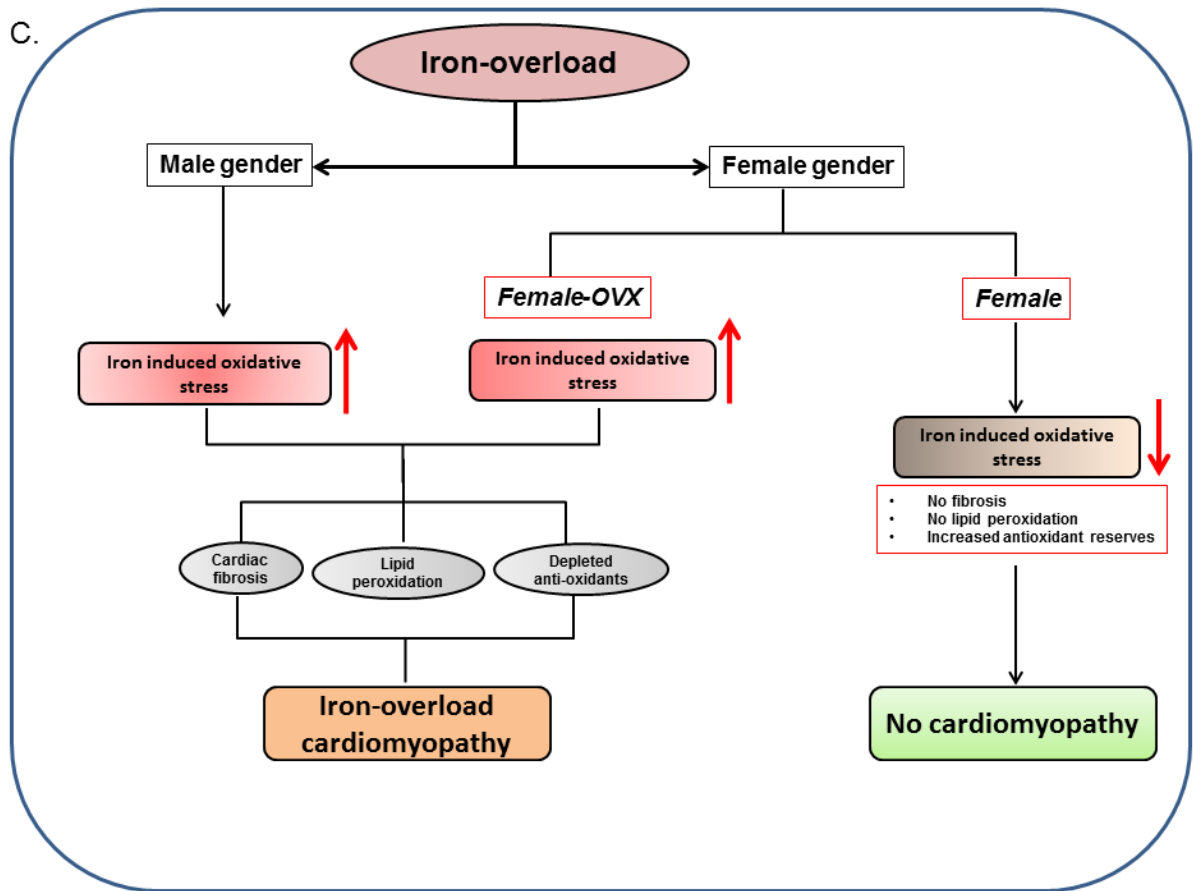


**Figure 7.4 Schematic presentation showing summary of iron-overload pathophysiology.** Iron-overload cardiomyopathy associated with deposition of iron in heart and triggers iron induced oxidative stress favors the formation of free radicals which in turn promotes myocardial fibrosis,  $\text{Ca}^{2+}$  cycling defects and loss of anti-oxidant capacity (A). Iron-overload Liver disease associated with deposition of iron in liver parenchyma and triggers iron induced oxidative stress favors the formation of free radicals which in turn promotes hepatomegaly, hepatic fibrosis, lipid peroxidation and loss of anti-oxidant capacity (B). The pathophysiology of iron-overload cardiomyopathy in male and female gender. Male mice with iron-overload showed cardiomyopathy however female mice resistant to iron-overload cardiomyopathy. Ovariectomized females showed severe cardiomyopathy. Iron induced oxidative stress, lipid peroxidation, fibrosis and decreased anti-oxidant reserves are the major pathophysiology noticed (C).

**7.2 Future directions:** Future experiments should address the following areas:

1. During iron-overloaded conditions iron also deposits into different endocrine glands such as the pancreas, pituitary glands, and thyroid gland and leads to endocrinopathies including diabetes which are common co-morbidity found in iron-overload patients.<sup>313, 314, 320</sup> We did not study endocrinopathies in our murine models of iron-overload; studying the endocrine dysfunction in these murine models of iron-overload can shed light on the metabolic abnormalities associated with iron-overload.
2. Mitochondrial iron metabolism and mitochondrial iron-overload are also important aspects of iron-metabolism in diseased conditions. The study of mitochondrial iron metabolism during iron-overload cardiomyopathy, along with effects of resveratrol therapy on mitochondrial function could provide useful insights into the cellular metabolic perturbations associated with iron-overload cardiomyopathy and the therapeutic effects of resveratrol.
3. Our results showed that ovariectomized female mice are highly susceptible to iron induced oxidative stress and cardiomyopathy. To further investigate the protective properties of estrogen in this model, iron-overloaded ovariectomized female mice subjected to 17- $\beta$ -estradiol therapy can be used to rescue the worsened cardiomyopathy in these mice.

## References

1. Hentze MW, Muckenthaler MU, Andrews NC. Balancing acts: Molecular control of mammalian iron metabolism. *Cell*. 2004;117:285-297.
2. Silva B, Faustino P. An overview of molecular basis of iron metabolism regulation and the associated pathologies. *Biochimica et biophysica acta*. 2015;1852:1347-1359.
3. Hentze MW, Muckenthaler MU, Galy B, Camaschella C. Two to tango: Regulation of mammalian iron metabolism. *Cell*. 2010;142:24-38.
4. Andrews NC. Disorders of iron metabolism. *The New England journal of medicine*. 1999;341:1986-1995.
5. Napier I, Ponka P, Richardson DR. Iron trafficking in the mitochondrion: Novel pathways revealed by disease. *Blood*. 2005;105:1867-1874.
6. Fleming RE, Ponka P. Iron overload in human disease. *The New England journal of medicine*. 2012;366:348-359.
7. Conrad ME, Umbreit JN. Disorders of iron metabolism. *The New England journal of medicine*. 2000;342:1293-1294.
8. Anderson GJ, Vulpe CD. Mammalian iron transport. *Cellular and molecular life sciences : CMLS*. 2009;66:3241-3261.
9. Cheng Y, Zak O, Aisen P, Harrison SC, Walz T. Single particle reconstruction of the human apo-transferrin-transferrin receptor complex. *Journal of structural biology*. 2005;152:204-210.
10. Xu W, Barrientos T, Mao L, Rockman HA, Sauve AA, Andrews NC. Lethal cardiomyopathy in mice lacking transferrin receptor in the heart. *Cell reports*. 2015;13:533-545.

11. Robb A, Wessling-Resnick M. Regulation of transferrin receptor 2 protein levels by transferrin. *Blood*. 2004;104:4294-4299.
12. Johnson MB, Enns CA. Diferric transferrin regulates transferrin receptor 2 protein stability. *Blood*. 2004;104:4287-4293.
13. Pietrangelo A. Hereditary hemochromatosis--a new look at an old disease. *The New England journal of medicine*. 2004;350:2383-2397.
14. Roetto A, Daraio F, Alberti F, Porporato P, Cali A, De Gobbi M, Camaschella C. Hemochromatosis due to mutations in transferrin receptor 2. *Blood cells, molecules & diseases*. 2002;29:465-470.
15. Jandl JH, Inman JK, Simmons RL, Allen DW. Transfer of iron from serum iron-binding protein to human reticulocytes. *The Journal of clinical investigation*. 1959;38:161-185.
16. Jandl JH, Katz JH. The plasma-to-cell cycle of transferrin. *The Journal of clinical investigation*. 1963;42:314-326.
17. Andrews NC, Schmidt PJ. Iron homeostasis. *Annual review of physiology*. 2007;69:69-85.
18. Eckenroth BE, Steere AN, Chasteen ND, Everse SJ, Mason AB. How the binding of human transferrin primes the transferrin receptor potentiating iron release at endosomal pH. *Proceedings of the National Academy of Sciences of the United States of America*. 2011;108:13089-13094.
19. Chasteen ND. Transferrin: A perspective. *Advances in inorganic biochemistry*. 1983;5:201-233.
20. Dautry-Varsat A, Ciechanover A, Lodish HF. pH and the recycling of transferrin during receptor-mediated endocytosis. *Proceedings of the National Academy of Sciences of the United States of America*. 1983;80:2258-2262.
21. Richardson DR, Ponka P. The molecular mechanisms of the metabolism and transport of iron in normal and neoplastic cells. *Biochimica et biophysica acta*. 1997;1331:1-40.

22. Morgan EH. Inhibition of reticulocyte iron uptake by  $\text{nh}_4\text{cl}$  and  $\text{ch}_3\text{nh}_2$ . *Biochimica et biophysica acta*. 1981;642:119-134.
23. Armstrong NJ, Morgan EH. The effect of lysosomotropic bases and inhibitors of transglutaminase on iron uptake by immature erythroid cells. *Biochimica et biophysica acta*. 1983;762:175-186.
24. Fleming MD, Trenor CC, 3rd, Su MA, Foernzler D, Beier DR, Dietrich WF, Andrews NC. Microcytic anaemia mice have a mutation in *nramp2*, a candidate iron transporter gene. *Nature genetics*. 1997;16:383-386.
25. Gunshin H, Mackenzie B, Berger UV, Gunshin Y, Romero MF, Boron WF, Nussberger S, Gollan JL, Hediger MA. Cloning and characterization of a mammalian proton-coupled metal-ion transporter. *Nature*. 1997;388:482-488.
26. Gunshin H, Allerson CR, Polycarpou-Schwarz M, Rofts A, Rogers JT, Kishi F, Hentze MW, Rouault TA, Andrews NC, Hediger MA. Iron-dependent regulation of the divalent metal ion transporter. *FEBS letters*. 2001;509:309-316.
27. Ke Y, Chen YY, Chang YZ, Duan XL, Ho KP, Jiang DH, Wang K, Qian ZM. Post-transcriptional expression of *dmt1* in the heart of rat. *Journal of cellular physiology*. 2003;196:124-130.
28. Harrison PM, Arosio P. The ferritins: Molecular properties, iron storage function and cellular regulation. *Biochimica et biophysica acta*. 1996;1275:161-203.
29. Levi S, Corsi B, Bosisio M, Invernizzi R, Volz A, Sanford D, Arosio P, Drysdale J. A human mitochondrial ferritin encoded by an intronless gene. *The Journal of biological chemistry*. 2001;276:24437-24440.
30. Keel SB, Doty RT, Yang Z, Quigley JG, Chen J, Knoblauch S, Kingsley PD, De Domenico I, Vaughn MB, Kaplan J, Palis J, Abkowitz JL. A heme export protein is required for red blood cell differentiation and iron homeostasis. *Science*. 2008;319:825-828.

31. Quigley JG, Yang Z, Worthington MT, Phillips JD, Sabo KM, Sabath DE, Berg CL, Sassa S, Wood BL, Abkowitz JL. Identification of a human heme exporter that is essential for erythropoiesis. *Cell*. 2004;118:757-766.
32. Oudit GY, Trivieri MG, Khaper N, Liu PP, Backx PH. Role of l-type ca<sup>2+</sup> channels in iron transport and iron-overload cardiomyopathy. *Journal of molecular medicine*. 2006;84:349-364.
33. Donovan A, Brownlie A, Zhou Y, Shepard J, Pratt SJ, Moynihan J, Paw BH, Drejer A, Barut B, Zapata A, Law TC, Brugnara C, Lux SE, Pinkus GS, Pinkus JL, Kingsley PD, Palis J, Fleming MD, Andrews NC, Zon LI. Positional cloning of zebrafish ferroportin1 identifies a conserved vertebrate iron exporter. *Nature*. 2000;403:776-781.
34. Nemeth E, Tuttle MS, Powelson J, Vaughn MB, Donovan A, Ward DM, Ganz T, Kaplan J. Hepcidin regulates cellular iron efflux by binding to ferroportin and inducing its internalization. *Science*. 2004;306:2090-2093.
35. Abboud S, Haile DJ. A novel mammalian iron-regulated protein involved in intracellular iron metabolism. *The Journal of biological chemistry*. 2000;275:19906-19912.
36. Donovan A, Lima CA, Pinkus JL, Pinkus GS, Zon LI, Robine S, Andrews NC. The iron exporter ferroportin/slc40a1 is essential for iron homeostasis. *Cell metabolism*. 2005;1:191-200.
37. De Domenico I, Ward DM, di Patti MC, Jeong SY, David S, Musci G, Kaplan J. Ferroxidase activity is required for the stability of cell surface ferroportin in cells expressing gpi-ceruloplasmin. *The EMBO journal*. 2007;26:2823-2831.
38. De Domenico I, Ward DM, Nemeth E, Vaughn MB, Musci G, Ganz T, Kaplan J. The molecular basis of ferroportin-linked hemochromatosis. *Proceedings of the National Academy of Sciences of the United States of America*. 2005;102:8955-8960.

39. Muckenthaler MU, Galy B, Hentze MW. Systemic iron homeostasis and the iron-responsive element/iron-regulatory protein (ire/irp) regulatory network. *Annual review of nutrition*. 2008;28:197-213.
40. Recalcati S, Minotti G, Cairo G. Iron regulatory proteins: From molecular mechanisms to drug development. *Antioxidants & redox signaling*. 2010;13:1593-1616.
41. Ganz T, Nemeth E. Hepcidin and iron homeostasis. *Biochimica et biophysica acta*. 2012;1823:1434-1443.
42. Liu XB, Nguyen NB, Marquess KD, Yang F, Haile DJ. Regulation of hepcidin and ferroportin expression by lipopolysaccharide in splenic macrophages. *Blood cells, molecules & diseases*. 2005;35:47-56.
43. Bekri S, Gual P, Anty R, Luciani N, Dahman M, Ramesh B, Iannelli A, Staccini-Myx A, Casanova D, Ben Amor I, Saint-Paul MC, Huet PM, Sadoul JL, Gugenheim J, Srai SK, Tran A, Le Marchand-Brustel Y. Increased adipose tissue expression of hepcidin in severe obesity is independent from diabetes and nash. *Gastroenterology*. 2006;131:788-796.
44. Rochette J, Pointon JJ, Fisher CA, Perera G, Arambepola M, Arichchi DS, De Silva S, Vandwalle JL, Monti JP, Old JM, Merryweather-Clarke AT, Weatherall DJ, Robson KJ. Multicentric origin of hemochromatosis gene (hfe) mutations. *American journal of human genetics*. 1999;64:1056-1062.
45. Allen KJ, Gurrin LC, Constantine CC, Osborne NJ, Delatycki MB, Nicoll AJ, McLaren CE, Bahlo M, Nisselle AE, Vulpe CD, Anderson GJ, Southey MC, Giles GG, English DR, Hopper JL, Olynyk JK, Powell LW, Gertig DM. Iron-overload-related disease in hfe hereditary hemochromatosis. *The New England journal of medicine*. 2008;358:221-230.
46. Barton JC, Bertoli LF. Hemochromatosis: The genetic disorder of the twenty-first century. *Nature medicine*. 1996;2:394-395.

47. Hannuksela J, Leppilampi M, Peuhkurinen K, Karkkainen S, Saastamoinen E, Helio T, Kaartinen M, Nieminen MS, Nieminen P, Parkkila S. Hereditary hemochromatosis gene (hfe) mutations c282y, h63d and s65c in patients with idiopathic dilated cardiomyopathy. *European journal of heart failure*. 2005;7:103-108.
48. Feder JN, Gnirke A, Thomas W, Tsuchihashi Z, Ruddy DA, Basava A, Dormishian F, Domingo R, Jr., Ellis MC, Fullan A, Hinton LM, Jones NL, Kimmel BE, Kronmal GS, Lauer P, Lee VK, Loeb DB, Mapa FA, McClelland E, Meyer NC, Mintier GA, Moeller N, Moore T, Morikang E, Prass CE, Quintana L, Starnes SM, Schatzman RC, Brunke KJ, Drayna DT, Risch NJ, Bacon BR, Wolff RK. A novel mhc class i-like gene is mutated in patients with hereditary haemochromatosis. *Nature genetics*. 1996;13:399-408.
49. Townsend A, Drakesmith H. Role of hfe in iron metabolism, hereditary haemochromatosis, anaemia of chronic disease, and secondary iron overload. *Lancet*. 2002;359:786-790.
50. Papanikolaou G, Samuels ME, Ludwig EH, MacDonald ML, Franchini PL, Dube MP, Andres L, MacFarlane J, Sakellaropoulos N, Politou M, Nemeth E, Thompson J, Risler JK, Zaborowska C, Babakaiff R, Radomski CC, Pape TD, Davidas O, Christakis J, Brissot P, Lockitch G, Ganz T, Hayden MR, Goldberg YP. Mutations in hfe2 cause iron overload in chromosome 1q-linked juvenile hemochromatosis. *Nature genetics*. 2004;36:77-82.
51. Huang FW, Pinkus JL, Pinkus GS, Fleming MD, Andrews NC. A mouse model of juvenile hemochromatosis. *The Journal of clinical investigation*. 2005;115:2187-2191.
52. Celec P. Hemojuvelin: A supposed role in iron metabolism one year after its discovery. *Journal of molecular medicine*. 2005;83:521-525.
53. Niederkofler V, Salie R, Arber S. Hemojuvelin is essential for dietary iron sensing, and its mutation leads to severe iron overload. *The Journal of clinical investigation*. 2005;115:2180-2186.

54. Olivieri NF. The beta-thalassemiias. *The New England journal of medicine*. 1999;341:99-109.
55. Weatherall DJ, Clegg JB. Inherited haemoglobin disorders: An increasing global health problem. *Bulletin of the World Health Organization*. 2001;79:704-712.
56. Chen FE, Ooi C, Ha SY, Cheung BM, Todd D, Liang R, Chan TK, Chan V. Genetic and clinical features of hemoglobin h disease in chinese patients. *The New England journal of medicine*. 2000;343:544-550.
57. Weatherall DJ, Clegg JB. Thalassemia--a global public health problem. *Nature medicine*. 1996;2:847-849.
58. Shehee WR, Oliver P, Smithies O. Lethal thalassemia after insertional disruption of the mouse major adult beta-globin gene. *Proceedings of the National Academy of Sciences of the United States of America*. 1993;90:3177-3181.
59. Yang B, Kirby S, Lewis J, Detloff PJ, Maeda N, Smithies O. A mouse model for beta 0-thalassemia. *Proceedings of the National Academy of Sciences of the United States of America*. 1995;92:11608-11612.
60. Pennell DJ, Udelson JE, Arai AE, Bozkurt B, Cohen AR, Galanella R, Hoffman TM, Kiernan MS, Lerakis S, Piga A, Porter JB, Walker JM, Wood J, American Heart Association Committee on Heart F, Transplantation of the Council on Clinical C, Council on Cardiovascular R, Imaging. Cardiovascular function and treatment in beta-thalassemia major: A consensus statement from the american heart association. *Circulation*. 2013;128:281-308.
61. Cusma Piccione M, Piraino B, Zito C, Khandheria BK, Di Bella G, De Gregorio C, Oreto L, Rigoli L, Ferrau V, Salpietro CD, Carerj S. Early identification of cardiovascular involvement in patients with beta-thalassemia major. *The American journal of cardiology*. 2013;112:1246-1251.

62. Paszty C, Brion CM, Mancini E, Witkowska HE, Stevens ME, Mohandas N, Rubin EM. Transgenic knockout mice with exclusively human sickle hemoglobin and sickle cell disease. *Science*. 1997;278:876-878.
63. Paszty C. Transgenic and gene knock-out mouse models of sickle cell anemia and the thalassemias. *Current opinion in hematology*. 1997;4:88-93.
64. Ryan TM, Ciavatta DJ, Townes TM. Knockout-transgenic mouse model of sickle cell disease. *Science*. 1997;278:873-876.
65. Yamamoto M, Nakajima O, Furuyama K, Harigae H, Hayashi N. [molecular diagnosis of hereditary sideroblastic anemia and model mouse of the disease]. [*Rinsho ketsueki*] *The Japanese journal of clinical hematology*. 2000;41:540-543.
66. Nakajima O, Takahashi S, Harigae H, Furuyama K, Hayashi N, Sassa S, Yamamoto M. Heme deficiency in erythroid lineage causes differentiation arrest and cytoplasmic iron overload. *The EMBO journal*. 1999;18:6282-6289.
67. Heimpel H, Anselstetter V, Chrobak L, Denecke J, Einsiedler B, Gallmeier K, Griesshammer A, Marquardt T, Janka-Schaub G, Kron M, Kohne E. Congenital dyserythropoietic anemia type ii: Epidemiology, clinical appearance, and prognosis based on long-term observation. *Blood*. 2003;102:4576-4581.
68. Lim PS, Chan EC, Lu TC, Yu YL, Kuo SY, Wang TH, Wei YH. Lipophilic antioxidants and iron status in esrd patients on hemodialysis. *Nephron*. 2000;86:428-435.
69. Zager RA, Johnson AC, Hanson SY, Wasse H. Parenteral iron formulations: A comparative toxicologic analysis and mechanisms of cell injury. *American journal of kidney diseases : the official journal of the National Kidney Foundation*. 2002;40:90-103.
70. Kremastinos DT, Farmakis D. Iron overload cardiomyopathy in clinical practice. *Circulation*. 2011;124:2253-2263.

71. Wexler RK, Elton T, Pleister A, Feldman D. Cardiomyopathy: An overview. *American family physician*. 2009;79:778-784.
72. Gulati V, Harikrishnan P, Palaniswamy C, Aronow WS, Jain D, Frishman WH. Cardiac involvement in hemochromatosis. *Cardiology in review*. 2014;22:56-68.
73. Kremastinos DT, Tsetsos GA, Tsiapras DP, Karavolias GK, Ladis VA, Kattamis CA. Heart failure in beta thalassemia: A 5-year follow-up study. *The American journal of medicine*. 2001;111:349-354.
74. Murphy CJ, Oudit GY. Iron-overload cardiomyopathy: Pathophysiology, diagnosis, and treatment. *Journal of cardiac failure*. 2010;16:888-900.
75. Gujja P, Rosing DR, Tripodi DJ, Shizukuda Y. Iron overload cardiomyopathy: Better understanding of an increasing disorder. *Journal of the American College of Cardiology*. 2010;56:1001-1012.
76. Buja LM, Roberts WC. Iron in the heart. Etiology and clinical significance. *The American journal of medicine*. 1971;51:209-221.
77. Oudit GY, Sun H, Trivieri MG, Koch SE, Dawood F, Ackerley C, Yazdanpanah M, Wilson GJ, Schwartz A, Liu PP, Backx PH. L-type  $Ca^{2+}$  channels provide a major pathway for iron entry into cardiomyocytes in iron-overload cardiomyopathy. *Nature medicine*. 2003;9:1187-1194.
78. Loreal O, Gosriwatana I, Guyader D, Porter J, Brissot P, Hider RC. Determination of non-transferrin-bound iron in genetic hemochromatosis using a new hplc-based method. *Journal of hepatology*. 2000;32:727-733.
79. Hershko C, Graham G, Bates GW, Rachmilewitz EA. Non-specific serum iron in thalassaemia: An abnormal serum iron fraction of potential toxicity. *British journal of haematology*. 1978;40:255-263.

80. Das SK, Oudit GY. Voltage-gated  $Ca^{2+}$  channels as key mediators of iron-transport and iron-overload cardiomyopathy: L-type vs. T-type  $Ca^{2+}$  channels. *European journal of haematology*. 2012;88:476-477.
81. Kumfu S, Chattipakorn S, Srichairatanakool S, Settakorn J, Fucharoen S, Chattipakorn N. T-type calcium channel as a portal of iron uptake into cardiomyocytes of beta-thalassemic mice. *European journal of haematology*. 2011;86:156-166.
82. Eaton JW, Qian M. Molecular bases of cellular iron toxicity. *Free radical biology & medicine*. 2002;32:833-840.
83. Oudit GY, Trivieri MG, Khaper N, Husain T, Wilson GJ, Liu P, Sole MJ, Backx PH. Taurine supplementation reduces oxidative stress and improves cardiovascular function in an iron-overload murine model. *Circulation*. 2004;109:1877-1885.
84. Livrea MA, Tesoriere L, Pintaudi AM, Calabrese A, Maggio A, Freisleben HJ, D'Arpa D, D'Anna R, Bongiorno A. Oxidative stress and antioxidant status in beta-thalassemia major: Iron overload and depletion of lipid-soluble antioxidants. *Blood*. 1996;88:3608-3614.
85. Young IS, Trouton TG, Torney JJ, McMaster D, Callender ME, Trimble ER. Antioxidant status and lipid peroxidation in hereditary haemochromatosis. *Free radical biology & medicine*. 1994;16:393-397.
86. Kadiiska MB, Burkitt MJ, Xiang QH, Mason RP. Iron supplementation generates hydroxyl radical in vivo. An esr spin-trapping investigation. *The Journal of clinical investigation*. 1995;96:1653-1657.
87. Lee SH, Oe T, Blair IA. Vitamin c-induced decomposition of lipid hydroperoxides to endogenous genotoxins. *Science*. 2001;292:2083-2086.
88. Esterbauer H, Schaur RJ, Zollner H. Chemistry and biochemistry of 4-hydroxynonenal, malonaldehyde and related aldehydes. *Free radical biology & medicine*. 1991;11:81-128.

89. Folden DV, Gupta A, Sharma AC, Li SY, Saari JT, Ren J. Malondialdehyde inhibits cardiac contractile function in ventricular myocytes via a p38 mitogen-activated protein kinase-dependent mechanism. *British journal of pharmacology*. 2003;139:1310-1316.
90. Schwartz KA, Li Z, Schwartz DE, Cooper TG, Braselton WE. Earliest cardiac toxicity induced by iron overload selectively inhibits electrical conduction. *Journal of applied physiology*. 2002;93:746-751.
91. Das SK, Wang W, Zhabyeyev P, Basu R, McLean B, Fan D, Parajuli N, DesAulniers J, Patel VB, Hajjar RJ, Dyck JR, Kassiri Z, Oudit GY. Iron-overload injury and cardiomyopathy in acquired and genetic models is attenuated by resveratrol therapy. *Scientific reports*. 2015;5:18132.
92. Valenti L, Conte D, Piperno A, Dongiovanni P, Fracanzani AL, Fraquelli M, Vergani A, Gianni C, Carmagnola L, Fargion S. The mitochondrial superoxide dismutase a16v polymorphism in the cardiomyopathy associated with hereditary haemochromatosis. *Journal of medical genetics*. 2004;41:946-950.
93. Seznec H, Simon D, Bouton C, Reutenauer L, Hertzog A, Golik P, Procaccio V, Patel M, Drapier JC, Koenig M, Puccio H. Friedreich ataxia: The oxidative stress paradox. *Human molecular genetics*. 2005;14:463-474.
94. Perdomini M, Belbellaa B, Monassier L, Reutenauer L, Messaddeq N, Cartier N, Crystal RG, Aubourg P, Puccio H. Prevention and reversal of severe mitochondrial cardiomyopathy by gene therapy in a mouse model of friedreich's ataxia. *Nature medicine*. 2014;20:542-547.
95. Ramirez RL, Qian J, Santambrogio P, Levi S, Koeppen AH. Relation of cytosolic iron excess to cardiomyopathy of friedreich's ataxia. *The American journal of cardiology*. 2012;110:1820-1827.
96. Lodi R, Taylor DJ, Schapira AH. Mitochondrial dysfunction in friedreich's ataxia. *Biological signals and receptors*. 2001;10:263-270.

97. Rustin P, von Kleist-Retzow JC, Chantrel-Groussard K, Sidi D, Munnich A, Rotig A. Effect of idebenone on cardiomyopathy in friedreich's ataxia: A preliminary study. *Lancet*. 1999;354:477-479.
98. Borgna-Pignatti C, Rugolotto S, De Stefano P, Zhao H, Cappellini MD, Del Vecchio GC, Romeo MA, Forni GL, Gamberini MR, Ghilardi R, Piga A, Cnaan A. Survival and complications in patients with thalassemia major treated with transfusion and deferoxamine. *Haematologica*. 2004;89:1187-1193.
99. Pelzer T, Shamim A, Wolfges S, Schumann M, Neyses L. Modulation of cardiac hypertrophy by estrogens. *Advances in experimental medicine and biology*. 1997;432:83-89.
100. Grohe C, Kahlert S, Lobbert K, Meyer R, Linz KW, Karas RH, Vetter H. Modulation of hypertensive heart disease by estrogen. *Steroids*. 1996;61:201-204.
101. Grohe C, Kahlert S, Lobbert K, Stimpel M, Karas RH, Vetter H, Neyses L. Cardiac myocytes and fibroblasts contain functional estrogen receptors. *FEBS letters*. 1997;416:107-112.
102. Barkhem T, Carlsson B, Nilsson Y, Enmark E, Gustafsson J, Nilsson S. Differential response of estrogen receptor alpha and estrogen receptor beta to partial estrogen agonists/antagonists. *Molecular pharmacology*. 1998;54:105-112.
103. Rouayrenc JF, Vignon F, Bringer J, Pujol P. [non-genomic steroid effects: Estrogen action revisited]. *Annales d'endocrinologie*. 2000;61:517-523.
104. Klein-Hitpass L, Schorpp M, Wagner U, Ryffel GU. An estrogen-responsive element derived from the 5' flanking region of the xenopus vitellogenin a2 gene functions in transfected human cells. *Cell*. 1986;46:1053-1061.
105. Pietrangelo A. Iron and the liver. *Liver international*. 2016;36 Suppl 1:116-123.

106. Bacon BR, Adams PC, Kowdley KV, Powell LW, Tavill AS, American Association for the Study of Liver D. Diagnosis and management of hemochromatosis: 2011 practice guideline by the american association for the study of liver diseases. *Hepatology*. 2011;54:328-343.
107. Bacon BR, Britton RS. The pathology of hepatic iron overload: A free radical--mediated process? *Hepatology*. 1990;11:127-137.
108. Bacon BR, Park CH, Brittenham GM, O'Neill R, Tavill AS. Hepatic mitochondrial oxidative metabolism in rats with chronic dietary iron overload. *Hepatology*. 1985;5:789-797.
109. Singal PK, Khaper N, Palace V, Kumar D. The role of oxidative stress in the genesis of heart disease. *Cardiovascular research*. 1998;40:426-432.
110. De Marchi E, Baldassari F, Bononi A, Wieckowski MR, Pinton P. Oxidative stress in cardiovascular diseases and obesity: Role of p66shc and protein kinase c. *Oxidative medicine and cellular longevity*. 2013;2013:564961.
111. Tsutsui H, Kinugawa S, Matsushima S. Oxidative stress and heart failure. *American journal of physiology. Heart and circulatory physiology*. 2011;301:H2181-2190.
112. Adam-Vizi V, Chinopoulos C. Bioenergetics and the formation of mitochondrial reactive oxygen species. *Trends in pharmacological sciences*. 2006;27:639-645.
113. Ball AM, Sole MJ. Oxidative stress and the pathogenesis of heart failure. *Cardiology clinics*. 1998;16:665-675, viii-ix.
114. Rigoulet M, Yoboue ED, Devin A. Mitochondrial ros generation and its regulation: Mechanisms involved in h(2)o(2) signaling. *Antioxidants & redox signaling*. 2011;14:459-468.
115. Dhalla AK, Hill MF, Singal PK. Role of oxidative stress in transition of hypertrophy to heart failure. *Journal of the American College of Cardiology*. 1996;28:506-514.

116. Ide T, Tsutsui H, Kinugawa S, Utsumi H, Kang D, Hattori N, Uchida K, Arimura K, Egashira K, Takeshita A. Mitochondrial electron transport complex i is a potential source of oxygen free radicals in the failing myocardium. *Circulation research*. 1999;85:357-363.
117. Sawyer DB, Colucci WS. Mitochondrial oxidative stress in heart failure: "Oxygen wastage" revisited. *Circulation research*. 2000;86:119-120.
118. Goszcz K, Deakin SJ, Duthie GG, Stewart D, Leslie SJ, Megson IL. Antioxidants in cardiovascular therapy: Panacea or false hope? *Frontiers in cardiovascular medicine*. 2015;2:29.
119. Martinez-Cayuela M. Oxygen free radicals and human disease. *Biochimie*. 1995;77:147-161.
120. Curtin JF, Donovan M, Cotter TG. Regulation and measurement of oxidative stress in apoptosis. *Journal of immunological methods*. 2002;265:49-72.
121. Li Y, Huang TT, Carlson EJ, Melov S, Ursell PC, Olson JL, Noble LJ, Yoshimura MP, Berger C, Chan PH, Wallace DC, Epstein CJ. Dilated cardiomyopathy and neonatal lethality in mutant mice lacking manganese superoxide dismutase. *Nature genetics*. 1995;11:376-381.
122. Dennery PA. Regulation and role of heme oxygenase in oxidative injury. *Current topics in cellular regulation*. 2000;36:181-199.
123. Munoz-Sanchez J, Chanez-Cardenas ME. A review on hemeoxygenase-2: Focus on cellular protection and oxygen response. *Oxidative medicine and cellular longevity*. 2014;2014:604981.
124. Schipper HM. Heme oxygenase-1: Role in brain aging and neurodegeneration. *Experimental gerontology*. 2000;35:821-830.
125. Yoshida T, Migita CT. Mechanism of heme degradation by heme oxygenase. *Journal of inorganic biochemistry*. 2000;82:33-41.
126. Garcia-Santos D, Schranzhofer M, Horvathova M, Jaber MM, Bogo Chies JA, Sheftel AD, Ponka P. Heme oxygenase 1 is expressed in murine erythroid cells where it controls the level of regulatory heme. *Blood*. 2014;123:2269-2277.

127. Rossi R, Milzani A, Dalle-Donne I, Giustarini D, Lusini L, Colombo R, Di Simplicio P. Blood glutathione disulfide: In vivo factor or in vitro artifact? *Clinical chemistry*. 2002;48:742-753.
128. Rahman I, Kode A, Biswas SK. Assay for quantitative determination of glutathione and glutathione disulfide levels using enzymatic recycling method. *Nature protocols*. 2006;1:3159-3165.
129. Reed DJ. Glutathione: Toxicological implications. *Annual review of pharmacology and toxicology*. 1990;30:603-631.
130. Rahman I, Biswas SK, Jimenez LA, Torres M, Forman HJ. Glutathione, stress responses, and redox signaling in lung inflammation. *Antioxidants & redox signaling*. 2005;7:42-59.
131. Pastore A, Federici G, Bertini E, Piemonte F. Analysis of glutathione: Implication in redox and detoxification. *Clinica chimica acta; international journal of clinical chemistry*. 2003;333:19-39.
132. Gambhir JK, Lali P, Jain AK. Correlation between blood antioxidant levels and lipid peroxidation in rheumatoid arthritis. *Clinical biochemistry*. 1997;30:351-355.
133. Samiec PS, Drews-Botsch C, Flagg EW, Kurtz JC, Sternberg P, Jr., Reed RL, Jones DP. Glutathione in human plasma: Decline in association with aging, age-related macular degeneration, and diabetes. *Free radical biology & medicine*. 1998;24:699-704.
134. Hadi Yasa M, Kacmaz M, Serda Ozturk H, Durak I. Antioxidant status of erythrocytes from patients with cirrhosis. *Hepato-gastroenterology*. 1999;46:2460-2463.
135. Li S, Li X, Rozanski GJ. Regulation of glutathione in cardiac myocytes. *Journal of molecular and cellular cardiology*. 2003;35:1145-1152.
136. Aon MA, Stanley BA, Sivakumaran V, Kembro JM, O'Rourke B, Paolocci N, Cortassa S. Glutathione/thioredoxin systems modulate mitochondrial h<sub>2</sub>O<sub>2</sub> emission: An experimental-computational study. *The Journal of general physiology*. 2012;139:479-491.

137. Yamawaki H, Haendeler J, Berk BC. Thioredoxin: A key regulator of cardiovascular homeostasis. *Circulation research*. 2003;93:1029-1033.
138. Holmgren A. Thioredoxin. *Annual review of biochemistry*. 1985;54:237-271.
139. Taniguchi Y, Taniguchi-Ueda Y, Mori K, Yodoi J. A novel promoter sequence is involved in the oxidative stress-induced expression of the adult t-cell leukemia-derived factor (adf)/human thioredoxin (trx) gene. *Nucleic acids research*. 1996;24:2746-2752.
140. Tanaka T, Hosoi F, Yamaguchi-Iwai Y, Nakamura H, Masutani H, Ueda S, Nishiyama A, Takeda S, Wada H, Spyrou G, Yodoi J. Thioredoxin-2 (trx-2) is an essential gene regulating mitochondria-dependent apoptosis. *The EMBO journal*. 2002;21:1695-1703.
141. Miranda-Vizueté A, Ljung J, Damdimopoulos AE, Gustafsson JA, Oko R, Pelto-Huikko M, Spyrou G. Characterization of sptx, a novel member of the thioredoxin family specifically expressed in human spermatozoa. *The Journal of biological chemistry*. 2001;276:31567-31574.
142. Ejima K, Nanri H, Araki M, Uchida K, Kashimura M, Ikeda M. 17beta-estradiol induces protein thiol/disulfide oxidoreductases and protects cultured bovine aortic endothelial cells from oxidative stress. *European journal of endocrinology / European Federation of Endocrine Societies*. 1999;140:608-613.
143. Das KC, Lewis-Molock Y, White CW. Elevation of manganese superoxide dismutase gene expression by thioredoxin. *American journal of respiratory cell and molecular biology*. 1997;17:713-726.
144. Okuda M, Inoue N, Azumi H, Seno T, Sumi Y, Hirata K, Kawashima S, Hayashi Y, Itoh H, Yodoi J, Yokoyama M. Expression of glutaredoxin in human coronary arteries: Its potential role in antioxidant protection against atherosclerosis. *Arteriosclerosis, thrombosis, and vascular biology*. 2001;21:1483-1487.

145. Schulze PC, De Keulenaer GW, Yoshioka J, Kassik KA, Lee RT. Vitamin d3-upregulated protein-1 (vdup-1) regulates redox-dependent vascular smooth muscle cell proliferation through interaction with thioredoxin. *Circulation research*. 2002;91:689-695.
146. Niederau C, Fischer R, Purschel A, Stremmel W, Haussinger D, Strohmeyer G. Long-term survival in patients with hereditary hemochromatosis. *Gastroenterology*. 1996;110:1107-1119.
147. Niederau C, Fischer R, Sonnenberg A, Stremmel W, Trampisch HJ, Strohmeyer G. Survival and causes of death in cirrhotic and in noncirrhotic patients with primary hemochromatosis. *The New England journal of medicine*. 1985;313:1256-1262.
148. Muncunill J, Vaquer P, Galmes A, Obrador A, Parera M, Bargay J, Besalduch J. In hereditary hemochromatosis, red cell apheresis removes excess iron twice as fast as manual whole blood phlebotomy. *Journal of clinical apheresis*. 2002;17:88-92.
149. Rombout-Sestrienkova E, De Jonge N, Martinakova K, Klopping C, van Galen KP, Vink A, Wajon EM, Smit WM, van Bree C, Koek GH. End-stage cardiomyopathy because of hereditary hemochromatosis successfully treated with erythrocytapheresis in combination with left ventricular assist device support. *Circulation. Heart failure*. 2014;7:541-543.
150. Kim HC, Dugan NP, Silber JH, Martin MB, Schwartz E, Ohene-Frempong K, Cohen AR. Erythrocytapheresis therapy to reduce iron overload in chronically transfused patients with sickle cell disease. *Blood*. 1994;83:1136-1142.
151. Barton JC, McDonnell SM, Adams PC, Brissot P, Powell LW, Edwards CQ, Cook JD, Kowdley KV. Management of hemochromatosis. Hemochromatosis management working group. *Annals of internal medicine*. 1998;129:932-939.
152. Olivieri NF, Nathan DG, MacMillan JH, Wayne AS, Liu PP, McGee A, Martin M, Koren G, Cohen AR. Survival in medically treated patients with homozygous beta-thalassemia. *The New England journal of medicine*. 1994;331:574-578.

153. Olivieri NF, Brittenham GM. Iron-chelating therapy and the treatment of thalassemia. *Blood*. 1997;89:739-761.
154. Brittenham GM, Griffith PM, Nienhuis AW, McLaren CE, Young NS, Tucker EE, Allen CJ, Farrell DE, Harris JW. Efficacy of deferoxamine in preventing complications of iron overload in patients with thalassemia major. *The New England journal of medicine*. 1994;331:567-573.
155. Modell B, Khan M, Darlison M. Survival in beta-thalassaemia major in the uk: Data from the uk thalassaemia register. *Lancet*. 2000;355:2051-2052.
156. Noetzli LJ, Carson SM, Nord AS, Coates TD, Wood JC. Longitudinal analysis of heart and liver iron in thalassemia major. *Blood*. 2008;112:2973-2978.
157. Hahalis G, Alexopoulos D, Kremastinos DT, Zoumbos NC. Heart failure in beta-thalassemia syndromes: A decade of progress. *The American journal of medicine*. 2005;118:957-967.
158. Anderson LJ, Wonke B, Prescott E, Holden S, Walker JM, Pennell DJ. Comparison of effects of oral deferiprone and subcutaneous desferrioxamine on myocardial iron concentrations and ventricular function in beta-thalassaemia. *Lancet*. 2002;360:516-520.
159. Rombout-Sestrienkova E, Nieman FH, Essers BA, van Noord PA, Janssen MC, van Deursen CT, Bos LP, Rombout F, van den Braak R, de Leeuw PW, Koek GH. Erythrocytapheresis versus phlebotomy in the initial treatment of hfe hemochromatosis patients: Results from a randomized trial. *Transfusion*. 2012;52:470-477.
160. Belguendouz L, Fremont L, Linard A. Resveratrol inhibits metal ion-dependent and independent peroxidation of porcine low-density lipoproteins. *Biochemical pharmacology*. 1997;53:1347-1355.
161. Wong YT, Gruber J, Jenner AM, Ng MP, Ruan R, Tay FE. Elevation of oxidative-damage biomarkers during aging in f2 hybrid mice: Protection by chronic oral intake of resveratrol. *Free radical biology & medicine*. 2009;46:799-809.

162. Chung JH, Manganiello V, Dyck JR. Resveratrol as a calorie restriction mimetic: Therapeutic implications. *Trends in cell biology*. 2012;22:546-554.
163. Das SK, Patel VB, Oudit GY. Beneficial effects of grape resveratrol on serum adiponectin and inflammation: Clinical trial in patients with stable coronary artery disease: Editorial to: "Grape resveratrol increases serum adiponectin and downregulates inflammatory genes in peripheral blood mononuclear cells: A triple-blind, placebo-controlled, one-year clinical trial in patients with stable coronary artery disease" by j. Tome-carneiro et al. *Cardiovascular drugs and therapy / sponsored by the International Society of Cardiovascular Pharmacotherapy*. 2013;27:1-4.
164. Dolinsky VW, Chan AY, Robillard Frayne I, Light PE, Des Rosiers C, Dyck JR. Resveratrol prevents the prohypertrophic effects of oxidative stress on Ikb1. *Circulation*. 2009;119:1643-1652.
165. Lagouge M, Argmann C, Gerhart-Hines Z, Meziane H, Lerin C, Daussin F, Messadeq N, Milne J, Lambert P, Elliott P, Geny B, Laakso M, Puigserver P, Auwerx J. Resveratrol improves mitochondrial function and protects against metabolic disease by activating sirt1 and pgc-1alpha. *Cell*. 2006;127:1109-1122.
166. Edwards AG, Donato AJ, Lesniewski LA, Gioscia RA, Seals DR, Moore RL. Life-long caloric restriction elicits pronounced protection of the aged myocardium: A role for ampk. *Mechanisms of ageing and development*. 2010;131:739-742.
167. Hardie DG, Ross FA, Hawley SA. Ampk: A nutrient and energy sensor that maintains energy homeostasis. *Nature reviews. Molecular cell biology*. 2012;13:251-262.
168. Dasgupta B, Milbrandt J. Resveratrol stimulates amp kinase activity in neurons. *Proceedings of the National Academy of Sciences of the United States of America*. 2007;104:7217-7222.
169. Um JH, Park SJ, Kang H, Yang S, Foretz M, McBurney MW, Kim MK, Viollet B, Chung JH. Amp-activated protein kinase-deficient mice are resistant to the metabolic effects of resveratrol. *Diabetes*. 2010;59:554-563.

170. Canto C, Gerhart-Hines Z, Feige JN, Lagouge M, Noriega L, Milne JC, Elliott PJ, Puigserver P, Auwerx J. Ampk regulates energy expenditure by modulating nad<sup>+</sup> metabolism and sirt1 activity. *Nature*. 2009;458:1056-1060.
171. Fulco M, Cen Y, Zhao P, Hoffman EP, McBurney MW, Sauve AA, Sartorelli V. Glucose restriction inhibits skeletal myoblast differentiation by activating sirt1 through ampk-mediated regulation of nampt. *Developmental cell*. 2008;14:661-673.
172. Canto C, Jiang LQ, Deshmukh AS, Matakic C, Coste A, Lagouge M, Zierath JR, Auwerx J. Interdependence of ampk and sirt1 for metabolic adaptation to fasting and exercise in skeletal muscle. *Cell metabolism*. 2010;11:213-219.
173. Das SK, DesAulniers J, Dyck JR, Kassiri Z, Oudit GY. Resveratrol mediates therapeutic hepatic effects in acquired and genetic murine models of iron-overload. *Liver international*. 2016;36:246-257.
174. Price NL, Gomes AP, Ling AJ, Duarte FV, Martin-Montalvo A, North BJ, Agarwal B, Ye L, Ramadori G, Teodoro JS, Hubbard BP, Varela AT, Davis JG, Varamini B, Hafner A, Moaddel R, Rolo AP, Coppari R, Palmeira CM, de Cabo R, Baur JA, Sinclair DA. Sirt1 is required for ampk activation and the beneficial effects of resveratrol on mitochondrial function. *Cell metabolism*. 2012;15:675-690.
175. Li Y, Xu S, Mihaylova MM, Zheng B, Hou X, Jiang B, Park O, Luo Z, Lefai E, Shyy JY, Gao B, Wierzbicki M, Verbeuren TJ, Shaw RJ, Cohen RA, Zang M. Ampk phosphorylates and inhibits srebp activity to attenuate hepatic steatosis and atherosclerosis in diet-induced insulin-resistant mice. *Cell metabolism*. 2011;13:376-388.
176. Horton JD, Goldstein JL, Brown MS. Srebps: Activators of the complete program of cholesterol and fatty acid synthesis in the liver. *The Journal of clinical investigation*. 2002;109:1125-1131.

177. Sulaiman M, Matta MJ, Sunderesan NR, Gupta MP, Periasamy M, Gupta M. Resveratrol, an activator of sirt1, upregulates sarcoplasmic calcium atpase and improves cardiac function in diabetic cardiomyopathy. *American journal of physiology. Heart and circulatory physiology.* 2010;298:H833-843.
178. Conti M, Beavo J. Biochemistry and physiology of cyclic nucleotide phosphodiesterases: Essential components in cyclic nucleotide signaling. *Annual review of biochemistry.* 2007;76:481-511.
179. Sung MM, Das SK, Levasseur J, Byrne NJ, Fung D, Kim TT, Masson G, Boisvenue J, Soltys CL, Oudit GY, Dyck JR. Resveratrol treatment of mice with pressure-overload-induced heart failure improves diastolic function and cardiac energy metabolism. *Circulation. Heart failure.* 2015;8:128-137.
180. Dong Q, Wu Z, Li X, Yan J, Zhao L, Yang C, Lu J, Deng J, Chen M. Resveratrol ameliorates cardiac dysfunction induced by pressure overload in rats via structural protection and modulation of ca(2+) cycling proteins. *Journal of translational medicine.* 2014;12:323.
181. Gu XS, Wang ZB, Ye Z, Lei JP, Li L, Su DF, Zheng X. Resveratrol, an activator of sirt1, upregulates ampk and improves cardiac function in heart failure. *Genetics and molecular research : GMR.* 2014;13:323-335.
182. Xuan W, Wu B, Chen C, Chen B, Zhang W, Xu D, Bin J, Liao Y. Resveratrol improves myocardial ischemia and ischemic heart failure in mice by antagonizing the detrimental effects of fractalkine\*. *Critical care medicine.* 2012;40:3026-3033.
183. Kanamori H, Takemura G, Goto K, Tsujimoto A, Ogino A, Takeyama T, Kawaguchi T, Watanabe T, Morishita K, Kawasaki M, Mikami A, Fujiwara T, Fujiwara H, Seishima M, Minatoguchi S. Resveratrol reverses remodeling in hearts with large, old myocardial infarctions through enhanced autophagy-activating amp kinase pathway. *The American journal of pathology.* 2013;182:701-713.

184. Aguirre L, Portillo MP, Hijona E, Bujanda L. Effects of resveratrol and other polyphenols in hepatic steatosis. *World journal of gastroenterology*. 2014;20:7366-7380.
185. Wang S, Moustaid-Moussa N, Chen L, Mo H, Shastri A, Su R, Bapat P, Kwun I, Shen CL. Novel insights of dietary polyphenols and obesity. *The Journal of nutritional biochemistry*. 2014;25:1-18.
186. Holthoff JH, Wang Z, Seely KA, Gokden N, Mayeux PR. Resveratrol improves renal microcirculation, protects the tubular epithelium, and prolongs survival in a mouse model of sepsis-induced acute kidney injury. *Kidney international*. 2012;81:370-378.
187. Ji G, Wang Y, Deng Y, Li X, Jiang Z. Resveratrol ameliorates hepatic steatosis and inflammation in methionine/choline-deficient diet-induced steatohepatitis through regulating autophagy. *Lipids in health and disease*. 2015;14:134.
188. Raj P, Louis XL, Thandapilly SJ, Movahed A, Zieroth S, Netticadan T. Potential of resveratrol in the treatment of heart failure. *Life sciences*. 2014;95:63-71.
189. Movahed A, Ostovar A, Iranpour D, Thandapilly SJ, Raj P, Louis XL, Smoliga JM, Netticadan T. The efficacy of resveratrol in controlling hypertension: Study protocol for a randomized, crossover, double-blinded, placebo-controlled trial. *Trials*. 2016;17:296.
190. Tome-Carneiro J, Gonzalez M, Larrosa M, Yanez-Gascon MJ, Garcia-Almagro FJ, Ruiz-Ros JA, Tomas-Barberan FA, Garcia-Conesa MT, Espin JC. Grape resveratrol increases serum adiponectin and downregulates inflammatory genes in peripheral blood mononuclear cells: A triple-blind, placebo-controlled, one-year clinical trial in patients with stable coronary artery disease. *Cardiovascular drugs and therapy / sponsored by the International Society of Cardiovascular Pharmacotherapy*. 2013;27:37-48.

191. Faghihzadeh F, Adibi P, Hekmatdoost A. The effects of resveratrol supplementation on cardiovascular risk factors in patients with non-alcoholic fatty liver disease: A randomised, double-blind, placebo-controlled study. *The British journal of nutrition*. 2015;114:796-803.
192. Walle T, Hsieh F, DeLegge MH, Oatis JE, Jr., Walle UK. High absorption but very low bioavailability of oral resveratrol in humans. *Drug metabolism and disposition: the biological fate of chemicals*. 2004;32:1377-1382.
193. Sung MM, Dyck JR. Therapeutic potential of resveratrol in heart failure. *Annals of the New York Academy of Sciences*. 2015;1348:32-45.
194. Mukherjee R, Spinale FG. L-type calcium channel abundance and function with cardiac hypertrophy and failure: A review. *Journal of molecular and cellular cardiology*. 1998;30:1899-1916.
195. Catterall WA. Structure and regulation of voltage-gated  $Ca^{2+}$  channels. *Annual review of cell and developmental biology*. 2000;16:521-555.
196. Bers DM. Cardiac excitation-contraction coupling. *Nature*. 2002;415:198-205.
197. Picht E, Zima AV, Shannon TR, Duncan AM, Blatter LA, Bers DM. Dynamic calcium movement inside cardiac sarcoplasmic reticulum during release. *Circulation research*. 2011;108:847-856.
198. Schulla V, Renstrom E, Feil R, Feil S, Franklin I, Gjinovci A, Jing XJ, Laux D, Lundquist I, Magnuson MA, Obermuller S, Olofsson CS, Salehi A, Wendt A, Klugbauer N, Wollheim CB, Rorsman P, Hofmann F. Impaired insulin secretion and glucose tolerance in beta cell-selective  $Ca_v1.2$   $Ca^{2+}$  channel null mice. *The EMBO journal*. 2003;22:3844-3854.
199. Rorsman P, Renstrom E. Insulin granule dynamics in pancreatic beta cells. *Diabetologia*. 2003;46:1029-1045.
200. Xu X, Colecraft HM. Engineering proteins for custom inhibition of  $Ca_v$  channels. *Physiology*. 2009;24:210-218.

201. Bodi I, Mikala G, Koch SE, Akhter SA, Schwartz A. The L-type calcium channel in the heart: The beat goes on. *The Journal of clinical investigation*. 2005;115:3306-3317.
202. Abernethy DR, Schwartz JB. Calcium-antagonist drugs. *The New England journal of medicine*. 1999;341:1447-1457.
203. Freher M, Challapalli S, Pinto JV, Schwartz J, Bonow RO, Gheorgiade M. Current status of calcium channel blockers in patients with cardiovascular disease. *Current problems in cardiology*. 1999;24:236-340.
204. Mason RP, Marche P, Hintze TH. Novel vascular biology of third-generation L-type calcium channel antagonists: Ancillary actions of amlodipine. *Arteriosclerosis, thrombosis, and vascular biology*. 2003;23:2155-2163.
205. Elkayam U. Calcium channel blockers in heart failure. *Cardiology*. 1998;89 Suppl 1:38-46.
206. Burges RA, Gardiner DG, Gwilt M, Higgins AJ, Blackburn KJ, Campbell SF, Cross PE, Stubbs JK. Calcium channel blocking properties of amlodipine in vascular smooth muscle and cardiac muscle in vitro: Evidence for voltage modulation of vascular dihydropyridine receptors. *Journal of cardiovascular pharmacology*. 1987;9:110-119.
207. Fitts DA. Ethics and animal numbers: Informal analyses, uncertain sample sizes, inefficient replications, and type I errors. *Journal of the American Association for Laboratory Animal Science : JAALAS*. 2011;50:445-453.
208. Ludbrook J. Statistics in biomedical laboratory and clinical science: Applications, issues and pitfalls. *Medical principles and practice : international journal of the Kuwait University, Health Science Centre*. 2008;17:1-13.
209. Dakhale GN, Hiware SK, Shinde AT, Mahatme MS. Basic biostatistics for post-graduate students. *Indian journal of pharmacology*. 2012;44:435-442.

210. Festing MF, Altman DG. Guidelines for the design and statistical analysis of experiments using laboratory animals. *ILAR journal / National Research Council, Institute of Laboratory Animal Resources*. 2002;43:244-258.
211. Felker GM, Thompson RE, Hare JM, Hruban RH, Clemetson DE, Howard DL, Baughman KL, Kasper EK. Underlying causes and long-term survival in patients with initially unexplained cardiomyopathy. *The New England journal of medicine*. 2000;342:1077-1084.
212. Olynyk JK, Cullen DJ, Aquilia S, Rossi E, Summerville L, Powell LW. A population-based study of the clinical expression of the hemochromatosis gene. *The New England journal of medicine*. 1999;341:718-724.
213. Tsushima RG, Wickenden AD, Bouchard RA, Oudit GY, Liu PP, Backx PH. Modulation of iron uptake in heart by l-type  $ca^{2+}$  channel modifiers: Possible implications in iron overload. *Circulation research*. 1999;84:1302-1309.
214. Goldhaber JJ, Qayyum MS. Oxygen free radicals and excitation-contraction coupling. *Antioxidants & redox signaling*. 2000;2:55-64.
215. Becker LB. New concepts in reactive oxygen species and cardiovascular reperfusion physiology. *Cardiovascular research*. 2004;61:461-470.
216. Wood JC, Otto-Duessel M, Aguilar M, Nick H, Nelson MD, Coates TD, Pollack H, Moats R. Cardiac iron determines cardiac  $t_2^*$ ,  $t_2$ , and  $t_1$  in the gerbil model of iron cardiomyopathy. *Circulation*. 2005;112:535-543.
217. Milne JC, Lambert PD, Schenk S, Carney DP, Smith JJ, Gagne DJ, Jin L, Boss O, Perni RB, Vu CB, Bemis JE, Xie R, Disch JS, Ng PY, Nunes JJ, Lynch AV, Yang H, Galonek H, Israelian K, Choy W, Iffland A, Lavu S, Medvedik O, Sinclair DA, Olefsky JM, Jirousek MR, Elliott PJ, Westphal CH. Small molecule activators of sirt1 as therapeutics for the treatment of type 2 diabetes. *Nature*. 2007;450:712-716.

218. Lavu S, Boss O, Elliott PJ, Lambert PD. Sirtuins--novel therapeutic targets to treat age-associated diseases. *Nature reviews. Drug discovery*. 2008;7:841-853.
219. Baur JA, Pearson KJ, Price NL, Jamieson HA, Lerin C, Kalra A, Prabhu VV, Allard JS, Lopez-Lluch G, Lewis K, Pistell PJ, Poosala S, Becker KG, Boss O, Gwinn D, Wang M, Ramaswamy S, Fishbein KW, Spencer RG, Lakatta EG, Le Couteur D, Shaw RJ, Navas P, Puigserver P, Ingram DK, de Cabo R, Sinclair DA. Resveratrol improves health and survival of mice on a high-calorie diet. *Nature*. 2006;444:337-342.
220. Baur JA, Sinclair DA. Therapeutic potential of resveratrol: The in vivo evidence. *Nature reviews. Drug discovery*. 2006;5:493-506.
221. Hajjar RJ. Potential of gene therapy as a treatment for heart failure. *The Journal of clinical investigation*. 2013;123:53-61.
222. Cutler MJ, Wan X, Plummer BN, Liu H, Deschenes I, Laurita KR, Hajjar RJ, Rosenbaum DS. Targeted sarcoplasmic reticulum  $Ca^{2+}$  ATPase 2a gene delivery to restore electrical stability in the failing heart. *Circulation*. 2012;126:2095-2104.
223. Zhong J, Basu R, Guo D, Chow FL, Byrns S, Schuster M, Loibner H, Wang XH, Penninger JM, Kassiri Z, Oudit GY. Angiotensin-converting enzyme 2 suppresses pathological hypertrophy, myocardial fibrosis, and cardiac dysfunction. *Circulation*. 2010;122:717-728, 718 p following 728.
224. Patel VB, Bodiga S, Basu R, Das SK, Wang W, Wang Z, Lo J, Grant MB, Zhong J, Kassiri Z, Oudit GY. Loss of angiotensin-converting enzyme-2 exacerbates diabetic cardiovascular complications and leads to systolic and vascular dysfunction: A critical role of the angiotensin ii/at1 receptor axis. *Circulation research*. 2012;110:1322-1335.
225. Basu R, Oudit GY, Wang X, Zhang L, Ussher JR, Lopaschuk GD, Kassiri Z. Type 1 diabetic cardiomyopathy in the akita (ins2wt/c96y) mouse model is characterized by lipotoxicity and

- diastolic dysfunction with preserved systolic function. *American journal of physiology. Heart and circulatory physiology*. 2009;297:H2096-2108.
226. Wang W, McKinnie SM, Patel VB, Haddad G, Wang Z, Zhabyeyev P, Das SK, Basu R, McLean B, Kandalam V, Penninger JM, Kassiri Z, Vederas JC, Murray AG, Oudit GY. Loss of apelin exacerbates myocardial infarction adverse remodeling and ischemia-reperfusion injury: Therapeutic potential of synthetic apelin analogues. *Journal of the American Heart Association*. 2013;2:e000249.
227. Basu R, Fan D, Kandalam V, Lee J, Das SK, Wang X, Baldwin TA, Oudit GY, Kassiri Z. Loss of timp3 gene leads to abdominal aortic aneurysm formation in response to angiotensin ii. *The Journal of biological chemistry*. 2012;287:44083-44096.
228. Patel VB, Wang Z, Fan D, Zhabyeyev P, Basu R, Das SK, Wang W, Desaulniers J, Holland SM, Kassiri Z, Oudit GY. Loss of p47phox subunit enhances susceptibility to biomechanical stress and heart failure because of dysregulation of cortactin and actin filaments. *Circulation research*. 2013;112:1542-1556.
229. Erdelmeier I, Gerard-Monnier D, Yadan JC, Chaudiere J. Reactions of n-methyl-2-phenylindole with malondialdehyde and 4-hydroxyalkenals. Mechanistic aspects of the colorimetric assay of lipid peroxidation. *Chemical research in toxicology*. 1998;11:1184-1194.
230. Brunet A, Sweeney LB, Sturgill JF, Chua KF, Greer PL, Lin Y, Tran H, Ross SE, Mostoslavsky R, Cohen HY, Hu LS, Cheng HL, Jedrychowski MP, Gygi SP, Sinclair DA, Alt FW, Greenberg ME. Stress-dependent regulation of foxo transcription factors by the sirt1 deacetylase. *Science*. 2004;303:2011-2015.
231. Ennis IL, Li RA, Murphy AM, Marban E, Nuss HB. Dual gene therapy with serca1 and kir2.1 abbreviates excitation without suppressing contractility. *The Journal of clinical investigation*. 2002;109:393-400.

232. Ching LC, Kou YR, Shyue SK, Su KH, Wei J, Cheng LC, Yu YB, Pan CC, Lee TS. Molecular mechanisms of activation of endothelial nitric oxide synthase mediated by transient receptor potential vanilloid type 1. *Cardiovascular research*. 2011;91:492-501.
233. O'Connell TD, Rodrigo MC, Simpson PC. Isolation and culture of adult mouse cardiac myocytes. *Methods in molecular biology*. 2007;357:271-296.
234. Kabaeva Z, Zhao M, Michele DE. Blebbistatin extends culture life of adult mouse cardiac myocytes and allows efficient and stable transgene expression. *American journal of physiology. Heart and circulatory physiology*. 2008;294:H1667-1674.
235. Parkes JG, Liu Y, Sirna JB, Templeton DM. Changes in gene expression with iron loading and chelation in cardiac myocytes and non-myocytic fibroblasts. *Journal of molecular and cellular cardiology*. 2000;32:233-246.
236. Liu Y, Templeton DM. Iron-loaded cardiac myocytes stimulate cardiac myofibroblast DNA synthesis. *Molecular and cellular biochemistry*. 2006;281:77-85.
237. del Monte F, Harding SE, Schmidt U, Matsui T, Kang ZB, Dec GW, Gwathmey JK, Rosenzweig A, Hajjar RJ. Restoration of contractile function in isolated cardiomyocytes from failing human hearts by gene transfer of serca2a. *Circulation*. 1999;100:2308-2311.
238. Bird SD, Doevendans PA, van Rooijen MA, Brutel de la Riviere A, Hassink RJ, Passier R, Mummery CL. The human adult cardiomyocyte phenotype. *Cardiovascular research*. 2003;58:423-434.
239. Kawano H, Do YS, Kawano Y, Starnes V, Barr M, Law RE, Hsueh WA. Angiotensin ii has multiple profibrotic effects in human cardiac fibroblasts. *Circulation*. 2000;101:1130-1137.
240. Borra MT, Smith BC, Denu JM. Mechanism of human sirt1 activation by resveratrol. *The Journal of biological chemistry*. 2005;280:17187-17195.
241. Crowell JA, Korytko PJ, Morrissey RL, Booth TD, Levine BS. Resveratrol-associated renal toxicity. *Toxicological sciences : an official journal of the Society of Toxicology*. 2004;82:614-619.

242. Lee A, Jeong D, Mitsuyama S, Oh JG, Liang L, Ikeda Y, Sadoshima J, Hajjar RJ, Kho C. The role of sumo-1 in cardiac oxidative stress and hypertrophy. *Antioxidants & redox signaling*. 2014;21:1986-2001.
243. Kho C, Lee A, Jeong D, Oh JG, Chaanine AH, Kizana E, Park WJ, Hajjar RJ. Sumo1-dependent modulation of serca2a in heart failure. *Nature*. 2011;477:601-605.
244. Balderas-Villalobos J, Molina-Munoz T, Mailloux-Salinas P, Bravo G, Carvajal K, Gomez-Viquez NL. Oxidative stress in cardiomyocytes contributes to decreased serca2a activity in rats with metabolic syndrome. *American journal of physiology. Heart and circulatory physiology*. 2013;305:H1344-1353.
245. Esposito BP, Breuer W, Sirankapracha P, Pootrakul P, Hershko C, Cabantchik ZI. Labile plasma iron in iron overload: Redox activity and susceptibility to chelation. *Blood*. 2003;102:2670-2677.
246. Leszek P, Sochanowicz B, Szperl M, Kolsut P, Brzoska K, Piotrowski W, Rywik TM, Danko B, Polkowska-Motrenko H, Rozanski JM, Kruszewski M. Myocardial iron homeostasis in advanced chronic heart failure patients. *International journal of cardiology*. 2012;159:47-52.
247. Sale S, Verschoyle RD, Boocock D, Jones DJ, Wilsher N, Ruparelia KC, Potter GA, Farmer PB, Steward WP, Gescher AJ. Pharmacokinetics in mice and growth-inhibitory properties of the putative cancer chemopreventive agent resveratrol and the synthetic analogue trans 3,4,5,4'-tetramethoxystilbene. *British journal of cancer*. 2004;90:736-744.
248. Amri A, Chaumeil JC, Sfar S, Charrueau C. Administration of resveratrol: What formulation solutions to bioavailability limitations? *Journal of controlled release : official journal of the Controlled Release Society*. 2012;158:182-193.
249. Johnson JJ, Nihal M, Siddiqui IA, Scarlett CO, Bailey HH, Mukhtar H, Ahmad N. Enhancing the bioavailability of resveratrol by combining it with piperine. *Molecular nutrition & food research*. 2011;55:1169-1176.

250. Mori J, Patel VB, Abo Alrob O, Basu R, Altamimi T, Desaulniers J, Wagg CS, Kassiri Z, Lopaschuk GD, Oudit GY. Angiotensin 1-7 ameliorates diabetic cardiomyopathy and diastolic dysfunction in db/db mice by reducing lipotoxicity and inflammation. *Circulation. Heart failure*. 2014;7:327-339.
251. Nixon JP, Zhang M, Wang C, Kuskowski MA, Novak CM, Levine JA, Billington CJ, Kotz CM. Evaluation of a quantitative magnetic resonance imaging system for whole body composition analysis in rodents. *Obesity*. 2010;18:1652-1659.
252. Abu Rajab M, Guerin L, Lee P, Brown KE. Iron overload secondary to cirrhosis: A mimic of hereditary haemochromatosis? *Histopathology*. 2014;65:561-569.
253. Ko C, Siddaiah N, Berger J, Gish R, Brandhagen D, Sterling RK, Cotler SJ, Fontana RJ, McCashland TM, Han SH, Gordon FD, Schilsky ML, Kowdley KV. Prevalence of hepatic iron overload and association with hepatocellular cancer in end-stage liver disease: Results from the national hemochromatosis transplant registry. *Liver international*. 2007;27:1394-1401.
254. Pietrangelo A. Non-hfe hemochromatosis. *Hepatology*. 2004;39:21-29.
255. Trombini P, Paolini V, Pelucchi S, Mariani R, Nemeth E, Ganz T, Piperno A. Hepcidin response to acute iron intake and chronic iron loading in dysmetabolic iron overload syndrome. *Liver international*. 2011;31:994-1000.
256. Mehlem A, Hagberg CE, Muhl L, Eriksson U, Falkevall A. Imaging of neutral lipids by oil red o for analyzing the metabolic status in health and disease. *Nature protocols*. 2013;8:1149-1154.
257. Bacon BR, Britton RS, O'Neill R. Effects of vitamin e deficiency on hepatic mitochondrial lipid peroxidation and oxidative metabolism in rats with chronic dietary iron overload. *Hepatology*. 1989;9:398-404.
258. Seki E, Schwabe RF. Hepatic inflammation and fibrosis: Functional links and key pathways. *Hepatology*. 2015;61:1066-1079.

259. Wynn TA, Ramalingam TR. Mechanisms of fibrosis: Therapeutic translation for fibrotic disease. *Nature medicine*. 2012;18:1028-1040.
260. Adams PC, Reboussin DM, Barton JC, McLaren CE, Eckfeldt JH, McLaren GD, Dawkins FW, Acton RT, Harris EL, Gordeuk VR, Leiendecker-Foster C, Speechley M, Snively BM, Holup JL, Thomson E, Sholinsky P, Hemochromatosis, Iron Overload Screening Study Research I. Hemochromatosis and iron-overload screening in a racially diverse population. *The New England journal of medicine*. 2005;352:1769-1778.
261. Carthew P, Edwards RE, Smith AG, Dorman B, Francis JE. Rapid induction of hepatic fibrosis in the gerbil after the parenteral administration of iron-dextran complex. *Hepatology*. 1991;13:534-539.
262. Pietrangelo A, Gualdi R, Casalgrandi G, Montosi G, Ventura E. Molecular and cellular aspects of iron-induced hepatic cirrhosis in rodents. *The Journal of clinical investigation*. 1995;95:1824-1831.
263. Pietrangelo A. Hemochromatosis: An endocrine liver disease. *Hepatology*. 2007;46:1291-1301.
264. Angelucci E, Baronciani D, Lucarelli G, Baldassarri M, Galimberti M, Giardini C, Martinelli F, Polchi P, Polizzi V, Ripalti M, et al. Needle liver biopsy in thalassaemia: Analyses of diagnostic accuracy and safety in 1184 consecutive biopsies. *British journal of haematology*. 1995;89:757-761.
265. Telfer PT, Prestcott E, Holden S, Walker M, Hoffbrand AV, Wonke B. Hepatic iron concentration combined with long-term monitoring of serum ferritin to predict complications of iron overload in thalassaemia major. *British journal of haematology*. 2000;110:971-977.
266. Brown KE, Dennery PA, Ridnour LA, Fimmel CJ, Kladney RD, Brunt EM, Spitz DR. Effect of iron overload and dietary fat on indices of oxidative stress and hepatic fibrogenesis in rats. *Liver international*. 2003;23:232-242.

267. Matsumoto M, Poci A, Rossetti L, Depinho RA, Accili D. Impaired regulation of hepatic glucose production in mice lacking the forkhead transcription factor foxo1 in liver. *Cell metabolism*. 2007;6:208-216.
268. Friedman SL. Mechanisms of hepatic fibrogenesis. *Gastroenterology*. 2008;134:1655-1669.
269. Yoshiji H, Kuriyama S, Miyamoto Y, Thorgeirsson UP, Gomez DE, Kawata M, Yoshii J, Ikenaka Y, Noguchi R, Tsujinoue H, Nakatani T, Thorgeirsson SS, Fukui H. Tissue inhibitor of metalloproteinases-1 promotes liver fibrosis development in a transgenic mouse model. *Hepatology*. 2000;32:1248-1254.
270. Nagai H, Matsumaru K, Feng G, Kaplowitz N. Reduced glutathione depletion causes necrosis and sensitization to tumor necrosis factor-alpha-induced apoptosis in cultured mouse hepatocytes. *Hepatology*. 2002;36:55-64.
271. Luedde T, Kaplowitz N, Schwabe RF. Cell death and cell death responses in liver disease: Mechanisms and clinical relevance. *Gastroenterology*. 2014;147:765-783 e764.
272. Bataller R, Brenner DA. Liver fibrosis. *The Journal of clinical investigation*. 2005;115:209-218.
273. Popov Y, Schuppan D. Targeting liver fibrosis: Strategies for development and validation of antifibrotic therapies. *Hepatology*. 2009;50:1294-1306.
274. Kawada N, Seki S, Inoue M, Kuroki T. Effect of antioxidants, resveratrol, quercetin, and n-acetylcysteine, on the functions of cultured rat hepatic stellate cells and kupffer cells. *Hepatology*. 1998;27:1265-1274.
275. Munzel T, Gori T, Keaney JF, Jr., Maack C, Daiber A. Pathophysiological role of oxidative stress in systolic and diastolic heart failure and its therapeutic implications. *European heart journal*. 2015
276. Iorga A, Li J, Sharma S, Umar S, Bopassa JC, Nadadur RD, Centala A, Ren S, Saito T, Toro L, Wang Y, Stefani E, Eghbali M. Rescue of pressure overload-induced heart failure by estrogen therapy. *Journal of the American Heart Association*. 2016;5

277. Konhilas JP, Leinwand LA. The effects of biological sex and diet on the development of heart failure. *Circulation*. 2007;116:2747-2759.
278. Miller VM. Why are sex and gender important to basic physiology and translational and individualized medicine? *American journal of physiology. Heart and circulatory physiology*. 2014;306:H781-788.
279. Witt H, Schubert C, Jaekel J, Fliegner D, Penkalla A, Tiemann K, Stypmann J, Roepcke S, Brokat S, Mahmoodzadeh S, Brozova E, Davidson MM, Ruiz Noppinger P, Grohe C, Regitz-Zagrosek V. Sex-specific pathways in early cardiac response to pressure overload in mice. *Journal of molecular medicine*. 2008;86:1013-1024.
280. Mendelsohn ME, Karas RH. The protective effects of estrogen on the cardiovascular system. *The New England journal of medicine*. 1999;340:1801-1811.
281. Murphy E. Estrogen signaling and cardiovascular disease. *Circulation research*. 2011;109:687-696.
282. Bendale DS, Karpe PA, Chhabra R, Shete SP, Shah H, Tikoo K. 17-beta oestradiol prevents cardiovascular dysfunction in post-menopausal metabolic syndrome by affecting sirt1/ampk/h3 acetylation. *British journal of pharmacology*. 2013;170:779-795.
283. van Eickels M, Grohe C, Cleutjens JP, Janssen BJ, Wellens HJ, Doevendans PA. 17beta-estradiol attenuates the development of pressure-overload hypertrophy. *Circulation*. 2001;104:1419-1423.
284. Satoh M, Matter CM, Ogita H, Takeshita K, Wang CY, Dorn GW, 2nd, Liao JK. Inhibition of apoptosis-regulated signaling kinase-1 and prevention of congestive heart failure by estrogen. *Circulation*. 2007;115:3197-3204.

285. Sharkey LC, Holycross BJ, Park S, Shiry LJ, Hoepf TM, McCune SA, Radin MJ. Effect of ovariectomy and estrogen replacement on cardiovascular disease in heart failure-prone shhf/mcc- fa cp rats. *Journal of molecular and cellular cardiology*. 1999;31:1527-1537.
286. Krijt J, Cmejla R, Sykora V, Vokurka M, Vyoral D, Necas E. Different expression pattern of hepcidin genes in the liver and pancreas of c57bl/6n and dba/2n mice. *Journal of hepatology*. 2004;40:891-896.
287. Widdowson EM, McCance RA. Sexual differences in the storage and metabolism of iron. *The Biochemical journal*. 1948;42:577-581.
288. Ramakrishnan U, Kuklina E, Stein AD. Iron stores and cardiovascular disease risk factors in women of reproductive age in the united states. *The American journal of clinical nutrition*. 2002;76:1256-1260.
289. Sullivan JL. Iron and the genetics of cardiovascular disease. *Circulation*. 1999;100:1260-1263.
290. MacDonald JK, Pyle WG, Reitz CJ, Howlett SE. Cardiac contraction, calcium transients, and myofilament calcium sensitivity fluctuate with the estrous cycle in young adult female mice. *American journal of physiology. Heart and circulatory physiology*. 2014;306:H938-953.
291. Musumeci M, Maccari S, Sestili P, Massimi A, Corritore E, Marano G, Catalano L. The c57bl/6 genetic background confers cardioprotection in iron-overloaded mice. *Blood transfusion = Trasfusione del sangue*. 2013;11:88-93.
292. Idris AI. Ovariectomy/orchidectomy in rodents. *Methods in molecular biology*. 2012;816:545-551.
293. McLean BA, Zhabyeyev P, Patel VB, Basu R, Parajuli N, DesAulniers J, Murray AG, Kassiri Z, Vanhaesebroeck B, Oudit GY. Pi3kalpha is essential for the recovery from cre/tamoxifen cardiotoxicity and in myocardial insulin signalling but is not required for normal myocardial contractility in the adult heart. *Cardiovascular research*. 2015;105:292-303.

294. Patel VB, Bodiga S, Fan D, Das SK, Wang Z, Wang W, Basu R, Zhong J, Kassiri Z, Oudit GY. Cardioprotective effects mediated by angiotensin ii type 1 receptor blockade and enhancing angiotensin 1-7 in experimental heart failure in angiotensin-converting enzyme 2-null mice. *Hypertension*. 2012;59:1195-1203.
295. Berdoukas V, Coates TD, Cabantchik ZI. Iron and oxidative stress in cardiomyopathy in thalassemia. *Free radical biology & medicine*. 2015
296. Jansova H, Machacek M, Wang Q, Haskova P, Jirkovska A, Potuckova E, Kielar F, Franz KJ, Simunek T. Comparison of various iron chelators and prochelators as protective agents against cardiomyocyte oxidative injury. *Free radical biology & medicine*. 2014;74:210-221.
297. Sipido KR, Volders PG, Vos MA, Verdonck F. Altered na/ca exchange activity in cardiac hypertrophy and heart failure: A new target for therapy? *Cardiovascular research*. 2002;53:782-805.
298. Hou Y, Zhang S, Wang L, Li J, Qu G, He J, Rong H, Ji H, Liu S. Estrogen regulates iron homeostasis through governing hepatic hepcidin expression via an estrogen response element. *Gene*. 2012;511:398-403.
299. Meyer S, van der Meer P, van Tintelen JP, van den Berg MP. Sex differences in cardiomyopathies. *European journal of heart failure*. 2014;16:238-247.
300. Zacharski LR, Ornstein DL, Woloshin S, Schwartz LM. Association of age, sex, and race with body iron stores in adults: Analysis of nhanes iii data. *American heart journal*. 2000;140:98-104.
301. Brewer C, Otto-Duessel M, Wood RI, Wood JC. Sex differences and steroid modulation of cardiac iron in a mouse model of iron overload. *Translational research : the journal of laboratory and clinical medicine*. 2014;163:151-159.
302. Berdoukas V, Coates TD, Cabantchik ZI. Iron and oxidative stress in cardiomyopathy in thalassemia. *Free radical biology & medicine*. 2015;88:3-9.

303. Berndt C, Lillig CH, Holmgren A. Thiol-based mechanisms of the thioredoxin and glutaredoxin systems: Implications for diseases in the cardiovascular system. *American journal of physiology. Heart and circulatory physiology*. 2007;292:H1227-1236.
304. Lagranha CJ, Deschamps A, Aponte A, Steenbergen C, Murphy E. Sex differences in the phosphorylation of mitochondrial proteins result in reduced production of reactive oxygen species and cardioprotection in females. *Circulation research*. 2010;106:1681-1691.
305. Richter K, Konzack A, Pihlajaniemi T, Heljasvaara R, Kietzmann T. Redox-fibrosis: Impact of tgfbeta1 on ros generators, mediators and functional consequences. *Redox biology*. 2015;6:344-352.
306. Saito K, Ishizaka N, Aizawa T, Sata M, Iso-o N, Noiri E, Mori I, Ohno M, Nagai R. Iron chelation and a free radical scavenger suppress angiotensin ii-induced upregulation of tgf-beta1 in the heart. *American journal of physiology. Heart and circulatory physiology*. 2005;288:H1836-1843.
307. Lancel S, Qin F, Lennon SL, Zhang J, Tong X, Mazzini MJ, Kang YJ, Siwik DA, Cohen RA, Colucci WS. Oxidative posttranslational modifications mediate decreased serca activity and myocyte dysfunction in galphaq-overexpressing mice. *Circulation research*. 2010;107:228-232.
308. Chirico V, Rigoli L, Lacquaniti A, Salpietro V, Piraino B, Amorini M, Salpietro C, Arrigo T. Endocrinopathies, metabolic disorders, and iron overload in major and intermedia thalassemia: Serum ferritin as diagnostic and predictive marker associated with liver and cardiac t2\* mri assessment. *European journal of haematology*. 2015;94:404-412.
309. Mousa AA, Ghonem M, Elhadidy EH, Azmy E, Elbackry M, Elbaiomy AA, Elzehery RR, Shaker GA, Saleh O. Iron overload detection using pituitary and hepatic mri in thalassemic patients having short stature and hypogonadism. *Endocrine research*. 2016:1-6.
310. Breuer W, Hershko C, Cabantchik ZI. The importance of non-transferrin bound iron in disorders of iron metabolism. *Transfusion science*. 2000;23:185-192.

311. Liu Y, Parkes JG, Templeton DM. Differential accumulation of non-transferrin-bound iron by cardiac myocytes and fibroblasts. *Journal of molecular and cellular cardiology*. 2003;35:505-514.
312. Gutteridge JM, Rowley DA, Griffiths E, Halliwell B. Low-molecular-weight iron complexes and oxygen radical reactions in idiopathic haemochromatosis. *Clinical science*. 1985;68:463-467.
313. Schafer AI, Cheron RG, Dluhy R, Cooper B, Gleason RE, Soeldner JS, Bunn HF. Clinical consequences of acquired transfusional iron overload in adults. *The New England journal of medicine*. 1981;304:319-324.
314. Pelusi C, Gasparini DI, Bianchi N, Pasquali R. Endocrine dysfunction in hereditary hemochromatosis. *Journal of endocrinological investigation*. 2016
315. Hare DJ, Arora M, Jenkins NL, Finkelstein DI, Doble PA, Bush AI. Is early-life iron exposure critical in neurodegeneration? *Nature reviews. Neurology*. 2015;11:536-544.
316. Leinwand LA. Sex is a potent modifier of the cardiovascular system. *The Journal of clinical investigation*. 2003;112:302-307.
317. Rossouw JE, Anderson GL, Prentice RL, LaCroix AZ, Kooperberg C, Stefanick ML, Jackson RD, Beresford SA, Howard BV, Johnson KC, Kotchen JM, Ockene J, Writing Group for the Women's Health Initiative I. Risks and benefits of estrogen plus progestin in healthy postmenopausal women: Principal results from the women's health initiative randomized controlled trial. *Jama*. 2002;288:321-333.
318. Grandi AM, Venco A, Barzizza F, Scalise F, Pantaleo P, Finardi G. Influence of age and sex on left ventricular anatomy and function in normals. *Cardiology*. 1992;81:8-13.
319. Adams PC, Valberg LS. Evolving expression of hereditary hemochromatosis. *Seminars in liver disease*. 1996;16:47-54.

320. Economou M, Katzos G, Koussi A, Tsatra I, Athanassiou-Metaxa M. Hypoparathyroidism in beta-thalassemic patients. *Journal of pediatric hematology/oncology*. 2003;25:275-276; author reply 276.